Isolation and Functional Studies of The F-type ATP Synthase

from Spinach Chloroplasts and *Heliobacterium modesticaldum*

by

Jay-How Yang

A Dissertation Presented in Partial Fulfillment
of the Requirements for the Degree
Doctor of Philosophy

Approved February 2015 by the
Graduate Supervisory Committee:

Petra Fromme, Chair
Kevin Redding
Ian Gould

ARIZONA STATE UNIVERSITY

May 2015

ABSTRACT

Adenosine triphosphate (ATP) is the universal chemical energy currency in most living cells, used to power many cellular reactions and generated by an enzyme supercomplex known as the ATP synthase, consisting of a hydrophilic F_1 subcomplex and a membrane-bound F_O subcomplex. Driven by the electrochemical gradient generated by the respiratory or photosynthetic electron transport chain, the rotation of the F_O domain drives movements of the central stalk in response to conformational changes in the F_1 domain, in which the physical energy is converted into chemical energy through the condensation of ADP and P_i to ATP. The exact mechanism how ATP synthesis is coupled to proton translocation is not known as no structure of the intact ATP-synthase nor the intact F_O subcomplex has been determined to date. Structural information may shed light on these mechanisms and aid in understanding how structural changed relate to its coupling to ATP synthesis. The work in this thesis has successful established a defined large-scale CF_1F_O isolation procedure resulting in high purity and high yield of this complex from spinach thylakoid membranes by incorporating a unique combination of biochemical methods will form the basis for the subsequent structural determination of this complex. Isolation began from the isolation of intact chloroplasts and the separation of intact thylakoid membranes. Both native and denaturing electrophoresis analyses clearly demonstrated that the purified CF_1F_O retains its quaternary structure consisting of the CF_1 and CF_O subcomplexes and nine subunits (five F_1 subunits: α, β, γ, δ and ε, and four F_O subunits: a, b, b' and c). Moreover, both ATP synthesis and hydrolysis activities were successfully detected using protein reconstitution in combination with acid-base incubation and in-gel ATPase assays, respectively. Furthermore, the ATP-synthase of *H. modesticaldum*, an anaerobic photosynthetic bacterium, was also isolated and characterized at the biochemical level.

These biochemical characterizations directly influenced recent studies on the high-resolution structure determination of intact CF_1F_O using electron crystallography on two-dimensional crystals. The availability of the functionally intact CF_1F_O purified at a large scale will lead to studies that investigate the possible crystallization conditions to ultimately determine its three-dimensional structure at atomic resolution.

DEDICATION

I express deep gratitude to my parents for their support and encouragement. I also dedicate this dissertation to the laboratory equipment.

ACKNOWLEDGMENTS

I am grateful to my supervisor, Dr. Petra Fromme for her great experience in photosynthesis and in particular with the ATP synthase enzyme, with many years of excellent insight into a challenge project. Petra's guidance changed the course of my career and I deeply appreciate her generosity. I am thankful for the support and advice of the members of my committee, Dr. Ian Gould and Dr. Kevin Redding. Former students from the group, Dr. Benjamin Varco-Merth and Dr. Robert Michael Lawrence provided initial instruction related to the purification of the native chloroplast ATP synthase. Their encouragement lasted the duration of my PhD years and helped me troubleshoot in complicated times.

I convey my regards to Dr. Matthias Frank, Dr, James Evans and Dr. Barry Bruce for their time, enthusiasm and support at various stages of my project. I would also like to acknowledge the contributions of Dr. Peter Graber and Dr. Markus Burger for demonstrating the reconstitution measurement of ATP synthase. I owe immense thanks to Dr. Ingo Grotjohann and Dr. Raimund Fromme for additional advice related to ATP synthase (especially help with spinach party) and many thoughtful discussions regarding biochemical techniques and for being dear friends. Many thoughtful discussions with my good friends Dr. Katerina Dorner, Dr. Thomas Spatzal and Dr. Jose Martin Garcia immensely helped me regain both knowledge and sanity. Finally, I would like to thank all members of Fromme group for enduring and even understanding my quirks.

TABLE OF CONTENTS

Page

CHAPTER Page

CHAPTER Page

CHAPTER Page

CHAPTER Page

CHAPTER Page

LIST OF TABLES

Table Page

LIST OF FIGURES

Figure Page

LIST OF ABBREVIATIONS

Abbreviation

A_{280}.....280 nm Absorbance

A_{278}.....278 nm Absorbance

A_{645}.....645 nm Absorbance

A_{700}.....700 nm Absorbance

CHAPTER 1

INTRODUCTION

1.1 Oxygenic Photosynthesis

Chlorophyll which is present in photosynthetic organisms and gives them the green color, is the most plentiful pigment on Earth, and photosynthesis is the most important process on Earth. In the absence of these photosynthetic organisms, sunlight cannot be absorbed, and the energy of sunlight cannot be stored, ultimately resulting in all living things on Earth becoming extinct. The oxygenic photosynthetic reaction, which can be represented using the simple chemical equation 6 CO_2 + 6 H_2O ------> $C_6H_{12}O_6$ (carbohydrate) + 6 O_2, converts energy from sunlight into biochemical energy and produces molecular oxygen which is used for energy supply by all higher organisms on Earth. Oxygenic photosynthesis, which takes place in cyanobacteria, algae, and chloroplasts of higher plants, can also be regarded as the sum of a series of multiple electron-transfer steps, which are driven by the light-induced charge separation carried out by two integral membrane-bound pigment-protein complexes (photosystems I and II), which are coupled by a membrane-bound electron carrier complex (cytochrome b_6f complex) and the mobile electron carriers plastoquinone (PQ) and plastocyanin (Pc). These large protein membrane complexes with various cofactors as well as their relative orientation in the thylakoid membrane are depicted in Figure 1.1. They are shown as the structural models derived from X-ray crystallography in Figure 1.1A. A schematic picture of the cofactors involved in the multiple electron-transfer steps is shown in Figure 1.1B. The reactions carried out by each of the complexes are described in detail below. Both photosystem I (PSI) and photosystem II (PSII) are multisubunit pigment-protein complexes that perform the transduction of light energy into electrical energy by catalyzing the light-induced charge separation across the thylakoid membrane. In

the heart of PSII the photoreaction center is located which is coupled to the oxygen-evolving complex (Levy, Mosser et al. 1999). After light has been absorbed by the internal antenna system, the excitation energy is transferred to the photoreaction center, where a special pair of chlorophyll molecules (P680) ($P_{D1}P_{D2}$) act in the primary charge separation. The excited state $P680^{*}$ is formed and catalyzes the primary charge separation leads to the oxidation of P680* to $P680^{+}$. One electron is transferred to the chlorophyll (Chl_{D1}), which acts as the primary electron acceptor, which also acts as an immediate electron donor for pheophytin (Phe_{D1}).

A.

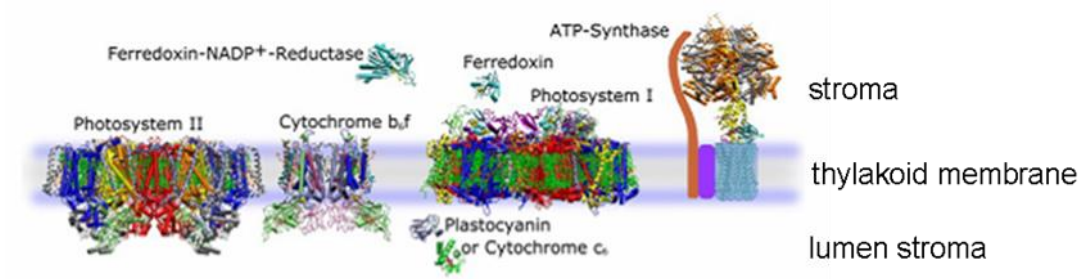

B.

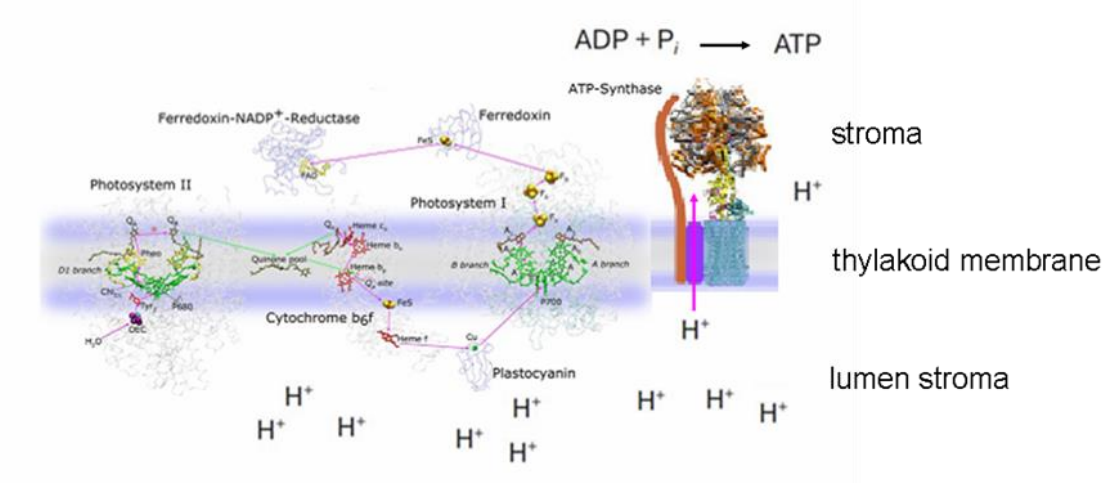

Figure 1.1 Overview of Oxygenic Photosynthesis. The image shows the major protein complexes responsible for electron transfer in oxygenic photosynthesis and their respective positions in the thylakoid membrane, with the lumen depicted below the membrane and the stroma depicted above the membrane (A) and emphasis on the electron transfer route with the involved protein cofactors (B). The electron transfer reactions create and electrochemical gradient of protons that is used by the ATP synthase to synthesize ATP from ADP and Phosphate (Lawrence 2011).

Immediately after receiving an electron from Phe_{D1}, the electron is passed to the primary tightly-bound plastoquinone (PQ_A) and then to the secondary mobile plastoquinone (PQ_B). After being reduced twice (two charge separations), the PQ_B molecule ultimately binds two protons ($2\ H^+_{out}$) that are translocated from the stroma to form the plastoquinol (PQ_BH_2) molecule, which acts as a mobile electron ($2\ e^-$) and a proton carrier ($2\ H^+$). The protonated PQ_BH_2 molecule dissociates from the PQ_B quinone binding site of PSII to exchange with an oxidized plastoquinone molecule from the PQ pool. The released hydrophobic PQ_BH_2 molecule diffuses into the thylakoid membrane until it reaches the membrane-bound cytochrome *b*$_6$*f* complex, which serves as an electron acceptor for the oxidation of PQ_BH_2. Simultaneously, the oxidized $P680^+$ with high redox potential of 1.1V extracts an electron from the Mn_4Ca cluster in the OEC via a tyrosine residue, which serves as the immediate electron donor for $P680^+$. The oxidized $P680^+$ is reduced to P680, which is able to catalyze the next subsequent charge separation. In each of the 4 consecutive charge-separation events catalyzed by by P680, one electron and one proton are extracted from 2 water molecules bound to the Mn_4Ca cluster which form the catalytic center of the oxygen evolving complex (Levy, Mosser et al. 1999). The OEC finally splits two water molecules ($2\ H_2O$) to produce one oxygen molecule (O_2) after 4 charge separation events and in the process four protons ($4\ H^+$) are released into the lumen. The cytochrome *b*$_6$*f* complex (cyt *b*$_6$*f*) acts as a bridge in the electron transfer chain between PSII and PSI. It oxidizes PQH_2 to PQ, the $2\ H^+$ are released into the lumen and the 2e- subsequently reduce 2 plastocyanin molecules (Pc). The cytochrome *b*$_6$*f* complex (cyt *b*$_6$*f*) contains two quinone-binding sites (Q_o and Q_i) for the PQ_BH_2 and the quinone (Q) molecules and, in a process called Q-cycle, shuttles two additional H^+ from the stromal to the lumenal side across the membrane.The reduced PQ_BH_2 is oxidized at the Q_o site between heme

b_6^L and the [Fe_2S_2] cluster, which is oriented toward the lumen side of the thylakoid membrane. One of the two electrons donated by PQ_BH_2 is transferred to plastocyanin (Pc) (or cytochrome c_6 in cyanobacteria) through the [Fe_2S_2] cluster and the cyt *f*, which semi-oxidizes PQ_BH_2 to semi-plastoquinol PQ_BH and subsequently releases one proton (H^+) into the lumen side of the thylakoid membrane. The other electron from PQ_BH is directed through the low-potential heme b_6^L and the high-potential heme b_6^H to reduce a Q molecule to semi-quinone Q at the Q_i site oriented toward the stromal side of the thylakoid membrane, which is known as half of the Q cycle. The semi-plastoquinol PQ_BH is completely oxidized to plastoquinone (PQ), and the other proton (H^+) is subsequently released into the lumen of the thylakoid membrane. The second half of Q-cycle involves the oxidation of a second PQH_2, which donates two electrons (2 e^-) to the cytochrome *b6f* complex and releases two proton carriers (2 H^+) into the lumen side of the thylakoid membrane. At the lumenal side, the soluble mobile one-electron carrier protein, namely plastocyanin (Pc), is reduced to Cu^{1+}Pc through cytochrome *f* by one PQ_BH_2 molecule and is then dissociated from the cytochrome *b6f* complex to diffuse through the lumen until it migrates to photosystem I (PSI). Photosystem I contains P700, which acts as the primary electron donor formed by a special pair of chlorophyll molecules (Chl_{1A} and Chl_{1B}). PSI contains a large intrinsic antenna system of 90 chlorophylls and 22 carotenoids which are tightly functionally coupled to the reaction center core. After absorbing light by one of these antenna pigments the excitation energy is transferred to the core of the reaction center leading to the excitation of P700 to a higher energy level, resulting in the excited state $P700^{*}$. An electron is donated from $P700^*$ to one of the next chlorophyll molecules (Chl_{2A} or Chl $_{3B}$), resulting in the formation of the oxidized $P700^+$. Later, this oxidized $P700^+$ is reduced to P700 by accepting an electron from the reduced plastocyanin (Cu^{1+}Pc), which is thereby

oxidized to plastocyanin ($Cu^{2+}Pc$). The electron in $Chl_{2A/B}$ is immediately transferred to the next chlorophyll molecules ($Chl_{3A/B}$) and then to one of the two phylloquinone molecule (A_{1A} or A_{1B}, respectively). PSI contains two branches (A and B) of the electron transfer chain. The branch from Chl_{2A} and Chl_{3A} to PhQ_A is called A-branch, whereas the branch from Chl_{2B} and Chl_{3B} to PhQ_B is called B-branch. Although both branches A and B are functional, the ratio of A and B branch electron transfer differs between different photosynthetic organisms (Cohen, Shen et al. 2004, Dashdorj, Xu et al. 2005, Mula, Savitsky et al. 2012, Tikhonov 2013). The electron of one of the reduced phylloquinone molecules (A_{1A} and A_{1B}) is transferred to the first 4Fe4S iron sulfur center (F_x), then to the second 4Fe4S cluster (F_A), and finally to a terminal acceptor, the 4Fe4S cluster (F_B). The electron in the reduced F_B is passed to the soluble mobile electron carrier protein ferredoxin (Fd) on the stromal side of the thylakoid membrane. In the stroma, the reduced Fd^{e-} molecule dissociates from PSI and diffuses in the stroma until it binds to ferredoxin-$NADP^+$-reductase (FNR). The electron of the reduced Fd molecule is delivered to ferredoxin-$NADP^+$-reductase (FNR), which serves as a one-electron to two-electron converter. FNR contains a functional group (FAD) that can accept and then store one electron from the first-reduced Fd^{e-}, and the other electron is subsequently delivered by a second reduced Fd. The final step in the non-cyclic electron transfer process involves the transfer of two electrons (2 e^-) from the double-reduced FNR to an oxidized $NADP^+$ molecule, which is a two-electron carrier. The reduced $NADP^+$ molecule with two accepted electrons (2 e^-) is coupled to one proton (H^+_{out}) from the stromal side to form the first high energy biochemical energy NADPH. Several of the descriptions above were adapted from Tikhonov (2013).

1.2 Electrochemical Gradient

During the non-cyclic electron transfer process in oxygenic photosynthesis, an electrochemical gradient, which consists of the proton gradient (ΔpH) and an electrical potential (ΔΨ), is created between the stroma and lumen sides of the thylakoid membrane. This electrochemical gradient is then used for the synthesis of ATP from ADP and inorganic phosphate by the ATP synthase protein complex bound to the thylakoid membrane. The proton concentration at the stromal side decreases as the plastoquinone (PQ_B^{2e-}) molecule in PSII and the reduced $NADP^{+2e-}$ molecule become coupled to protons (H^+_{out}) at the stromal side to form the plastoquinol $PQ_B^{2e-}H_2$ molecule and an oxidized NADPH, respectively. In contrast to the decrease of the proton concentration at the stromal side, the lumenal side is acidified by an increase in the proton concentration through the oxidation of water molecules and release of protons via the OEC and the oxidation of the plastoquinol PQ_BH_2 molecule in the cytochrome b_6f complex and Q-cylce proton transfer, which results in the release of protons (H^+) into the lumen. Therefore, a proton gradient is created by the difference in the proton concentration between the two sides that occurs through these processes. An electric gradient (ΔΨ) is formed by the transfer of electron through the oxidation of a water molecule at the lumenal side to an oxidized NADP+ molecule at the stromal side. Therefore, the lumenal side of the thylakoid membrane becomes positively charged (loss of e^-), whereas the stromal side of the membrane becomes negatively charged (gain of e^-). The electrochemical gradient (ΔpH and ΔΨ) is not only the essential driving force of ATP synthesis but also a feedback control mechanism of electron transfer in the chloroplast.

1.3 Overview of the ATP Synthase Protein Complex

Adenosine triphosphate (ATP) is the universal chemical energy currency in living cells and is used to power many biochemical processes. ATP molecules can be synthesized through a number of cellular processes, such as glycolysis, citric acid cycle, beta-oxidization, and fermentation. However, of the majority of ATP is synthesized by the ATP synthase protein complex via oxidative phosphorylation in the mitochondria or photo-phosphorylation in the chloroplasts. The ATP synthase protein complex is a universal rotary nanomachine, which is essentially a super-complex consisting of two sub-complexes (soluble factor and membrane-bound factor) with multiple subunits. The primary function of the ATP synthase complex is to generate ATP molecules from ADP and Pi. However, some ATP synthase complexes function in ion transport by hydrolyzing ATP (the reverse direction). Several types of ATP synthase complexes have been identified; these include F-type ATP synthases, which are found in bacterial plasma membranes, mitochondrial inner membranes and chloroplast thylakoid membranes, the A-type ATP synthases, which are found is archaeal plasma membranes, and the V-type ATP synthases, which are found in the plasma membranes of a wide variety of cells, such as eukaryotic vacuoles, endosomes, lysosomes, and secretory vesicles. The function of F-type ATP synthases are similar to that of A-type ATP synthases, which major function is ATP synthesis. They use an electrochemical gradient of protons or ions to drive ATP synthesis, whereas V-ATPase uses the energy from ATP hydrolysis to pump protons (H^+) or other ions across the intracellular and plasma membranes of organelles. The core of the molecular architecture of ATP synthase complexes is widely conserved among the three types of ATP synthase complexes and species, and it include at least five dissimilar subunits in the soluble factor (F_1) and at least three dissimilar subunits in the membrane-bound factor

(Arechaga and Fotiadis). However large structural differences exist in the composition of the rotor in the membrane integral part of the enzyme, the peripheral stalk(s) and the accessory subunits which may play important regulatory roles.

1.4 Molecular Structure of the Chloroplast ATP Synthase Protein Complex

The membrane-bound F-type ATP synthase protein complex is a universal rotary nanomachine found in the energy-transducing membranes of bacteria, mitochondria, and chloroplasts (Turina, Samoray et al. 2003). The main role of the ATP synthase complexes is the formation of ATP (Boyer 1997, Rexroth, Meyer Zu Tittingdorf et al. 2004, Nakamoto, Baylis Scanlon et al. 2008, von Ballmoos, Wiedenmann et al. 2009, Walker 2013). The subunit composition and nomenclatures of ATP synthase complexes in bacteria, mitochondria, and chloroplasts are compared in Table 1.1.

Table 1.1 Subunit Nomenclature for the Bacterial, Mitochondrial, and Chloroplast ATP Synthase Complexes.

Type		Bacteria	Mitochondria	Chloroplast
F_1 domain	catalytic sites	α	α	α
		β	β	β
	central stalk	γ	γ	γ
		ε	ε	ε
			δ	
	peripheral stalk	δ	OSCP[a]	δ
F_O domain	H^+ access channel	a	a, e, f, g, A6L	a (IV)
	peripheral stalk	b_2, or b/b'	b_2, d, F_6	b/b' (I/II)
	Oligomeric rotor	c_{10-15}	c_{10}	c_{10-15} (III_{10-15})

(A) [a] OSCP, oligomycin sensitivity conferral protein. (B) The bacterial and chloroplast ATP synthases share similar subunit organization, whereas the mitochondrial ATP synthase contains more subunits in its peripheral stalk (F6, OSCP (inhibitor) and d-subunits in addition to its a-subunit (AL6, e-, f-, and g-subunits). (C) The *E. coli* ATP synthase possesses two identical copies of the b-subunit, whereas the cyanobacterial and chloroplast ATP synthases contain two homologous b-subunits (b- and b'-subunits). Table taken and adapted from Nakamoto et al. (2008) and Walker (2013) (Nakamoto, Baylis Scanlon et al. 2008, Walker 2013).

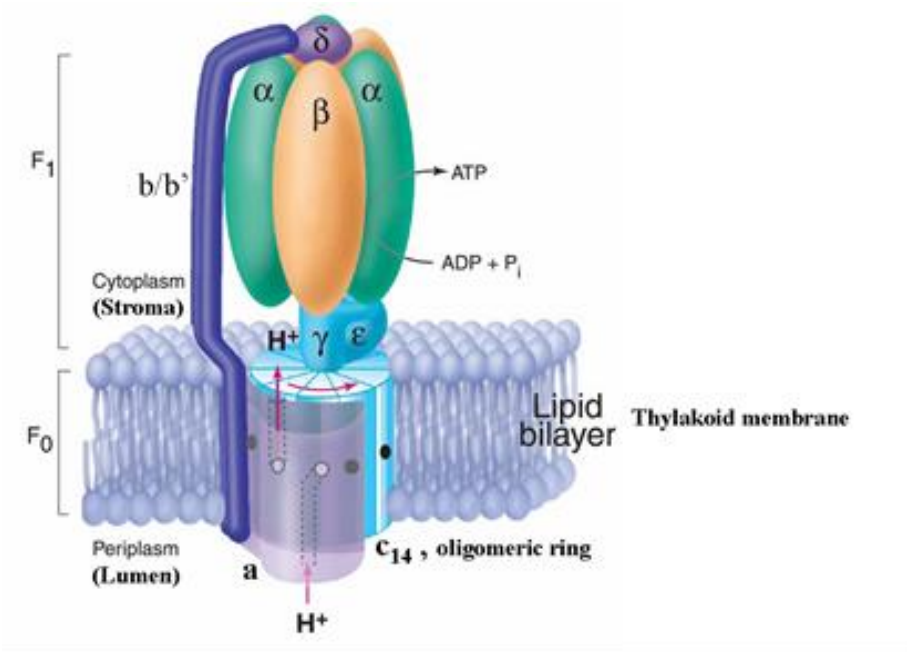

Figure 1.2 General Subunit Arrangement of the Chloroplast F-type ATP Synthase Complex. Latin characters are used for the subunits of the membrane-bound Fo domain, and Greek characters are used for the 5 different subunits of the hydrophilic F_1 domain which is composed of $\alpha_3,\beta_3,\gamma,\delta,\varepsilon$. In chloroplasts, the subunits of the Fo domain have traditionally been denoted with roman numbers but more recently names a, b and c are used to allow for easier comparison with other F-type ATP synthases. The Fo domain consists of 4 different subunits: IV (a), I (b), II (b'), and III_{14} (c_{14}). The proton translocation through the Fo domain is coupled with catalytic ATP formation in F1. Protons enter from the lumenal (periplasmic) side (lumen) and exit to the cytoplasmic side (stroma) through the a-subunit. Rotation of the c-oligomeric ring in the F_O domain driven by the proton potential is coupled with the rotation of the central stalk, resulting in conformational changes in the catalytic sites of the F_1 domain, where the 3 catalytic sites synthesize ATP in a conformational-coupled binding change mechanism(Boyer 1979, Boyer 1997). The image was taken and adapted from Fillingame et al. (2003), Lawrence et al. (2011) (Fillingame, Angevine et al. 2003, Lawrence, Varco-Merth et al. 2011).

The chloroplast ATP synthase protein complex is coupled to the electron transfer processes in the thylakoid membrane. The electrochemical proton gradient ($\Delta pH + \Delta\psi$) between the stromal and lumenal sides (intra thylakoid space) in the chloroplast is generated through the electron transfer process and drives ATP synthesis. In the process of ATP synthesis, protons (H^+) are translocated across the thylakoid membrane from the lumenal side (intra thylakoid space) to the stromal side thereby driving rotation and ATP synthesis by the ATP synthase protein complex. This driving force of the

electrochemical gradient is thereby converted into chemical energy by the formation of ATP from ADP and inorganic phosphate by the ATP synthase protein complex (Groth. G. and Strotmann 1999). The chloroplast ATP protein synthase protein complex (CF_1F_o) is a super-complex comprising two sub-complexes, namely the hydrophilic subcomplex F_1 and the hydrophobic F_O subcomplex. The hydrophilic subcomplex is a membrane extrinsic head domain designated the CF_1 domain, which comprises five dissimilar subunits, i.e., the α-, β-, γ-, δ-, and ε-subunits (Figure 1.2). In contrast, three (or four) different subunits, namely the a-, b-(b'), and c-subunits, comprise a hydrophobic membrane-bound subcomplex designated the CF_O domain (Figure 1.2). Hence, the chloroplast ATP synthase protein complex is often synonymously denoted CF_1F_O. The CF_1 and CF_O domains are integrated into the CF_1F_O protein complex by two stalks: the rotational central interior stalk, which consists of the CF_1-γ-subunit and ε-subunit, and the peripheral stationary stalk, which contains the CF_O-b and b' subunits as well as the CF_1-δ-subunit (Bottcher, Schwarz et al. 1998).

1.5 Overview of the Functional Activity in the Chloroplast ATP Synthase Complex

The chloroplast ATP synthase protein complex consists of nine different subunits ($\alpha_3\beta_3\gamma\delta\varepsilon I_1 II_1$ $III_{10\text{-}15}$ IV_1; Figure 1.2) located in two major separable domains (CF_1 and CF_O). As first proposed through biochemical functional and structural studies and confirmed by the X-ray structures of F_1 (Abrahams, Leslie et al. 1994, Groth, Mills et al. 2000, Groth and Pohl 2001), the top view of the CF_1 domain shows an asymmetrically hexagonal ring consisting of three α-β pairs containing three ADP-binding sites located at each of the β subunits interfacing the α-subunits. During catalysis, three sequential conformational changes (open, tight and loose positions, respectively) interchange driven by a 360° rotation of the γ-subunit. This process has

been proposed by Paul Boyer who received the Nobel Prize for his hypothesis of the binding change mechanism (Boyer, Cross et al. 1973, Boyer 1979, Boyer 1989, Boyer 1993, Boyer 1997, Boyer 1998, Boyer 1998). The proton translocation process takes place at the CF_O domain, which is composed of a symmetrical oligomer ring that contains multiple copies$_{10\text{-}15}$ of the III (c) subunit (transmembrane helical hairpins) and the IV (a) subunit that is peripherally located on the ring (Feniouk 2008). The detailed proton translocation cycle is depicted and described in Figure 1.3. During proton translocation, a proton (H^+) on the lumen side is trapped through a lower channel of the IV (a) subunit, and this trapped proton (H^+) is immediately transferred to the III (c) subunit to bind the unprotonated glutamic acid residue on one of the monomeric subunits of the III (c) subunit, which is in contact with the IV (a) subunit.

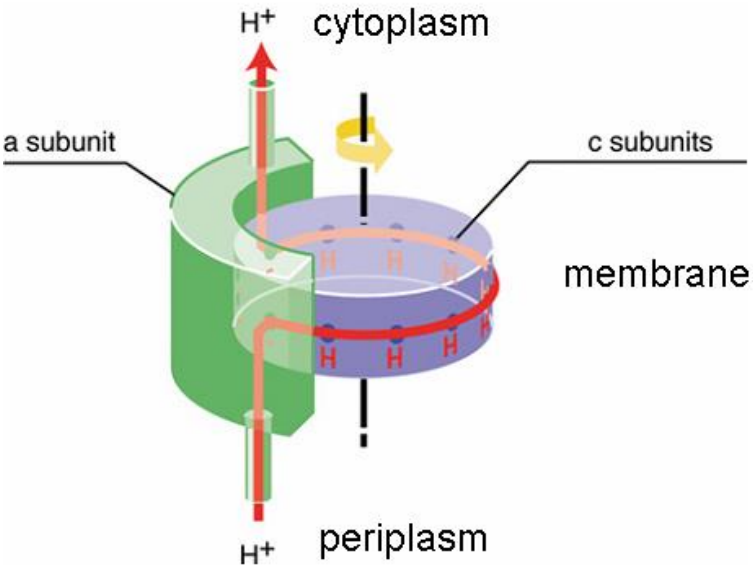

Figure 1.3 Model of the Coupling of Rotation and H^+ Translocation in the F_O Domain of ATP Synthases. The figure depicts the a-subunit (Pfeiffer, Gohil et al. 2003) which is in contact with the cylindrically oligomeric ring of c-subunits (blue). Each monomeric c-subunit contains an aspartate or glutamate residue (dark blue circles). The process of proton translocation and rotation are proposed to be coupled as follows: A single proton is shown entering from the lumenal (periplasmic) side via the entry half-channel of the a-subunit and then protonates a negatively charged carboxyl group of an aspartate or glutamate residue at the a-c subunit interface. Once protonated, this leads to a one step rotation of the c-ring, which thereby moves the protonated residue into the hydrophobic environment of the lipid bilayer. The stepwise rotation of the oligomeric c-ring brings

the next negatively charged carboxyl group into the a-c subunit interface, allowing another protonation. At the other side the rotor one of the protonated c-subunits reaches the exit half-channel of the a-subunit, where the protonated carboxyl group is deprotonated, finally releasing the proton to the stromal (cytoplasmic) side via the exit half-channel of the a-subunit on the opposite side of the membrane. The number of protons required to drive a complete 360° rotation of the oligomeric ring of the c-subunits corresponds to the number of monomeric c-subunits that form the oligomeric ring. Each complete 360° rotation of the c-ring rotor drives synthesis of three molecules of ATP in the F_1 domain, driven by the movement of the γ subunit that is firmly attached to the c-ring rotor. Figure taken and adapted from Junge (1999) and Walker (2013) (Junge 1999, Walker 2013).

Therefore, one entire 360° rotation is completed by the sequential protonation of the acid residues on each monomer of the III (c) subunit. After the first-protonated III (c) subunit forms contacts with the other side of the IV (a) subunit, glutamate is immediately deprotonated, and a proton (H^+) is then released via an upper channel of the IV (a) subunit on the stromal side (Junge and McLaughlin 1987, Junge, Lill et al. 1997, Junge 1999, Richter, Hein et al. 2000). The rotation of the central stalk (γ-subunit and ε-subunit), which is mechanically and structurally coupled with the III-(c) ring of CF_O, drives the stepwise synthesis of three ATP molecules on three catalytic sites (one on each of the three β-subunits) via the binding change mechanism (Diez, Zimmermann et al. 2004). In other words, ATP-synthesis is driven by the rotation of the rotor moiety ($III_{10\text{-}15}\gamma\varepsilon$) relative to the stator moiety ($\alpha_3\beta_3\delta I_1 II_1$). Hence, it can be concluded that the cyclical sequence of rotation produces three ATP molecules and driven by the flow of protons along a concentration gradient from the lumenal side to the stromal side. In principle all enzyme reactions are reversible, so all ATP synthases could also catalyze the reverse reaction where ATP hydrolysis drives the pumping of protons or ions against a concentration gradient. However in chloroplasts the hydrolytic function of CF_1F_O is inactivated during the night to prevent the futile hydrolysis of ATP synthesized during the day by redox modulation of a disulfide bridge on its γ subunit via thioredoxin and inactivation of the enzyme that involves regulatory binding sites at

the alpha subunits (Mills and Mitchell 1982, Junesch and Graber 1991, Ort 1992, Evron, Johnson et al. 2000, Hisabori, Konno et al. 2002, Hisabori, Ueoka-Nakanishi et al. 2003, Richter 2004, Kohzuma, Dal Bosco et al. 2013) . A few bacterial F-type ATP synthases, such as that in *Ilyobacter tartaricus*, can primarily function in active ion transport in the reverse direction, which uses the energy of ATP hydrolysis to translocate ions across the plasma membrane. This hydrolysis direction of the F-type ATP synthase complex is particularly important for anaerobic bacteria to generate a membrane potential (ΔpH) (Dimroth and Cook 2004). Hence, both the synthesis and hydrolysis directions of the F-type ATP synthase are relevant in the physiological state.

1.6 The F_1 Domain is Responsible for ATP Synthesis and Hydrolysis

The subcomplex of the F_1 domain, which consists of a hexagonally arranged catalytic core ($\alpha_3\beta_3$-subunits), a central stalk (γ-subunit and ε-subunit) and part of the peripherally stationary stalk (δ-subunit). It can act as a rotary molecular motor in concert with a central stalk consisting of a γ-subunit and a ε-subunit (Boyer 1981, Abrahams, Leslie et al. 1994, Noji, Yasuda et al. 1997, Weber and Senior 1997, Weber and Senior 1997, Kinosita, Yasuda et al. 2000, Kinosita, Yasuda et al. 2000, Nadanaciva, Weber et al. 2000, Senior, Weber et al. 2000, Weber and Senior 2000, Weber and Senior 2000, Yoshida, Muneyuki et al. 2001, Kinosita, Adachi et al. 2004). Full rotation causes a series of conformational changes in the asymmetry of the $\alpha_3\beta_3$-subunits, resulting in the release of the product (ATP) and the binding of substrates (ADP and inorganic phosphate). To describe the unusual features involving multiple catalytic sites, the "catalytic site model" and the "binding change mechanism" were proposed by Celik Kayalar and Paul Boyer based on the results of the enzymatic kinetics analysis (Kayalar, Rosing et al. 1977, Boyer 1993, Boyer 1997). The

mechanism underlying the changes in binding described by Boyer's model is supported by a direct visualization of the γ-subunit, which is found in the center of a hexagonal catalytic core and moves from one of three αβ-subunits to the next in each 120° rotation (Gogol, Johnston et al. 1990). According to the high-resolution structure of the F_1 domain isolated from bovine heart mitochondria, the catalytic core (three copies of αβ-subunit) shows imperfect rotational symmetry with a hydrophobic sleeve surrounding the C-terminal tip of the γ-subunit, which traverses deeply into the central cavity of the hexagonal core. Each of the catalytic sites (αβ-subunit) reveals three sequentially different conformational changes between the open, tight, and loose states (sequence in synthesis direction) after a full 360° rotation of the central stalk (Abrahams, Leslie et al. 1994). The rotation of the F_1 domain occurs in steps of 120°, as predicted by the binding change mechanism proposed by Boyer, and this was directly observed through time-resolved fluorescence microscopy. They fixed the histidine-tagged $s\alpha_3\beta_3\gamma$-subcomplex on a glass plate and then attached a fluorescently labeled actin filament to the γ-subunit (Noji, Yasuda et al. 1997, Yasuda, Noji et al. 1998, Adachi, Yasuda et al. 2000). ATP addition then leads to a rotation of actin filament attached to the gamma subunit which was life monitored in a fluorescence microscope. In the proposed model of the coupling of the binding change mechanism and catalysis by 120° stepwise rotations, three sequential catalytic sites are required in ATP catalysis, and all three catalytic sites undergo conformational changes simultaneously as each 120° rotation of the central stalk (γ-subunit and ε-subunit) occurs, corresponding to either the binding of substrates (ADP molecule and inorganic phosphate, P_i), the formation of ATP, or the release of ATP. The process in which ATP is synthesized in the catalytic core involves three copies of the αβ-subunits. The binding sites directly involved in ATP catalysis are all located on the three β-subunits, the biding site is located at the interface between the

alpha and beta subunits. Each catalytic site is equally capable of carrying out ATP synthesis/hydrolysis, whereas α-subunits are probably involved in the regulatory mechanism (Cross and Nalin 1982, Yoshida and Allison 1986).

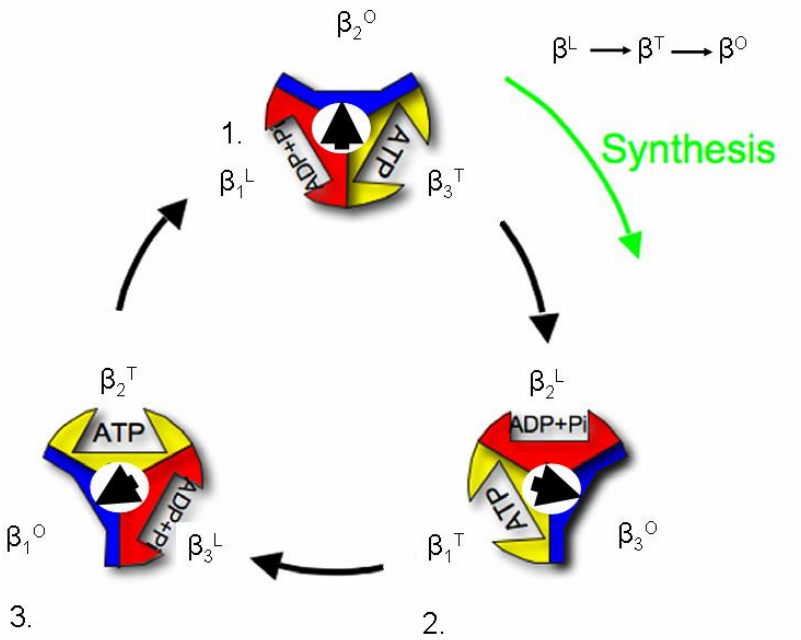

Figure 1.4 Conformational Changes in Three Catalytic Sites (β-subunits). The alternately sequential conformational changes in three catalytic sites (β subunits) during rotational catalysis. The figure depicts the following: The binding change in one catalytic β subunit by a 120° stepwise rotation of the γ subunit (block arrows).The sites are designated as O (open), T (tight) (ATP bound) or L (loose) (ADP and Pi bound). The sequence of states (curved block arrows) that appear as ATP synthesis occurs is shown in a clockwise direction (green arrow). (D) The order of the conformational changes in ATP synthesis is $\beta^{Loose} \rightarrow \beta^{tigth} \rightarrow \beta^{opene}$. Image taken and caption adapted from Nakamoto et al (2008) (Nakamoto, Baylis Scanlon et al. 2008).

Figure 1.4 shows the binding change mechanism in three catalytic sites, and this mechanism will be briefly discussed below. Some of the included descriptions are adapted from (Boyer 2000, Nakamoto, Baylis Scanlon et al. 2008). Each of catalytic sites in the ATP synthesis cycle can be associated with one of three alternately sequential conformational changes from the loose (partly open), tight (closed), and open (empty) states. In the loose the binding site is ready for new substrate binding (ADP and P_i). It converts to the tight state, where the previously bound ADP and P_i form ATP.

The In the loose state is formed when the binding site is pushed open by the gamma subunit and in this process ATP is released. The conformational changes in one β-subunit occur between the initial loose states, and the tight states, and between the tight and open states (L→T→O) after each 120° stepwise rotation of the central stalk, where the γ-subunit contacts the alpha beta interfaces leading to their conformation changes. The three β-subunits are designated β_1-subunit (loose), β_2-subunit (open) and β_3-subunit (tight). The cycle starts with the binding site (β_1-subunit) in the loose state (β_1^L), which is considered the original conformation, where the γ-subunit stops the rotation to 0°. Immediately after the binding of ADP and P_i to the binding site of the β_2-subunit, β_2-subunit changes its conformation from the open state to the loose state via the first 120° rotation of the central stalk (0°→120°). The binding site of the β_2-subunit is occupied by ADP and P_i. This conformational change triggers conformational changes in the other two binding sites (β_1- and β_3-subunits). The binding side in the β_1-subunit in the loose state changes to the tight state ($\beta_1^L \rightarrow \beta_1^T$), resulting in the synthesis of ATP by previously bound substrates, and the synthesized ATP is then ready to be released during the subsequent conformational change, which is considered the first conformation change as well as the initial step ($\beta_1^L \rightarrow \beta_1^T$). In contrast, the β_3-subunit in the tight state changes to the open state ($\beta_3^T \rightarrow \beta_3^O$), resulting in the release of the synthesized ATP, and this step makes the β_3-subunit ready for new substrate binding. After the second successive 120° rotation of the central stalk (120°→240°), the conformation of the β_1-subunit converts the site from the tight to the open state ($\beta_1^T \rightarrow \beta_1^O$). This is considered the second conformation change as well as the intermediate step, in which ATP is formed from the bound ADP and P_i. Simultaneously, the conformational changes in the other two binding sites ($\beta_2^L \rightarrow \beta_2^T$ and $\beta_3^O \rightarrow \beta_3^L$, respectively) are triggered again. In the last step, which is considered the third

conformational change, the β_1-subunit in the open state changes its conformation back to its original conformation (loose state) ($\beta_1^O \rightarrow \beta_1^L$) via the third successive 120° rotation of the central stalk (240°→360°), leading to the occupation of the binding site of the β_1-subunit by ADP and P_i and resetting the cycle to its starting position (β_1^L) (Boyer 1997; Boyer 2000). The states of the β_2- and β_3-subunits are re-converted to the subsequent states ($\beta_2^T \rightarrow \beta_2^O$ and $\beta_3^L \rightarrow \beta_3^T$) via triggering conformational changes in the last step. Therefore, the coupling of a complete 360° rotation of the γ-subunit (120°→120°) with a return of each catalytic site to its original conformation for the formation of a single ATP molecule can completely generate three ATP molecules in three catalytic sites in the F_1 domain. However, the binding change mechanism in 120° steps have been further resolved at sub-millisecond resolution, indicating that the 120° step can be dissected into a 80° substep and a 40° substep (Hirono-Hara, Noji et al. 2001, Shimabukuro, Yasuda et al. 2003, Nishizaka, Oiwa et al. 2004). Figure 1.5 shows a scheme of the binding change mechanism of ATP hydrolysis in three catalytic sites. The three β-subunits are designated as the β_1-subunit (open), which is ready for substrate binding (ATP), the β_2-subunit (tight), which is occupied by the previously bound substrates (ATP) and is ready to hydrolyze ATP in the subsequent state (loose), and the β_3-subunit (loose), which means that the ADP and P_i are ready to be released. The cycle starts with the binding site (β_1-subunit) in the open state (β_1^O), which means that the binding site is ready for ATP binding, and this is considered the original conformation. Immediately after ATP binding, the γ-subunit is driven to rotate 80° counterclockwise (0°:360°→-80°:280°), which causes the release of ADP from the β_3-subunit in the loose state. The γ-subunit dwells on the 80° position for approximately 2 ms (millisecond) prior to the subsequent 40° rotational movement. In the first 1-ms transition step of the 80° substep, ATP bound at 240° in the β_2-subunit in the tight state

is hydrolyzed to ADP and P_i. In the second 1-ms transition step, P_i is waiting to be released from the β_3-subunit in the loose state. Immediately after approximately 2 ms, P_i found in the waiting state attached to the β_3-subunit in the loose state is released, which immediately triggers the last 40° substep (-80°:280° →-120°:240°).

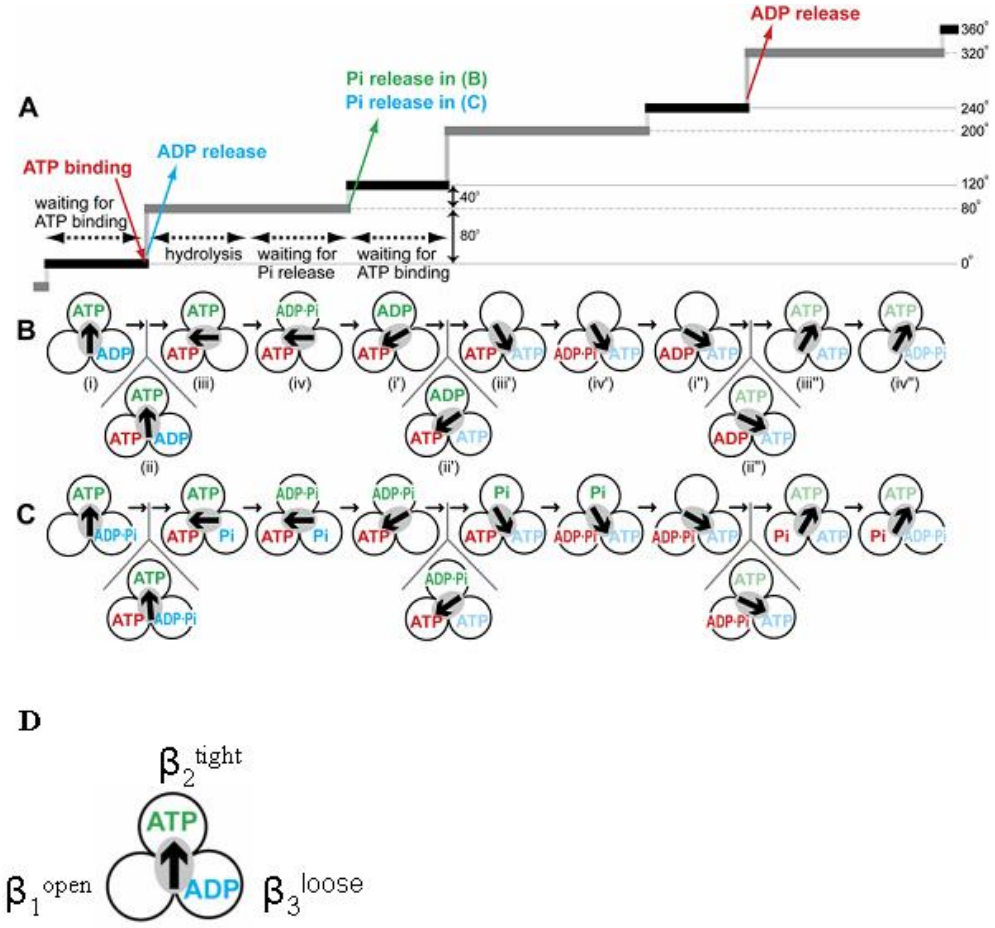

Figure 1.5 The Binding Change Mechanism at Sub-Millisecond Resolution. Rotation and catalysis of the binding change mechanism of F1-ATP synthase in hydrolysis.The figure depicts the following: (A) Schematic time course of the stepping rotation. The vertical axis is the rotary angle of the γ subunit, and the horizontal axis is time. Colored events occurring in the catalytic site are shown in the same color as in (B) or (C). (B) Corresponding nucleotide states in the three catalytic sites. The three circles represent three catalytic sites (αβ subunits). The central gray ellipsoid represents the γ subunit, and the thick arrow shows its orientation; the twelve o'clock position in (i) corresponds to 0° in (A). Molecular species derived from the same ATP molecule are shown in the same color. Small arrows show the progress in this major reaction pathway; the configurations (ii), (ii'), and (ii'') shown below the major path represent the instant immediately following ATP binding, i.e., the beginning of an 80° substep. (C) An alternative scheme in which P_i release lags behind ADP release. (D) Three alternately sequential conformational changes from the open (empty), tight (closed), or loose (partially open) state in the three catalytic sites (β subunits). Figure taken and caption adapted from (Adachi, Oiwa et al. 2007).

At the 120° position of the γ-subunit (after the two 80° and 40° rotations), the β_1-subunit changes its conformation from the open state to the tight state ($\beta_1^O \rightarrow \beta_1^T$), the β_2-subunit converts from the tight state to the loose state ($\beta_2^T \rightarrow \beta_2^L$), which means that the hydrolyzed ADP and P_i are ready to be released, and the β_3-subunit in the loose state undergoes a conformational change to the open state ($\beta_3^L \rightarrow \beta_3^O$). However, the time that the γ-subunit is maintained in the 120° position remains unresolved, and the temporal resolution is currently 0.125 ms (Adachi, Oiwa et al. 2007). During this extremely short time resolution, the β_3-subunit in the open state (β_3^O) is waiting for new ATP binding. Immediately after ATP binding to the β_3-subunit, the γ-subunit drives the next 80° substep (-120°:240°→-200°:160°). During this step, the hydrolyzed ADP in the β_2-subunit is simultaneously dissociated from the binding site of the β_2-subunit, and P_i is then ready to be released after approximately 2 ms. Those reactions that occur in the subsequent time frame of approximately 2 ms after the 80° substep represent those reactions that occurred in the previous time frame. ATP bound at 0° to the β_1-subunit in the open state starts to be hydrolyzed to ADP and P_i during the first half of the 2-ms time frame, and P_i bound to the β_2-subunit then waits to be released until approximately 2 ms later. After approximately 2 ms, P_i attached to the β_2-subunit is released, and the γ-subunit is immediately rotated 40° (-200°:160°→-240°:120°). When the γ-subunit is at the 240° position (the second 120° rotation), the β_1-subunit in the tight state undergoes a change to the loose state ($\beta_1^T \rightarrow \beta_1^L$). Then, the hydrolyzed ADP and P_i are released in the third 120° rotation, and the β_3-subunit in the open state undergoes a conformational change to the tight state ($\beta_3^O \rightarrow \beta_3^T$), which is occupied by ATP. In contrast, the β_2-subunit changes its state from loose to open ($\beta_2^L \rightarrow \beta_2^O$) for subsequent ATP binding. The reaction of ATP binding to the β_2-subunit immediately triggers the third 80° substep (-240°:120°→-320°:40°). Simultaneously, ADP in the β_1-subunit is

dissociated, whereas P_i in the β_1-subunit is in the waiting state. ATP bound to the β_3-subunit then starts to be hydrolyzed. After approximately 2 ms, the third 40° substep is triggered by the release of P_i from the β_1-subunit (-320°:40°→-360°:0°). After the third 40° substep, which causes the γ-subunit to return to the 0° position (-320°:40°→-360°:0°), the β_1-subunit at the open state undergoes a change to the loose state ($\beta_1^L \rightarrow \beta_1^O$), making it ready for ATP binding, and the β_2-subunit is then occupied by ATP ($\beta_2^O \rightarrow \beta_2^T$). The β_3-subunit is occupied by hydrolyzed ADP and P_i ($\beta_3^T \rightarrow \beta_3^L$).

1.7 The F_O Domain Couples Proton Transport between the a- and c-subunits

The membrane-bound F_O domain of the F-type ATP synthase complex is composed of the a-subunit, which is peripherally attached to the ring, the b and b"subunits, which serve as a peripheral stationary stalk, and a symmetric oligomer ring that contains multiple (8-15) copies of the monomeric c-subunit (Feniouk 2008). The F_O domain acts as an energy converter between the chemical state and the physical state. In the direction of ATP synthesis, the F_O domain of the F-type ATP synthase complex converts a transmembrane proton potential into physical torque to drive the coupling of the rotary γ-subunit with ATP formation between three alternating catalytic sites in the F_1 domain (Noji, Yasuda et al. 1997), whereas in the reverse direction, physical torque can be generated via ATP hydrolysis in the F_1 domain to drive rotation of the γ-subunit, which in turn is coupled to rotation of the F_O domain to promote reverse proton transport. In contrast to the well-characterized hydrophilic F_1 domain, the structural information and the detailed proton translocation mechanism of the F_O domain remain difficult to characterize due to the extreme hydrophobicity of the F_O domain. In the proposed proton translocation mechanism, each monomer of an oligomeric ring of the c-subunit in the F_O domain is protonated via a proton access channel of the a-subunit in the

lumenal (periplasmic)) site and is then deprotonated and the proton released at the other side of the access channel of the a-subunit to the stromal (cytoplasmic) site. The sequential protonation and deprotonation of the c-subunit is coupled with a stepwise movement of an oligomeric ring of the c-subunit in the F_O domain (Vik and Antonio 1994, Engelbrecht and Junge 1997, Elston, Wang et al. 1998).

In the overview of the c-subunit, based on evidence from nuclear magnetic resonance (NMR) structure and disulfide cross-linking experiments, each c-subunit monomer spans the membrane as two extended transmembrane helical hairpins (TMH), designated cTMH1 and cTMH2 (Girvin, Rastogi et al. 1998, Jones, Jiang et al. 1998, Dmitriev, Jones et al. 1999, Rastogi and Girvin 1999, Fillingame, Angevine et al. 2002, Fillingame, Angevine et al. 2003). As shown in Figure 1.6 A, cTMH1s pack toward the center of the c-ring structure, and cTMH2s are located at the periphery of the c-ring structure. The essential residue cAsp-61 (D61) involved in the cycle of protonation and deprotonation is located on the center of cTMH2 (Dmitriev, Jones et al. 1999, Fillingame, Angevine et al. 2002, Fillingame, Angevine et al. 2003). For the protonated side chain of cAsp-61 to be stabilized, cAsp-61 at the front face of one monomer (cTMH2") packs in close proximity to cAla-24, cIle-28, and cAla-62 of the neighboring monomer (cTMHs 1-2"), with the side chains of these residues facing toward each other, as shown in Figure 1.6 B (Dmitriev, Jones et al. 1999). According to the NMR structures of the monomeric c-subunit (Figure 1.7), TMH1 and TMH2 reveal two different conformational states at pH 5.0 and 8.0, as shown in Figures 1.7 A and B. At pH 5.0, the protonated residue Asp-61 side chain is located on the front face of TMH2, whereas at pH 8.0, TMH2 rotates 140° clockwise such that the side chain of the deprotonated residue Asp-61 moves from the front to the back faces of TMH2 to later

interact with residue aArg-210 in aTMH4 at the interface between cTMH2 and aTMH4 (Jiang and Fillingame 1998, Fillingame, Angevine et al. 2002).

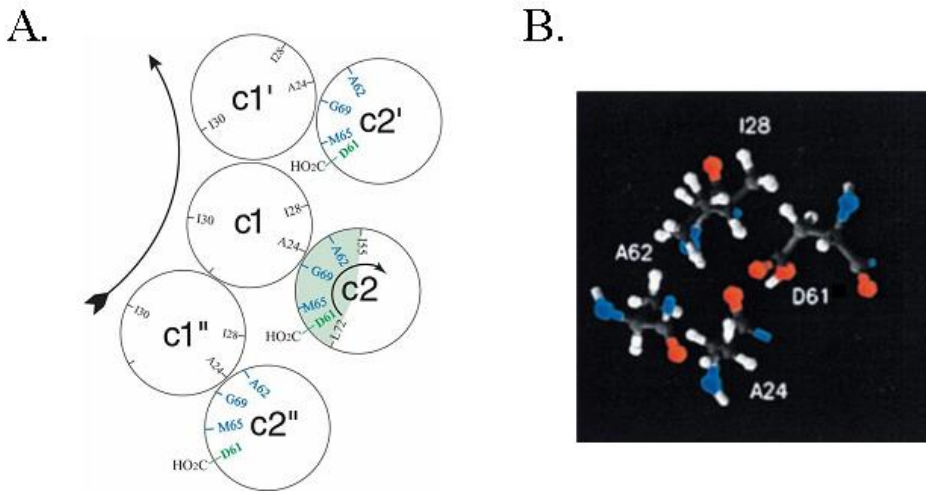

Figure 1.6 The Relative Packing of Three Monomeric c-subunits in the c-oligomeric Ring. (A) Each C-subunit consists of 2 transmembrane helices (c1 and c2). (A) Depiction of the orientation of cAsp-619 of one monomer in proximity to aAla-24, aIle-28, and aAla-62 of a neighboring monomer. (B) Proposed interaction face of cTMH-2 with the a-subunit is shown in green shading. The position of the protonated side chains of the essential residue cAsp-61 is shown in blue. Images taken and captions adapted from (Dmitriev, Jones et al. 1999, Fillingame, Angevine et al. 2003).

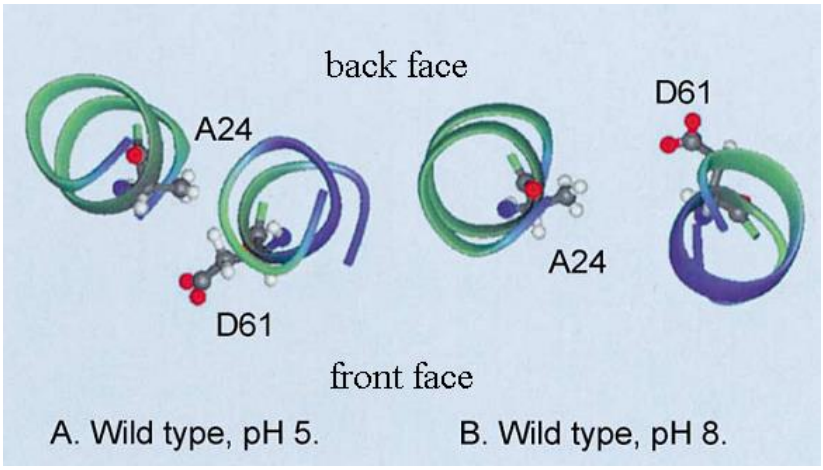

Figure 1.7 NMR Structures of TMH-1 and TMH-2 of the Monomeric c-subunit. (A) Wild-type monomer of c-subunits at pH 5.0 with positions of the side chains of TMH-1 residue Ala-24 and TMH-2 residue Asp-61 indicated. The protonated Asp-61 side chain packs at the face designated ‘‘front’’. (B) Wild-type monomer of c-subunits at pH 8.0 with the positions of the side chains of TMH-1 residue Ala-24 and TMH-2 residue Asp-61 indicated. In this conformation, the deprotonated Asp-61 side chain now packs at the ‘‘back’’ face. Figure taken and caption adapted from (Fillingame, Angevine et al. 2003)

For the overview of the a-subunit, there is NO experimental structure from the a-subunit from any organism. The existing model is a computational model from the Schulten's lab (University of Illinois Urbana-Champaign). However, according to a model of the cross-sectional arrangement, the a-subunit folds in the membrane with five transmembrane helices (TMH), which are designated aTMH1, aTMH2, aTMH3, aTMH4 and aTMH5. It was proposed that 4 of these helices (aTMHs 2-5) are packed as a helical bundle that lies at the periphery of the c-ring, as shown in Figure 1.8 (Hakulinen, Klyszejko et al. 2012).

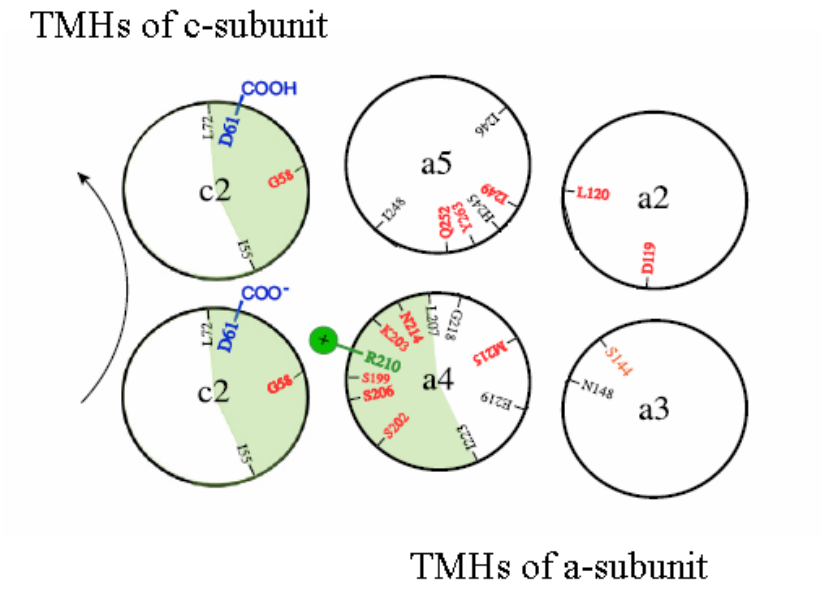

Figure 1.8 Packing of TMHs of the a-subunit in a Four-Helix Bundle with TMH-2 of the c-subunit. The predicted relative packing of TMHs 2–5 of the a-subunit in a four-helix bundle with TMH-2 of the c-subunit**.** The predicted faces of the helix-helix interaction between the a- and c-subunit are shown in cyan. Residues cAsp-61 (D61), with either protonated or deprotonated carboxyl groups, and the aArg-210 side chain are shown in blue and green, respectively. The arrow indicates the direction of c-ring rotation during ATP synthesis. Image taken and caption adapted from Fillingame and steed (2014) (Fillingame and Steed 2014).

The juxtaposition of aTMH2, aTMH4 and aTMH5 is suggested to create an aqueous cavity at the center of the membrane to allow the entry of a single proton from the lumenal (periplasmic) site. The Ag^{+}- and Cd^{2+}-sensitive residues located at the interior

of the helix bundle are thought to form the lumenal (periplasmic) channel; these include aAsp-119 and aLeu-120 in aTMH2, aAsn-214 and Met-215 in aTMH4, and His-245 and Gln-252 in aTMH5 (Valiyaveetil and Fillingame 1998, Fillingame and Steed 2014). Both aTMH4 and aTMH5 are proposed to act as gates for the entry of a single proton by the simultaneous swiveling of aTMH4 in the counterclockwise direction and of aTMH5 in the clockwise direction in response to acidification of the lumenal (periplasmic) channel in the helix bundle. Residues aAsn-214 and aGln-252 are brought to sufficiently close proximity to the ionized side chain of cAsp-61 to create a free pathway through which a single proton from the lumenal (periplasmic) channel can access and protonate the ionized side chain of cAsp-61 (Valiyaveetil and Fillingame 1998, Fillingame, Angevine et al. 2003, Fillingame and Steed 2014) (Fillingame and Steed, 2014; Fillingame et al., 2003). Based on the hypothesis of Fillingame and coworkers, the protonation of cAsp-61 could be facilitated by breaking the formation of a salt-bridge between residues cAsp-61 and aArg-210 coupled to the simultaneous rotation of both aTMH4 and aTMH5 (Fillingame and Steed 2014). Figure 1.8 shows the proposed packing position of the TMHs of a-subunit and the interaction interface between the a- and c-subunits. The movements of the aTMHs coupled with mechanisms of proton translocation are discussed in the subsequent subsection. Overall, all these models have been made based on crosslinking studies and biochemical cys screening mutation and due to the lack of experimental structural information on the a-subunit, they are only hypothesis

1.8 Mechanism of H^+ transport between the a-subunit and c-subunit

The conformational changes that occur in the catalytic F_1 domain of the F-type ATP synthase complex involved in the mechanism of ATP synthesis or hydrolysis are well

established, but the mechanism through which a single proton is translocated across the membrane through the hydrophobic F_O domain remains unclear. The basic mechanism of proton translocation involves the interaction between the a- and c-subunits and a cycle of sequential protonation and deprotonation reactions of the conserved aspartic acid residue (Arg-210) of the a-subunit that intacts with the carboyl side chain of ASP or Glu in helix 2 of the c-subunit (c-ring). Sequential conformational changes at the interface between the a- and c-subunits during proton translation generate torque for driving the rotation of the c-ring-γ–ε complex coupled with changes in the catalytic structure of the αβ-subunits to catalyze the synthesis of ATP.

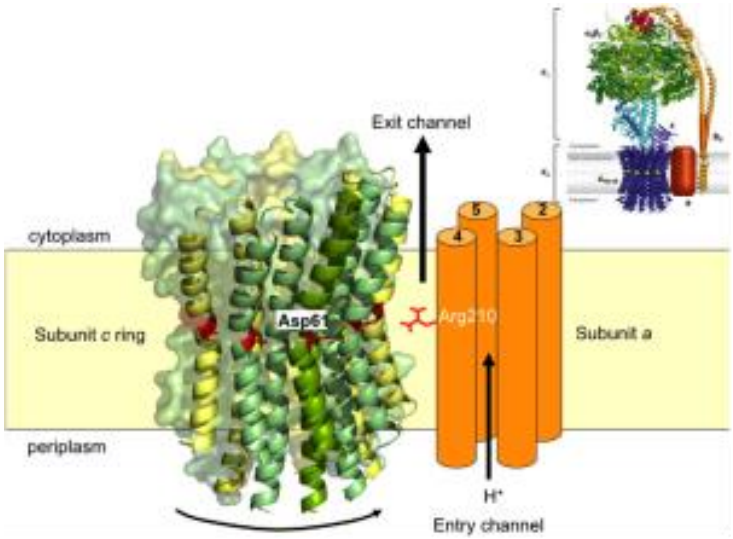

Figure 1.9 The Proposed Model of the Proton Translocation. Schematic structural model of the proposed translocation of a single proton across the membrane via the interaction between the a- and c-subunit in the H^+-transporting F-type ATP synthase complex. A single proton enters via the lumenal (periplasmic) channel and is released via the stromal (cytoplasmic) channel. The process of the proton translocation will be discussed in subsequent subsections. Figure taken and caption adapted from Fillingame and Steed (2014) (Fillingame and Steed 2014).

Several proposed models describe structural changes between the a- and c-subunits as the basis for mechanisms to try to explain the coupling of proton transfer to the interaction of the a- and c-subunits coupled to the movement of the c-ring, and these will be briefly discussed below. Figure 1.9 shows a basic route for the entry of a single

proton from the lumenal (periplasmic) site to the stromal (cytoplasmic) site via two separating channels, namely a lumenal (periplasmic) (P, positively charged side of the membrane) channel and a stromal (cytoplasmic) (N, negatively charged side of the membrane) channel. A detailed mechanistic model (Figure 1.10) proposed by Rastogi and Girvin (1999) describes the coupling of helix movements of the a- and c-subunits with stepwise rotation of the c-ring rotor. Residues cAsp-61 and aArg-210 are located in cTMH2 and aTMH4, repressively. Figure 1.10 shows the proposed structural changes involved in the transfer of a single proton, and these will be briefly discussed below. Some of the descriptions in the content are adapted from Rastogi and Girvin (1999). In the initial state (C), the aArg-210 residue is positioned between the deprotonated cAsp-61 residue of one monomer (shown in green) and the previously protonated cAsp-61 residue of an adjacent monomer (shown in yellow). After protonation of cAsp-61 (shown in green) by a single proton entering from the lumenal (periplasmic) channel, the newly protonated monomer, including cTMH1 and cTMH2, rotates back to its originally protonated position (the stable state). Simultaneously, the aArg-210 residue moves in the clockwise direction from the interface of the a- and c-subunits (green and yellow) to the next c-subunit monomer (shown in blue) in this intermediate state (D). In the following step (E), the protonated aAsp-61 of the next c-subunit monomer is deprotonated at the new a-c-subunit interface (blue and green), resulting in the release of a single proton that are originally bound to the aAsp-61 (blue) to the stromal (cytoplasmic) site. In the final step (F), the initial state is regenerated such that the aArg-210 residue lies between the newly deprotonated residue cArg-61 (blue) and the protonated residue cArg-61 (Pfeiffer, Gohil et al.) in step E, making it ready for the next proton transfer. The helix movements involved in step D can generate sufficient torque to drive the stepwise rotation of the c-ring in the clockwise direction.

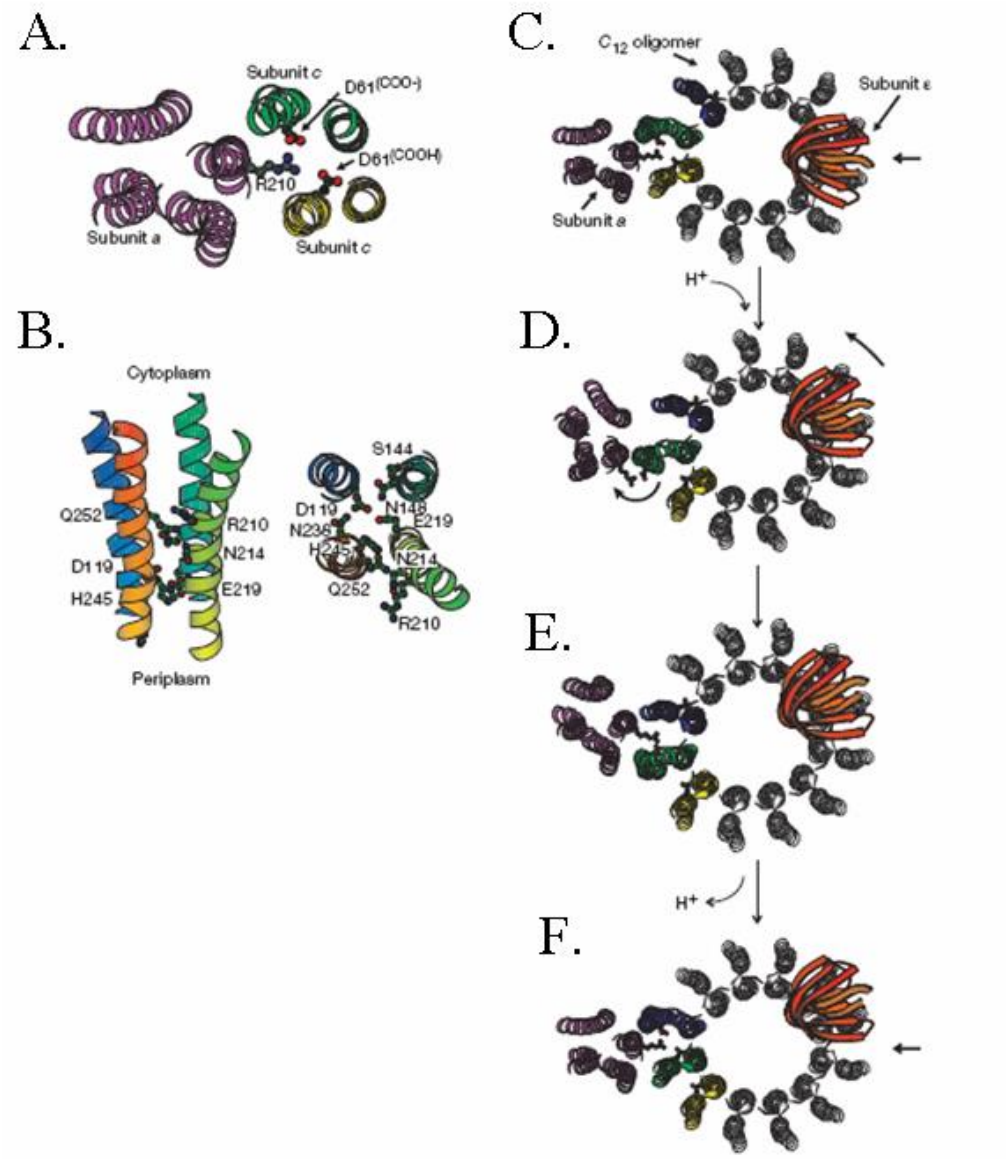

Figure 1.10 The Rastogi and Girvin's Mechanism Model of the Proton Translocation. A Model of the Mechanism of Proton Translocation via the Interaction of the a-c-subunits. (A) The active site of proton translocation in the *E. coli* a- and c_{12}-ring is presented. (B) The residues involved in the entrance of a proton from the lumenal (periplasmic) side to aArg-210 and binding to cAsp-61. (C, D, E, and F) One cycle of a single proton translocation, which is briefly described in this subsection. Figure taken and caption adapted from Rastogi and Girvin, (1999) (Rastogi and Girvin 1999).

Compared with the model proposed by Rastogi and Girvin (1999), which proposes that the deprotonation of cAsp-61 drives the rotation of cTMH2 in the counterclockwise direction, resulting in the exposure of the ionized cAsp-61 side chain at the a-c subunit interface, Fillingame et al. (2003) made some modifications and proposed a model in

which cTMH2 swivels clockwise to bring the protonated cAsp-61 side chain to sufficiently close proximity to aArg-210 at the a-c-subunit interface to facilitate deprotonation. Figure 1.11 shows the proposed helix movements coupled with the interaction between cAsp-61 and aArg-210, and the proposed mechanism will be briefly discussed in the following section. Several of the descriptions were adapted from Fillingame et al. (2003).

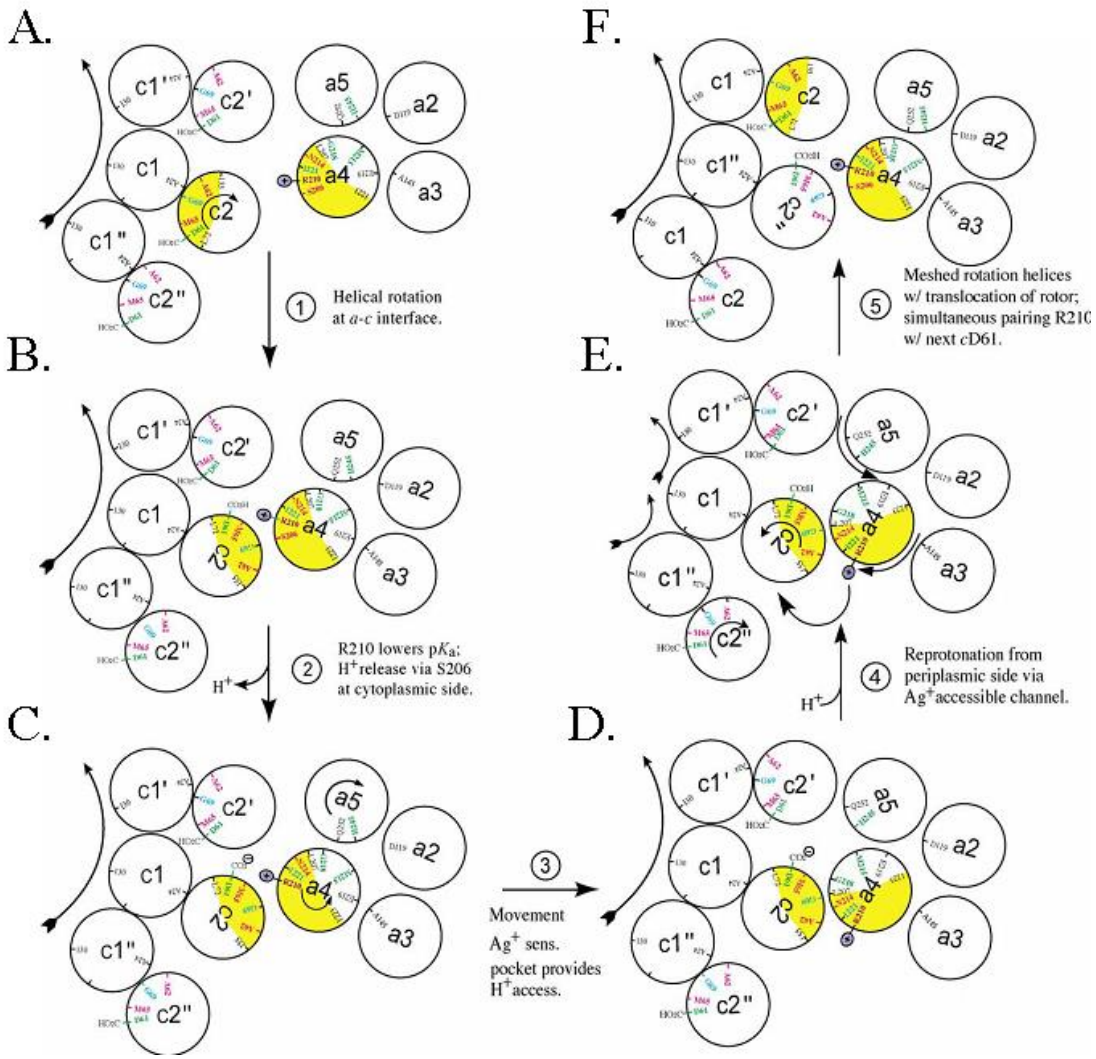

Figure 1.11 The Fillingame's Mechanism Model of the Proton Translocation. A model of a single proton transfer coupled with the concerted helix movement of TMHs that drives the stepwise rotation of the c-ring rotor. The model presents the residues and transmembrane helices (TMHs) of the a- and c_{10}-ring of *E. coli* ATP synthase. The capital letters, from A to F, represent the cycle of a single proton transfer from the initial to the final state (regenerating the initial state). Steps 1 to 5 represent the intermediate states. A brief description of this model is found in this subsection. Figure taken and caption adapted from Fillingame et al. (2003) (Fillingame, Angevine et al. 2003).

In the initial state (A and step 1), cTMH2 spins 140° in the clockwise rotation relative to cTMH1, resulting in the movement of the protonated cAsp-61 (cTMH2) residue from the stable site (front face) to the active site (back face) of one monomer of the c-subunit (c2) for its subsequent interaction with aArg-210 (aTMH4) at the a-c-subunit interface. In the second step (2), the critical aArg-210 residue lowers the pKa of the essential carboxyl group of the cAsp-61 residue to facilitate deprotonation of cAsp-61 at the a-c-subunit interface (aTMH4 and cTMH2). The dissociated proton originally bound to cAsp-61 exits to the stromal (cytoplasmic) side via the stromal (cytoplasmic) channel (aSer-206 in aTMH4). At the C state, the side chain of aArg-210 is proposed to move away from the carboxyl group of the currently deprotonated cAsp-61 residue. In this model, the deprotonated cAsp-61 can be reprotonated by increasing the pKa of its carboxyl group. The movement of the aArg-210 side chain is driven by the simultaneous rotation of aTMH4 and aTMH5. In the third step (3), prior to the movement of aArg-210, a single proton from the lumenal (periplasmic) site enters via the lumenal (periplasmic) half-channel to the center of the helix bundle. The proton binding to the binding site in the lumenal (periplasmic) channel likely involves interactions between various residues, including aGly-218 and aMet-215 in aTMH4 and aHis-245 in aTMH5. In the fourth step (4), immediately after the rotation of aTMH4 coupled with the movement of aArg-210, deprotonated cAsp-61 is reprotonated through a proton potential at the a-c-subunit interface. In the E state, after the reprotonation of cAsp-61, the concerted rotation of four TMHs (aTMH4 and aTMH5, cTMH2 of the initial monomeric c-subunit and cTMH2 of the next monomer) immediately occurs, and this is coupled with the stepwise rotation of the c-ring rotor to drive movement of the next monomer (c2") to the position of the initial c-subunit monomer (c2). At this state, the counterclockwise swiveling of cTMH2 of the initial

monomer of the c-subunit (c2) moves the currently reprotonated cAsp-61 to its original state (the front face). Furthermore, the reverse swiveling of aTMH4 and aTMH5 return aArg-210 to its initial position at the a-c-subunit interface. In the final step (5), after all concerted helix movements, the initial state (F) is regenerated, and this state is equivalent to (A). The clockwise rotation of cTMH2 of the next monomer of the c-subunit (c2") exposes the previously protonated cArp-61 at the a-c-subunit interface for the next proton-transfer cycle.

The latest mechanism model updated by Fillingame and Steed (2014) shown in Figure 1.12 simply and clear illustrates that the helical movements (TMHS) at the interface between the a- and c-subunits (the a-c-subunit interface) may be coupled with the translocation of a single proton with the stepwise rotation of the c-ring rotor, and these will be briefly discussed below. Some of the descriptions are adapted Fillingame and Steed (2014) (Fillingame and Steed 2014). The inner ring consisting of cTMH1 is located toward the center of the c-ring rotor and cTMH2 is located on the outside of the c-ring. The cTMH2 helcies are located proximally to aTMH4 and aTMH5, which act as a gate that only allows a single proton from the lumenal (periplasmic) site to enter the a-c-subunit interface for protonation of the ionized cAsp-61 residue (cTMH2 in the c^2 monomer). In the initial state (A), which is regenerated from the previous cycle, a salt bridge is formed between the side chain of the aArg-210 residue (aTMH4) and the cAsp-61 carboxyl group (cTMH2 in the c^2 monomer). In the second state (B), a single proton enters the lumenal (periplasmic) channel and then binds to the proton-binding site (aHis-245 in aTMH5; aAsp-119 in aTMH2) within the lumenal (periplasmic) channel; this proton-binding process is considered an acidification step of the lumenal (periplasmic) channel that immediately promotes the simultaneous helical swiveling of both aTMH4 (counterclockwise direction) and aTMH5 (clockwise direction).

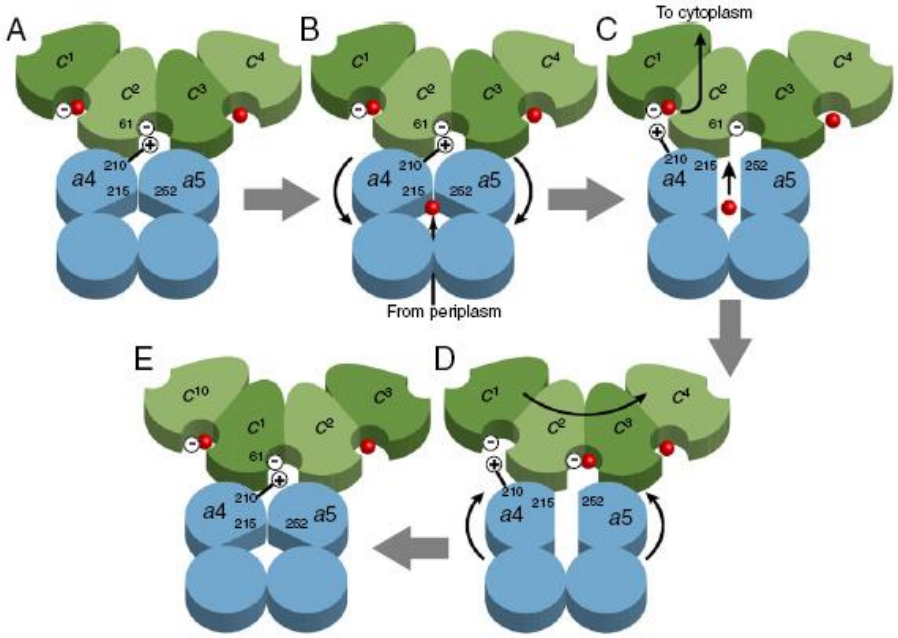

Figure 1.12 The Latest Fillingame's Mechanism Model of the Proton Translocation. Schematic model of the conformational changes between the TMHs that drive the translocation of a single H^+ and the 36° stepwise rotation of the c-ring rotor. The peripheral helix of the c-ring is shown in green, numbered from 1 to 10, and packs proximally to TMH-4 and TMH-5 of the a-subunit (blue). (A) Representative model of the initial state. (B, C and D) Representative models of the intermediate states. (E) The final state that is equivalent to the initial state (A) following the translocation of a single H^+ with the coupled stepwise 36° rotation of the c-ring rotor. Image taken and caption adapted from Fillingame and Steed (2014) (Fillingame and Steed 2014).

In the transition between the B and C states, the salt bridge formed between residues aArg-210 (aTMH4) and cAsp-61 (cTMH2 in c^2 monomer) is forced to break with the acidified (H^+)-driven movement of aTMH4. Simultaneously, the rotation of both aTMH4 and aTMH5 induces opening of the proton gate such that the aMet-215 (aTMH4) and aGln-252 (aTMH5) residues are moved to sufficiently close proximity to the ionized cAsp-61 residue (cTMH2 in the c^2 monomer) to create a pathway for a single lumenal (periplasmic) proton to access the a-c-subunit interface for subsequent protonation of the ionized cAsp-61 residue. In the third state (C), the ionized residue Asp-61 in cTMH2 (c^2-subunit monomer) is protonated by a single lumenal (periplasmic) proton at the a-c-subunit interface. Simultaneously after the counterclockwise

swiveling of aTMH4, the cAsp-61 residue in cTMH2 of the c^1-subunit monomer is deprotonated by the formation of a new salt bridge coupled with the release of a single proton originally bound to the cAsp-61 residue in c-TMH2 of the c^1-subunit monomer to the cytoplasmic channel. The formation of a new salt bridge occurs between the ionized side chain of the aArg-210 residue (aTMH4) and the carboxyl group of the cAsp-61 residue in the counterclockwise-positioned cTMH2 of the c^1-subunit monomer. In the fourth state (D), after protonation of the cAsp-61 residue in cTMH2 of the c^2-subunit monomer and deprotonation of the adjacent one in cTMH2 of the c^1-subunit monomer, both aTMH4 and aTMH5 swivel in reverse directions relative to the directions in the second step (B) to return to their original positions, resulting in closing the proton gate such that protons cannot access the a-c-subunit interface from the lumenal (periplasmic) channel. In contrast, the reverse swiveling can generate sufficient torque to rotate the entire c-ring by 36° in the clockwise direction, which regenerates a new interface (in the initial state) between the a-subunit and the subsequent c-subunit monomer. The final step (E) is equivalent to the initial state (A): cTMH2 of the c^1-subunit monomer is rotated in the clockwise direction to the position of cTMH2 of the c^2-subunit monomer, which is assumed to be the position in the initial state, and becomes ready for the next proton translocation cycle.

CHAPTER 2

MOTIVATION

2.1 Structure Availability of ATP Synthase

The structure determination of biomolecules is the ultimate goal to aid in the understanding of how biomolecules can perform such complex functional mechanisms observed in everyday life. Membrane proteins, one of these attractive biomolecules, play essential roles in cell structure, enzymatic activity, signaling, and the transport of nutrients. To date, over 100,000 protein structures have been determined using various combinations of techniques such as crystallization and X-ray crystallography, nuclear magnetic resonance (MNR) and electron microscopy (EM). Most of the determined protein structures are water-soluble proteins, and less than 550 integral membrane protein structures are available due to their hydrophobic properties. In particular, structures of protein supercomplexes such as photosynthetic protein complexes and ATP synthase complexes are much more difficult to determine not only due to their extremely large molecular size but also due to additional cofactors that may be essential in the formation and function of these supercomplexes. A challenging target for the structure determination of protein supercomplexes is the ATP synthase complex, which is a universal energy transduction machine that is present in nearly all living organisms and catalyzes the synthesis of ATP from ADP and inorganic phosphate ions driven by a transmembrane proton (or sodium ion) motive force. Due to the amphipathic nature of the ATP synthase, no structure has been determined so far of the whole ATP synthase complex; the most detailed structural information to date on the F_1 subcomplex of ATP synthase has been obtained for bovine heart mitochondrial ATP synthase at a resolution of 2.8 Å using X-ray crystallography (Abrahams, Leslie et al. 1994). However, crystal

structures of the F_1 domain from other organisms such as the thermophile *Bacillus* PS3 at 3.2 Å resolution (Shirakihara, Leslie et al. 1997) and yeast mitochondria at 2.8 Å resolution (Kabaleeswaran, Puri et al. 2006) have been reported. In contrast, the only available structural information on the chloroplast F_1-ATP synthase is that from spinach chloroplasts at 3.2 Å and 3.4 Å resolution (Groth and Pohl 2001, Groth 2002). Due to the extreme hydrophobicity of the F_O domain, in contrast to the hydrophilic F_1 domain, structural information on the integral F_O domain is lacking, although structural information on the b- and c-subunits of the F_O domain is available. The first crystal structure of the F_O-integral rotor ring (c_{10}-ring) was determined at a resolution of 3.9 Å from yeast (Stock, Leslie et al. 1999). Additionally, structural information on the c_{11}-ring of the Na^+-ATP synthase from the thermophilic bacteria *Ilyobacter tartaricus* and *Acetobacterium woodii* is available at 2.4 Å and 2.1 Å resolution, respectively (Meier, Polzer et al. 2005, Matthies, Zhou et al. 2014). The structure of the F_O-c_{14} ring from spinach chloroplasts and the F_O-c_{15} ring of *Spirulina platensis* is also available at 3.8 Å and 2.1 Å resolution, respectively (Vollmar, Schlieper et al. 2009, Krah, Pogoryelov et al. 2010). The structure of the b-subunit from *Escherichia coli* has been determined using nuclear magnetic resonance spectroscopy (Dmitriev, Jones et al. 1999). An overview of the structural information on subcomplexes or individual subunits of ATP synthase is provided in Table 2.1. However, complete detailed structural information on intact ATP synthase remains lacking. The current accepted structure of intact F-type ATP synthase is a mosaic model of the mitochondrial ATP synthase, which still lacks structural information for both a- and b-subunits in the F_O domain and additional supernumerary subunits such as e, f, g and A6L. However, three-dimensional crystals of intact ATP synthase have not been reported, presumably due to several possible reasons. One possible reason is that the ATP synthase is inherently unstable *in vitro* due

to the solubilization step that uses detergents instead of native lipids that surround its hydrophobic domain. Furthermore, the a-subunit is lost during purification because of its low affinity for the contact region of the F_O-c ring.

Table 2.1 Stoichiometry of Subcomplexes and Subunits and Structural Information on the F-type H^+-ATP Synthase.

E. coli			Chloroplasts			Mitochondria		
Subunits (stoichiometry)		Structural data (method)	Subunits (stoichiometry)		Structural data (method)	Subunits (stoichiometry)		Structural data (method)
α	3		α	3		α	3	
β	3		β	3		β	3	
γ	1		γ	1		γ	1	
δ	1	NMR	δ	1		OSCP	1	
ε	1	NMR X-ray	ε	1		δ	1	
–			–			ε	1	
EF_1		EM	CF_1		EM	MF_1		X-ray EM
a	1		IV	1		a	1	
b	2	NMR	I, II	1		b	2	
c	12	NMR	III	12	EM	c	12	
						d	1	
						F_6	1	
						e	1	
						f	1	
						g	1	
EF_0		AFM EM	CF_0			MF_0		
EF_0F_1		EM	CF_0F_1		AFM EM	MF_0F_1 IF_1		EM

IF_1 is the inhibitor protein of MF_OF_1. EM, electron microscopy; NMR, nuclear magnetic resonance; X-ray, X-ray diffraction; AFM, atomic force microscopy. Table taken and caption adapted from (Bottcher and Graber 2000).

Therefore, the functional ATP synthase is difficult to isolate in high purity and in high yield (Delucas 2009, McPherson 2009). A second possible reason is that the isolated ATP synthase may be a mixture of structural isomers, differing in the conformation of the central stator and the peripheral stalk associated with the $\alpha_3\beta_3$ catalytic site. A third possible reason is that the dimensions of the F_1 domain are larger than those of the F_O domain, and the molecular architecture of the F-type ATP synthase is asymmetrical compared with that of the A-type ATP synthase, which is less favorable for the formation of well-ordered crystals in three dimensions. To determine the entire structure of ATP synthase in the near future, the structural determination of individual subunits from various organisms using advanced crystallographic techniques should be

continually pursued and greater effort must be directed at the structure determination of its subcomplexes, particularly that of the integral ATP synthase supercomplex, to understand the intersubunit interactions during ATP catalysis.

2.2 Motivation

Although structural information for several subcomplexes and individual subunits of ATP synthase from several organisms is available, detailed structural information on the intact ATP synthase remains lacking. The Holy Grail of the fields involved in the investigation of the ATP synthase is to obtain a high-resolution structure of intact ATP synthase. Although ATP synthase proteins can be isolated from several available organisms, spinach chloroplasts are likely a better source for several reasons. Primarily, although the chloroplast ATP synthase possesses an asymmetric molecular architecture, which renders it more difficult to form 3D crystals, it is possible for the chloroplast ATP synthase to present a single native conformation using a single simple physical treatment (no illumination) to induce its light-sensitive conformational changes, which will be briefly discussed in the subsequent subsection. Additionally, the subunit composition of the chloroplast ATP synthase is less complex than that of the mitochondrial ATP synthase. A second possible reason is that spinach leaves can be readily obtained and manipulated compared with other source materials. The goal of this project is to obtain three-dimensional crystals of intact chloroplast ATP synthase (CF_1F_O) for future structure determination. The initial work for this project began with the isolation of CF_1F_O from spinach according to the procedures of Turina et al. (2003) (Turina, Samoray et al. 2003) and Varco-Merth et al. (2008) (Varco-Merth, Fromme et al. 2008), and subsequent crystallization trails were evaluated using a broad range of conditions, including ionic strength, pH, specific anions and cations, precipitants and

additives. Comparisons of the results of these crystallization trails indicated that hexagonal or square-shaped salt crystals were readily observed in conditions containing 2% (w/v) PEG 3350 and 0.2 M $MgSO_4$, and a large number of small protein crystals were also detected by UV-fluorescence microscopy in modified conditions with a pH range from 6.5 to 8.5 (Figure 2.1).

Figure 2.1 Protein Crystals of Ribulose-1, 5-bisphosphate Carboxylase Oxygenase (RuBisCO). The shaped-crystals are grown from a starting solution that contains the isolation intact CF_1F_O. Please note that these pictures are taken under white and UV light.

Nice thin, square, clear crystals were harvested at the optimized condition containing 22% (w/v) PEG 3350, 0.26 M-0.32 M $MgSO_4$, and 0.1 M Tricine, pH 8.0. X-ray diffraction analysis of one of these crystals, which diffracted to 2.6 Å resolution, indicated that these crystals possess identical unit cell dimensions and space group as those for a previously reported crystal structure for RuBisCO, which is the most abundant protein on earth. In previous studies (Neff and Dencher 1999, Seelert, Poetsch et al. 2000), isolated CF_1F_O always contains significant amounts of RuBisCO observed either during ammonium sulfate precipitation or on the collected gradient fraction following sucrose gradient centrifugation. Inspection of these established steps in the isolation of CF_1F_O suggested that the majority of the isolated CF_1F_O is used for either chemiosmotic ATP synthesis or ATP hydrolysis assays or for the subsequent isolation of the CF_O c-ring. Therefore, although the small quantities of RuBisCO that contaminate CF_1F_O samples may be negligible for these applications, the presence of RuBisCO contamination will become a critical issue in crystallization trails of intact

CF_1F_O. Based on these results and observations, I was inspired to purify functionally intact CF_1F_O in extremely high purity and to produce this supercomplex in large quantities for future crystallization trails, which additionally represents a significant goal for future structure determination experiments. The work presented in this dissertation primarily focuses on the development and optimization of purification steps to entirely eliminate RuBisCO contamination from the CF_1F_O sample. Simultaneously, these steps can also stabilize CF_1F_O in its native state. The challenges and objectives are described in detail in Chapter 3.

2.3 The Regulation Mechanism of the Chloroplast ATP Synthase.

The F-type ATP synthase is a highly efficient reversible molecular motor capable of both ATP synthesis and hydrolysis; however, it also requires a mechanism to regulate its functional structural changes between active and inactive states to overcome certain energy or physiological conditions. The regulatory mechanism of chloroplast ATP synthase (CF_1F_O) is generally modulated depending on the proton motive force (*pmf*) across the thylakoid membrane (Tikhonov 2013, Walker 2013). In the dark, due to an extremely low proton gradient, the ATP synthesis of CF_1F_O cannot proceed, and a high ATP hydrolysis activity would apparently occur to expend ATP. To prevent this futile hydrolysis of ATP, a regulatory mechanism causes CF_1F_O to shift from an active state to an inactive state via intramolecular formation of a disulfide bond (-SH +HS- → -S-S-) between two cysteine residues (Cys_{199} and Cys_{205}) in the regulatory domain of the CF_1-γ subunit (Tikhonov 2013). Once illumination is restored, inactivated CF_1F_O will be reactivated to synthesize ATP until the initial generated *pmf* reaches the critical threshold level for reactivation of CF_1F_O to synthesize ATP and reduce the disulfide bond (-S-S- → -SH +HS-) in the CF_1-γ subunit (Tikhonov 2013, Walker 2013).

The CF_1-ε subunit, which is a subunit in the central stator that is attached to the CF_1-γ subunit, but is also attached to the CF_O-c ring, plays a critical role as an endogenous inhibitor to suppress the ATP hydrolysis direction of CF_1F_O. The ε subunit possesses two different conformations, down and up, in its two α-helical C-terminal domains. In the active state (Figure 2.2), the down conformation is observed in which two α-helices are turned toward the outer domain of the CF_1-γ subunit, precluding the subunit-subunit inhibition interaction between the ε subunit and the γ subunit and promoting the rotation in ATP synthesis.

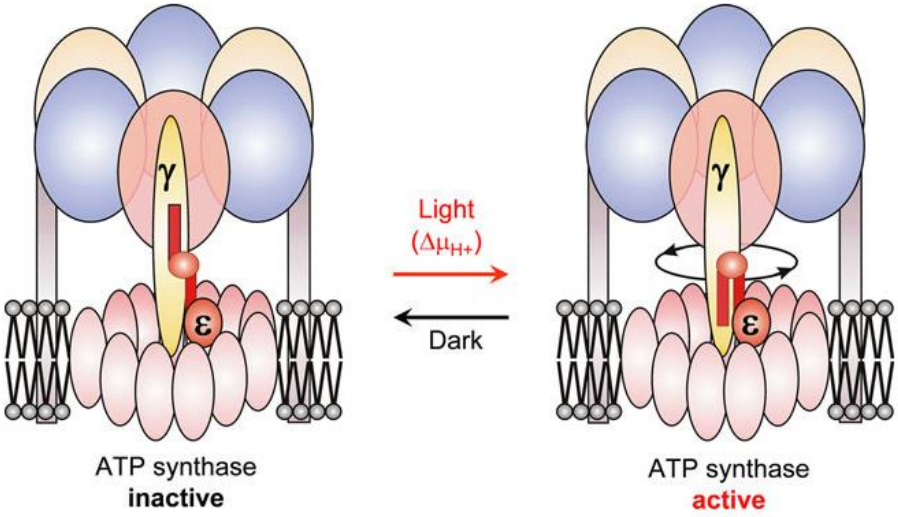

Figure 2.2 Conformational Changes in the Regulatory ε-subunit of CF_1F_O. Schematic Representation of Two Conformational Changes in the Regulatory ε-subunit between the Active and Inactive States of Chloroplast ATP Synthase. Figure taken and caption adapted from Tikhonov (2013) (Tikhonov 2013).

In the inactive state (Figure 2.2), two α-helices form a straight-up conformation, in which one α-helix turns toward the $\alpha_3\beta_3$ catalytic site and into the region of the $\alpha_3\beta_3$ catalytic cavity, thereby leading to an interaction between the ε subunit and the $\alpha_3\beta_3$ catalytic site that impedes the rotation of the γ subunit and inhibits CF_1F_O in the ATP hydrolysis direction (Konno, Suzuki et al. 2004, Tikhonov 2013, Walker 2013). This inhibition mechanism is also observed in ATP synthases from *Escherichia coli* and

Bacillus PS3 (Laget and Smith 1979, Kato-Yamada, Bald et al. 1999, Cingolani and Duncan 2011). Despite similar subunit compositions of the F_1 domain among mitochondrial, bacterial, and chloroplast ATP synthases, the mitochondrial ATP synthase possesses a different regulatory mechanism than that observed for bacterial and chloroplast ATP synthases. For the mitochondrial ATP synthase, an inhibitor protein known as IF_1 mediates the regulation between active and inactive states, in which IF_1 interacts with its αβ catalytic site to form an inhibition complex between its αβ catalytic site and the γ subunit (Walker 2013).

CHAPTER 3

OBJECTIVES AND CHALLENGES

3.1 Overview

The ATP synthase is a universal energy transduction machine that is present in nearly all living organisms and catalyzes the synthesis of ATP from ADP and inorganic phosphate ions driven by a transmembrane proton (or sodium ion) motive force. During the last several decades, hundreds of researchers worldwide have contributed their knowledge to unravel the attractive catalysis mechanism between proton conduction and ATP synthesis. An understanding of the molecular architecture of ATP synthase will certainly promote the elucidation of how conformational changes in each of its subunits relate to the catalytic mechanism. Although structural information for several subcomplexes and individual subunits of ATP synthase is available, detailed structural information for intact ATP synthase remains lacking. To obtain a high-resolution structure of intact ATP synthase, the growth of highly ordered three- or two-dimensional (3D or 2D, respectively) crystals of the intact ATP synthase is a prerequisite. However, to successfully achieve crystallization, a high purity of intact active ATP synthase is a prerequisite as the starting material. The overarching goal of the completed work described in this dissertation has been to produce intact active monodisperse chloroplast ATP synthase (CF_1F_O) in high purity. To this end, a progressive series of multiple purification steps have been experimentally optimized. These optimized steps are described in detail in Chapter 4. Four objectives and several challenges are outlined in this chapter below.

3.2 Isolation and Purification of Intact Thylakoid Membranes

The first objective of this project is to modify known isolation approaches and develop a new purification method in which intact chloroplast thylakoid membranes can be isolated in extremely high purity without contamination. As noted, the isolation of thylakoid membranes in extremely high purity is expected to be considerably difficult due to contaminating ribulose-1, 5-bisphosphate carboxylase oxygenase (RuBisCO) proteins that are present in chloroplasts in significant quantities. Although methods are well established for the isolation of intact thylakoid membranes from spinach leaves, most of these purified thylakoid membranes are mainly used for studies of in vitro protein insertion or transport assays. An optimized purification method offers two possible advantages. First, a significant amount of intact chloroplasts isolated from spinach leaves can be obtained by two rounds of centrifugation, which will exclude mitochondrial ATP synthase (MF_1F_O) contaminants from the subsequent purification of chloroplast ATP synthase (CF_1F_O). The subsequent isolation of intact thylakoid membranes is typically also facilitated because thylakoid membranes can form firm pellets in sucrose cushion centrifugation following lysis of intact chloroplasts, in which other membrane systems or soluble particles can be separated from thylakoid membranes. Second, the firm pellets formed by thylakoid membranes will enable additional purification manipulations to completely remove RuBisCO proteins. The removal of these proteins is essential for the subsequent purification of CF_1F_O and future crystallization trails. These advantages are all relevant to produce RuBisCO-free CF_1F_O ATP synthase. The isolation of other membrane proteins such as chloroplast transporters located on either the envelope or the thylakoid membrane systems will likely benefit from the availability of this optimized purification approach.

3.3 Isolation and Purification of Intact Chloroplast CF_1F_O ATP Synthase

Following successful isolation of intact thylakoid membranes, the second objective is to isolate and purify intact CF_1F_O ATP synthase in its native form and active state. The CF_1F_O purification typically begins with whole plant tissues and skillfully combines various biochemical techniques to isolate CF_1F_O from numerous other proteins present in plant cells. Due to the availability of highly purified thylakoid membranes, CF_1F_O can be readily solubilized from thylakoid membranes using a unique detergent mixture composition. CF_1F_O can be initially separated from other solubilized thylakoid membrane proteins using ammonium sulfate precipitation and further purified by sucrose gradient centrifugation to completely remove possible remaining contaminants. Ideally, highly pure CF_1F_O is present in the gradient that marks its density. To further stabilize its native state, detergent replacement to β-DDM is also performed using sucrose gradient centrifugation. As the starting material for future crystallization trails, a highly pure and monodisperse CF_1F_O sample is a prerequisite. This process is typically performed in part using high pressure liquid chromatography (HPLC) and affinity columns. According to its binding properties, CF_1F_O does not bind to negatively charged affinity matrices, and the flow-through fractions are collected and loaded onto a subsequent anion affinity column, from which CF_1F_O is eluted using a sodium chloride gradient supplemented with β-DDM. The optimized purification method for CF_1F_O is developed through experimental refinement of these techniques that have been designed to exploit the biophysical characteristics of CF_1F_O. Completing this second objective of the production of highly pure intact CF_1F_O ATP synthase in significant quantities as a monodisperse sample in the absence of contaminating RuBisCO proteins is a notable prerequisite for the third objective, and

particularly for the fourth objective of two-dimensional crystallization trails of CF_1F_O on a lipid monolayer.

3.4 Functional Characterization of the Purified CF_1F_O ATP Synthase

Upon purification of the CF_1F_O ATP synthase, the third objective is to characterize its functional state using either qualitative or quantitative analysis. CF_1F_O is reconstituted in liposomes composed of a mixture of phosphatidylcholine (PC) and phosphatidic acid (PA). The hydrophobicity of CF_O causes CF_1F_O to readily insert into phospholipids, resulting in a unidirectional orientation with the CF_1 domain toward the outside of the phospholipids while the detergents are removed. The proteoliposome is energized using an acid-base transition and a K^+/valinomycin diffusion potential. Application of this principle can be quantitatively investigated by determining the enzymatic activity (the turnover rate of ATP synthesis or the H^+/ATP ratio) of the purified CF_1F_O. The ATP hydrolysis activity of CF_1F_O can also be qualitatively detected by skillfully incorporating in-gel ATPase hydrolysis assays with native electrophoresis. The released ADP that is hydrolyzed from ATP by CF_1F_O is precipitated with lead (II) ions to form white precipitates on native gels. Because the ATP hydrolysis activity can be monitored in native gels using an in-gel ATPase assay, this assay can be used to rapidly screen for the enzymatic activity of purified CF_1F_O directly in gels without the requirement of complicated reconstitution assays. The application of this in-gel ATPase assay as a screening method to determine the optimal detergent to stabilize the structure and function of the purified CF_1F_O in different protein-detergent complexes for future crystallization experiments will be additionally investigated. Detergent screening is not possible using current reconstitution assays, as these assays require the removal of the detergent during reconstitution into phospholipids. Successful qualitative or

quantitative characterization of the CF_1F_O functional state will ultimately lead to experiments that can be designed to investigate the composition of crystallization buffers in the presence of detergents that may critically influence crystal formation of intact CF_1F_O while simultaneously stabilizing its native structure.

3.5 Monolayer Two-dimensional Crystallization of Intact CF_1F_O

Due to the difficulty in growing three-dimensional crystals of intact CF_1F_O in light of ATP synthase's naturally amphiphilic properties, two-dimensional (2D) crystallization of intact CF_1F_O is an attractive alternative approach. The fourth objective is to obtain 2D crystals of intact CF_1F_O using a lipid monolayer technique rather than the typically used dialysis-mediated detergent removal techniques. The lipid monolayer is formed through an air-water interface technique. The detergent-solubilized CF_1F_O is absorbed onto the lipid layer due to its hydrophobic properties, and an ordered 2D arrangement of intact CF_1F_O is generated with the simultaneous removal of detergents using Bio-Beads. The successful completion of this objective will ultimately lead to the determination of a high-resolution structure of intact CF_1F_O using electron crystallography.

3.6 Other Challenges Related to Objectives

To avoid conformational changes of CF_1F_O during purification, the entire isolation and purification is completed under green light, making experiments much more difficult and more time consuming. The amphiphilic nature of this membrane protein supercomplex renders CF_1F_O not only difficult to purify and stabilize in its functional state but also difficult to detect using standard analytical lab techniques. Certain subunits such as the ε, a, and c subunits in denaturing gels are difficultly stained using

Coomassie Blue. Consequently, silver staining is used in place of the less sensitive Coomassie Blue staining method. Due to a lack of tryptophan residues in the c-subunit, the routine method of protein concentration determination at 280 nm cannot be performed, and a more time-consuming modified Lowry assay must be used instead. The detection of the native state of CF_1F_O using various native electrophoresis techniques is also difficult, particularly that which is combined with the in-gel ATPase assay for detection of the ATP hydrolysis activity. The imaging of the results of the in-gel ATPase assays is also extremely challenging due to the white lead precipitates, which cannot be visualized in the transparent gels. However, the related steps are skillfully incorporated and optimized to overcome these challenges and obstacles to accomplish this purification objective of obtaining large quantities of RuBisCO-free CF_1F_O for future crystallization experiments.

CHAPTER 4

MATERIALS AND METHODS

4.1 Plant Material Preparation

For isolation of chloroplast CF_1F_O ATP synthase protein complexes, approximately 20 bags (9 oz each) of fresh baby spinach leaves (Fresh Express, a brand of Chiquita) were purchased from a supermarket for each preparation and maintained at 4℃ in the dark for at least three days to remove the starch from contents in the spinach leaves. Because protease inhibitors can affect the ATP synthase kinetics (Cox, Downie et al. 1978, Jancarik 1991), no protease inhibitors were used in the following isolation procedure. Therefore, leaves containing any physical damage that can be visualized by the naked eye were removed because this damaged tissue may release proteases to destroy chloroplast CF_1F_O ATP synthase protein complexes. Approximately 1.5 kg of intact spinach leaves was removed from the pre-sorted leaves, the stalks were removed to reduce mitochondrial-ATP synthase contamination because stalks are rich in mitochondrial organelles and were then immediately immersed into ice-cold tap-water to reduce the proteolysis of chloroplast CF_1F_O ATP synthase protein complexes caused by the released proteases. The culling step should be completed within 2 h in a green room. The stem-removed spinach leaves were stored in ice-cold water, and the amount of water that adhered to the culled good spinach leaves was filtered out using kitchen screen filter mesh prior to isolation.

4.2 Isolation of Intact Chloroplasts

Intact chloroplast CF_1F_O ATP synthase protein complexes were isolated from spinach by described procedure reported by Perry et al. (1991) (Perry, Li et al. 1991), Hall et al. (2011) (Hall, Mishra et al. 2011), Pick (1982) (Pick 1982), and van Wijk et al. (2007) (van Wijk, Peltier et al. 2007) with modifications. All of the steps were performed at 4℃ under green light.

4.2.1 Crude Preparation of Intact Chloroplasts

Intact chloroplasts were isolated from sorted stem-removed spinach leaves using a procedure described by Perry et al. (1991) (Perry, Li et al. 1991) and von Wijk et al. (2007) (van Wijk, Peltier et al. 2007) with modifications. All of the steps were carried out at 4℃ under green light. Approximately 1 kg of stem-removed spinach leaves was placed in a chilled Waring homogenize chamber and then homogenized by blending three times for 30 s at high speed in 500 mL of 1X chilled **Homogenization Buffer** (50 mM HEPES-KOH pH 8.0, 330 mM Sorbital, 1 mM $MgCl_2$, 1 mM $MnCl_2$, 1 mM EDTA-Na_2 pH 8.0, 0.1% w/v BSA) and then for 1 min at low speed in an additional 500 mL of 1X **Homogenization Buffer**. The homogenate was filtered through eight layers of cheesecloth containing four layers of Miracloth (EMD Millipore, Part No. 475855) between the top two layers into a chilled 2000-mL glass beaker to remove the unhomogenized cell debris. The filtered homogenate was transferred to 250-mL centrifuge tubes (Nalgene, Part No. 3141-0250) and then centrifuged at 3,000xg_{max} using a TA-10-250 fixed-angle rotor (Beckman Coulter, Part No. 368293) and an Allegra-25R Benchtop centrifuge (Beckman Coulter, Part No. 369436) for 3 min at 4℃. The supernatant was decanted and discarded, and the green pellets containing crude chloroplasts were firmly attached to the bottom of the centrifuge tubes. The green

pellets of crude chloroplasts were resuspended in a small volume (~10 mL) of the chilled **Resuspend Buffer** (50 mM HEPES-KOH pH 8.0, 330 mM Sorbital, 1 mM EDTA-Na_2 pH 8.0) by swirling the suspension with a soft brush, and the chlorophyll concentration was then determined according to section 4.5.2. The chlorophyll concentration of the resuspended chloroplasts was adjusted to a value between 50 and 100 mg/mL using chilled **Resuspend Buffer** in a final volume of 16 mL for the following step of the linear Percoll gradient centrifugation.

4.2.2 Percoll Gradient Preparation

To use Percoll to prepare a linear self-generating gradient in a total of eight 50-mL polycarbonate centrifuge tubes (Nalgene, Part No. 3118), the Percoll gradient was freshly prepared by completely mixing 15 mL of the undiluted 100 % Percoll (GE Healthcare, Part NO. 17-0891-01) with 15 mL of chilled **Percoll Gradient Buffer** (100 mM HEPES-KOH pH 8.0, 660 mM Sorbital, 1 mM EDTA-Na_2 pH 8.0). The linear self-generating Percoll gradient was established by centrifugation at 43,000xg_{max} using a SS-34 fixed-angle rotor (Thermo Scientific, Part No. 28020) and a Sorvall RC6 plus centrifuge (Thermo Scientific, Part No. 46910) for 30 min at 4℃ with an acceleration of 9 and a deceleration of 0. Finally, centrifuge tubes containing the established linear self-generating Percoll gradient should be carefully kept away from any unwanted movement that may disturb the linear gradient and stored at 4℃ for later use.

4.2.3 Percoll Gradient Centrifugation

No more than 2 mL of the chloroplast suspension corresponding to the range of 500 to 1000 mg/mL chlorophyll in a 50-mL polycarbonate centrifuge tube was carefully transferred to the top of the pre-made linear Percoll gradient using a disposable plastic

pipette to avoid disturbance of the linear gradient. The 50-mL polycarbonate centrifuge tubes were centrifuged at 5,000xg_{max} using a TS-5.1-500 swinging-bucket rotor (Beckman Coulter, Part No. 368308) and an Allegra-25R benchtop centrifuge (Beckman Coulter, Part No. 369436) for 15 min at 4℃ with an acceleration of 9 and a deceleration of 1.

4.2.4 Fraction Collection from Percoll Gradient Centrifugation

After complete centrifugation, two well separated green bands were visible. The upper green band in the linear Percoll gradient contained broken chloroplasts, whereas the lower green band contained intact chloroplasts. The fraction containing broken chloroplasts was carefully removed and removed by aspiration, whereas the fraction enriched with intact chloroplasts was carefully collected using a disposable plastic pipette and stored on ice.

4.2.5 Removal of Percoll from the Collected Fraction

The collected fraction containing intact chloroplasts was diluted at least 1:3 with **Resuspend Buffer** and well mixed by hand to wash off the Percoll in the fraction. The diluted fraction was centrifuged at 1200xg_{max} using a TA-14-50 fixed-angle rotor (Beckman Coulter, Part No. 368303) and an Allegra-25R Benchtop centrifuge (Beckman Coulter, Part No. 369436) for 5 min at 4℃ with an acceleration of 9 and a deceleration of 9. After the supernatant was decanted and discarded, the green pellets were resuspended in 50 mL of chilled **Resuspend Buffer** by swirling the suspension and then centrifuging it using the previously decribed. The Percoll can be completely removed from the collected fraction by repeating this step twice. The completely washed green pellets were resuspended in a small volume of chilled **Resuspend Buffer**

by swirling the suspension and then stored on ice. The chlorophyll concentration in the resuspended intact chloroplasts was adjusted to a value between 50 and 100 mg/mL using chilled **Resuspend Buffer** in a maximum volume of 16 mL for the second round of intact chloroplast purification by linear Percoll gradient centrifugation.

4.2.6 Second Round of Intact Chloroplast Purification

To increase the purity of the intact chloroplasts from the crude intact chloroplasts, a second round of Percoll purification was performed using the same experimental conditions used in the first round of purification. Finally, the lower phase of the gradients, which contains the refined intact chloroplasts, was collected and recovered from the Percoll gradients by multiple washing steps (see section 4.2.5). The refined intact chloroplasts were pelleted and then stored on ice in the dark for isolation of intact thylakoid membranes.

4.3 Isolation of Intact Thylakoid Membranes

4.3.1 Crude Preparation of Intact Thylakoid Membranes

To separate the stromal fraction and thylakoid membrane fraction, the intact chloroplasts were lysed by hypotonic shock and then subjected to sucrose gradient centrifugation. A pellet of refined intact chloroplasts was resuspended in a small volume of chilled **Lysis Buffer** (10 mM HEPES-KOH pH 8.0, 1 mM $MgCl_2$) by swirling. The chlorophyll concentration in the intact chloroplast resuspension was determined as described in detail in section 4.5.2 and then adjusted to a final chlorophyll concentration of 1 mg/mL. The intact chloroplasts were ruptured by hypotonic shock with **Lysis Buffer** and then incubated on ice for 30 min in the dark to completely swell the chloroplasts. The swollen chloroplasts were completely ruptured using a Dounce

homogenizer to completely release the stromal fraction, the envelope membrane fraction, and the thylakoid membrane fraction into the lysed resuspension. To separate the stromal fraction from the membrane fraction, which included the envelope membranes and the thylakoid membranes, the lysed chloroplast suspension was centrifuged at 40,000xg_{max} using a SS-34 fixed-angle rotor (Thermo Scientific, Part No. 28020) and a Sorvall RC6 plus centrifuge (Thermo Scientific, Part No. 46910) for 30 min at 4℃ with an acceleration of 9 and a deceleration of 9. After centrifugation, the supernatant containing the stromal fraction was decanted and discarded, and the pellet from the chloroplast membrane fractions was resuspended with 6 mL of chilled **Thylakoid Membrane Isolation Buffer** (10 mM Tricine-KOH pH 7.5, 300 mM sucrose, 4 mM $MgCl_2$, 1 mM EDTA-Na_2 pH 8.0) with a soft brush.

4.3.2 Sucrose Density Gradient Preparation

One hundred milliliters (100 mL) of the sucrose density gradient solutions at different concentrations was freshly prepared and chilled at 4℃ to establish a discontinuous sucrose density gradient in six SW-32 Ti ultracentrifugation tubes (Beckman Coulter, Part No. 326823). The three layers of the discontinuous sucrose density gradient were established by carefully layering the sucrose gradient solutions upon one another via a disposable plastic pipette. The initial layer of the discontinuous sucrose gradient was established by first adding 11 mL of **1.2 M Sucrose Gradient Solution** (1.2 M sucrose, 10 mM Tricine-NaOH pH 7.5, 4 mM $MgCl_2$, 1 mM EDTA-Na_2) into a ultracentrifugation tube (Beckman Coulter, Part No. 326823), and a second layer of 13 mL of **1.0 M Sucrose Gradient Solution** (1.0 M sucrose, 10 mM Tricine-NaOH pH 7.5, 4 mM $MgCl_2$, 1 mM EDTA-Na_2) and then a top layer of 12 mL of **0.6 M Sucrose Gradient Solution** (0.6 M sucrose, 10 mM Tricine-NaOH pH 7.5, 4 mM $MgCl_2$, 1 mM

EDTA-Na_2) were then added. Finally, the discrete layers of the sucrose gradient were visible, and the gradients were kept away from any unwanted movement to avoid disturbing the formed sucrose gradient and stored at 4℃ to maintain the integrity of the layers in the sucrose gradient.

4.3.3 Sucrose Density Gradient Centrifugation

To minimize the disturbance of the top sucrose layer during the loading step, the resuspension consisting of chloroplast membranes was very carefully layered onto the top layer using a disposable plastic transfer pipette. Each of the SW-32 Ti ultracentrifugation tubes containing a pre-made sucrose gradient was filled up with 1 mL of the chloroplast membrane resuspension. The SW-32 Ti ultracentrifugation tubes were assembled with required parts and accessories according to the manufacturer's instructions and then ultracentrifuged at 175,000xg_{max} (32,000 rpm) using a SW-32 Ti swinging-Bucket rotor (Beckman Coulter, Part No. 369694) and an Optima-100K ultracentrifuge (Beckman Coulter, Part No. 393253) for 45 min at 4℃ with the maximum acceleration and a deceleration without braking.

4.3.4 Fraction Collection from Sucrose Density Gradient Centrifugation

After ultracentrifugation, the envelope membrane fraction was located between 0.6 M and 1 M sucrose layers, whereas the thylakoid membrane fraction was found on the bottom of the tube. For collection of the thylakoid membrane fraction, immediately after the supernatant was decanted and discarded, the surface of the pellet of the thylakoid membrane fraction was carefully washed twice with 1 mL of chilled **Washing Buffer** (10 mM Tricine-NaOH pH 8.0,150 mM sucrose, 4 mM $MgCl_2$) by swirling the suspension to remove any unwanted contamination and then resuspended

in 6 mL of chilled **Washing Buffer** with a soft brush prior to obtaining a refined preparation of intact thylakoid membranes.

4.3.5 Second Round of Intact Thylakoid Membrane Purification

To completely remove any possible envelope membranes from the crude preparation of intact thylakoid membranes, the crude intact thylakoid membrane fraction was purified using the same sucrose density gradient purification procedure that was used for the crude preparation of intact thylakoid membranes. Immediately after ultracentrifugation, the surface of the pellet of the purified thylakoid membrane fraction was carefully washed three times with 2 mL of chilled **Washing Buffer** (10 mM Tricine-NaOH pH 8.0,150 mM sucrose, 4 mM $MgCl_2$) by swirling the suspension to completely remove the envelope membrane fraction and, the suspension was then stored on ice prior to removing the possible stromal fraction from the thylakoid membranes.

4.3.6 Removal of the Possible Residual Stromal Fraction

It is known that ribulose-1,5-bisphosphate carboxylase (RuBisCO) is a plant enzyme involved in the first major step of carbon fixation to convert inorganic carbon into organic molecules, such as glucose, RuBisCO is probably the most abundant protein on Earth. To remove the possible stromal fraction from the thylakoid membrane fraction, the pellet of refined intact thylakoid membranes was resuspended with 100 mL of chilled **Washing (RuBisCO) Buffer** (150 mM NaCl, 10 mM Tricine-NaOH pH 8.0, 4 mM $MgCl_2$) with a soft brush and then centrifuged at 7,500xg_{max} using a TA-14-50 fixed-angle rotor (Beckman Coulter, Part No. 368303) and an Allegra-25R Benchtop centrifuge (Beckman Coulter, Part No. 369436) for 5 min at 4℃. The supernatant

should be decanted and discarded because the pellet of thylakoid membranes obtained in this step is quite loose. To completely remove the remaining stromal proteins, particularly RuBisCO proteins, the wash step was repeated at least five times. The well-washed fraction of thylakoid membranes was resuspended with a small volume of **Resuspension Buffer** (50 mM Tricine-NaOH pH 8.0, 400 mM sucrose, 4 mM $MgCl_2$) by swirling and then stored on ice in the dark prior to determining the chlorophyll concentration.

4.4 Isolation of Chloroplast CF_1F_O ATP Synthase Complexes

4.4.1 Determination of Chlorophyll Concentration

The total chlorophyll (chls) concentration is proportional to the relative protein concentration in the suspension of isolated thylakoid membranes. The total chlorophyll in the well-washed isolated thylakoid membranes was extracted with an 80% (v/v) aqueous acetone solution and was then measured spectrophotometrically at the wavelengths of 645 nm and 700 nm as described in detail in section 4.5.3. The total chlorophyll concentration in the original suspension was determined using Welburn's equation (see Appendix A) with a molar extinction coefficient (Wellburn 1984). The final chlorophyll concentration was adjusted by dilution with the appropriate volume of **Resuspension Buffer** to 5 mg/mL, which is the optimal concentration for the solubilization of the membrane proteins from isolated thylakoid membranes.

4.4.2 Solubilization of Membranes from Isolated Thylakoid Membranes

Before solubilization, a calculated amount of solid DL-dithiotreitol (DTT) was slowly added to the diluted thylakoid membrane suspension (chlorophyll concentration, 5 mg/mL) under slow stirring until the final concentration of DTT in the membrane

suspension reached 50 mM, which activates the CF_1F_O protein for reducing dithiol bonds. This mixture of membrane-suspension is stirred for additional 15 min at 4°C. The solubilization process was performed by adding the following freshly prepared solutions in the described order (see Appendix A) within 5 min into the suspension of reduced thylakoid membranes under stirring at 4°C. For example, 100 mL of the reduced thylakoid membrane suspension was solubilized with 25 mL of **Solubilization Buffer** (80 mM Tricine-NaOH pH 8.0, 800 mM sucrose, 20 mM $MgCl_2$, 20 mM KCl), 4 mL of 100 mM **Na_2-ATP**, 20 mL of 100% (w/v) **NH_4SO_4**, 14 mL of **deionized H_2O**, 20 mL of 500 mM **DL-dithiotreitol (DDT)**, 5 mL of 500 mM **Sodium Cholate**, and 12 mL of 500 mM **β-D-octylglucoside (OG)** to obtain final concentrations of 2.5 mg/ mL chlorophyll, 12.5 mM cholate and 30 mM β-D-octylglucoside in the solubilization mixture. Under the optimal solubilization conditions used above (the chlorophyll ratio and a mixture of the anionic sodium cholate and the non-ionic β-D-octylglucoside detergent), CF_1F_O complexes can be almost completed extracted, and most photosynthesis-associated membrane protein complexes can still be retained in the fraction of thylakoid membranes. The solubilization mixture was stirred for an additional 15 min at 4°C after β-D-octylglucoside was added. The solubilization mixture was filled into Type-70 Ti ultracentrifuge tubes (Beckman Coulter, Part No. 355654), and the mixture was then incubated for an additional 15 min. During filling, the solubilization continued to be processed such that the total duration of the solubilization process was exactly 35 min. To separate the solubilized membrane proteins from the fraction of unsolubilized thylakoid membranes, the solubilization mixture was ultracentrifuged at 208,000xg_{max} using a Type-70 Ti fixed-angle rotor (Beckman Coulter, Part No. 337922) and an Optima-90K ultracentrifuge (Beckman Coulter, Part No. 393253) for 60 min at 4°C with maximum acceleration and

deceleration. After ultracentrifugation, the retaining supernatant enriched in CF_1F_O ATP synthase protein complexes as well as other solubilized membrane proteins (i.e., PSI, PSII, and cyt b_6f complex) was carefully collected from the unsolubilized membrane pellets for subsequent ammonium sulfate precipitation.

4.4.3 Ammonium Sulfate Precipitation step

The volume of **Saturated ammonium sulfate solution** that has to be added in the following ammonium sulfate precipitation steps was estimated using the following equation 4.4.3 (see Appendix B). The initial percentage of ammonium sulfate in the collected supernatant was 10% (v/v). The initial ammonium sulfate precipitation was completed at 4℃ in a drop-wise manner by adding the estimated volume of **Saturated Ammonium Sulfate Solution** (100% (w/v) $(NH_4)_2SO_4$) into the supernatant with stirring until a final concentration of 32.5% (v/v) was reached. The mixture of the collected supernatant in the 10% to 32.5% (v/v) cut-off saturated solution of ammonium sulfate was stored at 4℃ without stirring for an additional 20 min and then stirred for 5 min at 4℃ prior to centrifugation. To separate the first supernatant enriched with CF_1F_O ATP synthase protein complexes from the first precipitate containing most of the non-CF_1F_O ATP synthase protein complexes, the mixture was centrifuged at 12,000xg_{max} using a TA-14-50 fixed-angle rotor (Beckman Coulter, Part No. 368303) and an Allegra-25R Benchtop centrifuge (Beckman Coulter, Part No. 369436) for 15 min at 4℃ with an acceleration of 9 and a deceleration of 9. CF_1F_O ATP synthase protein complexes in the retained first supernatant (containing 32.5% ammonium sulfate) were precipitated in the second ammonium sulfate precipitation step using the 32.5% to 45% (v/v) cut-off saturated solution of ammonium sulfate, which was added in a drop-wise manner under stirring at 4℃. The second mixture of the first supernatant

in the 32.5% to 45% (v/v) cut-off saturated solution of ammonium sulfate was stored at 4℃ without stirring for an additional 20 min and then stirred for 5 min at 4℃ prior to centrifugation. The second precipitate containing CF_1F_O ATP synthase protein complexes was collected from the second mixture using the same centrifugation conditions used previously. The centrifuge tubes containing the CF_1F_O-protein-complex-second precipitate were turned upside down and air-dried with KimWipes to remove the remaining small volume of the second supernatant.

4.4.4 Storage of the Ammonium Sulfate Precipitate Fraction

To stabilize CF_1F_o ATP synthase protein complexes, the second precipitate of CF_1F_O ATP synthase protein complexes was resuspended with at most 10 mL of **Freezing Buffer** (30 mM NaH_2PO_4-NaOH pH 7.2, 200 mM sucrose, 2 mM $MgCl_2$, 0.5 mM Na_2-EDTA pH 8.0, 4 mM n-dodecyl-β-D-maltoside,β-DDM) containing 200 mM sucrose. This enriched CF_1F_O protein resuspension can be either immediately subjected to the following steps (i.e., sucrose density gradient ultracentrifugation or other biochemical characterization analysis) or flash-frozen in liquid nitrogen as 450-μL aliquots in 500-μL storage straws and then stored in a liquid nitrogen dewar for future use.

4.4.5 Sucrose Gradient Centrifugation of the Crude Fraction of CF_1F_O

4.4.5.1 Preparation of Sucrose Density Gradient Solution

The sucrose density gradient protocol applied for the advanced purification of CF_1F_O ATP synthase protein complexes was slightly modified from the method described by Turina et al. (2003) (Turina, Samoray et al. 2003). A large volume of **10X Sucrose Gradient Solution** (300 mM NaH_2PO_4-NaOH pH 7.2, 20 mM $MgCl_2$, 5 mM Na_2-EDTA pH 8.0) was prepared in advance in 30-mL aliquots in Falcon 50-mL centrifuge

tubes and stored at -20℃ for future use. A large volume of **200 mM β-DDM Solution** was prepared in advance, filtered through a syringe filter unit with a 0.22-µm-pore-size hydrophilic polyethersulfone membrane and finally stored in 12-mL aliquots in Falcon 15-mL centrifuge tubes at -20℃ for future use. The **10 mg/mL Asolectin Solution** was freshly prepared by hydrating 1000 mg of solid asolectin in 100 mL of deionized H_2O overnight, and the following day, the hydrating asolectin suspension was extruded through at least 20 passes through a polycarbonate membrane with a pore size of 0.2 µm to yield homogenous liposomes with a diameter similar to the pore size and then immediately applied to the sucrose density gradient solution. 50 mL of each **Sucrose Gradient Solutions** at concentrations of **20**, **28**, **36**, **44**, **52**, and **60**% (w/v), was freshly prepared by completely dissolving sucrose in 5 mL of **10X Sucrose Gradient Buffer**, 2 mL of **200 mM β-DDM Solution** and 5 mL of **10 mg/mL Asolectin Solution**, filled with deionized H_2O to a final volume of 50 mL, and stored at 4℃ prior to preparing the discontinuous sucrose density gradient.

4.4.5.2 Home-made Gradient Former

The gradient former used in this study is home-made and composed of a 5 mL-syringe connected to a pipetting needle (Popper & Sons, Part No. 7942) via a two-way stopcocks (Bio-Rad Part No. 7328102) for controlling the flow rate of the prepared gradients. A VTi 50-OptiSeal centrifuge tube (Beckman Coulter, Part No. 362183) is held steady and an upright position by a clamp stand. The home-made gradient former was inserted in a straight position into the centrifuge tube and then clamped, and the tip of the needle should be adjusted to ensure that it is as close to the bottom of the centrifuge tube as possible.

4.4.5.3 Sucrose Density Gradient Preparation

The six layers of the discontinuous sucrose density gradient were established within 5 min per tube by layering the pre-made sucrose density gradient solutions from 20% to 60% (w/v) upon one another via the home-made gradient former. The initial layer of the sucrose gradient was established using 6 mL of chilled **20% Sucrose Gradient Solution** at a flow rate of at least 5 ml per min adjusted by a two-way stopcocks. Then, 5.9 mL of each of the following sucrose density gradient solutions (**28%**, **36%**, **44%**, **52%** and **60%**) started to be carefully added to the syringe as the previous sucrose density gradient solution was almost drained from the syringe chamber (almost close to the bottom of the syringe chamber). However, to successfully establish the sucrose gradient layers, a subsequent solution should not be either added too early into the syringe chamber, which would result in its mixing with the previously added solution, or added after the previous solution was completely drained, which would introduce air bubbles into the needle and force these up through the gradient to disturb the integrity of well-formed sucrose gradient layers. Until the last sucrose gradient solution (**60% Sucrose Gradient Solution**) was completely drained, the pipetting needle of the gradient former was very carefully and slowly pulled out straightly from the ultracentrifuge tube to minimize the disturbance of the established layers in the discontinuous sucrose gradient. Finally, the ultracentrifuge tubes containing the discretely visible sucrose layers were not disturbed with any unwanted movement and stored at 4℃ to avoid destroying the well-formed layers of the discontinuous sucrose gradient.

4.4.6 Sample Preparation for Sucrose Density Gradient Centrifugation

Eight storage straws of the fraction of 45% (w/v) ammonium sulfate precipitates that contains CF_1F_O protein complexes in **Freezing Buffer** were thawed at 4℃. The total protein concentration of the thawed ammonium sulfate fraction (~3.5 mL) was determined at the ultraviolet wavelength of 280 nm through appropriate dilution with **UV-VIS spectrum Buffer** (20 mM Tricine-NaOH pH 8.0, 20 mM succinate, 0.6 mM KOH, 2 mM β-DDM) (section 4.5.1). The total protein concentration in the thawed ammonium sulfate fraction was then adjusted to a value between 10 and 20 mg/mL using **Sucrose Gradient Centrifugation Dilution Buffer** (30 mM NaH_2PO_4-NaOH pH 8.0, 200 mM sucrose, 2 mM $MgCl_2$, 0.5 mM Na_2-EDTA pH 8.0, 4 mM β-DDM) in a final maximum volume of 8 mL.

4.4.7 Sucrose Dnsity Gradient Centrifugation

To minimize the disturbance of the top layer of the sucrose gradient during the loading step, the diluted ammonium sulfate fraction suspension was extremely carefully layered onto the top layer using a disposable plastic transfer pipette. Each of the VTi-50 ultracentrifuge tubes containing the pre-made sucrose gradient layers was filled with at most 1 mL of the diluted ammonium sulfate fraction suspension, which corresponds to a total concentration of 10~20 mg/mL in each tube with a maximum total volume of ~36 mL. The VTi-50 ultracentrifuge tubes, which were assembled with the required parts and accessories according to the manufacturer's instructions, were ultracentrifuged at 242,000xg_{max} (50,000 rpm) using a VTi-50 vertical rotor (Beckman Coulter, Part No. 362758) and an Optima-90K ultracentrifuge (Beckman Coulter, Part No. 393253) for 17 h at 4℃ with the maximum acceleration. During the ultracentrifugation process, the membrane proteins travel through the sucrose gradient

and then stop at the point of the sucrose gradient at which the proteins' density matches that of the surrounding sucrose gradient. After the ultracentrifugation, to avoid disturbing the proteins that had been previously sedimented in the sucrose layers, the rotor was decelerated without braking, which may require an additional 4 h for the rotor to completely stop spinning.

4.4.8 Fraction Collction through Sucrose Gradient Centrifugation

4.4.8.1 Fraction Collection from Bottom to Top Sucrose Gradients

Immediately after the spinning was completely stopped, the VTi-5o rotor should be disassembled, but the ultracentrifuge tubes can still be stored inside the rotor because the rotor remains sufficiently cold to maintain the integrity of the protein sedimentations in the sucrose gradient. The protein migration pattern in the sucrose gradient has a limited lifetime. Therefore, the ultracentrifugation tubes have to be stored at 4℃, and the sucrose gradient fractions have to be collected within 30 min after ultracentrifugation before the protein migration pattern starts to diffuse. For detailed fraction collection, the ultracentrifugation tube is maintained steady and in an upright position by a clamp stand in a refrigerator at 4℃. A tiny hole was introduced into the center of the bottom of the centrifuge tube using a fine needle. The needle was then slightly inserted into the pierced hole and glued onto the ultracentrifuge tube, and the connection around the hole and the needle was then completely sealed. The needle setup allows the sucrose gradient solution to drip out at a flow rate of approximately 1 drop per second. A total of 36 x 1 mL of the sucrose gradient fractions are collected at 4℃ from the bottom to the top of the gradient in 1.5-mL microcentrifuge tubes below the needle, immediately flash-frozen in liquid nitrogen as 450-µL aliquots in 500-µL storage straws and stored in a liquid nitrogen dewar for further biochemical analysis.

4.4.8.2 Fraction Collection from a Specific Sucrose Gradient Layer

To collect fractions from a specific sucrose layer, i.e., the layer corresponding to the 44% (w/v) sucrose gradient enriched in CF_1F_O-detergent-lipid ATP synthase complexes, the ultracentrifuge tube was also maintained steady and in a vertical position with a clamp in a refrigerator at 4℃. A tiny hole was introduced into the center of the 44% (w/v) sucrose layer from the side wall of the ultracentrifuge tube using a fine needle connected to a 3-mL sterilized syringe. Two milliliters of the 44% (w/v) sucrose gradient fraction were collected, immediately flash-frozen in liquid nitrogen as 450-μL aliquots in 500-μL storage straws and stored in a liquid nitrogen dewar for further biochemical analysis.

4.5 Protein and Chlorophyll Concentration Determination

4.5.1 Protein Concentration Determination at 278 nm and 280nm

The UV lamp of a UV-Visible absorbance spectrophotometer (Beckman Coulter DU-800) should be warmed up at least 15 min prior to any measurement and then calibrated at 278 nm and 280 nm using 1000 μL of **UV-VIS spectrum Buffer at 278nm/280 nm** (20 mM Tricine-NaOH pH 8.0, 20 mM succinaye, 0.6 mM KOH, 2 mM β-DDM) as the reference sample. A 1/100 dilution of the original protein sample mixture was prepared by mixing 10 μL of the original protein sample mixture with 990 μL of **UV-VIS spectrum Buffer at 278 nm/280 nm**, and the absorbance of this dilution was then measured at 278 nm and 280 nm. The absorbance value at 280 nm was used in equation 4.5.1.1 (see, Appendix B) to estimate the concentration of total proteins in the original protein sample mixture. The absorbance value at 278 nm was inputted into equation 4.5.1.2 (see Appendix B) based on the Lambert–Beer Law to estimate the concentration of CF_1F_O ATP synthase protein complexes in the original protein sample mixture.

4.5.2 Chlorophyll Concentration Determination at 652 nm

The total chlorophyll (chls) concentration is proportional to the relative number of chloroplasts in the chloroplast suspension. In general, 1 mg of chlorophyll contains between 1 and 2×10^9 chloroplasts. The chlorophyll concentration in the suspension of isolated intact chloroplasts was rapidly measured using the method described by Arnon (1949) (Arnon 1949)and Perry et al. (1991) (Perry, Li et al. 1991) with some modifications. Prior to measurement, the visible lamp of a UV-Visible absorbance spectrophotometer (Beckman Coulter DU-800) should be warmed up for at least 15 min and then calibrated at 652 nm using a "reference" sample prepared by mixing 1 μL of deionized H_2O instead of the sample with **80% (v/v) Acetone Sample Solution at 652 nm** (800 μL Acetone, 199 μL deionized H_2O). One microliter of an aqueous sample solution containing green chloroplasts was added into freshly prepared **80% (v/v) Acetone Sample Solution at 652 nm**, vortexed for 2 min, and maintained on ice for an additional 10 min in the dark to completely extract chlorophyll from the chloroplasts. The sample solution was then centrifuged at 14,000xg_{max} using a F-45-12-11 fixed-angle rotor (Eppendorf, Part No. 022668498) and MiniSpin (Eppendorf, Part No. 022620100) at room temperature for 5 min to separate the extracted chlorophylls from the insoluble chloroplast debris. The supernatant was carefully transferred to a new 1.5-mL microcentrifuge tube and then measured at 652 nm. The chlorophyll concentration in the original sample was then calculated using the absorbance value at 652 nm and the equation 4.5.3 (see Appendix B).

4.5.3 Chlorophyll Concentration Determination for the CF_1F_O Isolation

The total chlorophyll concentration in the sample solution was measured by the method described by Wellburn (1984) (Wellburn 1984). The characteristic peak of the

absorption spectrum of the total chlorophylls is found at 664 nm in 80% (v/v) acetone solution ($\varepsilon_{664\ nm}$ = 76,780 M^{-1} cm^{-1}) compared with the baseline at 700 nm. Hence, the total chlorophyll was extracted using 80% (v/v) acetone solution. Prior to measurement, the visible lamp of a UV-Visible absorbance spectrophotometer (Beckman Coulter DU-800) should be warmed up for at least 15 min and then calibrated at 664 nm and 700 nm using a "reference" sample prepared by mixing 1 μL of deionized H_2O instead of the sample and 999 μL of **80% (v/v) Acetone Sample Solution at 664 nm/700 nm** (800 μL Acetone, 199 μL deionized H_2O). Then, 1 μL of an aqueous sample solution containing thylakoid membranes was added into freshly prepared 999 μL of **80% (v/v) Acetone Sample Solution at 664 nm/700 nm**, and the mixture was vortexed for 2 min to completely extract chlorophyll molecules from the thylakoid membranes and then centrifuged at 14,000xg_{max} using a F-45-12-11 fixed-angle rotor (Eppendorf, Part No. 022668498) and MiniSpin (Eppendorf, Part No. 022620100) at room temperature for 5 min to separate the extracted chlorophylls from the insoluble thylakoid membrane debris. The supernatant was carefully transferred into a 1.5-mL microcentrifugation tube and then measured at 664 and 700 nm. The concentration of total chlorophyll in the original sample was then calculated using absorbance values of 664 nm and 700 nm and the equation 4.5.4 (see Appendix B).

4.5.4 Protein Concentration Determination via the Modified Lowry Assay

The protein concentration was determined according to the modified Lowry method as described by Hartree (1972) (Hartree 1972) and Lowry et al. (1951) (Lowry, Rosebrough et al. 1951). Although this assay is time-consuming, it does provide a more accurate determination of the concentration of membrane proteins because the membrane lipids in a suspension of membrane proteins, which may interfere with the

assay, can be effectively solubilized in reagent containing 1% (w/v) SDS. Prior to the assay, **Reagent C** was freshly prepared by completely mixing 15 mL of **Reagrent A** (2% (w/v) Na_2CO_3, 50 mM NaOH, 0.16% (w/v) Tartaric acid, 1% w/v sodium dodecyl sulfate, SDS) and 150 µL of **Reagent B** (4% (w/v) $CuSO_4$ 5 H_2O) in 20 assay test tubes. The BSA standard samples were also freshly prepared as described: A triplicate set of protein standards was prepared from bovine serum albumin (BSA) by serially diluting **BSA Stock Solution** (100 µg/mL) with distilled H_2O to obtain concentrations of 0, **20**, **40**, **60**, **80** and **100** µg/mL. To fit the diluted concentrations within the range of the BSA standard concentrations, 4 µL of each of the protein samples with unknown concentrations was diluted 200-fold with 796 µL of the appropriate buffer in triplicate. Then, 750 µL of **Reagent C** was added to each assay tube containing 250 µL of either the **BSA Standards** or the Diluted **Protein Samples**, and the mixture was vortexed and then incubated at room temperature for 20 min to ensure that all of the proteins, particularly the membrane proteins and lipids, were completely solubilized by SDS. Immediately after the first incubation, 75 µL of **50% (v/v) Folin-Ciocalteu Phenol Solution** was rapidly added to each assay tube, and the mixture was then vortexed and subjected to a second incubated at room temperature for 45 min. (Note that the intensity of the bluish color that develops is actually representative of the proportion of protein concentration in the assay tubes). Prior to measurement, the visible lamp of a UV-Visible absorbance spectrophotometer (Beckman Coulter DU-800) should be warmed up for at least 15 min and then calibrated at 660 nm using the 0% v/v BSA standard, and spectral measurements at 660 nm were then obtained for each of the BSA standards and protein samples. Therefore, the unknown concentrations were calculated using the BSA standard curve, which was plotted to correlate the absorbance values of the BSA standards to the known concentrations.

4.6 Electrophoresis

4.6.1 Tricine SDS-PAGE Denaturing Electrophoresis

The protein composition was analyzed through one-dimensional denaturing discontinuous electrophoresis. Tricine SDS-PAGE is a powerful electrophoretic system for separating proteins in the molecular weight range of 1 to 100 kD (Wittig, Braun et al. 2006). The reagent setup of Tricine SDS-PAGE used in this research is based on the method developed by Schagger (2006) (Schagger 2006) The procedures used for polyacrylamide gel preparation and the electrophoresis apparatus assembly, including the glass-plate cassettes, followed the instructions provided by Bio-Rad and Short Protocols in Molecular Biology (Fourth Edition, unit 10, 1999).

4.6.1.1 Tricine SDS-PAGE Gel Preparation

A Tricine-SDS-PAGE polyacrylamide gel with dimensions of 7 × 8 × 0.1 cm was cast in a 4% stocking gel and a 15% separating gel. Then, 5 mL of the **Separating-gel Solution** containing 15% acrylamide was freshly prepared by mixing 2.5 mL of Acrylamide/Bis-acrylamide solution 30% (v/v), 29:1, 1.65 mL of 3X Tricine gel buffer (3 M Tris-NaOH pH 8.45, 0.3% (w/v) SDS) and 0.45 mL of deionized H_2O. After the polymerizing reagents (10 μL of 40% (w/v) **Ammonium Persulfate Solution (APS)** and 7.5 μL of **TEMED**) were added, 4.5 mL of the gel solution was immediately applied into the assembled glass-plate cassette, and a layer of 200 μL of 100% methanol was then immediately added and incubated at room temperature until the solution (gel) was completely polymerized (approximately 30 min). After the separating gel was completely polymerized, the overlaying solution (methanol) was discarded, and the gel was allowed to dry in air for 15 min to evaporate the remaining methanol. Immediately after 15 min of incubation, 1.8 mL of the freshly prepared **Stocking-gel Solution**

containing 4% acrylamide, prepared by mixing 0.4 mL of Acrylamide/Bis-acrylamide solution 30% (v/v), 29:1, 0.75 mL of 3X Tricine gel buffer (3 M Tris-NaOH pH 8.45, 0.3% (w/v) SDS), 1.85 mL of deionized H_2O, 5 μL of 40% (w/v) **Ammonium Persulfate Solution** and 2.5 μL of **TEMED**, was poured onto the top of the polymerized separating gel until reaching the top of the short glass-plate cassette. A 10-well comb was immediately inserted into the fresh stocking solution, and the gel solution with the comb was incubated at room temperature for at least 60 min until the stocking solution (gel) was completely polymerized. The cast gel could be freshly used or stored at 4℃ for one week.

4.6.1.2 Tricine SDS-AGE Denaturing Sample Preparation

The samples were prepared based on previously described methods (Fromme, Boekema et al. 1987, Schagger 2006, Lawrence, Varco-Merth et al. 2011) with some modifications. The denaturing buffer was chosen based on the protein source. For proteins eluted from a chromatographic column, part of the protein sample was mixed with three volumes of **3X Sample Loading Buffer with non-reducing reagent** (150 mM Tris-HCl pH 7.0, 30% (w/v) glycerol, 12% (w/v) SDS, 0.05% (w/v) Bromophenol Blue). If the proteins were collected through sucrose gradient purification, part of the protein sample was mixed with three volumes of **3X Sample Loading Buffer with non-glycerol** (150 mM Tris-HCl pH 7.0, 12% (w/v) SDS, 0.05% (w/v) Bromophenol Blue. For pelleted proteins, the pellet was resuspended in 20 μL of one-fourth-diluted **3X Sample Loading buffer with non-reducing reagent**. The mixture of the protein sample with the appropriate denaturing buffer was well mixed in a 1.5-mL microcentrifuge tube and completely denatured by incubation at 80℃ for at least 30 min, cooled down on ice, and centrifuged at 3000xg_{max} using a F-45-12-11 fixed-angle

rotor (Eppendorf, Part No. 022668498) and MiniSpin (Eppendorf, Part No. 022620100) at room temperature for 1 min prior to loading.

4.6.1.3 Tricine SDS-PAGE Electrophoresis Buffer preparation

The **Anode electrophoresis buffer** (100 mM Tris-HCl pH 8.9) and **Cathode-electrophoresis buffer** (100 mM Tris-HCl pH 8.9, 100 mM Tricine, 0.1% (w/v) SDS, adjust pH to 8.25) were prepared based on a previously described method (Wittig, Braun et al. 2006) at 4℃ until future use. The cast gel was mounted in the electrophoresis chamber according to the instructions provided by Bio-Rad Mini-Protein Tetra Cell (Bio-Rad, 165-8000). Then, 180 mL of **Cathode-electrophoresis Buffer** was then added to the upper chamber (cathode electrode), and 300 mL of **Anode-electrophoresis Buffer** was added to the lower chamber (anode electrode). An appropriate amount of the denatured protein and 10 μL of the protein dual-color standards (Bio-Rad, Part No. 161-0374) were loaded via a gel loading tip (Bio-Rad, Part No. 223-9911).

4.6.1.4 Tricine SDS-PAGE Electrophoresis Running Condition

The electrophoresis running conditions are recommended by a previously described method (Wittig, Braun et al. 2006). Electrophoresis is typically run in an ice box at an initial voltage of 30 V until all of the loading samples have completely migrated from the gel wells into the stocking gel. Subsequently, the samples are migrated at a constant voltage of 50 V in the stocking gel, and the voltage was then increased to 150 V after the samples had completely entered the separating gel. The gel was then maintained at this high voltage until the separation was completed.

4.6.2 Native Electrophoresis

For further characterization of the CF_1F_O ATP synthase protein complex in its physical state, native electrophoresis including blue native electrophoresis (BN-PAGE), clear native electrophoresis (CN-PAGE), and high-resolution clear native electrophoresis (hrCN-PAGE), was performed according to previously described protocols with slight modifications.

4.6.2.1 Blue Native Electrophoresis (BN-PAGE)

4.6.2.1.1 BN-PAGE Gel Preparation

The resolution of a gradient gel allows the detection of a much broader range of protein sizes than that obtained with a single-concentration gel by increasing the percentages of acrylamide from top to bottom. Depending on the gradient, the resolution generally covers from a low molecular weight of ~10 kDa) to a high molecular weight of ~250 kDa. The gradient gel setup (see Appendix C), including a gradient former (Model 385, Bio-Rad) and a peristaltic pump with other essential apparatuses, follows the instructions provided by Bio-Rad and Short Protocols in Molecular Biology (Fourth Edition, unit 10, 1999) with slight modifications. **4X Native Gel Buffer** (100 mM Imidazole-HCl pH 7.0, 2 M 6-Aminohexanoic acid) and **30% (w/v) Acrylamide/Bis-acrylamide, 32:1 Solution** (7 mL of **Acrylamide/Bis-acrylamide Solution, 30 % (w/v)**, **29:1**, 9.75 mL of **Acrylamide/Bis-acrylamide Solution, 40% (w/v), 37.5:1**, 3.75 mL of **deionized H_2O**) were prepared and stored at 4℃ for future use. The light (4%) (0.53 mL of **30% (w/v) Acrylamide/Bis-acrylamide Soluton, 30% (w/v), 32:1**, 1 mL of **4X Native Gel Buffer**, 2.47 mL of **deionized H_2O**] and heavy (16%) (2.13 mL of **30% (w/v) Acrylamide/Bis-acrylamide Solution, 30% (w/v), 32:1**, 1 mL of **4X Native Ggel Buffer**, 0.64 mL of **100% Glycerol**, 0.23 mL of **deionized H_2O**)

acrylamide gel solutions of a gradient gel are freshly prepared with the exception of the **Polymerizing Reagents** (**APS Solution** and **TEMED**), which are added just before use, and stored at 4℃. All tubing connections and valve positions have to be set up before the gel solutions are applied. Both solutions without polymerizing reagents are pipetted into the mixing (16%) and reservoir (4%) chambers. The appropriate amount of **Polymerizing Reagents** (5 μL of **40% (w/v) APS Solution** and 2 μL of **TEMED**) in the light acrylamide solution, 5.5 μL of **40% (w/v) APS Solution** and 2.2 μL of **TEMED** in the heavy acrylamide solution] was added to each chamber and quickly mixed with a disposable pipet. The interconnecting valve between the chambers and the stir-bar in the mixing chamber were turned on, resulting in a gradient gel solution prepared by mixing the light and heavy solutions. The outlet valve was then immediately turned on, and the flow rate was adjusted to 2 mL/min. The gradient gel solution collected through the outlet from the mixing chamber was slowly cast from the top to bottom of a glass-plate sandwich via a peristaltic pump. After the gel was completely cast, a layer of 200 μL of 100% Methanol was added to the top of the gradient gel and then incubated at room temperature until the solution (gel) was completely polymerized (~30 min). After the gradient gel was completely polymerized, the overlaying solution (methanol) was discarded, and gel was allowed to dry in air for 15 min to evaporate any remaining methanol. Immediately after 15 min of incubation, 1.8 mL of the freshly prepared **3.5% Stocking-gel Solution** (0.35 mL of **30% (w/v) Acrylamide/Bis-acrylamide Solution, 30% (w/v), 32:1**, 0.75 mL of **4X Native Gel Buffer**, 1.9 mL of **deionized H_2O**, 6.23 μL of **40% (w/v) APS Solution**, 2.5 μL of **TEMED**] was pipetted on the top of the polymerized separating gel until the top of the short glass-plate cassette was reached. A 10-well comb was immediately inserted into the unpolymerized stocking solution, and the gel solution with the comb was incubated

at room temperature for at least 60 min until the stocking solution (gel) was complete polymerized. The cast gel could be freshly used or stored at 4℃ for one week.

4.6.2.1.2 BN-PAGE Sample Preparation

The preparation of samples for native electrophoresis is based on previously described methods (Wittig, Braun et al. 2006, Meyer, Wittig et al. 2007, Wittig, Carrozzo et al. 2007) with some modifications. The protein fractions of interest were prepared by either density centrifugation or FPLC (Fast Protein Liquid Chromatography). To avoid protein aggregation, the protein samples were either dialyzed or desalted against **Low Ionic Strength Buffer** (50 mM NaCl, 50 mM Imidazole-HCl pH 7.0, 5 mM $MgCl_2$, 8 mM β-DDM) just prior to electrophoresis. Ten microliters of the BN-PAGE protein sample loading buffer containing 10 μg of protein was freshly prepared as the following formula: 2.5 μL of **4X BN-PAGE Sample Loading Buffer** (200 mM NaCl, 200 mM Imidazole-HCl pH 7.0, 8 mM 6-Aminohexanoic acid, 4 mM Na_2-EDTA pH 8.0, 16% (v/v) Glycerol)," x" μL of **5% (w/v) Coomassie Blue G-250**, "y" μL of **200 mM β-DDM Solution**, 10-x-y-z μL of **deionized H_2O**, "z" μL **desalted Protein Sample**, to yield a final protein concentration of 1 μg/μL. To formula above, a sufficient amount of detergent (β-DDM) is added to yield a detergent-to-protein ratio of 2.5:1 g/g, and Coomassie Blue G-250 dye is added to obtain a ratio of detergent to Coomassie of 8:1 g/g. It is not necessary to heat the native sample loading buffer, but this buffer was subjected to a 1-min centrifugation at 10,000x*g* prior to loading. The maximum loading volume per well was 20 μL. However, the loading volume depended on the desired mass of proteins per well.

4.6.2.1.3 BN-PAGE Native Electrophoresis Buffer Preparation

The native electrophoresis conditions for BN-PAGE are based on previously described methods (Wittig, Braun et al. 2006, Meyer, Wittig et al. 2007, Wittig, Carrozzo et al. 2007) with some modifications. Prior to running, the **BN-PAGE Cathode-electrophoresis Buffer** (50 mM Tricine-HCl pH 7.0, 7.5 mM Imidazole-HCl pH 7.0) was freshly supplemented with the anionic Coomassie Blue G-250 dye to obtain a final concentration of 0.02% (w/v). The casted native gel was mounted in the vertical electrophoresis apparatus according to the instructions provided by Bio-Rad Mini-PROTEIN Tetra Cell (Bio-Rad, 165-8000). The cathode (inside) chamber was filled with 200 mL of the chilled cathode buffer, and the anode (outside) chamber was filled with 300 mL of chilled **Anode-electrophoresis Buffer** (25 mM Imidazole-HCl pH 7.0). An appropriate volume containing a specific mass of the native protein sample and 10 µL of the NativeMark unstained protein standard (Life Technologies, Part No. LC0725) were then loaded via a gel loading tip (Bio-Rad, Part No. 223-9911).

4.6.2.1.4 BN-PAGE Native Electrophoresis Running Condition

Electrophoresis is typically performed at 4℃. The BN-PAGE running conditions start with an initial voltage of 100 V until the loaded protein samples have completely entered into the stocking gel, and this is followed by an increase in voltage to 150 V with a maximum current of 16 mA per gel until the process is finalized. However, to achieve better detection of faint protein bands, after the loading dye has run approximately one-third of the total gel length, a **Slight-blue Cathode-electrophoresis Buffer** (50 mM Tricine-HCl pH 7.0, 7.5 mM Imidazole-HCl pH 7.0) supplemented with 0.002% (w/v) Coomassie Blue G-250 is applied to the remaining running distance instead of the original BN-PAGE cathode buffer containing 0.02% (w/v) Coomassie

Blue G-250. The electrophoresis is stopped after 2-2.5 h, and at the end, the current is increase decreased to 2 mA from 16 mA as the Coomassie Blue dye approaches the gel front.

4.6.2.2 Clear Native Electrophoresis (CN-PAGE)

4.6.2.2.1 CN-PAGE Gel Preparation

The preparation of the gradient gel for **CN-PAGE** is based on the method for BM-PAGE described in Section BN-PAGE gel preparation.

4.6.2.2.2 CN-PAGE Sample Preparation

The **CN-PAGE** samples were prepared based on the method used for BN-PAGE described in Section BN-PAGE sample preparation with the exception that **Ponceau S Dye** (0.01%, w/v) was used instead of Coomassie Blue G-250 dye in the sample loading buffer.

4.6.2.2.3 CN-PAGE Native Electrophoresis Buffer Preparation

The native electrophoresis running buffers for CN-PAGE were prepared based on the method for BN-PAGE described in Section Preparation of BN-PAGE native electrophoresis buffer. The **Anode-electrophoresis Buffer** (20 mM Imidazole-HCl pH 7.0) and **Cathode-electrophoresis Buffer** (50 mM Tricine-HCl pH 7.0, 7.5 mM Imidazole-HCl pH 7.0) for CN-PAGE are identical to those used for BN-PAGE with the exception that no additive (Coomassie Blue G-250 dye) was added to the cathode buffer for CN-PAGE.

4.6.2.2.4 CN-PAGE Native Electrophoresis Running Condition

CN-PAGE native electrophoresis is typically performed at 4℃. The electrophoretic conditions start with an initial voltage of 100 V until the loaded native protein sample has completely entered into the stocking gel, and this step was followed by an increase in the voltage to 150 V with a maximum current of 16 mA per gel until the end of the process. The total running time from the beginning to the time at which the Ponceau S dyes approach the gel front is approximately 2-2.5 h, and the current was decreased to 1 mA from 16 mA.

4.6.2.3 High-resolution Clear Native Electrophoresis (hrCN-PAGE)

4.6.2.3.1 hrCN-PAGE Gel Preparation

The preparation of the gradient gel used for **hrCN-PAGE** is based on the method for BM-PAGE described in Section BN-PAGE gel preparation.

4.6.2.3.2 hrCN-PAGE Sample Preparation

The samples for **hrCN-PAGE** were prepared based on the method for CN-PAGE described in Section CN-PAGE sample preparation.

4.6.2.3.3 hrCN-PAGE Native Electrophoresis Buffer Preparation

The native electrophoresis running conditions for **hrCN-PAGE** are based on those described in Section Preparation of CN-PAGE native electrophoresis buffer. Identical **Anode-electrophoresis Buffer** (25 mM Imidazole-HCl pH 7.0) and **Cathode-electrophoresis Buffer** (50 mM Tricine-HCl pH 7.0, 7.5 mM Imidazole-HCl pH 7.0) are applied for CN-PAGE and hrCN-PAGE with the exception that the cathode buffer used for hrCN-PAGE is freshly supplemented with anionic sodium deoxycholate (DOC)

and non-ionic β-DDM at final concentrations of 0.05% (w/v) and 0.02% (w/v), respectively, to form mixed micelles prior to use.

4.6.2.3.4 hrCN-PAGE Native Electrophoresis Running Conditions

The native electrophoresis running conditions for **hrCN-PAGE** are based on the CN-PAGE running conditions described in Section CN-PAGE native electrophoresis running conditions.

4.6.3 Two-dimensional Electrophoresis (1-D: Blue-PAGE or hrCN-PAGE and 2-D: Tricine-SDS-PAGE)

Two-dimensional gel electrophoresis consists of a combination of two high-resolution electrophoresis techniques to obtain better resolution than that obtained with either technique alone. Either BN-PAGE or CN-PAGE (hrCN-PAGE) is used for the first electrophoresis dimension to separate native protein complexes from biological membranes in order to determine their masses and oligomeric states, and this is followed by the second SDS-PAGE dimension, which allows resolution of subunits of the native protein complexes obtained by BN-PAGE.

4.6.3.1 2D-PAGE Gel Preparation

A 4%~12% native gradient gel is typically used for the first electrophoresis dimension (Section BN-PAGE, CN-PAGE, or hrCN-PAGE gel preparation), and A 4%~12% denaturing gradient gel is used for the second electrophoresis dimension (Section Tricine SDS-PAGE gel preparation).

4.6.3.2 2D-PAGE Sample Preparation

The method used to prepare the samples for the first electrophoresis dimension depended on the native gel applied (Section BN-PAGE, CN-PAGE or hrCN-PAGE sample preparation). For the second electrophoresis dimension, a 0.5-cm gel strip from BN-PAGE (or hrCN-PAGE stained with Coomassie blue) was placed on a Petri dish, incubated for at least 15 min with 1% (w/v) SDS containing 1% (v/v) β-mercaptoethanol, and then washes with deionized H_2O to remove the excess β-mercaptoethanol. Immediately after the gel strip was trimmed to fit the space for SDS-PAGE, the strip was horizontally squeezed into the space for SDS-PAGE, and SDS-PAGE sample buffer was then on top of the horizontal gel strip until the chamber was filled.

4.6.3.3 2D-PAGE Electrophoresis Running Buffer Preparation

The running buffers for the first electrophoresis dimension (1D) are based on the buffer compositions of the buffers used for the native electrophoresis applied (Section Preparation of BN-PAGE, CN-PAGE or hrCN-PAGE native electrophoresis buffer), and those used for the second electrophoresis dimension (2D) are based on the buffer composition of Tricine-SDS-PAGE (Section Preparation of Tricine SDS-PAGE denaturing electrophoresis buffer).

4.6.3.4 2D-PAGE Electrophoresis Running Condition

The running conditions for the first and second electrophoresis dimensions are based on the conditions previously described (Section BN-PAGE, CN-PAGE or hrCN-PAGE native electrophoresis running conditions and Section Running condition for Tricine SDS-PAGE denaturing electrophoresis).

4.6.4 Native Protein Electroelution

The electroelution of the CF_1F_O ATP synthase complexes is based on a method using the H-shaped elution device described by Seelert and Krause (2008) (Seelert and Krause 2008) and Krause et al. (2008) (Krause and Seelert 2008). The H-shaped elution device (C.B.U. Scientific, Part No. ECU-040-25) was set up according to the manufacturer's recommended instructions. Both electrode chambers in the tank were filled with **1X Electroelution Buffer** (25 mM Tricine-HCl pH 7.0, 7.5 mM Bis-Tris pH 7.0). The cathodic arm of the H-shaped eluter with a 5-kDa dialysis membrane (Harvard Apparatus, Part No. 74-2100) was also filled with **1X Electroelution Buffer** up to half of the distance from the dialysis membrane to the connecting bridge. To achieve better and faster elution, the native gel strips of BN-PAGE or CN-PAGE that contain the target proteins were carefully cut into multiple small pieces and then placed in a disposable syringe. The gel materials that were compressed out of the syringe to become smaller particles were injected into the buffer solution of the cathodic arm of the eluter during compression, and this step was followed by incubation for at least 10 min to allow the gel particles to precipitate onto the dialysis membrane. The H-shaped eluter was then carefully filled with **1X Electroelution Buffer** until both arms of the eluter and the connecting bridge were completed filled with buffer. Electroeluting was performed overnight at 4℃ with a voltage of 75 V. After overnight elution, a blue layer can be observed on the dialysis membrane of the anodic arm. For collection of the blue eluate, the supernatant in the anodic arm was carefully removed to avoid any turbulence. The more supernatant was removed, the more concentrated the eluate has become. For quantitative recovery, after most of the eluate was removed, the dialysis membranes were rinsed with an additional 100 μL of **1X Electroelution Buffer.**

4.7 Staining of Proteins in a Polyacrylamide Gel

4.7.1 Coomassie Blue Staining

The protein bands on polyacrylamide gels were detected using the method described in Short Protocols in Molecular Biology (Fourth Edition, unit 10.4). After electrophoresis, the gel was quickly rinsed twice with a large amount of distilled H_2O and was incubated with 40 mL of distilled H_2O for 15 min at room temperature. The washed gel was then either heated with 40 mL of **Stain Reagent** (0.1% (w/v) Coomassie Blue R-250, 30% (v/v) Methanol, 10% (v/v) Acetic acid) in a microwave (0.95 kW) for 30 s or incubated with **Stain Reagent** for 1 h (or overnight, if necessary). The stained gel was quickly rinsed with an excess amount of distilled H_2O to remove any excess Coomassie Blue. For the initial destaining step, the gel was incubated twice with 20 mL of **Destain A** (50% (v/v) Methanol, 10% (v/v) Acetic acid) for 10 min, with 30 mL of **Destain A** for 30 min, and then with 30 mL of **Destain A** for 60 min. During the first destaining step, the protein bands were visualized as the blue dyes were being removed. The gel was deeply destained twice with 30 mL of **Destain B** (5% (v/v) Methanol, 10% (v/v) Acetic acid) for 30 min and then incubated with 40 mL of **Destain B** either until the desired protein bands were resolved or overnight. The destined gel was quickly rinsed with distilled H_2O twice for **Destain B** removal prior to imaging.

4.7.2 Silver Staining

The highly sensitive silver staining method was used to detect protein bands at amounts higher than 0.25 ng per band in polyacrylamide gels as described by Merril et al. (1981) (Merril, Dunau et al. 1981) with minor modifications. This protocol was optimized for mini gels (7 cm x 8 cm x 10 mm). **Reagents A** and B must be prepared immediately before use, but **Reagents C** and **D** may be prepared in advance. After electrophoresis,

the protein gel was quickly washed twice with a large volume of deionized H_2O to remove any excess SDS and subsequently incubated with 40 mL of deionized H_2O prior to the fixation step. The proteins bands on a gel were fixed either with **Reagent A** (12.5% (v/v) Glutaraldehyde, 50%, v/v) for 60 min at room temperature or with two-fold diluted Reagent A (6.25%) overnight. The fixed gel was quickly rinsed multiple times with deionized water to remove excessive glutaraldehyde and subsequently incubated with 40 mL of deionized water or 15 min twice to remove all remaining glutaraldehyde. The protein bands were stained with 40 mL of **Reagent B** (1% (w/v) silver nitrate) for 60 min and rinsed for 30 min with deionized water to remove excess silver prior to developing the protein bands. To develop the bands, the gel was incubated with 10 mL of **Reagent C** (0.25% (v/v) Formaldehyde solution, 6.25% (w/v) sodium carbonate) until the protein bands of interest could be distinctly visualized. The gel was then immediately fixed with 20 mL of **Reagent D** (8% (w/v) Glycerol, 10% (v/v) Acetic acid) to preserve overdevelopment and rinsed for 15 min with a large volume of deionized water prior to being photographed. The stained gel was rapidly rinsed twice with deionized water for removal of **Reagent D** prior to imaging.

4.8 Immunoblotting and Immunodetection

Immunoblot analysis was performed using a previously described method (Lawrence, Varco-Merth et al. 2011) with slight modifications. All immunoblot buffers were freshly prepared just prior to immunoblotting and chilled on ice. An Immuno-Blot PVDF membrane (Bio-Rad, part No. 162-0255) was activated by soaking in 20 mL of 100% (v/v) methanol for at least 1 h. The gel was pre-washed with a large volume of deionized water for 30 min, incubated with **1X Protein Transfer Buffer** (25 mM Tris base, 192 mM Glycine, 20 % v/v Methanol), and electroblotted onto an activated PVDF

membrane at 350 mA for 35 min in chilled **1X Protein Transfer Buffer** through a Bio-Rad Mini Trans-Blot Cell (Bio-Rad, part No. 170-3930) according to the manufacturer's instructions (Bio-Rad, part No. M1703930). A blotted PVDF membrane was quickly rinsed with **1X Tris-buffered saline with Tween-20 Buffer** (TBST) (50 mM Tris base, 150 m NaCl, 0.05% (v/v) Tween-20) to remove an remaining 1X protein transfer buffer and was then equilibrated with **1X Blocking Buffer** (50 mM Tris base, 150 m NaCl, 0.05% (v/v) Tween-20) containing 5% (w/v) non-fat dry milk for 60 min at room temperature (or overnight at 4℃). The PVDF membrane was quickly rinsed in **1X TBST Buffer** prior to incubation with the primary antibody. The membrane was incubated in 20 mL of **1X Blocking Buffer** (50 mM Tris base, 150 m NaCl, 0.05% (v/v) Tween-20, 5% (w/v) non-fat dry milk) containing the" x" µL of **Polyclonal-primary-antibody** at an appropriate dilution for 60 min at room temperature (or overnight at 4℃) and then washed three times with 20 mL of **1X TTBS Buffer** prior to incubation with the secondary antibody. For secondary antibody incubation, the membrane was incubated with 20 mL of **1X Blocking Buffer** (50 mM Tris base, 150 m NaCl, 0.05% (v/v) Tween-20, 5% (w/v) non-fat dry milk) containing "y" µL **HRP- conjugated-goat-anti-rabbit-IgG** at 1:5000 dilution (Santa Cruz Biotechnology, Part No. SC-2301) and "z" µL **StrepTactin-HRP-conjugate** in 1:5000 dilution (Bio-Rad, Part No. 161-0380) for an additional 60 min at room temperature and then washed three times for 10 min with 20 mL of **1X TTBS Buffer**. The secondary antibody luminescence was activated with the Immun-Star HRP substrate (Bio-Rad, part No. 170-0541), and chemiluminescent images of the bound conjugates were taken with a Kodak Gel Logic 440 CCD camera using a 2-min dark exposure period.

4.9. Chromatography

4.9.1 Desalting and Buffer Exchange

The **PD-10 column** is a gel filtration column containing **Sephadex G-25 medium**, which allows separation based on differences in size. Typically, the PD-10 column (GE Healthcare Life Sciences, Part No. 17-0851-01) is used for desalting and buffer exchange. The column was prepared using methods recommended by GE Healthcare (GE Healthcare Life Sciences, Part No. 52-1308-00 BB). The fractions collected through a sucrose gradient containing CF_1F_O ATP synthase protein complexes were desalted by passing through a PD-10 desalting column. The desalting column was equilibrated with 25 mL of the **Desired Desalting Buffer** or the **Equilibration Buffer**) at 4℃ via gravity flow, and a maximum of 2.5 mL of fraction was then added to the top of the column. After the fraction completely enters the packed bed of the column, the fraction was eluted with 4 mL of equilibration buffer at 4℃ via gravity flow. Immediately after desalting, the collected fraction (4 mL) was concentrated with an Amicon centrifugal filter unit over a 100-KDa cutoff membrane (EMD Millipore, Part No. UFC-910096) according to manufacturer's recommended instructions at 3,000xg_{max} using a TS-5.1-500 swinging-bucket rotor (Beckman Coulter, Part No. 368308) and an Allegra-25R Benchtop centrifuge (Beckman Coulter, Part No. 369436) at 4°C. The final volume of the retained concentrated fraction was close to 500 μL, and this fraction was then immediately either subjected to the desired experiments or flash-frozen in liquid nitrogen as 450-μL aliquots in 500-μL storage straws and stored in a liquid nitrogen dewar for future use.

4.9.2 Dye-ligand Chromatography

The protocol used for affinity chromatography is based on a previously described protocol (Poetsch, Seelert et al. 1999, Seelert, Poetsch et al. 2000) with slight modifications. The **1X R120 Pre-equilibration Buffer (**10 mM Tris-NaOH pH 8.0), **1X R120-equilibration Buffer** (20 mM Tris-NaOH pH 8.0, 20% (w/v) Glycerol; 5 mM $MgSO_4$, 4 mM β-DDM) and **1X R120 Elution Buffer** (1.5 M NaCl, 20 mM Tris-HCl pH 8.0, 20% (w/v) Glycerol, 5 mM $MgSO_4$, 4 mM β-DDM) were freshly prepared and the detergent was added after deaeration prior to use, filtration was performed through a 0.22-µm-pore-size filter (EMD Millipore, Part No. SLGP033RB) and deaeration was performed for 60 min. The detergents have to be added and then completely dissolved prior to chromatographic purification. The protein sample in the presence of the β-DDM detergent was desalted by passage through a PD-10 column with **1X R120 Equilibration Buffer** containing 4 mM β-DDM at 4℃, concentrated with an Amicon centrifugal filter unit over a 100-KDa cutoff membrane (EMD Millipore, Part No. UFC-910096) according to the manufacturer's instructions at 3,000xg_{max} using a TS-5.1-500 swinging-bucket rotor (Beckman Coulter, Part No. 368308) and an Allegra-25R benchtop centrifuge (Beckman Coulter, Part No. 369436) at 4℃ and finally adjusted to a final concentration of 4 mg of protein/mL. Then, 4 mL of the **Reactive Red-120 Agarose Resin** (Sigma, Part No. R0503) was manually packed in **1X R120 Pre-equilibration Buffer** with GE column XK 26/20 kit (GE Healthcare Life Sciences, Part No. 28-9889-48) according to the AKTA manufacturer's instruction manual and then equilibrated with at least six column volumes of **1X R120 Equilibration Buffer** at 4℃ prior to application of the protein samples. The run parameters used for negative chromatography are listed in Appendix E. The intact ATP synthase complexes were eluted with **1X R120 Elution Buffer**. Thereafter, the minor

impurities were eluted with 12 column volumes of **1X R120 Elution Buffer**. The column was regenerated with at least six column volumes of **1X R120 Equilibration Buffer** prior to the next run. The column was cleaned with at least six column volumes of **1X R120 Pre-equilibration Buffer** and then stored in 20% (v/v) ethanol solution at 4℃.

4.9.3 Anion Exchange Chromatography

The anion affinity chromatography procedure for purification is based on a previously described protocol (Poetsch, Seelert et al. 1999) with slight modifications. The **1X Equilibration Buffer** (10 mM Tris-NaOH pH 8.0, 10 mM $MgCl_2$, 1 mM β-DDM) and **1X Elution Buffer (**2 M NaCl, 10 mM Tris-NaOH pH 8.0, 10 mM $MgCl_2$, 1 mM β-DDM) were freshly prepared with the exception that the detergent was added prior to use, filtration was performed through a 0.22-μm-pore-size filter (EMD Millipore, Part No. SLGP033RB) and deaeration was performed for 60 min. The detergents have to be added and then completely dissolved prior to chromatographic purification. The protein sample in the presence of the β-DDM detergent was desalted by passage through a PD-10 column with **1X Equilibration Buffer** containing **1 mM β-DDM Solutuion** at 4℃, then concentrated with an Amicon centrifugal filter unit over a 100-KDa cutoff membrane (EMD Millipore, Part No. UFC-910096) according to manufacturer's instructions at 3,000xg_{max} using a TS-5.1-500 swinging-bucket rotor (Beckman Coulter, Part No. 368308) and an Allegra-25R benchtop centrifuge (Beckman Coulter, Part No. 369436) at 4℃ and adjusted to a final concentration of 10 mg of protein/mL. The **POROS 20 HQ column** (Life technologies, Part No. 12322-26) was used for anion affinity chromatography. The column was prepared according to the Applied Biosystems's instructions manual by washing with 10 column volumes (17 mL) of

deionized water to remove all of the storage reagent and subsequently equilibrating with at least 10 column volumes (17 mL) of **1X Equilibration Buffer** at 4℃ prior to application of the protein sample. The chromatographic parameters are described in Appendix E. The ATP synthase protein was eluted with a linear gradient from 0% to 25% (v/v) of **1X Elution Buffer** in 30 column volumes (51 mL) at a flow rate of 5 mL/min. The collected fractions (0.5 mL per fraction) containing the protein of interest were pooled for the subsequent experiments. Thereafter, the minor impurities were eluted from 25% to 100% of **1X Elution Buffer** with another 10 column volumes (17 mL) at a flow rate of 5 mL/min. The column was cleaned with 10 column volumes (17 mL) of deionized water and regenerated with another 10 column volumes of **1X Equilibration Buffer** (17 mL) at a flow rate of 5 mL/min prior to application of the next protein sample.

4.10 ATP Synthase Hydrolysis Assay

The assay of the in-gel ATP hydrolysis activity basically follows the principles of the protocol established for mitochondrial complex V by Zerbetto et al. (1997) (Zerbetto, Vergani et al. 1997) and the method for the measurement of the chloroplast ATP synthase developed by Suhai et al. (2009) (Suhai, Heidrich et al. 2009) with the following minor modifications. The principle of this qualitative assay is that free phosphate ions released from ATP molecules during ATP hydrolysis would react with lead ions to form white lead phosphate precipitates. The assay buffers were freshly prepared with the exception of the detergents, which were added as described in Appendix 1 and have to be completely dissolved in the buffers. The solid ATP (Sigma, Part No. A2383) has to be freshly added just before the assay to avoid ATP hydrolysis in the buffers. The native gel was pre-equilibrated with **1X Pre-incubation Buffer** (40

mM Tris-HCl pH 8.0, 1.5 mM $MgCl_2$, 4 mM ATP-Na_2) supplemented with the following detergents at a concentration of 30 mM for 3 h at room temperature: n-octyl β-D-glucopyranoside (OG) (Glycon Biochemicals, Part No. D97001-C), n-dodecyl β-maltoside (β-DDM) (Glycon Biochemicals, Part No. D97002-C), N,N-dimethyl-1-dodecanamine-N-oxide (LDAO) (Affymetrix/Anatrace, Part No. D360), or taurodeoxycholate (TDOC) (Sigma-Aldrich, Part No. T0875). This pre-equilibration step was followed by a 1-min wash with deionized water and incubation with **1X Development Buffer** (35 mM Tris-HCl pH 8.0, 270 mM Glycine; 14 mM $MgSO_4$, 0.075% (w/v) $Pd(NO_3)_2$, 0.8 mM ATP-Na_2, 20% (v/v) Methanol) for 30 min up to 24 h at room temperature. The increase in the activity of ATP hydrolysis corresponds to the increase in the development of white lead phosphate precipitates. The white bands of lead phosphate precipitates could be visualized after incubation for only 30 min. The hydrolysis reaction could be stopped by incubating with 50% (v/v) methanol for 30 min and subsequently transferring to deionized H_2O, and this step was followed by imaging under a specific blue background (UV light box) with a Nikon COOLPIX P600 digital camera. The lead phosphate precipitates could be dissolved by incubating with the acidic fixing solution (50% methanol and 10% acetic acid) for re-staining with either Coomassie Blue G-250 dye or silver stain.

4.11 ATP Synthesis Assay

4.11.1 Liposome Preparation

The ATP synthesis activity of purified ATP synthase was measured using a previously described assay (Turina, Samoray et al. 2003). For the assay, a liposome preparation was first prepared, and this step was followed by protein reconstitution and then measurement. The liposome preparation was performed based on the detergent-dialysis

method adapted from Fischer and Gräber (1999) (Fischer and Graber 1999). Liposomes are prepared from phosphatidylcholine (PC) and phosphatidic acid (PA). Stocks of **PC Solution** (25 g/L L-α-phosphatidylcholine (Avanti, Part No. 840051) in chloroform storage at -20℃, light protected) and **PA solution** (2.5 g/L L-α-phosphatidylcholine (Avanti, Part No.840101) in chloroform storage at -20℃, light protected) were prepared in chloroform and stored at -20℃ as directed. The **1X Lipid Solubilization Buffer** (10 mM Tricine-NaOH pH 8.0, 100 µM EDTA-Na_2 pH 8.0, 500µM DTT, 7.2 g/L Sodium cholate, 3.6 g/L Sodium desoxycholate) and **15X Dialysis Buffer** (150 mM Tricine-NaOH pH 8.0; 3 mM EDTA-Na_2 pH 8.0; 3.75 mM DTT; 37.5 $MgCl_2$) were freshly prepared as described. The lipid mixture (16 g/L) containing phosphatidylcholine and phosphatidic acid in a mass ratio of 19:1 was prepared by mixing 6.8 mL of **PC Stock Solution** and 3.6 mL of **PA Stock Solution**. The chloroform in the mixture was completely removed under a stream of nitrogen gas through a rotary evaporator to obtain a lipid film cake. The dried lipid mixture was completely resuspended in 10 mL of **1X Lipid Solubilization Buffer** through repeating hand-swing vortexing under a stream of nitrogen gas. This lipid-loosening suspension was sonicated three times in a tip sonicator (Branson Sonifier 250 at 20 kHz and 150 W) in an ice bath for 30 s at 30-s intervals to form an emulsion (liposome cream) under a stream of nitrogen gas. The lipid-emulsion solution was frozen at -20℃ overnight. The **1X Dialysis Buffer** was prepared by mixing 1 L of **15X Dialysis Buffer** with 14 L of deionized water and heated to 30℃ prior to dialysis. Custom-built dialysis chambers were assembled with dialysis membranes (5 kDa) that were previously soaked with 1X dialysis buffer for a few hours. The frozen lipid-emulsion solution was thawed at room temperature, and then 2 mL of the thawed lipid-emulsion solution was pipetted into each of the assembled dialysis chambers. This lipid emulsion solution was

dialyzed against 15 L of **1X Dialysis Buffer** at 30℃ for 5 h using a custom-built rotary device. At the end of the dialysis, this lipid emulsion solution was transformed to an egg-white-like lipid suspension. The collected egg-white-like lipid suspension (~10 mL) was extruded by passing through a polycarbonate membrane with a pore size of 0.2 µm (GE Healthcare Life Sciences, Part No. 800281) for at least 10 cycles (total of 20 passes through the membrane) via a mini-extruder (Avanti, Part No. 610000) to yield homogenous liposomes with a diameter close to the pore size. After extrusion, the egg-white-like lipid suspension should transform to a slightly hazy transparent lipid solution. The extruded liposomes have to be immediately applied for protein reconstitution.

4.11.2 CF_1F_O Protein Reconstitution

ATP synthase was reconstituted into the prepared liposomal membrane using the protocol described by Richard et al. (1990) (Richard, Rigaud et al. 1990). The liposomal membrane was destabilized with the freshly prepared **Triton X-100 solution** (100 g/L) detergent to allow their reconstitution into the protein-detergent micelles. The **1X Reconstitution Buffer** (20 mM Succinic acid, 20 mM Tricine-NaOH pH 8.0, 0.6 mM KCl, 80 mM NaOH) have to be freshly prepared just prior to reconstitution. The SM_2 Bio-Beads were activated according to either the Bio-Rad manufacturer's instruction manual or the method described by Holloway (1973) (Holloway 1973). Then, 200 µL of the reconstitution solution was freshly prepared by pipetting the reagents in the sequence shown in Appendix D. The reconstitution reaction was stirred at 50 rpm for 1 h at room temperature, and 70 mg of activated SM_2 Bio-Beads was then added to remove the detergent and re-stabilize the liposomal membranes. The mixture was then incubated for another hour at room temperature. After reconstitution, the proteoliposome solution was carefully transferred into new microcentrifugation tubes

without any SM_2 Bio-Beads and immediately used for the activity measurement; however, the proteoliposome solution could be stored at 4℃ for one week without loss of activity

4.11.3 Measurement of Enzymatic Activity

4.11.3.1 Calibration and Baseline Recording

The ATP synthesis activity was measured using the established method described by Richard et al. (1990), Fischer et al. (1994), Fischer and Graber (1999), and Turina et al. (2003) (Richard, Rigaud et al. 1990, Fischer, Etzold et al. 1994, Fischer and Graber 1999, Turina, Samoray et al. 2003). **15 µM ATP Sock Solution** and **100 nM ADP Stock Solution** were prepared and stored in 10-µL aliquots at -20℃ for future use. The **1X Basic Incubation Buffer** (200 mM Tricine-NaOH pH 8.0, 5 mM NaH_2PO_4, 160 mM KOH, 2.5 mM $MgCl_2$, 100 µM ADP, adjust pH up to 8.8 with NaOH) was freshly prepared and immediately used for activity measurement. The **2X Luciferin/Luciferase Reagent** (Roche, Part No. 11699695001) was prepared according to Roche's instruction manual. It is known that a low amount of ATP molecules is present in the **100 mM ADP Stock Solution**, which can exert a negative influence on the measurement of newly synthesized ATP molecules. To determine the amount of ATP molecules contaminating the basic incubation buffer, 885 µL of **1X Basic Incubation Buffer** was mixed with 15 µL of **2X Luciferin/Luciferase Reagent** (Roche, Part No. 11699695001), and the mixture was then incubated for 1 min in the dark and then placed in an LKB-1250 luminometer connected to a chart recorder to record the baseline measurement. The concentration of ATP molecules in the basic incubation buffer was detected by the increase in luminescence just after placement in an LKB-1250 luminometer (Equation 4.11.3.1, see Appendix F). After the signal

reaches a constant level, an additional 1 µL of **10 nM ATP Standard Solution** was added. The amount of ATP contamination in the basic incubation buffer was calculated using the equation 4.11.3.1 (see Appendix F).

4.11.3.2 Measurement of ATP Synthesis

The **10 mM Valinomycin Stock Solution** was prepared in 100 % (v/v) methanol and stored in 10-µL aliquots at -20℃ for future use. The **1X Acidic-incubation Solution** (20 mM Succinic acid, 5 mM NaH_2PO_4, 0.6 mM KOH, 2.5 mM $MgCl_2$, 20 µM Valinomycin, freshly added, 100 µM ADP, freshly added, adjust pH up to 4.7 with NaOH) was freshly prepared and immediately used for the activity measurements. The proteoliposomes are energized by acid-base incubation with the K+/valinomycin diffusion potential. The $\Delta\varphi$ between the internal and external proteoliposomes was generated by low internal and high external K^+ concentrations in the presence of valinomycin, and the ΔpH was generated by acid-base incubation. Then, 885 µL of the **1X Basic-incubation Buffer** (200 mM Tricine-NaOH pH 8.0, 5 mM NaH_2PO_4, 160 mM KOH, 2.5 mM $MgCl_2$, 100 µM ADP, adjust pH up to 8.8 with NaOH) was mixed with 15 µL of **2X Luciferin/Luciferase Reagent** (Roche, Part No. 11699695001), and the mixture was then incubated for 1 min in the dark and placed in an LKB-1250 luminometer to determine the baseline measurement. Then, 15 µL of the proteoliposome suspension adjusted to a final concentration of 100 nM was mixed with 100 µL of **1X Acidic -incubation Buffer** , and the mixture was subsequently incubated at room temperature for 3 min in the dark. Then, 100 µL of the acidified proteoliposomes was immediately injected using a Hamilton model 710 syringe (Hamilton, Part No. 7638-01) connected with a custom-made 5-in 23s-gauge needle (Hamilton, Part No. 7804-09) directly into the **1X Basic-incubation Buffer** that was

previously placed in the chamber of an LKB-1250 luminometer. The increasing concentration of newly synthesized ATP molecules was immediately detected by the increase in luminescence just after injection (Equation 4.11.2, see Appendix F). After the synthesis of new ATP reaches saturation, an additional 1 μL of the **10 nM ATP Standard Solution** was added for calibration. The turnover rate of ATP synthesis per ATP synthase was calculated from the initial slope and the equation 4.11.3.2 (see Appendix F).

4.12 Monolayer Two-dimensional Crystallization of Intact CF_1F_O

The purpose of the two-dimensional crystallization of the CF_1F_O ATP synthase protein complex on a lipid monolayer is to produce 2D crystals of the CF_1F_O ATP synthase protein complex for future structural studies using electron crystallography at high resolution. We also plan to attempt fixed target femtosecond X-ray diffraction studies in the future. Two approaches were applied to establish a lipid monolayer, and these are based on the air-water interface method described by Lebeau and Vénien-Bryan (2013) (Lebeau and Venien-Bryan 2013) with some modifications.

4.12.1 Preparation of Membrane Protein Solution and Lipid Solution

Immediately after their isolation and concentration, the CF_1F_O ATP synthase protein complexes were dialyzed against **2D Crystal Buffer** (10 mM Tris-NaOH pH 8.0, 5 mM $MgCl_2$, 4 mM β-DDM, freshly added) via a disposable PD-10 desalting column (GE Healthcare Life Sciences, Part No. 17-0851-01) as described in detail in Section 4.9.1. The concentration of buffer-exchanged CF_1F_O ATP synthase protein complexes was determined and adjusted to a final concentration of 10 mg/mL (Section 4.5.4). The lipids in chloroform: POPA (Avanti Polar Lipids, Part No. 840857C), POPC (Avanti

Polar Lipids, Part No. 850457C), POPE (Avanti Polar Lipids, Part No. 850757C), and POPG (Avanti Polar Lipids, Part No. 840457C) were dried under a stream of argon gas to completely remove chloroform, and the dried lipids were subsequently hydrolyzed in 100 % (v/v) methanol and stored under an argon atmosphere at -20℃ in air-tight Amber glass bottles for later use. Prior to formation of the lipid monolayer, the **Lipid Working Solutions** (95% (v/v) of 25 mg/mL POPC, 25% (v/v) of 25mg/mL POPA in methanol; 49% (v/v) of 25 mg/mL POPC, 49% (v/v) of 25 mg/mL POPE, 2% v/v of 25 mg/mL POPG in methanol; 49% (v/v) of 5 mg/mL POPC, 49% (v/v) of 25 mg/mL POPE,1% (v/v) of 25 mg/mL POPG, 1% (v/v) of 25 mg/mL POPA in methanol) were freshly prepared as described in Appendix 1 to obtain a final concentration of 25 mg/mL and stored under an argon atmosphere in air-tight Amber glass bottles for the subsequent experiments.

4.12.2 Teflon Block Preparation

A homemade eight-well Teflon block provided by Dr. James Evans (The Pacific Northwest National Laboratory) was designed for formation of the lipid monolayer according to the method described by Lebeau and Vénien-Bryan (Lebeau and Venien-Bryan 2013). Each well in the Teflon block contains a reservoir with a volume of approximately 62 μL of **2D Crystal Buffer** for formation of the lipid monolayer and a small-angled side channel for adding either protein samples or the SM-2 Bio-Beads resin (Bio-Rad, Part No. 152-3920). After use, the Teflon block should be thoroughly cleaned with chloroform to completely dissolve any lipids on the block and then extensively rinsed with deionized water. In addition, the block should be immersed in 100% (v/v) methanol for long-term storage. Prior to use, the Teflon block should be cleaned with 100% (v/v) chloroform and deionized water to ensure that there is no lipid

on the block and then subjected to hydrophobic treatment in clean methanol for at least 30 min. The block should then be air-dried in an upside-down position inside a Petri dish with Kimwipes in the clean bench for late use.

4.12.3 Formation of a Lipid Monolayer

The dried hydrophobic Teflon trough was placed on top of a water-saturated paper towel in a Petri dish as the humidity chamber. A volume of approximately 62 μL of **2D Crystal Buffer** was slowly added to each reservoir of the Teflon block to obtain the maximum surface tension. Prior to lipid deposition, a 2.5-μL Hamilton syringe (Hamilton, Part No. 87942) was cleared with 100% (v/v) chloroform at least five times to remove any lipid contamination. The tip of the needle of the 2.5-μL Hamilton syringe filled with 2.5 μL of the **Lipid Working Solution** (25 mg/mL) was brought as close as possible to the center of the top of the solution in the reservoir, and the lipid was then gently deposited on top of the solution to yield a final lipid concentration as close to 1 mg/mL as possible, which is higher than the concentration required to form a lipid monolayer in such a small volume. Immediately after lipid deposition, the block was incubated for 1 h in the closed Petri dish to allow the deposited lipid to spread out and form a lipid monolayer at the air-water interface as methanol evaporates.

4.12.4 Membrane Protein Insertion

Immediately after incubation, an approximate volume of 7 μL of freshly prepared protein solution containing CF_1F_O ATP synthase protein complexes (10 mg/mL), which was solubilized in the presence of 4 mM β-DDM, was gently injected through the side channel into the bottom of the reservoir via a 10-μL Hamilton syringe (Hamilton, Part No. 80301) to obtain a final protein concentration of approximately 1 mg/mL and a

protein-to-lipid ratio of approximately 1 (w/w). Because the solution in the reservoir may evaporate during the previous incubation, an appropriate volume of **2D Crystal Buffer** should be added (if necessary) through the side channel into the reservoir via a 10-μL Hamilton syringe to obtain the maximum surface tension prior to additional incubation. The trough was incubated at room temperature for 4 h in the closed Petri dish sealed with parafilm and was maintained as stable as possible to minimize disturbance of the protein reconstituted in the lipid monolayer.

4.12.5 Detergent Removal from Reconstitution Solution via Bio-Beads

The SM-2 Bio-Beads resin (Bio-Rad, Part No. 152-3920) used to adsorb detergents from the reconstitution solution have to be activated by washing with excess methanol and then with excess deionized water to completely remove the methanol. The activated Bio-Beads then have to be maintained in deionized water in a glass bottle and stored at 4℃ for future use. After incubation, 10 activated Bio-Beads collected from the bottom of the bottle were gently added through the side channel into the bottom of the reservoir using forceps and then incubated for an additional 2 h to allow the detergents in the reconstitution solution to be adsorbed onto the Bio-Beads. Prior to overnight incubation, an additional 10 Bio-Beads were added, and a few microliters of **2D Crystal Buffer**, were then added, if necessary, to maintain the surface tension. The Teflon block was incubated at room temperature overnight in a closed Petri dish sealed with parafilm to prevent water evaporation.

4.12.6 Imaging through Transmission Electron Microscopy

After overnight incubation, most detergents in the reconstitution solution should be trapped on the Bio-Beads. CF_1F_O ATP synthase protein complexes are supposed to

spontaneously insert into the lipid monolayer. The Veco carbon-coated 400 mesh copper grid (Electron Microscopy Sciences, Part No. 0400-Cu) was freshly glow-discharged to give the carbon coating on the grid an overall hydrophilic surface (supplied by Dr. James Evans). The lipid monolayer was transferred to the shiny side of the grid (dull side up) by touching the top of the reconstitution solution in the reservoir for at least 2 s using EM reverse grip forceps (Electron Microscopy Sciences, Part No. 78317-2AX), and this step was followed by negative staining. The sample side of the grid was gently touched to the top of the reconstitution solution with the lipid monolayer for 1 s, and this step was followed by negative staining. Immediately after the monolayer was transferred, the grid was stained by laying the grid shiny-side down and allowing it to touch the surface of a drop of 2% uranyl acetate solution for at least 3 s, and this step was followed by rinsing with water by touching a drop of deionized water for 3 s. Prior to air-drying, the excess staining solution and deionized water on the grid were completely soaked up by touching only the outer copper ring of the grid using a piece of a Whatman filter paper wedge (GE Healthcare, Part No. 1001-100). The shiny side of the grid was placed face-side down to allow the grid to air dry until the surface of the shiny side of the grid looks like shiny again. Both the negative-stained and EM images obtained with a JEOL JSM-6300 transmission electron microscope equipped with a CCD camera were obtained at the Electron Microscopy (EM) Laboratory, Department of Life Sciences, Arizona State University. Technical support for negative staining and EM imaging was provided by Dr. Robert Roberson (EM Laboratory Facility Supervisor) and Dr. David Lowry (EM Laboratory Manger).

CHAPTER 5

RESULTS AND DISCUSSION

5.1 Isolation of Intact Chloroplasts

The first step in a large-scale purification procedure of the intact CF_1F_O ATP synthase from spinach chloroplasts was the isolation of intact spinach chloroplasts to completely remove non-chloroplast ATP synthase contamination. The isolation step was based on published procedures with some modifications (Perry, Li et al. 1991, van Wijk, Peltier et al. 2007). The intact chloroplasts were isolated from approximately 1 kg of prepared spinach leaves via discontinuous Percoll gradient centrifugation (Figure 5.1 B, lane 1). For optimal yield of isolated intact chloroplasts, prior to and during the isolation procedure, the spinach leaves typically must be stored at 4°C in the dark at least three days to avoid high levels of starch accumulation (Figure 5.1 A). The majority of unhomogenized cell debris was removed via multiple layers of cheesecloth and Miracloth. Organelles other than chloroplasts were removed by low-speed centrifugation. A thin layer of starch pellet was identified on top of the sedimentation of the green pellets that contained crude chloroplasts. Hence, a greater amount of organelles and starch was removed with multiple centrifugations. The crude chloroplasts were resuspended by gently swirling the suspension. Although most of the intact chloroplasts were present in the crude chloroplast fraction, broken chloroplasts were found in the fraction that was separated from undamaged chloroplasts by Percoll gradient centrifugations. In the Percoll gradients, broken chloroplasts, which have a much lighter density compared to intact chloroplasts, formed a band on the upper gradient, whereas intact chloroplasts sediment to the lower gradient as a narrow green band (Figure 5.1 C, lane 4 and lane 5). Poor separation was observed when an excess of chloroplasts overloaded the gradient (Figure 5.1 C, lane 3).

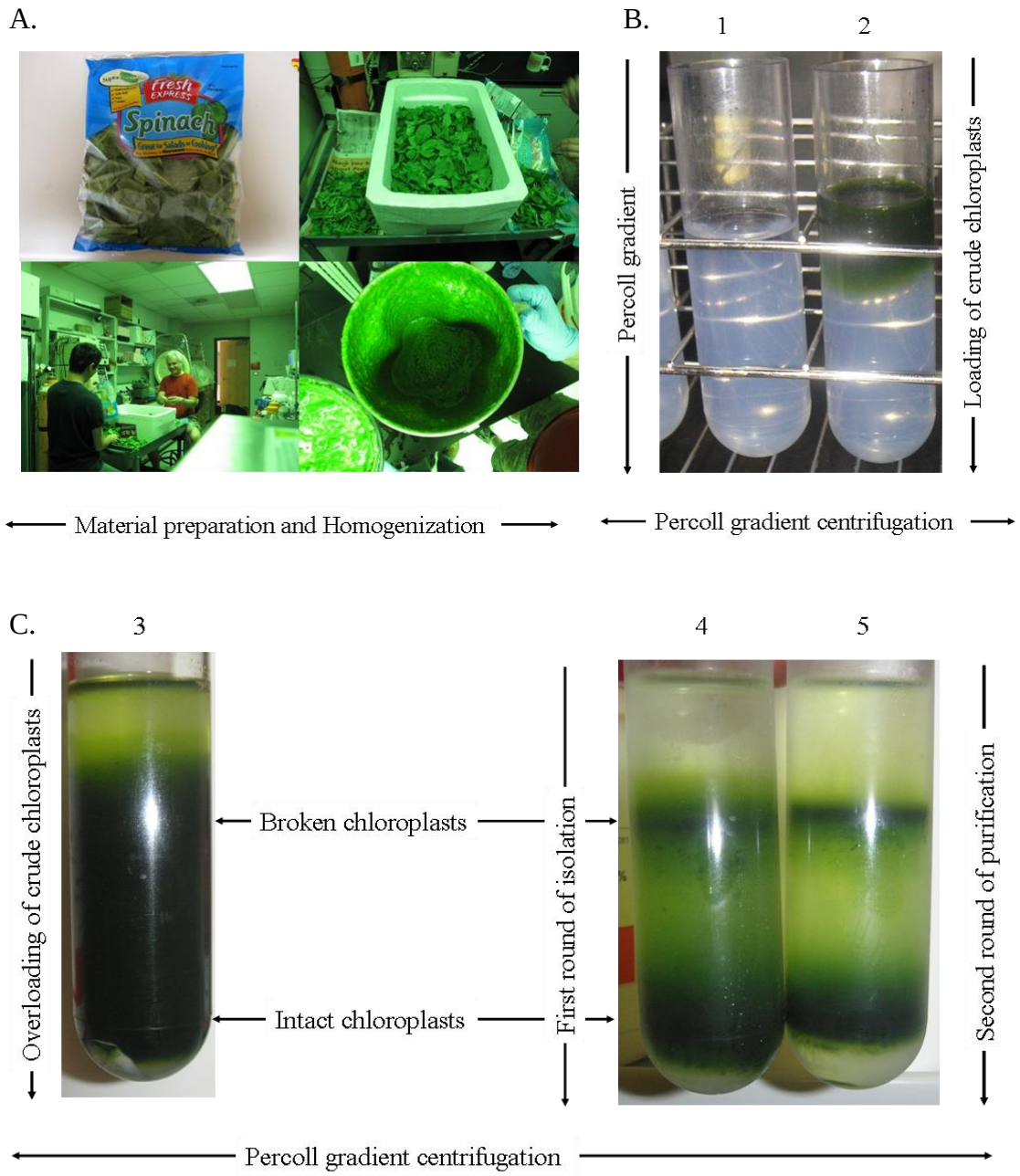

Figure 5.1 Isolation of Intact Chloroplasts via Percoll Gradient Centrifugation. Isolation of intact chloroplasts from spinach via Percoll gradient centrifugation. (A). Spinach leaves are sorted and homogenized under green light. (B and C). Isolation of intact chloroplasts via Percoll gradient centrifugation. Following the first isolation (lane 4), two green fractions appear in the Percoll gradient. The upper fraction contains broken chloroplasts, and the intact chloroplasts are found in the lower fractions. The collected fractions containing crude intact chloroplasts are applied to the second round of purification (lane 5). Approximately 150–200 g (wet weight) of intact chloroplasts of higher purity can be collected after two rounds of centrifugation. [Lane 1: ready Percoll density gradient; Lane 2: crude chloroplasts loaded on top of the Percoll gradient; Lane 3: poor separation due to overloading; Lane 4: the first isolation; Lane 5: the second round of purification].

To increase the efficiency of the Percoll gradient purification, the maximum loading volume on Percoll gradients was optimized by determining a unit chlorophyll basis (mg of total chlorophyll). Therefore, every 2 mL of loading volume of resuspended chloroplasts contained among 500 to 1000 mg of chlorophyll. Following centrifugation, immediately after stripped chloroplasts were removed using a vacuum aspirator collection system, the lower fractions that contained refined intact chloroplasts were carefully collected. Notably, although Percoll can form self-forming gradients that are useful in separating organelles according to their density, one disadvantage of Percoll gradients is that Percoll particles must be completely removed prior to performing subsequent experiments, particularly chloroplast envelope preparation. Percoll removal can be accomplished by either centrifugation of the collected gradient fraction at high speed (100,000x*g*, 2 h, 4℃), resulting in the sedimentation of the target organelles on a layer of compact Percoll, or dilution of the target organelles with washing buffer with recovery as a pellet following centrifugation for multiple cycles, which was used for the further preparation of refined intact chloroplasts.

5.2 Isolation of Intact Thylakoid Membranes

The second step in the isolation of the CF_1F_O ATP synthase was to isolate intact thylakoid membranes. The stromal fraction contains significant quantities of water-soluble proteins. The most notable protein found in the stromal fraction is ribulose-1,5-bisphosphate carboxylase, commonly known by the abbreviation RuBisCO, which is an enzyme involved in the first step of carbon fixation, a process by which atmospheric carbon dioxide and ribulose-1,5-bisphosphate are converted into 3-phosphoglycerate and other intermediate products, and, ultimately, into energy-rich molecules.

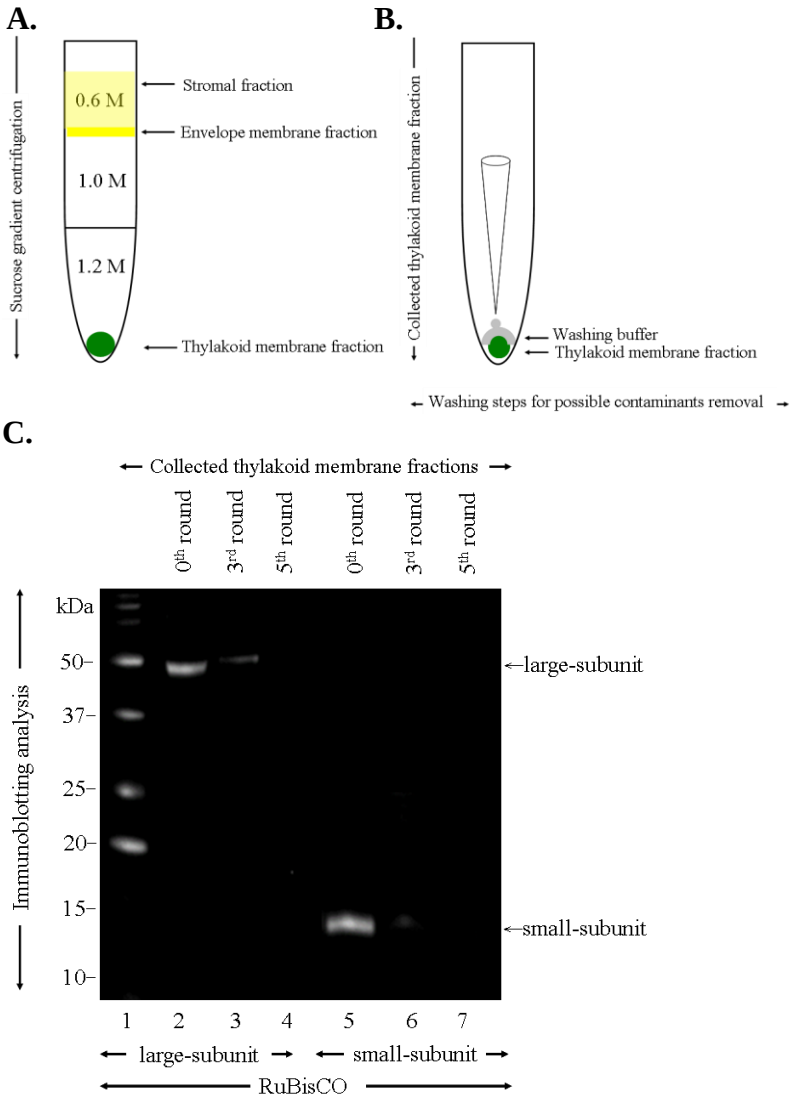

Figure 5.2 Insolation of Intact Thylakoid Membranes. Schematic diagram of the separation of thylakoid membrane and envelope membrane fractions and immunoblotting analysis of the purified thylakoid membrane fractions. (A). Thylakoid membranes are separated from stroma and envelope membranes using serial sucrose gradient centrifugation, resulting in thylakoid pellets. (B). Prior to suspension of the thylakoid pellets, the pellet surfaces must be rinsed multiple times to remove possible contaminants. (C). To remove possible contaminants from the thylakoid membrane fraction, the collected fraction undergoes multiple rounds of the washing-centrifugation step. The fractions collected after each round are analyzed by immunoblot analysis against the large and small subunits of RuBisCO proteins. [Lane 1: Precision Plus Protein™ Dual Color Standards (Bio-Rad, USA); Lane 2: original fraction of the thylakoid membranes (against the RuBisCO large subunit) (LSU, ~52 kDa) (Agrisera, No. AS03 037); Lane 3: third round of the thylakoid membrane fraction (against the RuBisCO large subunit); Lane 4: fifth round of the thylakoid membrane fraction (against the RuBisCO large subunit); Lane 5: original fraction of the thylakoid membranes (against the RuBisCO small subunit) (SSU, ~14 kDa) (Agrisera, No. AS07 259); Lane 6: third round of the thylakoid membrane fraction (against the RuBisCO small subunit); and Lane 7: fifth round of the thylakoid membrane fraction (against the RuBisCO small subunit)].

RuBisCO is most likely the most abundant protein on Earth. In contrast to the stromal fraction, the thylakoid membrane fraction only contains membrane-bound photosynthetic protein complexes including CF_1F_O ATP synthase. To separate the thylakoid membrane fraction from both stromal and envelope membrane fractions, the intact chloroplasts were ruptured by hypotonic shock and subsequently applied on a discontinuous sucrose gradient. Two rounds of centrifugation resulted in the sedimentation of the thylakoid membrane fraction on the bottom of the tube, whereas the envelope membrane fraction was located at the interface between 0.6 M and 1 M sucrose. Figure 5.2 A shows a schematic diagram of the result of the separation of the thylakoid membrane and envelope membrane fractions using sucrose gradient centrifugation. The analytical results indicated that the thylakoid membrane fraction was contaminated by RuBisCO proteins. Two strategies to reduce any unexpected contamination were introduced for these thylakoid membrane fractions. The surface of the thylakoid membrane pellet was carefully rinsed in washing buffer diagrammatically shown in Figure 5.2 B. A greater number of rinsing steps led to greater removal of contaminants. The thylakoid membrane fractions underwent multiple cycles of washing and centrifugation steps to completely remove any possibly remaining stromal proteins, particularly RuBisCO proteins. The immunoblot analysis of these multiple washing-centrifugation cycles is shown in Figure 5.2 C. A comparison of the immunoblot analyses indicated that the thylakoid membrane fraction contained lower levels of the large and small subunits of RuBisCO proteins in the third round of washing and centrifugation (Figure 5.2C, lane 3 and lane 6), and in the last round (Figure 5.2 C, lane 4 and lane 7), no RuBisCO proteins remained in the thylakoid fraction compared with the original fraction (Figure 5.2C, lane 2 and lane 5).

5.3 Isolation of the Intact CF_1F_O ATP Synthase

The isolation of intact CF_1F_O ATP synthase complexes was performed as described in the Materials and Methods using a protocol modified from previou literatures (Fromme, Boekema et al. 1987, Fromme 1988, Turina, Samoray et al. 2003, Varco-Merth, Fromme et al. 2008). The isolated thylakoid membrane fragments were solubilized using a combination of nonionic detergent (β-D-octylglucoside, OG) and anionic detergent (sodium cholate) in the presence of solid DTT. Most of the CF_1F_O ATP synthase complexes, including other membrane proteins, were extracted from the thylakoid membrane fragments with 30 mM OG and 12.5 mM sodium cholate at total chlorophyll concentration of 5 mg/mL. Subsequently, the solubilized membrane proteins were separated from insoluble membrane fragments via ultracentrifugation. The solubilized membrane proteins were precipitated by ammonium sulfate. The first precipitation at 4℃ between 10% and 30% (v/v) saturated ammonium sulfate attempted to precipitate most of the photosynthetic proteins. An insignificant amount of CF_1F_O ATP synthase complexes was precipitated in the second precipitation between 30% and 35% (v/v), as indicated by both Tricine SDS-PAGE (Figure 5.3 A, lane 4) and immunoblot analysis, which identified the c-subunit of the ATP synthase (Figure 5.3 B, lane 12). In the third precipitation step from 35% to 45% (v/v), most of the CF_1F_O ATP synthase complexes were quantitatively precipitated with 45% (v/v) saturated ammonium sulfate at 4℃, as shown in Tricine SDS-PAGE and immunoblot analysis (Figure 5.3 A, lane 6 and Figure 5.3 B, lane 14, respectively). An extremely low concentration of CF_1F_O ATP synthase complexes remained in the supernatant (3S) of the 45% (v/v) precipitation, as shown in Figure 5.3 A, lane 7 and Figure 5.3 B, lane 15. The remaining CF_1F_O ATP synthase complexes were precipitated with 50% (v/v) saturated ammonium sulfate (Figure 5.3 A, lanes 8, 9, and Figure 5.3 B, lanes 16 and

17). Notably, the final precipitates enriched in the CF_1F_O ATP synthase complexes possessed a greenish color. Attempts to prepare "colorless" precipitated enzymes through multiple rounds of resuspension and precipitation steps were unsuccessful.

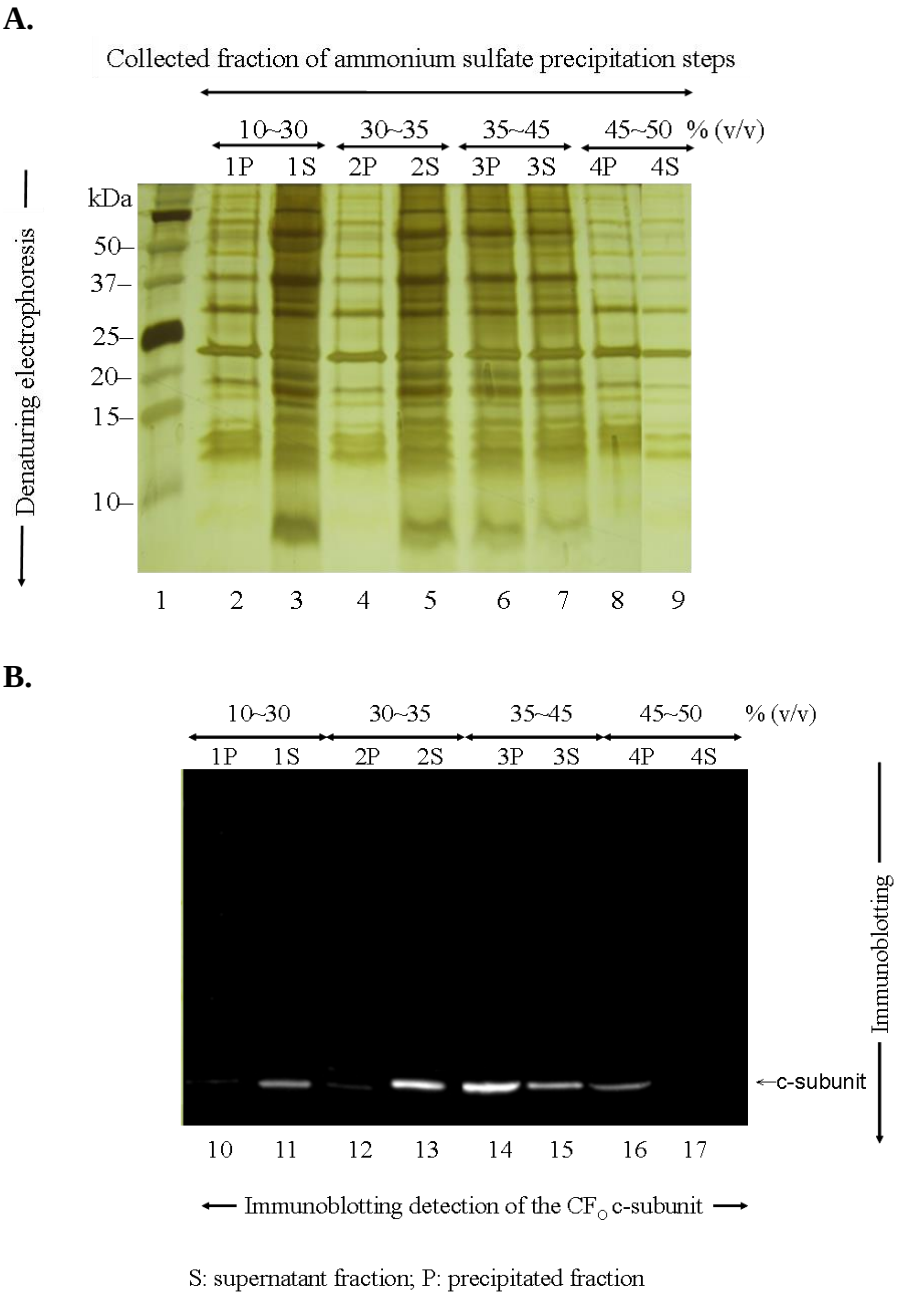

Figure 5.3 Analysis of Collected Fractions from Ammonium Sulfate Precipitation steps. Denaturing electrophoresis (A) and immunoblot analysis (B) of collected fractions from an ammonium sulfate precipitation of solubilized thylakoid membrane proteins. Silver staining of a 15% Tricine-SDS polyacrylamide gel and immunoblot detection of the ~8-kDa c-subunit (AptH: Agrisera, No. AS05 071) indicate that the majority of the CF_1F_O ATP synthase complex is precipitated by 45% (v/v) saturated ammonium sulfate (lane 14). The remainder of the CF_1F_O ATP synthase complex is further precipitated by 50% (v/v) saturated ammonium sulfate (lane 16). [Lane 1: kDa, Precision Plus

Protein™ Dual Color Standards (Bio-Rad, USA); Lanes 2 and 10: 15% Tricine SDS-PAGE and immunoblot analysis of the supernatant of the 30% (v/v) saturated ammonium sulfate precipitation; Lanes 3 and 11: 15% Tricine SDS-PAGE and immunoblot analysis of the precipitate of the 30% (v/v) saturated ammonium sulfate precipitation; Lanes 4 and 12: 15% Tricine SDS-PAGE and immunoblot analysis of the supernatant of the 35% (v/v) saturated ammonium sulfate precipitation; Lanes 5 and 13: 15% Tricine SDS-PAGE and immunoblot analysis of the precipitate of the 35% (v/v) saturated ammonium sulfate precipitation; Lanes 6 and 14: 15% Tricine SDS-PAGE and immunoblot analysis of the supernatant of the 45% (v/v) saturated ammonium sulfate precipitation; Lanes 7 and 15: 15% Tricine SDS-PAGE and immunoblot analysis of the precipitate of the 45% (v/v) saturated ammonium sulfate precipitation; Lanes 8 and 16: 15% Tricine SDS-PAGE of the supernatant of the 50% (v/v) saturated ammonium sulfate precipitation; and Lanes 9 and 17: 15% Tricine SDS-PAGE and immunoblot analysis of the precipitate of the 50% (v/v) saturated ammonium sulfate precipitation].

However, some non-target proteins were washed out via resuspension and precipitation steps, and a significant amount of related photosynthetic proteins remained in the precipitates. Discontinuous sucrose gradient ultracentrifugation served as an advanced purification method of precipitated CF_1F_O ATP synthase complexes to remove other remaining contaminants from photosynetic proteins. Using sucrose gradient consisting of steps of 12, 15, 18, 21, 24, 27 and 30% (w/v) sucrose (Varco-Merth, Fromme et al. 2008), the CF_1F_O ATP synthase complex was found in the yellow-olive band at 24% (w/v) sucrose (Figure 5.4 A). Silver staining of Tricine SDS-PAGE analysis (Figure 5.4 B) indicated that the 8 kDa monomer of the c-subunit complex (c-ring) was distinctly present in the collected fractions at the 24% (w/v) sucrose layer (Figure 5.4 B, lane 9) and was confirmed by antibody reactivity, as shown in Figure 5.4 C, lane 10. The two detergents (OG and sodium cholate) previously used in the solubilization step were replaced with 4 mM n-dodecyl-β-D-maltoside (β-DDM), which is a milder detergent, upon density gradient ultracentrifugation to stabilize the CF_1F_O ATP synthase complex and ensure higher activity (Varco-Merth, Fromme et al. 2008).

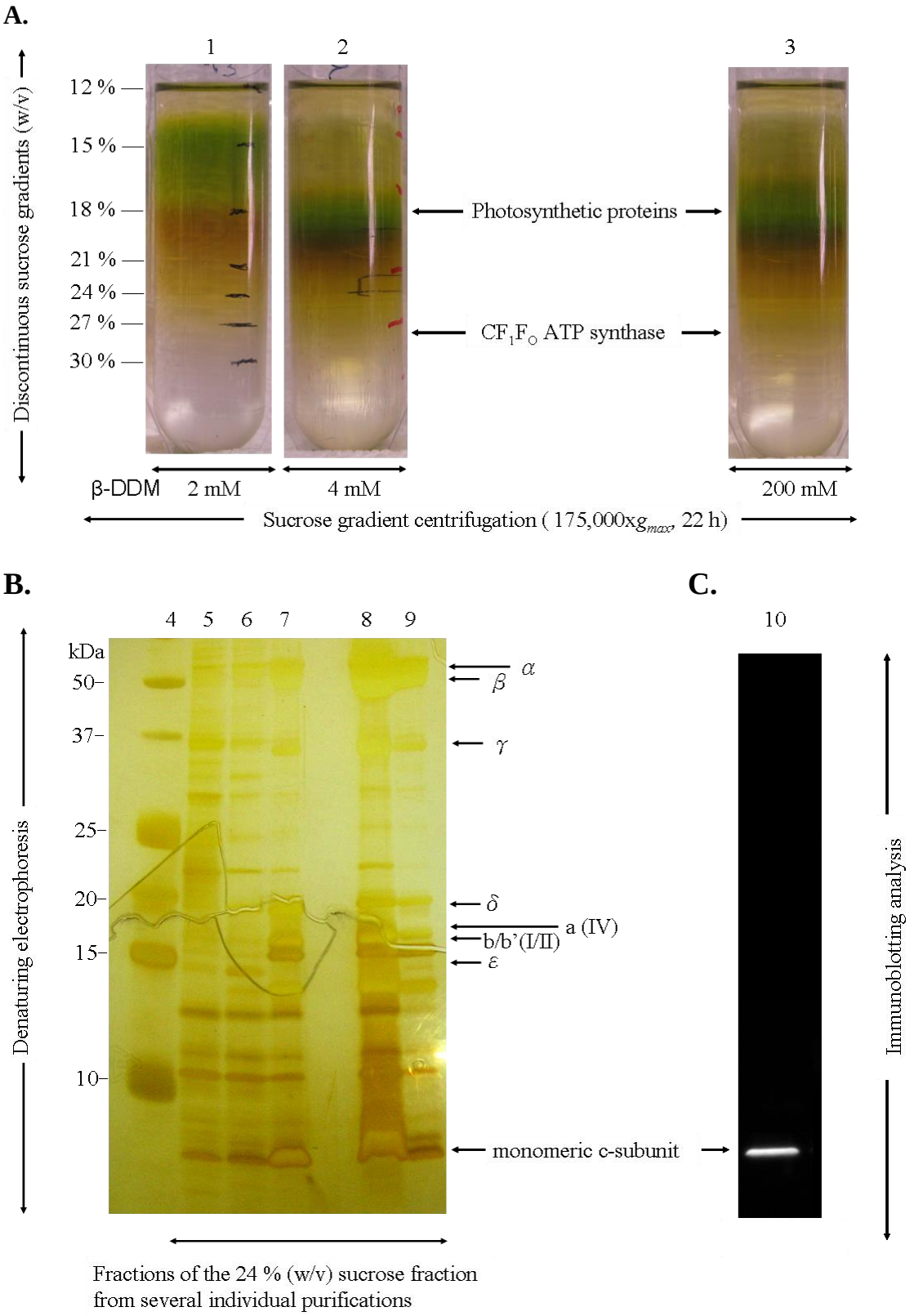

Figure 5.4 Sucrose Density Gradient Centrifugation of the CF_1F_O ATP synthase. Sucrose gradient centrifugation of the CF_1F_O ATP synthase, denaturing electrophoresis and immunoblot analysis of sucrose fractions following sucrose gradient Centrifugation. (A). The intact CF_1F_O ATP synthase is purified using sucrose density gradient centrifugation. The lower yellow band at ~24% is enriched in the CF_1F_O ATP synthase

[lane 2: 4 mM β-DDM]. The indicated numbers represent the concentration of sucrose (w/v) in each step. The lower yellow band at ~24% is not compacted if an insufficient or excess amount of DDM is added, resulting in the possible aggregation of CF_1F_O or the possible dissociation of the CF_1F_O ATP synthase complex into individual subunits [lane 1: 2 mM β-DDM; lane 3; 200 mM β-DDM]. (B). Silver-stained Tricine SDS-PAGE analysis of the 24% (w/v) sucrose fractions collected after the sucrose density gradient centrifugation from several individual CF_1F_O purifications [lanes 2 to 6]. (C). Immunoblot analysis indicates that the 8-kDa monomer of the c-subunit complex (c-ring) is distinctly present in the collected fractions at the 24% (w/v) sucrose fractions. [Lane 4: kDa, Precision Plus Protein™ Dual Color Standards (Bio-Rad, USA); lanes 5 to 9: sucrose fractions collected from several individual CF_1F_O purifications; lanes 25 to 36; lane 10; antibody against the c-subunit of CF_1F_O].

It should be noted that the CF_1F_O ATP synthase complex may either aggregate or dissociate to individual subcomplexes or/and lose some subunits in the presence of higher detergent concentrations during ultracentrifugation (Figure 5.4 A, lane 3). Using an alternative sucrose step density gradient (20, 28, 36, 44, 52 and 60%, w/v) (Turina, Samoray et al. 2003) with optimization (Figure 5.5 A), collected fractions from the bottom to the top of the gradient were analyzed using denaturing electrophoresis and immunoblotting. The results indicated that the monomeric c-subunits were clearly present in the collected fractions between No. 26 and No. 31 (Figure 5.5 B and C), indicating that the majority of the CF_1F_O ATP synthase complex migrated into the interface between the 44% (w/v) and 52% (w/v) sucrose layers. Some unidentified greenish insoluble fragments and precipitates were observed on the wall and on the bottom of tubes, respectively, by preparing sucrose gradient solutions in the presence of 8 mM β-DDM and 1 mg/mL extruded asolectin. A comparison of these separation results from different sucrose gradients clearly indicated that the optimal step gradient contained steps of 20, 28, 36, 44, 52 and 60% (w/v) sucrose in the presence of both β-DDM and asolectin, as shown in Figure 5.5

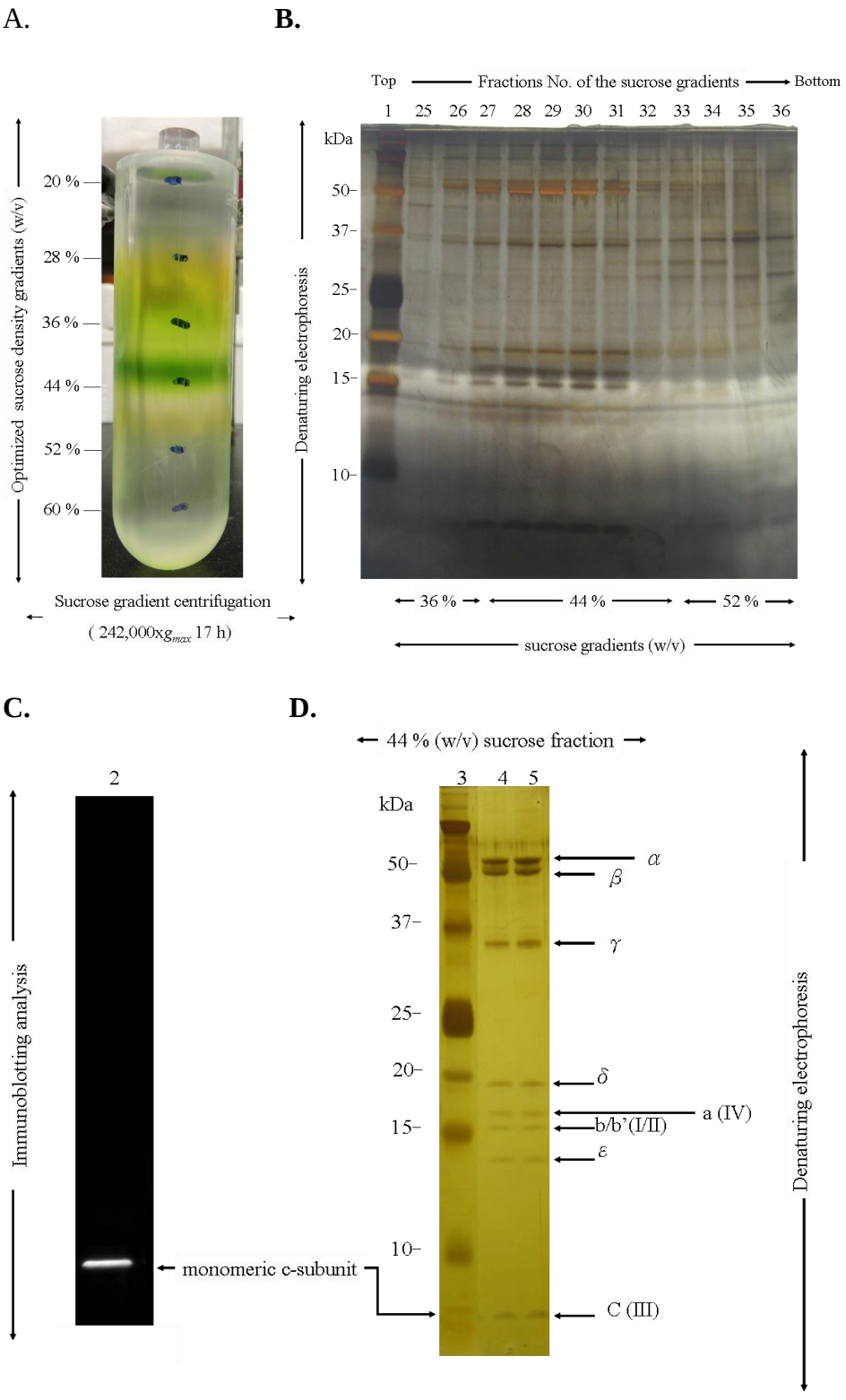

Figure 5.5 An Optimized Sucrose Density Gradient Centrifugation. An optimized sucrose gradient centrifugation, denaturing electrophoresis and immunoblot analysis of the 44% (w/v) sucrose fraction. (A) Intact CF_1F_O ATP synthase is purified using an optimized sucrose density gradient centrifugation. (B.) Silver-stained Tricine SDS-PAGE analysis of the sucrose fractions collected from the bottom to the top of the gradients after sucrose density gradient centrifugation. (C). Immunoblotting analysis indicates that the 8-kDa monomer of the c-subunit complex (c-ring) is distinctly present

in the collected fractions at the interface between the 44% and 52% (w/v) sucrose fractions. (D). Silver-stained Tricine SDS-PAGE analysis of the CF_1F_O ATP synthase. Individual subunits of CF_1F_O is assigned according to their molecular mass. [lanes 1 and 3: kDa, Precision Plus Protein™ Dual Color Standards (Bio-Rad, USA); lanes 25 to 36: corresponding to the sucrose fraction numbers; lane 2; antibody against the c-subunit of CF_1F_O; lanes 4 and 5: CF_1F_O proteins are collected fractions at the 44% (w/v) sucrose fraction].

The individual subunits of the CF_1F_O-detergent-lipid complex that were enriched at the yellowish interface between 44% and 52% (w/v) sucrose were separated by denaturing electrophoresis in high resolution and were also assigned according to the molecular weight pattern in denaturing gels (Fromme 1988), as shown in Figure 5.5 D.

5.4 Pigment Analysis of the Sucrose Gradient Fractions

Although the gradient fraction of the CF_1F_O ATP synthase possessed a yellowish color, the question arose whether pigments were bound to the CF_1F_O ATP synthase. Pigments extracted from the collected gradient fractions were characterized by UV-visible absorption spectroscopy. A comparison of the absorption results revealed that fractions containing the CF_1F_O ATP synthase exhibited strong absorption in two spectral regions (Figure 5.6). A major absorption was observed in the blue region of the spectrum between 400 nm and 500 nm, which corresponds to carotenoids, and a minor absorption was observed at 650 nm, which corresponds to photosynthetic pigments. Attempts to purify pigment-free CF_1F_O ATP synthase were unsuccessful. This pigment association also is observed in the native chloroplast C_{14} crystals (Varco-Merth, Fromme et al. 2008). These pigments may play possible roles in formation of the chloroplast ATP synthase.

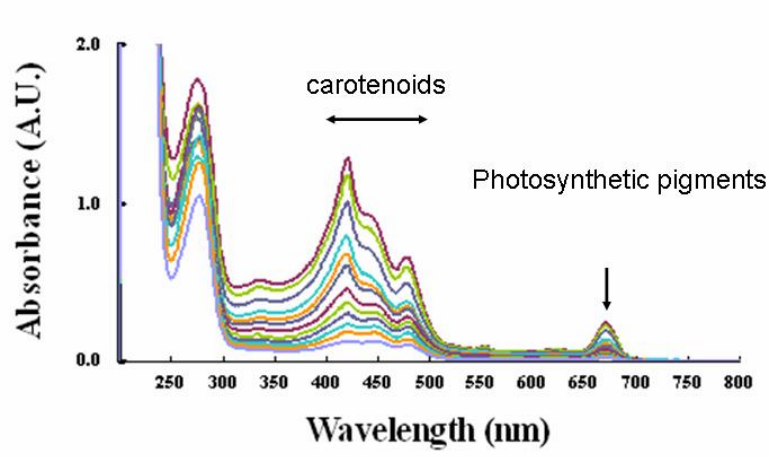

Figure 5.6 UV-Visible Absorption Spectra of the CF_1F_O Sucrose Gradient Fractions. UV-Visible absorption spectra of 80% acetone extracts of the sucrose fractions enriching CF_1F_O ATP synthase. The sucrose fractions that enrich CF_1F_O have absorption values characteristic of chlorophyll and carotenoids. The chlorophyll absorption near 680 nm is blue shifted relative to photosynthetic proteins. Colored lines are representative to the sucrose fractions from No. 25 to No. 36.

5.5 Native Electrophoresis Analysis of the CF_1F_O ATP Synthase

The ability of native electrophoresis techniques to isolate ATP synthase complexes from mitochondria and chloroplasts using various detergents (i.e., β-DDM or digitonin) in either analysis of enzymatically active oligomeric states or 2D crystallization studies has been well recognized (Poetsch, Neff et al. 2000, Schagger and Pfeiffer 2000, Krause, Reifschneider et al. 2005, Wittig and Schagger 2005, Meyer, Wittig et al. 2007). Typically, in native electrophoresis, the separation of membrane proteins in native gels is influenced by their native size in native gels while the separation in denaturing gels is achived according to the charge/mass. Blue native PAGE (BN-PAGE) uses the anionic Coomassie Blue dye to impart a net negative charge by binding membrane protein surfaces via its hydrophobic properties. Because the binding of Coomassie Blue to membrane proteins results in a negatively charged surface, membrane proteins in the native state migrate toward the anode during BN-PAGE. Furthermore, membrane proteins exhibit less aggregation and more hydrophilic character following masking of the hydrophobic regions upon dye binding.

Therefore, detergent is not required in BN-PAGE once the membrane protein surfaces are bound by Coomassie Blue, resulting in the minimization of denaturation in some detergent-sensitive membrane proteins during BN-PAGE (Wittig, Braun et al. 2006). However, prior to crystallization trials of the intact CF_1F_O ATP synthase, it was unclear whether CF_1F_O preserves its native structure in a functional state following the series of purification steps. Therefore, β-DDM-solubilized CF_1F_O samples were analyzed by various native gradient polyacrylamide gels to characterize its oligomeric state and its subcomplexes. These comparisons are shown in Figure 5.7. Preparative BN-PAGE analysis (Figure 5.7 A) identified the intact CF_1F_O supercomplex according to its known migration pattern in BN-PAGE. The most intense blue bands (Figure 5.7 A, lane 2 and lane 3) were assigned to the intact CF_1F_O supercomplex based on its native molecular mass (~570 kDa), as previously described (Neff and Dencher 1999). The CF_1 subcomplex (~420 kDa) migrated between 242 and 480 kDa, corresponding to the second most intense blue bands (Figure 5.7 A, lane 2 and lane 3). Furthermore, the membrane-bound CF_O subcomplex was not observed in BN-PAGE, according to its characteristic molecular mass (~150 kDa). Presumably, the Coomassie Blue staining may not be sufficiently sensitive to stain this hydrophobic CF_O domain at such low quantities compared with the staining intensity of the CF_1 bands. The slight dissociation of the supercomplex to the CF_1 subcomplex was also observed in BN-PAGE analysis (cathode buffer containing 0.02% Coomassie Blue dye). Presumably, this dissociation was due to mixed anionic micelles that formed between β-DDM used to solubilize CF_1F_O and the anionic Coomassie Blue dye. It gas been hyprothesis that an increase in the concentration of Coomassie Blue used in BN-PAGE may be related to an increase in the dissociation of the intact F_1F_O supercomplex into F_1 and F_O subcomplexes, respectively (Neff and Dencher 1999).

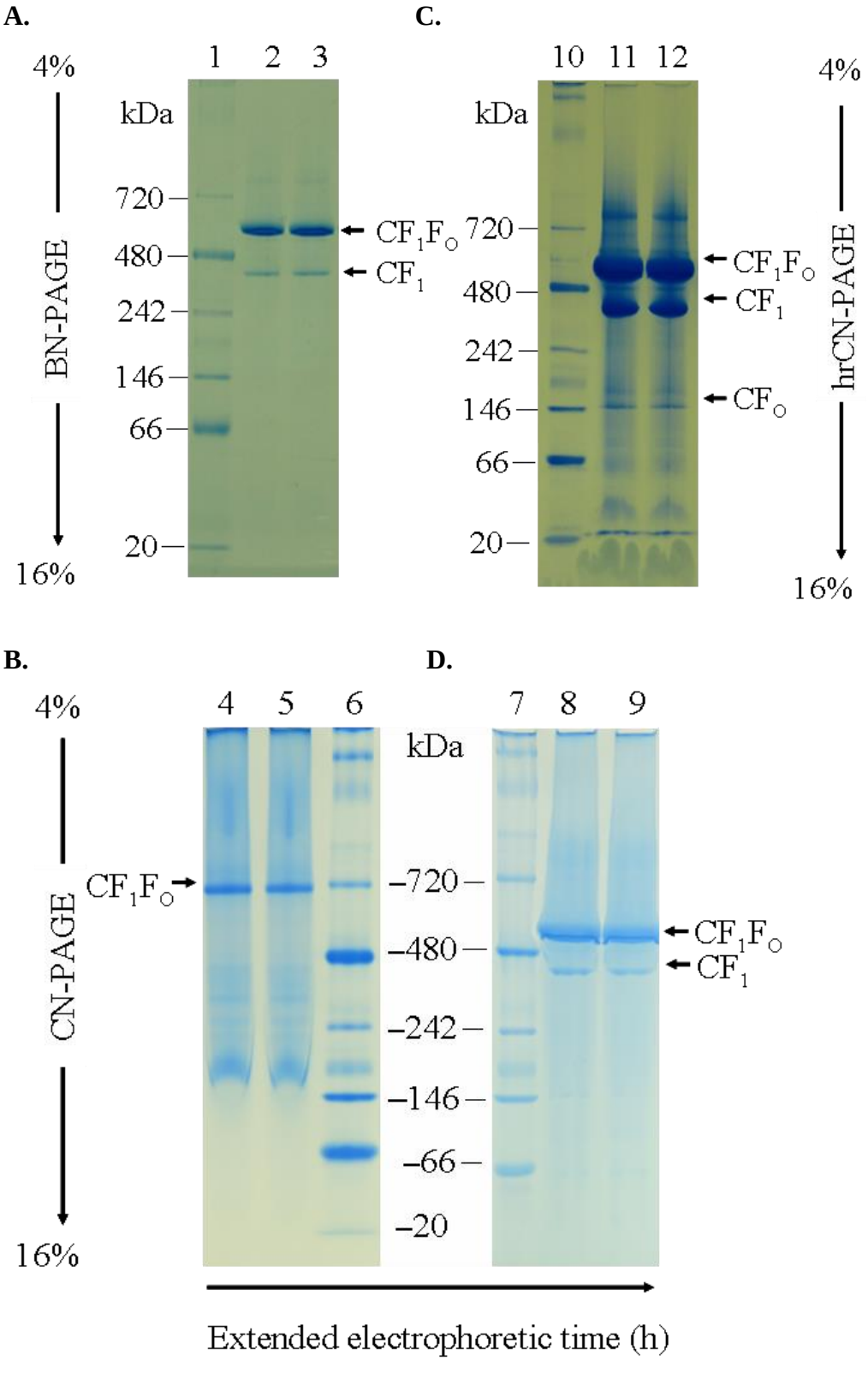

Figure 5.7 Native Electrophoresis Analysis of the Intact CF_1F_O ATP Synthase. Various native electrophoresis analysis of the β-DDM-solubilized intact CF_1F_O ATP synthase complex.Native CF_1F_O proteins are analyzed by the 4% ~ 16% Blue-native PANG (A), the 4% ~ 16% Clear-native PANG (B) and the 4% ~ 16% hrClear-native PANG (C). The native intact CF_1F_O supercomplex and the CF_1 subcomplex are identified on the gels of the blue native electrophoresis (BN-PAGE) (lanes 2 and 3),

clear native electrophoresis (CN-PAGE) (lanes 8 and 9) and high-resolution clear native electrophoresis (hrCN-PAGE) (lanes 11 and 12) according to their molecular mass, ~570 kDa and ~420 kDa, respectively. The ~150 kDa CF_O subcomplex is weakly stained only on the hrCN-PAGE gels (lanes 11 and 12). The separation resolution of CF_1F_O can be improved by extending the electrophoretic time. [lanes 1, 6, 7 and 10: kDa, unstained native protein standard (Life Technologies, USA); lanes 2 and 3: BN-PAGE of native CF_1F_O proteins; lanes 4 and 5: CN-PAGE of native CF_1F_O proteins; lanes 8 and 9: CN-PAGE of native CF_1F_O proteins by extending the electrophoretic time; lanes 11 and 12, hrCN-PAGE of native CF_1F_O proteins].

However, according to the comparisons of the staining intensity between CF_1F_O and CF_1, the experienced ratio (Coomassie Blue:protein:detergent) used in this BN-PAGE sample preparation appeared not to result in a significant dissociation. To prevent this deleterious effect of Coomassie Blue in the dissociation efficiency of the CF_1F_O supercomplex, colorless native PAGE (CN-PAGE), which does not use Coomassie Blue in sample preparation or in the cathode buffer, was evaluated. In contrast to BN-PAGE, which uses the anionic dye Coomassie Blue to bind to membrane proteins, CN-PAGE does not utilize this dye. The separation of membrane proteins in CN-PAGE is dependent on the intrinsic charge of the proteins themselves and on their size, resulting in a limited separation resolution in CN-PAGE compared with BN-PAGE but without the influence of Coomassie Blue in supercomplex dissociation. The result of preparative CN-PAGE analysis stained with Coomassie Blue (Figure 5.7 B) indicates that the electrophoretic mobility of the CF_1F_O supercomplex in CN-PAGE differed from that observed in BN-PAGE analysis (Figure 5.7, A and B). According to the known migration properties of the intact CF_1F_O supercomplex in BN-PAGE, CF_1F_O migrated to approximately 720 kDa (Figure 5.7 B, lane 4 and lane 5), which differed from the position observed in BN-PAGE analysis and may be caused by an insufficient separation time. Hence, an extended electrophoretic time was necessary due to the absence of Coomassie Blue to mask the proteins with a negative charge. As shown in Figure 5.7 D, lane 8 and lane 9, CF_1F_O migrated to an identical position as that observed

in BN-PAGE analysis when the electrophoretic time was doubled. Typically, dissociation of the supercomplex into the CF_1 and CF_O subcomplexes was not also observed in CN-PAGE analysis (Figure 5.7, B and D) due to the absence of Coomassie Blue in the cathode buffer; therefore, CN-PAGE may represent a much milder technique than BN-PAGE to investigate the native CF_1F_O structure. However, partial dissociation was observed in CN-PAGE analysis (Figure 5.7 D, lane 8 and lane 9), which may be caused by either prolonged storage at -80℃ or multiple freeze-thaw cycles of the CF_1F_O samples. From a functional point of view, an alternative technique to CN-PAGE, high-resolution colorless native PAGE (hrCN-PAGE), is closer to BN-PAGE than CN-PAGE because of the use of mixed detergent micelles (a nonionic detergent, such as β-DDM, and an anionic detergent, such as sodium deoxycholate) instead of Coomassie Blue as the new charge carrier in native gels. The result of preparative hrCN-PAGE analysis shown in Figure 5.7 C indicates that the migration properties of the intact CF_1F_O supercomplex in hrCN-PAGE were consistent with those observed in BN-PAGE analysis. The resolution of hrCN-PAGE was much higher than those of both BN-PAGE and CN-PAGE analyses, and its electrophoretic time was much shorter than those of BN-PAGE and CN-PAGE. Unfortunately, a partial dissociation of the CF_1F_O supercomplex into the CF_1 and CF_O subcomplexes was observed compared with CN-PAGE. This dissociation may have been caused by excess detergent micelles supplemented in the cathode buffer in hrCN-PAGE. The intact CF_1F_O supercomplex and CF_1 subcomplex were assigned to the strongest and strongly intense blue bands, respectively, according to their known molecular masses (Figure 5.7 C, lane 11 and lane 12). Moreover, the weakly stained band at approximately 146 kDa was assigned to the CF_O subcomplex based on its known molecular mass (~150 kDa) (Figure 5. 7 C, lane 11 and lane 12). CF_1 was notably more abundant than CF_O in

both BN-PAGE and hrCN-PAGE, which may indicate that the hydrophobic CF_O domain is less sensitive to Coomassie Blue staining than the hydrophilic CF_1 domain. Furthermore, in contrast to the identified bands in BN-PAGE, CN-PAGE or hrCN-PAGE, a weak band appeared just below the CF_1F_O band at approximately 480 kDa, which may consist of subcomplexes of CF_1F_O that may have lost the a- and/or b-subunit of the F_O domain due to the detergent-containing cathode buffer during electrophoresis in hrCN-PAGE. In summary, the purified CF_1F_O ATP synthase was successfully analyzed using the three native PAGE techniques BN-PAGE, CN-PAGE, and hrCN-PAGE to characterize its oligomeric state and its monomeric state. hrCN-PAGE offers higher resolution and is more straightforward to perform than BN-PAGE and CN - PAGE. The native structure of the purified CF_1F_O ATP synthase supercomplex was maintained following a series of purification steps.

5.6 Two-dimensional (2D) Electrophoresis Analysis of the CF_1F_O ATP Synthase

To characterize the subunit composition of the CF_1F_O supercomplex, gel strips of both CN-PAGE (Figure 5.8 A, lane 2) and hrCN-PAGE (Figure 5.8 C, lane 5) analyses containing CF_1F_O were analyzed using a second dimension of electrophoresis (1-D CN-PAGE or hrCN-PAGE, 2-D SDS-PAGE). The results of preparative 2-D CN/SDS and hrCN/SDS analyses indicate that the subunit composition of CF_1F_O was well identified on the second dimension of electrophoresis, and each individual subunit was assigned based on the observed molecular mass (Figure 5.8 B and D). In addition to the direct handling of 1D native gel strips (Figure 5.8 C, lane 5) for 2D SDS-PAGE, the CF_1F_O supercomplex and CF_1 subcomplex were individually recovered from native gels through electroelution and were subsequently analyzed using a second dimension of electrophoresis.

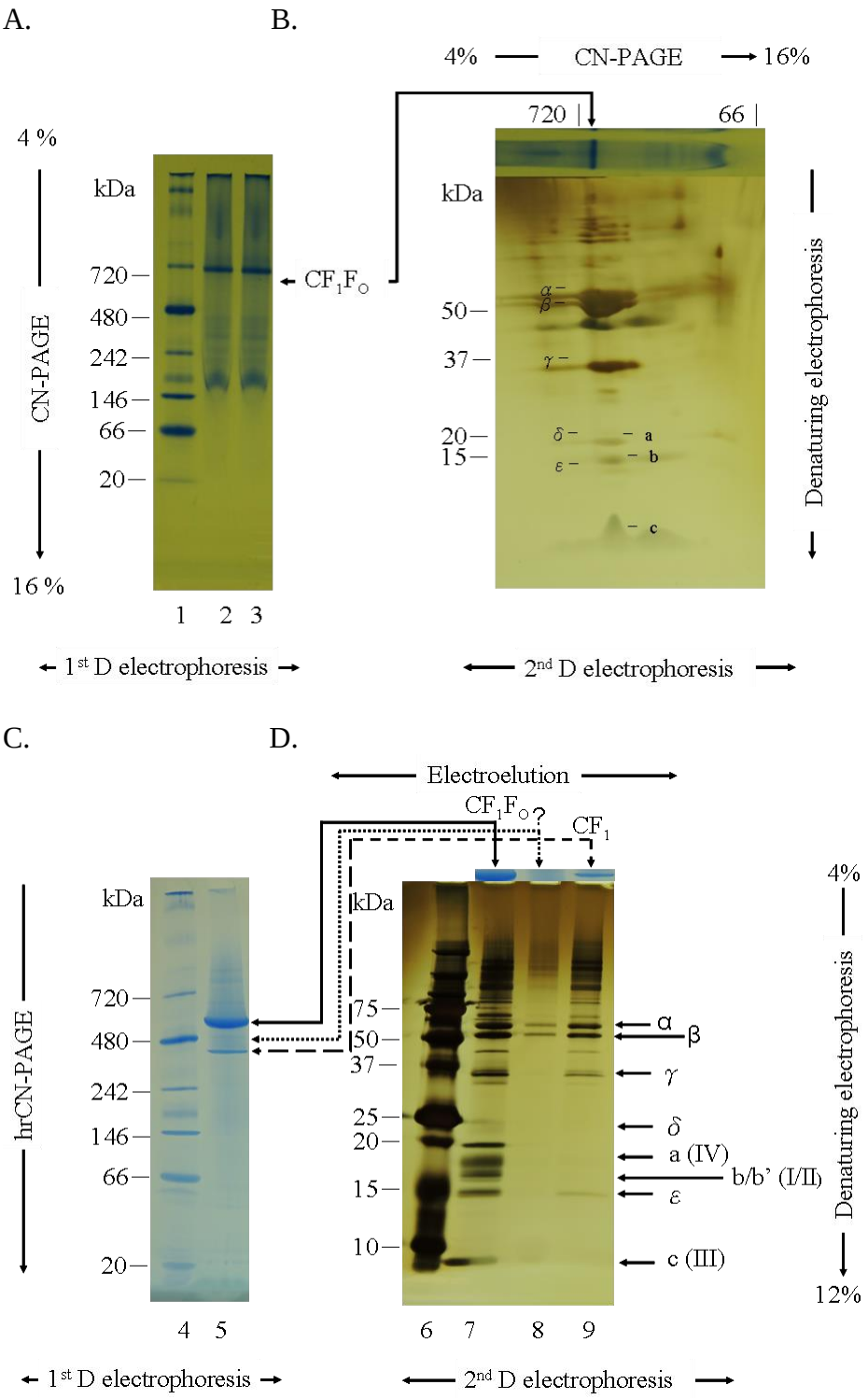

Figure 5.8 2D Electrophoresis Analysis of the Intact CF_1F_O-ATP Synthase. Native electrophoresis analysis and 2D electrophoresis analysis of the intact CF_1F_O-ATP synthase complex. Native CF_1F_O proteins are analyzed in the first-dimension by either 4% ~ 16% Clear-native PANG or hrClear-native PANG in the first dimension (A and C) and subsequently analyzed in the second-dimension by 4% ~ 12% Tricine SDS-PAGE (B and D). The Blue-stained CN-PAGE gel strip of the CF_1F_O ATP synthase complex (lane 2) is directly analyzed by 2D electrophoresis, showing the individual CF_1F_O subunits that are identified according to the molecular mass of each subunit (B).

The Blue-stained hrCN-PAGE gel slices (lane 5) that contain the intact CF_1F_O supercomplex (lane 7), the CF_1F_O subcomplex (lane 8) and the CF_1 subcomplex (lane 9), respectively, are electroeluted and subsequently analyzed by the denaturing electrophoresis that also shows the individual subunits of the CF_1F_O are identified according to the molecular mass of each subunit (D). [lanes 1 and 4: kDa, unstained native protein standard (Life Technologies, USA); lanes 2 and 3: CN-PAGE of native CF_1F_O proteins; lane 5: hrCN-PAGE of native CF_1F_O proteins; lane 6: kDa, Precision Plus Protein™ Dual Color Standards (Bio-Rad, USA); lane 7: electroeluted intact CF_1F_O supercomplex proteins; lane 8: electroeluted CF_1F_O subcomplex proteins; lane 9: electroeluted CF_1 subcomplex proteins].

As shown in Figure 5.8 D, the subunit composition of the recovered CF_1F_O was identified, and each subunit was assigned (Figure 5.8 D, lane 7). For the recovered CF_1 subcomplex, the subunits α, β, γ and ε were clearly identified, with the exception of the δ subunit (Figure 5.8 D, lane 9). Presumably, the unobserved δ subunit may be due to insufficient quantities. In addition to the recovery of both CF_1F_O and CF_1, recovery of the unidentified band (CF_1F_O subcomplex) that was scarcely observed at approximately 480 kDa between the CF_1F_O and CF_1 bands was attempted (continuous dashed line, Figure 5.8 C, lane 5). Unfortunately, the recovery rate was particularly low due to extremely low quantities as judged from hrCN-PAGE gels stained with Coomassie Blue (Figure 5.8 D, lane 8). The α- and β-subunits were readily identified compared with the γ, ε, and c subunits, which were scarcely observed due to their extremely low quantities (Figure 5.8 C, lane 5). This identified subunit composition confirmed the previous assumption that this band at approximately 480 kDa consists of subcomplexes of CF_1F_O that have lost the a- and/or b-subunit of the F_O domain due to the detergent micelles present in the cathode buffer during hrCN-PAGE electrophoresis.

5.7 Chromatographic Analysis of the CF_1F_O ATP Synthase

A prerequisite for the successful crystallization of the intact CF_1F_O ATP synthase supercomplex is a highly pure and monodisperse protein sample. Although the

previously described purification procedures are adequate to yield sufficient quantities of CF_1F_O, the purified CF_1F_O samples may still contain RuBisCO proteins and other contaminants. However, for CF_1F_O that requires additional chromatographic purification, the selection of an appropriate chromatography matrix that can be used at both large scale and low cost is challenging. This matrix must also maintain the native structure and functional catalytic mechanism of CF_1F_O following chromatography. Dye-ligand chromatography possesses these desired features and has been very effective in purifying the mitochondrial and chloroplast ATP synthases in the presence of various detergents (Seelert, Poetsch et al. 2000). Therefore, CF_1F_O purified using ultracentrifugation was additionally purified using R-120 chromatography in an optimal buffer composition in the presence of β-DDM. As a result of the purification chromatogram shown in Figure 5.9 A, a single pyramid-shaped peak with a high absorbance at 280 nm was observed nearly immediately following sample injection, and negligible peaks were observed following elution with a buffer containing 1.5 M NaCl. Figure 5.9 B shows the result of analysis of the corresponding flow-through fractions by denaturing electrophoresis, indicating that CF_1F_O was found in the flow-through fractions, in which each subunit of CF_1F_O was identified and assigned based on their corresponding molecular masses in SDS-PAGE (Figure 5.9 B, from lane 2 to lane 11). Only a negligible amount of proteins, which may include impurities such RuBisCO proteins that bind the R-120 resin, was eluted with buffers containing 1.5 M NaCl. A comparison of the results indicates that CF_1F_O does not bind the R-120 resin and immediately flows through, allowing its separation from other minor impurities such as RuBisCO proteins that strongly bind the column. Furthermore, immunoblot analysis of CF_1F_O fractions using antibodies against the large and small subunits of RuBisCO proteins indicated a lack of RuBisCO contamination in the CF_1F_O fractions

(Figure 5.9 E, lane 25). Notably, the purification of CF_1F_O using R-120 chromatography can be alternatively preformed using a gravity flow column due to the lack of binding of CF_1F_O to the R-120 resin, which may save a significant amount of time in the chromatographic steps. Although the purification of CF_1F_O has also been successful using Superdex 200 size exclusion chromatography, POROS 20 HQ anion exchange chromatography is an alternative chromatographic purification technique that can separate CF_1F_O from other impurities, particularly RuBisCO proteins, on the time scale of minutes compared with that of size exclusion chromatography on the time scale of hours. The purified CF_1F_O using R-120 chromatography was applied to a POROS 20 HQ column as an additional purification step, if necessary, with an optimized buffer composition containing β-DDM and glycerol, which stabilizes CF_1F_O during the purification. As shown in Figure 5.9 C, the most significant peak was observed at the elution volume of 38.25 mL in the presence of 1.3 M NaCl. The corresponding fractions were analyzed using denaturing electrophoresis, as shown in Figure 5.9 D, indicating that this peak corresponded to intact CF_1F_O, and each subunit was identified based on their molecular masses in denaturing gels (Figure 5.9 D, lane 13). Additionally, other negligible peaks were subsequently eluted. However, the primary contaminants, RuBisCO proteins, or other minor impurities, if present in CF_1F_O samples, can be adequately separated from the CF_1F_O fraction using a linear NaCl gradient (Figure 5.9 D). The ratio of the CF_1F_O and RuBisCO fractions is dependent on the purity of the CF_1F_O sample applied to the POROS 20 HQ column (Poetsch, Seelert et al. 1999).

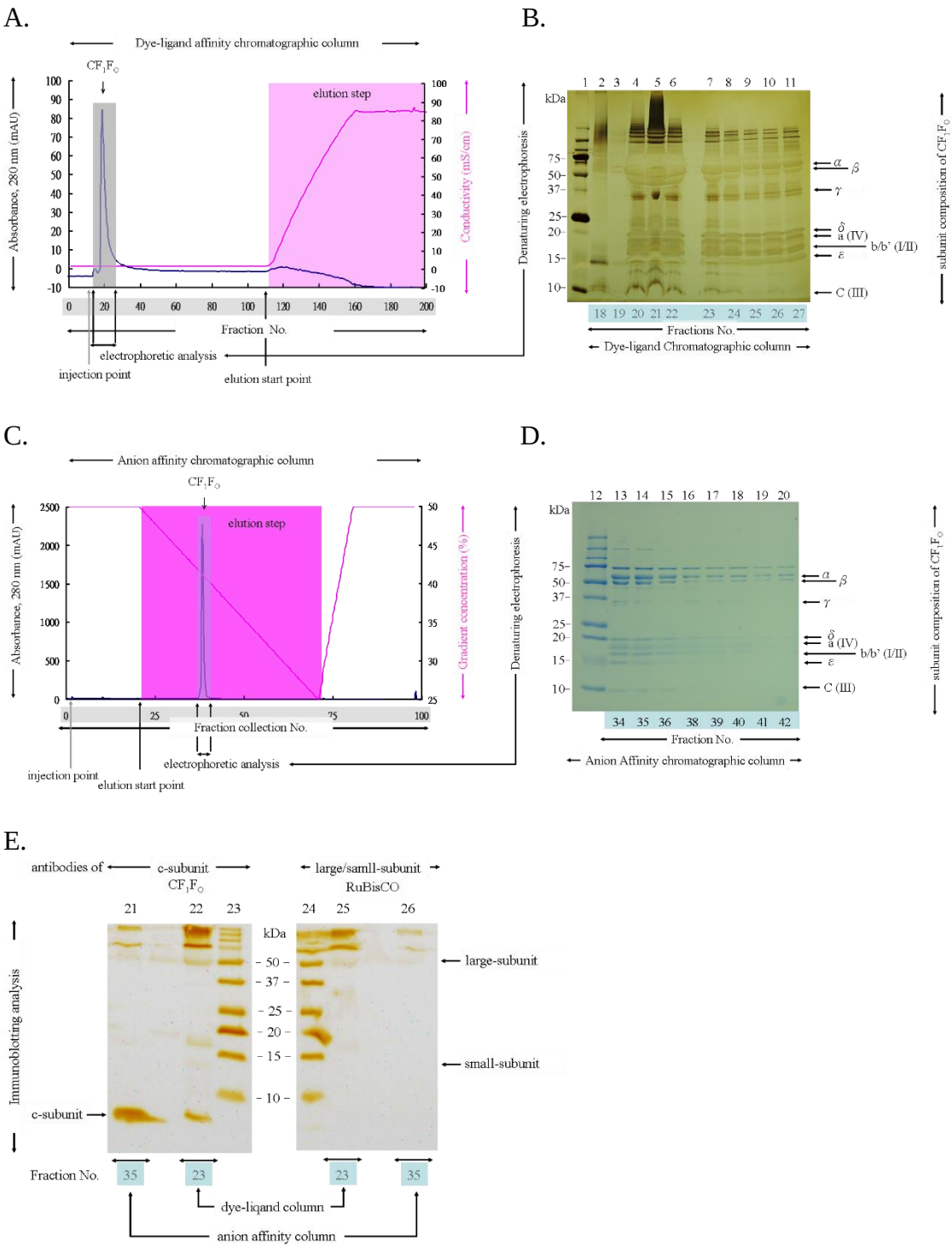

Figure 5.9 The Affinity Column Chromatograms of Intact CF_1F_O ATP Synthase. The affinity column chromatograms of intact CF_1F_O ATP synthase and denaturing electrophoresis and immunoblot analysis of the collected election fractions.The CF_1F_O samples are further purified by the dye-ligand affinity column (A) and anion affinity column (C), respectively. The flow-through fractions are analyzed by denaturing electrophoresis, which shows that these fractions contain the high purity of the intact CF_1F_O; the individual subunits of the CF_1F_O are identified according to their molecular mass of each subunit (B). The elution fractions collected from subsequent purification of the flow-through fractions by anion affinity column (C) are also analyzed by

denaturing electrophoresis, showing that these elution fractions contain intact CF_1F_O of extremely high purity; the individual subunits of the CF_1F_O are also assigned according to the molecular mass of each subunit (D). The chromatographic fractions from both dye-ligand and anion affinity columns are analyzed by immunoblotting against antibodies of both the c-subunit of CF_1F_O and the large/small-subunit of RuBisCO proteins, indicating that both fractions are RuBisCO free (E). [lanes 1 and 12: kDa, Precision Plus Protein^{TM} Dual Color Standards (Bio-Rad, part N. 161-0374); lanes 2 to 11: corresponding to the dye-ligand chromatographic flow-through fractions; lanes 13 to 20: corresponding to the anion chromatographic elution fractions; lanes 21 and 26: corresponding to the anion chromatographic elution fractions; lanes 22 and 25; corresponding to the dye-ligand chromatographic flow-through fractions; lanes 23 and 24: kDa, Precision Plus Protein™ WesternC™ Standards (Bio-Rad, Part No. 161-0376)].

A comparison of electrophoretic schemes (Figure 5.9 D) indicates that the eluted CF_1F_O was highly pure and the RuBisCO fraction was not present. Presumably, prior to POROS 20 HQ chromatography, CF_1F_O was additionally purified using R-120 chromatography following serial purification steps including sucrose gradient centrifugation. The intact CF_1F_O following sucrose gradient centrifugation can be additionally efficiently purified in significant quantities using either R-120 chromatography or POROS 20 HQ chromatography or a combination of both to remove impurities, particularly RuBisCO proteins, that possibly remain in the CF_1F_O sample following serial purification steps. Both chromatographies are based on ion exchange chromatography. Most importantly, the chromatographically purified CF_1F_O retains its functional native structure for subsequent crystallization trials. The significant differences between both chromatography methods are the time and cost spent in a single purification trial. In contrast to the low-cost R-120 resin that can alternatively be operated using an open gravity flow column, the POROS 20 HQ column is relatively more expensive and must be used with a commercial FPLC or HPLC system. To efficiently increase the purity of CF_1F_O for crystallization trials, chromatography using the low-cost R-120 resin is highly recommended as an additional purification step.

5.8 Functional Characterization of the CF_1F_O ATP Hydrolysis Activity

Although the H^+/ATP ratio in ATP synthesis and the ATP hydrolysis of ATP synthases isolated from different sources has been studied via liposome reconstitution and chemiosmotic PH jump experiments, the techniques involved are complex and time consuming. Therefore, the combination of native electrophoresis techniques and in-gel functional activity assays has emerged as a powerful tool for protein-protein interaction analysis of mitochondrial respiratory complexes (Wittig and Schagger 2009). One of these established in-gel assays, known as an in-gel ATP hydrolysis assay, is remarkably useful in both qualitative and quantitative analysis of the catalytic activity of the mitochondrial ATP synthase (complex V) (Wittig, Karas et al. 2007). The in-gel ATPase activity assay has previously been successfully applied for the detection of the activity of mitochondrial ATP synthases, spinach chloroplast ATP synthases, and ATP synthases of the cyanobacterium *T. elongatus* and the green algae *C. reinhardtii* for the study of ATP hydrolysis activity in the presence of different detergents (Suhai, Heidrich et al. 2009). In contrast to mitochondrial ATP synthases, for which high activities of ATP hydrolysis have been reported (Suhai, Heidrich et al. 2009), the chloroplast ATP synthase exhibits relatively lower ATPase activity due to the inhibition mechanism that prevents wasteful ATP hydrolysis in the dark. This inactivation is mediated by a conformational change of the ε subunit of CF_1 (Richter, Patrie et al. 1984, Gertz, Seelert et al. 2007), the binding of Mg^{2+}-ATP (Du and Boyer 1990, Digel, Hightower et al. 1996, Digel, Kishinevsky et al. 1996, Du, Tucker et al. 2001), the lack of a proton gradient, and oxidation of cysteine residues in the γ subunits to a disulfide bond (Nalin and McCarty 1984, Ort and Oxborough 1992). Several studies have used harsh pretreatments of the chloroplast enzyme, including heating, organic solvents, and trypsin, to stimulate the ATPase activity of the hydrophilic portion of the enzyme, CF_1,

as previously described (Farron 1970, Sakurai, Shinohara et al. 1981, Anthon and Jagendorf 1983, McCarty 2005). In particular, the interaction of some harsher detergents with the solubilized CF_1 domain of chloroplast ATP synthases led to an enhancement of the ATPase activity, as previously described (Pick and Bassilian 1982, Yu and McCarty 1985, Suhai, Heidrich et al. 2009). The stimulated ATPase activity of CF_1 by harsh detergents that form small micelles may be induced by the dissociation of the ε subunit from the chloroplast CF_1. Various detergents, including alkyl glucosides, LDAO, and TDOC have previously been evaluated to study the effect of the dissociation on the CF_1-ε subunit (Pick and Bassilian 1982, Yu and McCarty 1985, Suhai, Heidrich et al. 2009). With increasing micelle size by increasing the chain length, the interaction of alkyl glucosides with CF_1 becomes less and less effective in the removal of the ε subunit, resulting in lower ATPase activity (Yu and McCarty 1985). For the in-gel ATPase assay, also known as the lead phosphate method, which is based on the formation of a white lead phosphate precipitate following incubation of the phosphate released during ATP hydrolysis with lead nitrate, either CN-PAGE or hrCN-PAGE is highly preferred compared with BN-PAGE due to the deleterious side effect of Coomassie Blue used in BN-PAGE that may either dissociate detergent-labile subunits from the supercomplex or disassemble the supercomplex into subcomplexes. Furthermore, detection of the lead precipitate is extremely difficult in the presence of Coomassie Blue. Therefore, a significant advantage of using colorless native gels is that they can be directly used to perform the in-gel assays without interference of Coomassie Blue (Wittig and Schagger 2005, Wittig, Carrozzo et al. 2007, Wittig, Karas et al. 2007, Wittig and Schagger 2008, Wittig and Schagger 2009). Recently, the sensitivity of the in-gel ATPase activity assay has been remarkably improved using CN-PAGE compared with BN-PAGE (Wittig and Schagger 2005). Because the ATP hydrolysis activity can

be monitored in native gels via an in-gel ATPase assay, this assay can be used not only to rapidly screen for the enzymatic activity of isolated ATP synthase complexes directly in the gel without the need for complicated experiments but also to screen for the best detergent to stabilize the structure and function of the isolated ATP synthase in different protein-detergent complexes. Detergent screening is impossible to perform using ATP synthesis assays because these assays require the removal of the detergent during reconstitution into lipid membranes. Because the ATP hydrolysis activity of the chloroplast CF_1F_O supercomplex can be improved by activating this supercomplex via detergent treatments (Pick and Bassilian 1982, Yu and McCarty 1985, Suhai, Heidrich et al. 2009) prior to the in-gel ATPase activity assay, gel strips from hrCN-PAGE were treated with select detergents at room temperature, as described in detail in the Materials and Methods. Using OG treatment, ATP hydrolysis activity of CF_1F_O or CF_1 was not detected within the 0.5 h or 1 h incubation periods (Figure 5.10, AD panel, lane 1; BD panel, lane 2). Extremely weak bands were visible only after 24 h of incubation, indicating hydrolysis activity (Figure 5.10, CD panel, lane 3). Using β-DDM, ATP hydrolysis activity of CF_1F_O or CF_1 was not detected after 0.5 h of incubation (Figure 5.10, AE panel, lane l); their activities were scarcely detected after only 1 h of incubation (Figure 5.10, BE panel: lane) and fully detected after 24 h of incubation. In contrast to the extremely low activity of CF_1F_O and CF_1 following the first two incubation periods, the defective CF_1F_O supercomplex that had lost subunits a and b exhibited strong ATP hydrolysis activity after 0.5 h and 1 h of incubation (indicated by an question mark), which may be caused by the loss of subunits δ and ε during the β-DDM treatment. A comparison of these results indicates that CF_1F_O is inactive in ATP hydrolysis and requires activation in the presence of very mild detergents (such as β-DDM); furthermore, the removal of the proton translocating CF_O domain does not

stimulate ATP hydrolysis as ATP hydrolysis was detected only after 24 h for CF_1 in β-DDM. Using LDAO, very weak ATP hydrolysis activities for CF_1F_O and CF_1 were detected after 0.5 and 1 h of incubation (Figure 5.10, AF panel, lane 1; BF panel, lane 2), and their hydrolysis activities were fully detected only after 24 h of incubation.

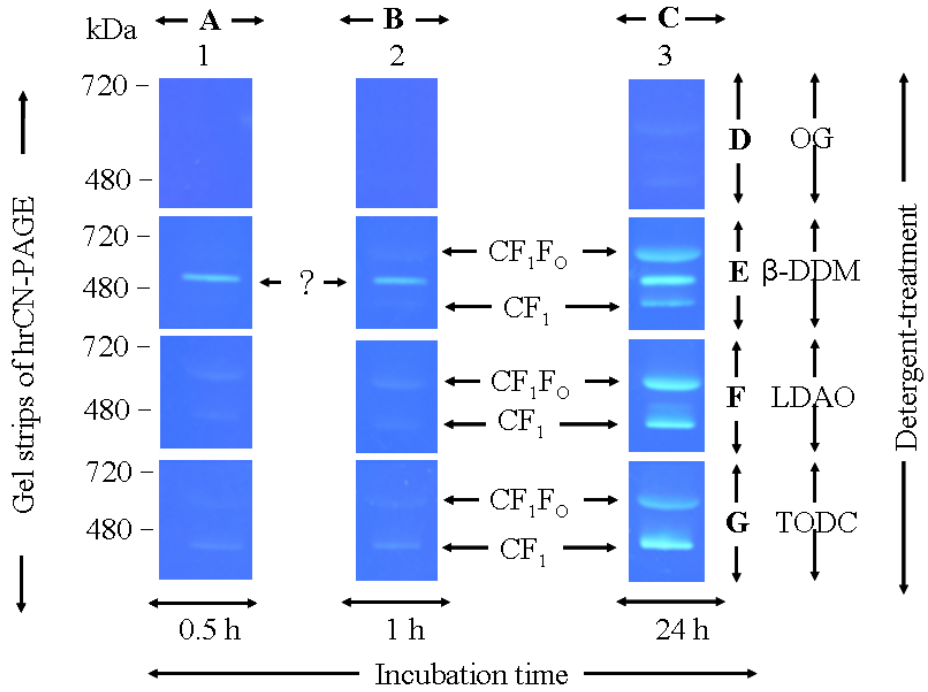

Figure 5.10 The CF_1F_O In-gel ATPase Hydrolysis Assay. The Functional characterization of the CF_1F_O ATP synthase by an in-gel ATPase hydrolysis assay. The hrCN-PAGE gel strips, each containing CF_1F_O, are incubated in buffers with different detergents to detect whether the ATPase activity depends on the detergent. The gel strips are preincubated with buffer containing OG (D), β-DDM (E), LDAO (F), or TDOC (G). In the in-gel ATPase activity assay, ATP hydrolysis can be visualized as the white band comprising precipitated lead phosphate. Images of the in-gel assays are taken under a special blue background after 0.5 h (A), 1 h (B) and 24 h (C) incubations, respectively. Both CF_1F_O and CF_1 are labeled, respectively. Please note that under β-DDM treatment, a band indicated by a question mark is identified by 2D electrophoresis that comprises CF_1F_O sub-complexes that could have lost the a-subunit and/or b-subunit of the CF_O domain by detergent micelles supplemented in the cathodic buffer during hrCN-PAGE electrophoresis.

Interestingly, in LDAO, the hydrolysis activity of the defective CF_1F_O supercomplex faintly appeared only after 24 h of incubation, and only a weak band appeared after 24 h of incubation (Figure 5.10, CF panel, lane 3). In contrast to results obtained following treatment with the detergents OG, β-DDM and LDAO, CF_1F_O treated with the harsh

detergent TDOC exhibited extremely low ATP hydrolysis activity after 0.5 h and 1 h of incubation (Figure 5.10, AG panel, lane 1 and BG panel, lane 2, respectively), and this activity substantially increased after 24 h of incubation (Figure 5.10, CG panel, lane3). The CF_1 ATP hydrolysis activity was clearly visible after 0.5 h as a low precipitate-stained intensity and a considerable increase in this activity was not observed after 1 h of incubation. After 24 h of incubation, the ATP hydrolysis activity of CF_1 was dramatically increased to an extremely higher precipitate-stained intensity (Figure 5.10, CG panel, lane3). In summary, comparisons of these results indicate that after 24 h of incubation, CF_1F_O exhibited higher ATPase activities in mild detergents such as LDAO and β-DDM, whereas lower ATP hydrolysis activity was detected in harsher detergents such as TDOC, and extremely low activity was detected in the harsher detergent OG. In contrast to the ATP hydrolysis activities of CF_1F_O after 24 h of incubation, CF_1 exhibited higher activities in TDOC and LDAO, low activity in β-DDM, and minimal activity in OG. Both CF_1F_O and CF_1 exhibited extremely low activities in LDAO and TDOC after 0.5 h and 1 h of incubation compared with those after 24 h of incubation, whereas no or minimal activities were observed for both CF_1F_O and CF_1 following either OG or β-DDM treatment after 0.5 h and 1 h of incubation. Due to the regulatory mechanism of CF_1F_O that prevents the futile hydrolysis of ATP in the dark, either short-chain detergents (e.g., OG and TDOC) or long-chain detergents (e.g., β-DDM and LDAO) could not drive intact CF_1F_O in the hydrolysis direction. In contrast, the CF_1F_O subcomplex observed in only the β-DDM treatment exhibited much higher ATP hydrolysis activity than either CF_1F_O or CF_1. Presumably, β-DDM, but not other detergents, enhanced the dissociation of the ε subunit, which is thought to inhibit the hydrolysis of ATP, from the head of intact CF_1F_O. Therefore, ATP hydrolysis in the CF_1F_O subcomplex was fully activated.

5.9 Functional Characterization of the CF_1F_O ATP Synthesis Activity

Although the functional state of the purified CF_1F_O can be qualitatively characterized using an in-gel ATP hydrolysis assay, quantitative functional characterization such as determining the H^+/ATP ratio is essential for understanding CF_1F_O in both bioenergetic and mechanistic considerations. The synthesis of a single ATP molecule catalyzed by one of three catalytic sites (β subunit) in the F_1 domain of the F_1F_O ATP synthase is driven by both free energy components of a transmembrane electrochemical potential ($\Delta\psi$) and a transmembrane proton gradient (ΔpH). The formation of ATP is coupled to the translocation of protons across the membrane. The number of protons required to be translocated for three synthesized ATP molecules is based on the number of monomers composing the c-oligomer motor. The number of c-subunit monomers varies according to species (currently between 8 and 15), leading to the prediction that the H^+/ATP ratio can vary among different species, which is identical to the stoichiometric ratio of c-subunits to β subunits between 2.7 (c/β=8/3) in *Bos taurus* and 5.0 (c/β=15/3) in *Arthrospira platensis*. The H^+/ATP ratio of chloroplast CF_1F_O in *Spinacia oleracea* is 4.7 (c/β=14/3). Only a few isolated F_1F_O ATP synthases have been well characterized in terms of either the H^+/ATP ratio or the rate of ATP synthesis (turnover rate), including the mitochondrial ATP synthase from yeast and *E. coli* and the chloroplast ATP synthase, due to the requirement of quantitative analysis techniques at high precision (Turina, Samoray et al. 2003, Steigmiller, Turina et al. 2008, Petersen, Forster et al. 2012). Currently, the chemiosmotic model system is extensively used for quantitative functional characterization in quantitative studies. In the early system, CF_1F_O was reconstituted into an asolectin liposome, and its maximal rate of ATP synthesis was 200 s^{-1} per CF_1F_O by energizing proteoliposomes with an acid-base transition to generate a transmembrane proton gradient (ΔpH), in combination with a

K^+/valinomycin diffusion potential, to create a transmembrane electrochemical potential ($\Delta\psi$) (Sone, Yoshida et al. 1977, Schmidt 1985, Fromme 1987). In the asolectin proteoliposome, the ATP synthesis rate must be measured within an extremely short time frame because the generated ΔpH is only available for approximately 300 ms. Presumably, the asolectin liposome exhibits relatively high H^+ permeability, and its size distribution is not homogeneous, resulting in a slower decrease in ΔpH in a large liposome than in a small liposome. Moreover, evidence from electron microscopy indicates that some of the asolectin liposomes contain more than one CF_1F_O, but some are completely empty. This consequence of the inhomogeneous distribution of CF_1F_O in the asolectin liposome also leads to a decrease in ΔpH in liposomes with multiple CF_1F_O much faster than those with a single CF_1F_O (Richard, Rigaud et al. 1990). Due to these disadvantages, the currently employed reconstitution procedure in the ATP synthesis assay was optimized with several crucial parameters by (Richard, Rigaud et al. 1990). CF_1F_O is first mixed with Triton X-100 to produce monodisperse protein prior to addition to the liposome, which also aids in the distribution of CF_1F_O in the liposome. The purified CF_1F_O was reconstituted into liposomes, composed of a mixture of phosphatidylcholine (PC) and phosphatidic acid (PA), which exhibit much lower proton permeability. However, CF_1F_O in the string-like structure that reduces its homogenous distribution into the liposome is another critical parameter, leading to low activity (Boekema, van Heel et al. 1988, Boekema 1988, Boekema, Schmidt et al. 1988, Richard, Rigaud et al. 1990). During the reconstitution step, the ratio of Triton X-100 to liposome was 1.0 and the incubation time was 1 h. Following reconstitution, the buffer composition between the internal and external phases of the proteoliposome was fully equilibrated.

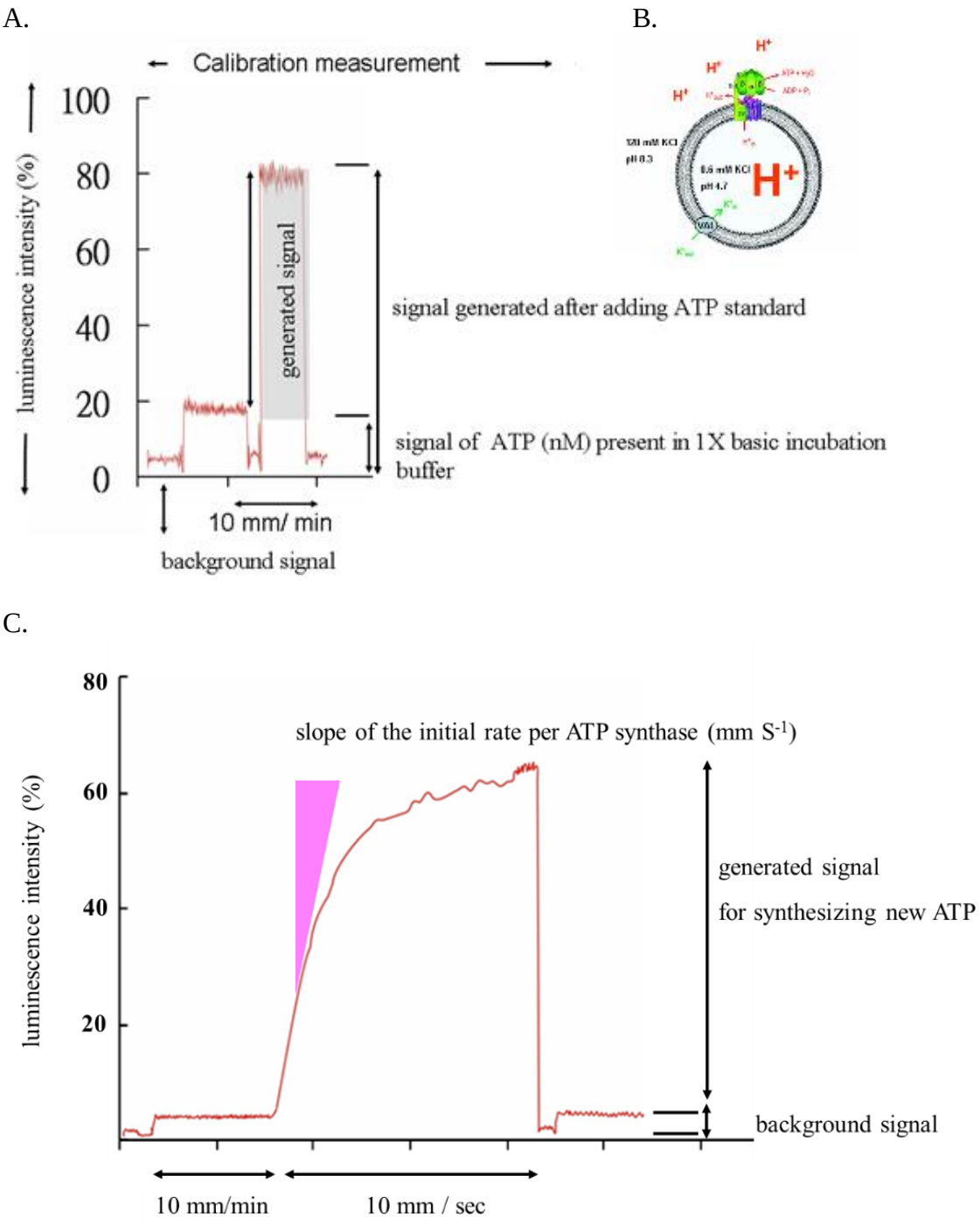

Figure 5.11 The CF_1F_O ATP Synthesis Activity Assay. Functional characterization of the ATP synthesis activity of CF_1F_O by the reconstitution assay with an acid-base transition. (A).The baseline recording and calibration measurement for determining the amount of free-ATP contaminants in the basic incubation buffer. (B). Scheme of the chemiosmotic system adapted from Turina et al. (2003) (Turina, Samoray et al. 2003). CF_1F_O is reconstituted into a liposome to form a proteoliposome that is energized with an acid-base transition, ΔpH, combined with a K^+/valinomycin diffusion potential, Δψ. (K). (C). The new ATP molecules synthesize after the generation of a transmembrane ΔpH. The luminescence intensity and slope correspond to the ATP yield and the initial rate of ATP synthesis per CF_1F_O, respectively.

Therefore, the corresponding pH value in the internal phase (pH_{in}) became identical to the pH value of the reconstitution buffer, which was measured with a pH electrode.Subsequently, these proteoliposomes were energized with acid–base transitions to generate a proton motive force, in combination with a K^+/valinomycin diffusion potential, to create a transmembrane electrochemical potential. In the acid–base transition step, the transmembrane ΔpH was established by mixing the acidified proteoliposome into the basic medium, corresponding to the initial pH_{out} value (Figure 5.11 B). Due to impurities in the ADP substrate, which is always contaminated by ATP, an unknown amount of ATP would contribute significant calculation errors in the stoichiometry. Figure 5.11 A shows the calibration scheme produced by luminescence signals to determine the unknown amount of ATP present in related media by the addition of a known amount of ATP, suggesting that 26 nM of ATP was found. Therefore, the final nucleotide concentrations present in the solution are 26 nM of ATP and 76 nM of ADP. The results of serial quantitative experiments (Figure 5.11 C) indicate that the catalyzed rates of ATP synthesis ranged between 150 s^{-1} and 200 s^{-1} per a single purified CF_1F_O (general average rate of 150 s^{-1}) suggesting that the purified CF_1F_O exhibited ATP synthesis activities in the physiological range.

5.10 Two-dimensional Crystallization of the CF_1F_O ATP Synthase

The structure determination of biomolecules is of the utmost importance to aid in understanding how such "simple" biomolecules, which are composed of amino acid residues, can perform such complex functional mechanisms observed in life. To date, over 100,000 protein structures have been determined by various combination techniques of crystallization, X-crystallography, electron microscopy, and NMR. Most of the determined protein structures are of water-soluble proteins, and less than 550

membrane protein structures are available, particularly difficult to integral membrane protein supercomplexes such as the photosynthetic protein complexes and ATP synthase complexes. Due to the hydrophobic nature of membrane proteins, the crystal growth of membrane proteins in three dimensions (3D) cannot be readily achieved compared with that of water-soluble proteins because the protein exists as a protein-detergent micelle and detergents cannot be present in the crystallization trial to maintain the protein-detergent micelle in three-dimensional crystals (exception: the membrane protein cyrstalization in the lipidic cubic phase). Because three-dimensional structures of membrane proteins can be successfully determined using two-dimensional (2D) crystals and electron crystallography at high resolution (Henderson and Unwin 1975, Henderson, Baldwin et al. 1990, Kuhlbrandt, Wang et al. 1994), electron crystallography of two-dimensional crystals has been rapidly developed as a powerful method to study membrane protein structures (Raunser and Walz 2009, Fujiyoshi 2011, Maeda, Shinzawa-Itoh et al. 2013). However, this method is limited by the 2D crystallization techniques, which involve several critical parameters including crystalline membrane proteins, the formation of a lipid monolayer, or the removal of detergents using Bio-Beads (Schmidt-Krey 2007). To date, only partial structures of the F-type ATP synthase including the F_1 domain, the F_1 domain with a partial peripheral stalk and the F_1–c_8 complex from mitochondrial ATP synthase F_1–c_{10} complex from yeast, and the c_{14}-ring complex from chloroplast ATP synthase have been determined (Abrahams, Leslie et al. 1994, Stock, Leslie et al. 1999, Rees, Leslie et al. 2009, Watt, Montgomery et al. 2010). Previous studies have also conducted atomic force microscopy (AFM) studies on the topography of the Na,K-ATPase and the F-type ATP synthase from *E. coli* and chloroplasts (Neff, Tripathi et al. 1997). However, a high-resolution crystal structure of an intact F-type ATP synthase is currently unavailable.

Hence, electron crystallography of 2D crystals is an alternative approach to achieve the final goal of the determination of the structure of intact F-type ATP synthase at high resolution. 2D crystal growth using dialysis-mediated detergent removal techniques have demonstrated success for the mitochondrial and chloroplast ATP synthases (Bottcher, Graber et al. 1995, Neff, Tripathi et al. 1997, Maeda, Shinzawa-Itoh et al. 2013).

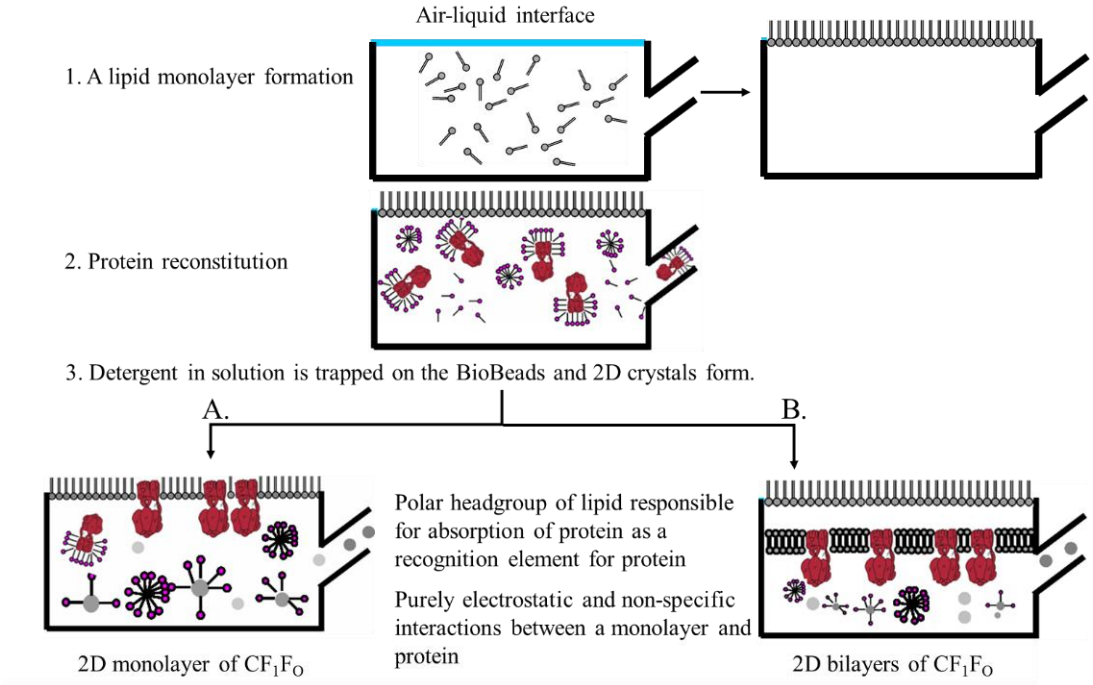

Figure 5.12 Method of the 2D Crystallization on a Lipid Monolayer or a Lipid Bilayer. Schematic method of two-dimensional (2D) crystallization of the intact CF_1F_O ATP synthase complex on a lipid monolayer or a lipid Bilayer. The growth of 2D crystals of the intact CF_1F_O ATP synthase complex on lipid mono- or bilayers is based on an air-liquid interface technique. Lipids are first solubilized in an organic solvent and deposited at the top of the subphase containing the detergent-free buffer. Then, the deposited lipids spread out toward the air-lipid interface. After typically 2 h of incubation, a monolayer is formed on the air-liquid interface while the organic solvent evaporates. A solution of β-DDM -solubilized CF_1F_O at an appropriate lipid: protein ratio that yields optimal results is injected through the side tube to the bottom of the well. Finally, CF_1F_O begins to be embedded into the lipid monolayer (A) or lipid bilayer (B) after a few hours of incubation. The detergents are absorbed by Bio-Beads injected through the side tube to the bottom of the well. Once the detergent is absorbed, the growth of 2D crystals occurs.

A lipid monolayer is an alternative approach for growing well-ordered 2D crystals in a shorter time period, so far which has only been successfully applied for the mitochondrial ATP synthase (Arechaga and Fotiadis 2007). The primary focus in this section is the formation of 2D CF_1F_O crystals on a lipid monolayer using an air-water interface technique. The successful formation of an ordered 2D arrangement of CF_1F_O on a lipid monolayer is critically dependent on two coupling processes: the absorption of CF_1F_O onto the lipid monolayer and the natural interaction between the protein and lipid monolayer. Figure 5.12 shows a schematic method for the two dimensional (2D) crystallization of the intact CF_1F_O ATP synthase complex. Initially, CF_1F_O will associate with the lipid monolayer and insert in to the lipid monolayer due to the hydrophobic nature of CF_O, leading to a unidirectional CF_1F_O insertion with the CF_1 domain toward the aqueous subphase on the lipid monolayer. This limits an orientation perpendicular to the monolayer and further facilitates CF_1F_O organization within the plane, ideally leading to the formation of 2D crystals in a unidirectional orientation (Figure 5.12 A). Alternatively, CF_1F_O could be alos reconstituted into a lipid bilayer and organized in a bidirectional orientation in the absence of an association between CF_1F_O and the lipid monolayer (Figure 5.12 B). Three different compositions of lipid mixtures (POPA, POPC, POPE and POPG) were used for the formation of the lipid monolayer. The 2D crystallization trials of CF_1F_O began with CF_1F_O solubilized with 4 mM β-DDM by optimizing the protein-to-lipid ratios to approximately 1.0 and imaged using negative-stain electron microscopy (see Materials and Methods). A comparison of electron micrographs in Figure 5.13 A, B and C indicates a lack of two-dimensional ordered arrays of CF_1F_O but rather string-like structures of CF_1F_O observed in these crystallization attempts, suggesting that CF_1F_O molecules were incorporated into the lipid bilayer, not the lipid monolayer.

A few of these string-like structures were observed in the mixture of POPC: POPA (19:1) (Figure 5.13 A) and the best results were obtained in the mixture of POPC:POPE: POPG: POPA (49:49:1:1) (Figure 5.14 C, D, E, F, G, and H). Unidentified string-like structures were observed in the mixture of POPC: POPE: POPG (49:49:2) (Figure 5.13 B). This finding may be due to poor negative staining. These string-like structures can be interpreted as side view projections of CF_1F_O in a one-dimensional packing (Figure 5.14 B), which were similar to structures observed in 2D crystallization trials from mitochondrial and chloroplast ATP synthases shown in Figure 5.14 A (Bottcher and Graber 2000) and Fromme (1988) (Fromme 1988, Bottcher and Graber 2000) and Figure 5.14 B (Arechaga and Fotiadis 2007) (Arechaga and Fotiadis 2007) and (Poetsch, Neff et al. 2000).

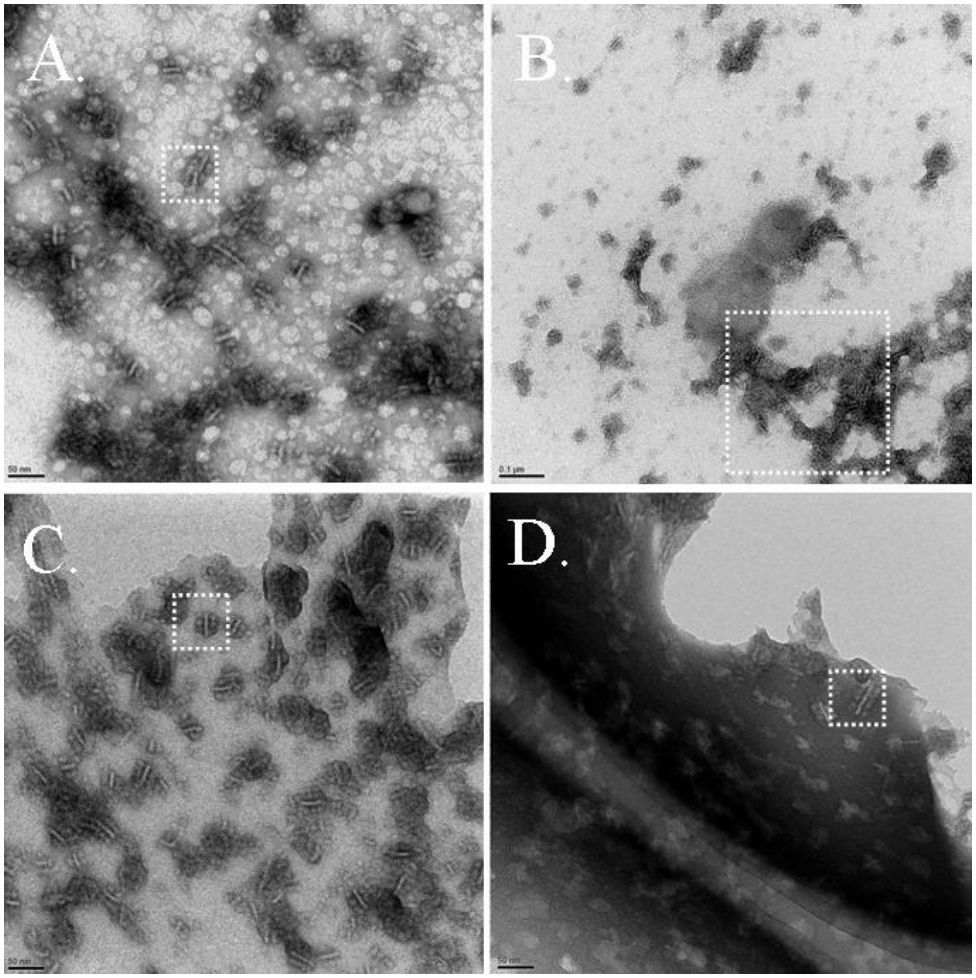

Figure 5.13 (continued on next page)

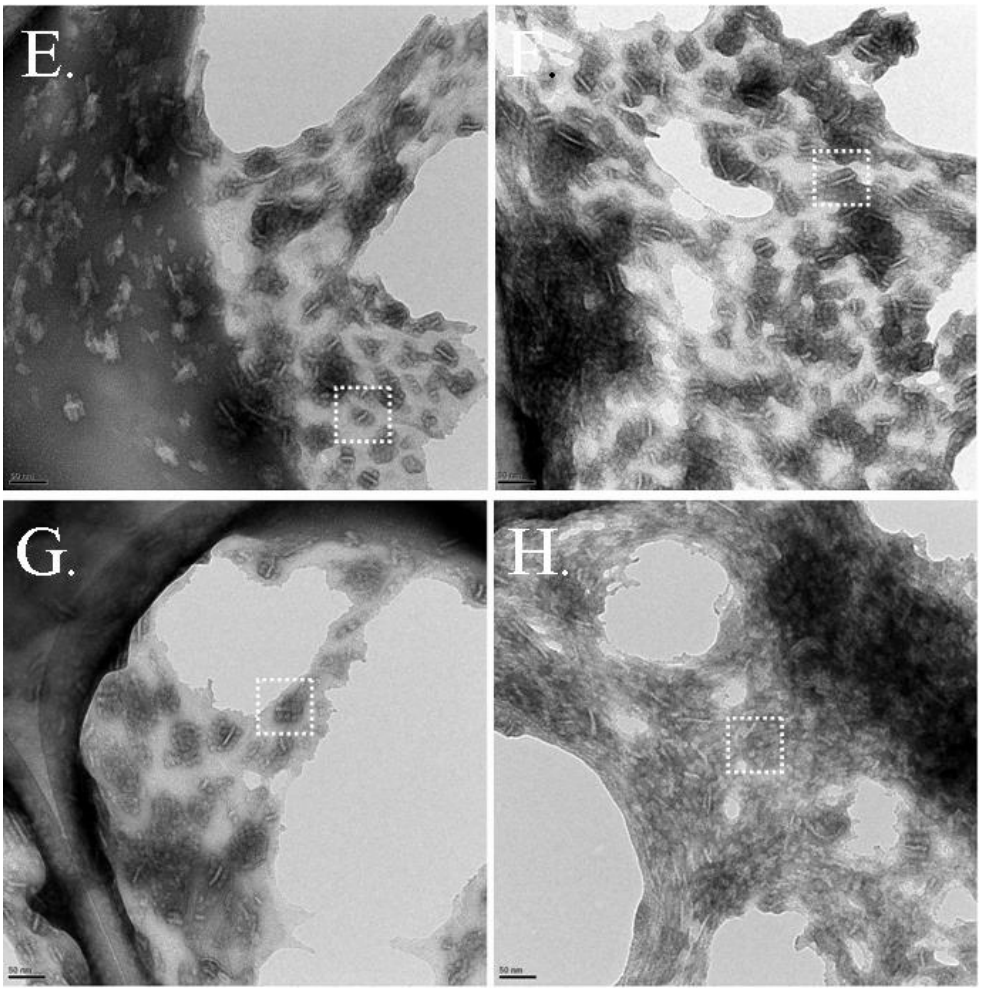

Figure 5.13 Transmission Electron Microscopy of 2D Crystals of CF_1F_O ATP Synthase. Transmission electron microscopy of negatively stained 2D crystals of CF_1F_O ATP synthase. (A). Overview electron micrograph of 2D crystals of CF_1F_O in the mixture of POPC: POPA. (B). Overview electron micrograph of 2D crystals of CF_1F_O in the mixture of POPC: POPE: POPG. (C, D, E, F, G, and H). Overview electron micrograph of 2D crystals of CF_1F_O in the mixture of POPC: POPE: POPG: POPA.The selected region marked by dashed square frame shows that CF_1F_O is reconstituted into the lipid bilayer and forms string-like structures. The selected regions marked by dashed square frames and magnified show in Figure 5.14.

Additionally, knob structures observed protruding from the lipid bilayer were considered to represent the hydrophilic CF_1 domains due to their dimensions of approximately 14–15 nm in height and 10–11 nm in width (Figure 5.14 D). Similar dimensions for the CF_1 domain were obtained by Arechaga and Fotiadis (2007) (Arechaga and Fotiadis 2007) (Figure 5.14 B). In contrast, the CF_O domains embedded into the lipid bilayer were parallel to the string-like structure and could be

not individually visualized because they did not appear as separate entities. Similarly, the dimensions of the CF_O domain could not be directly determined due to the difficulty in distinguishing the individual CF_O domains in the string-like structure. The size of the lipid bilayer in the area indicated by a dashed frame in the electron micrograph (Figure 5.14 C) and magnified (Figure 5.14 H) revealed an approximate length of 33.3 nm and a thickness of 3.7 nm, indicating that the CF_1F_O complexes were packed in an upside-down orientation. According to its length, three CF_1F_O complexes were packed along each side of the lipid bilayer. A total six CF_1F_O complexes were successfully observed on both sides. Currently, it is unclear whether the three closely packed CF_1F_O complexes possess identical conformations for the peripheral stalk or stator during reconstitution due to poor magnification of the images. Due to the observed thickness, the CF_O domains of adjacent CF_1F_O molecules were presumably alternating (Figure 5.14 D), which may also be due to the larger dimension of the CF_1 domain than that of the CF_O domain. However, a similar packing orientation was also observed by Arechaga and Fortiadis (2007) (Arechaga and Fotiadis 2007) (Figure 5.14 B). It is assumed that the CF_O domains are packed to face toward the CF_O domains on the other side (Figure 5.14 F and G). The average thickness of the lipid bilayer was observed to be approximately 4–5 nm. Furthermore, the hydrophobic CF_O domains appeared to interact and form string-like structures of different lengths (Figure 5.14 D, E, F, G, and H). Similar structures have also been reported by Bottcher and Graber (2000) (Bottcher and Graber 2000) and Fromme (1988) (Fromme 1988) (Figure 5.14 A), indicating that the CF_O domains can aggregate to form string-like structures of different lengths due to insufficient detergent to solubilize the strongly hydrophobic regions and that the thickness of these aggregated CF_O domains is 8.3 nm. Comparisons of the observed and previously reported thicknesses of the CF_O domains reveals that the formation of these

observed string-like structures was not due to insufficient detergent but due to the reconstitution of the CF_O domains into the lipid bilayer. Previous studies have indicated that protein reconstitution can be concomitant with the formation of 2D crystals in the latter (Poetsch, Neff et al. 2000, Arechaga and Fotiadis 2007).

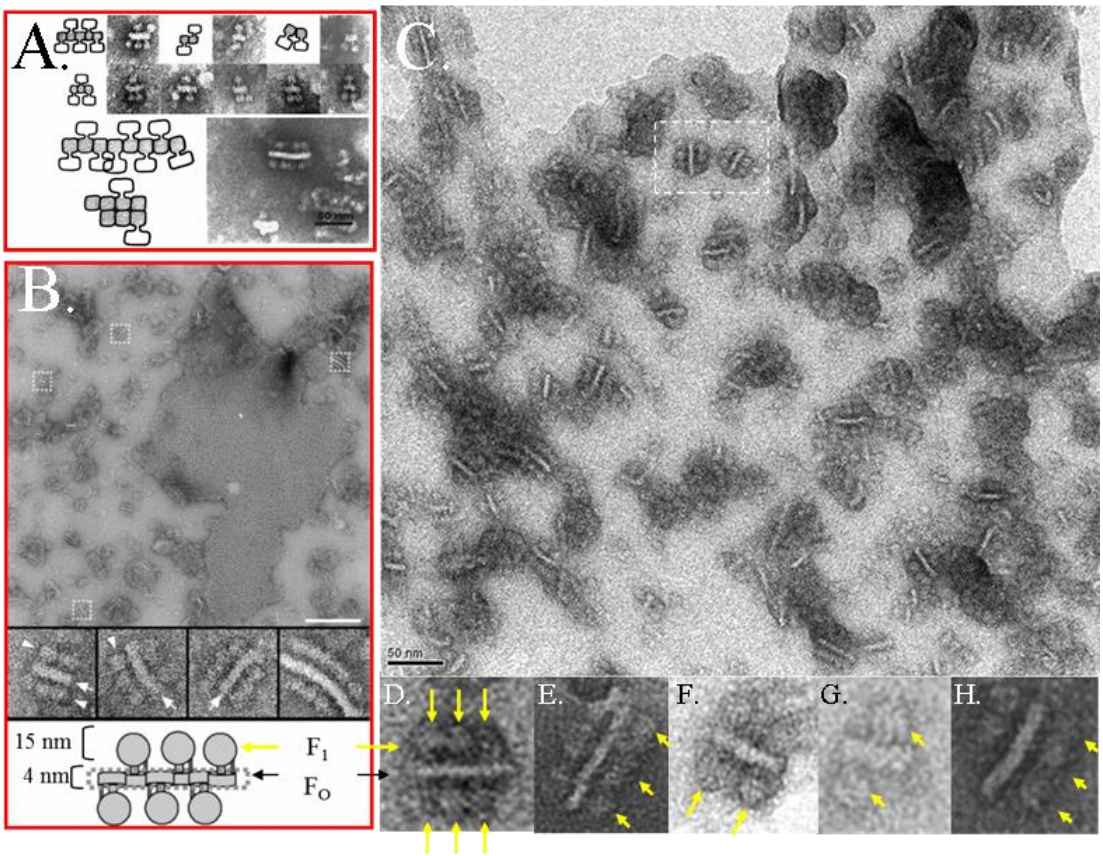

Figure 5.14 Transmission Electron Microscopy of 2D Crystals of CF_1F_O ATP Synthase. Transmission electron microscopy of negatively stained 2D crystals of CF_1F_O ATP synthase. (A). The CF_O domains can aggregate to form string-like structures of different lengths due to insufficient detergent to solubilize the strongly hydrophobic regions. Figure adapted from Bottcher and Graber (2000) and Fromme (1988) (Fromme 1988, Bottcher and Graber 2000). (B). Overview electron micrograph of bovine F_1F_O-ATP synthase and its side view of the string-like structure. Figure adapted from Arechaga and Fotiadis (2007) (Arechaga and Fotiadis 2007). (C). Overview electron micrograph of 2D crystals of CF_1F_O in the mixture of POPC: POPE: POPG: POPA. The selected region marked by dashed square frame shows that CF_1F_O is reconstituted into the lipid bilayer and forms string-like structures. (D, E, F, G, and H). The selected regions from Figure 5.14 and magnified show that CF_1F_O is reconstituted into the lipid bilayer and forms string-like structures with knobs, corresponding to CF_1, in an up-down orientation. The CF_1 and CF_O domains are indicated by the yellow hue of the arrowheads and the black hue of the arrowheads, respectively.

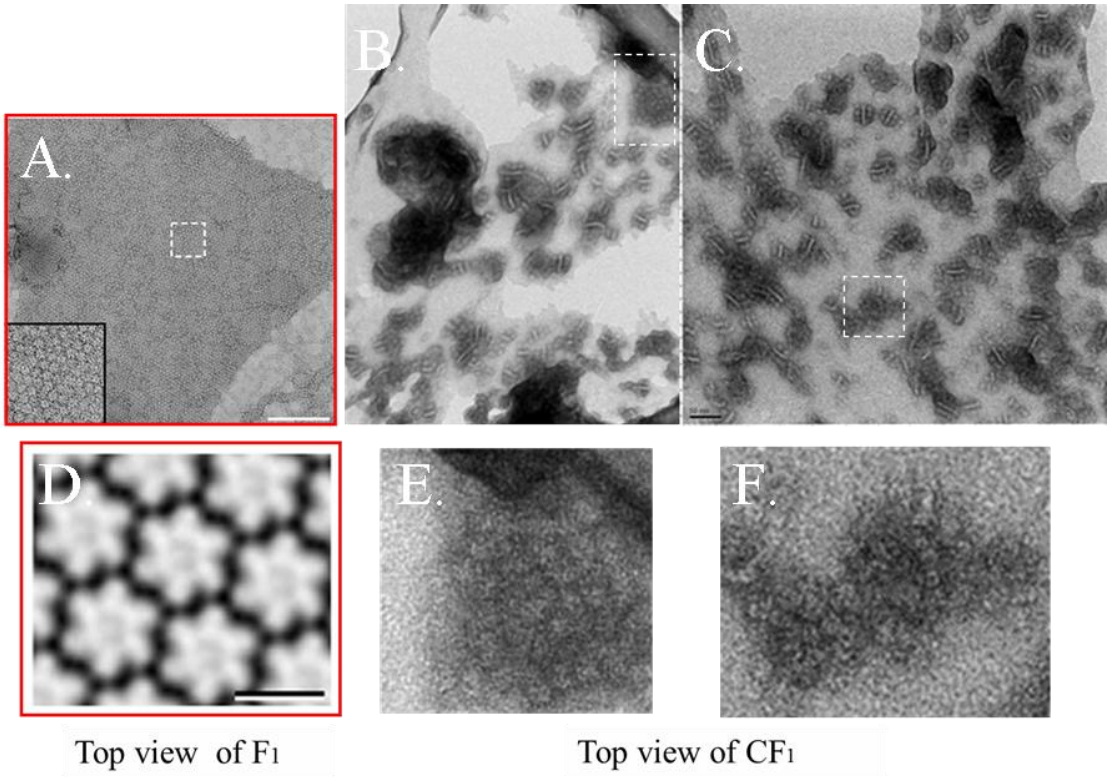

Figure 5.15 Transmission Electron Microscopy of 2D Crystals of CF_1F_O ATP Synthase. Transmission electron microscopy of negatively stained 2D crystals of CF1FO ATP synthase. (A). Overview electron micrograph of yeast F_1F_O-ATP synthase, adapted from Arechaga and Fotiadis (2007) (Arechaga and Fotiadis 2007). (B and C). Overview electron micrograph of 2D crystals of CF_1F_O in the mixture of POPC:POPE:POPG:POPA.The regions marked by dashed circular frames and magnified (E and F) show the top view of either CF_1 or CF_O due to the poor negative staining compared with the top view of MF_1 (D) in the high resolution images, adapted from Arechaga and Fotiadis (2007) (Arechaga and Fotiadis 2007).

Although no clear evidence indicated that these CF_1F_O string-like structures were organized into 2D crystals, it is believed that the regions marked by the dashed circle frame (Figure 5.15 B and C) and magnified (Figure 5.15 E and F) represent candidates for initial CF_1F_O 2D crystals due to the round ordered particles. Similar ordered structures have been observed in 2D crystallization trials of the mitochondrial and chloroplast ATP synthases showing in the Figure 5.15 A and D (Arechaga and Fotiadis 2007) and (Poetsch, Neff et al. 2000). These round ordered structures apparently represent the top view of initial 2D CF_1F_O crystals. Unfortunately, these structures could not be distinguished from either CF_1 or CF_O 2D crystals due to poor negative

staining. However, the primary reason for the lack of increased growth of initial 2D CF_1F_O crystals may be due to an insufficient incubation time. Therefore, a longer incubation time will be evaluated in subsequent 2D crystallization trials. Additional lipids at different compositions will be evaluated to form the lipid monolayer, particularly lipids such as DOPC that have been successfully used for the 2D crystallization of mitochondrial and chloroplast ATP synthase. Additionally, both $CaCl_2$ and phospholipase A_2, which have been successfully used for the formation of 2D crystals of chloroplast ATP synthase (Bottcher, Graber et al. 1995, Neff, Tripathi et al. 1997), will be included in subsequent crystallization trials.

CHAPTER 6

THE HELIOBACTERIAL ATP SYNTHASE

Purification and biochemical characterization of the ATP-synthase of *Heliobacterium modesticaldum*

6.1 Abstract

Heliobacterium modesticaldum is an anaerobic photosynthetic bacterium that grows optimally at pH 6-7 and 52℃ and is the only phototrophic member of the Firmicutes phylum family (gram-positive bacteria with low GC content). The ATP synthase of *H. modesticaldum* was isolated and characterized at the biochemical and biophysical levels. The isolated holoenzyme exhibited the subunit patterns of F-type ATP synthases containing a 5-subunit hydrophilic F_1 subcomplex and a 3-subunit hydrophobic F_O subcomplex. ATP hydrolysis by the isolated HF_1F_O ATP synthase was successfully detected after pretreatment with different detergents by an in-gel ATPase activity assay, which showed that the highest activity was detected in the presence of mild detergents such as LDAO; moreover, high catalytic activity in the gel was already detected after the initial incubation period of 0.5 h. In contrast, HF_1F_O showed extremely low ATPase activity in harsher detergents such as TODC. The isolated fully functional enzyme will form the basis for future structural studies.

6.2 Introduction

Heliobacterium modesticaldum is a thermophilic anoxygenic phototrophic bacterium that grows either photoheterotrophically or chemotrophically in the dark by fermentation but does not grow photoautotrophically due to the lack of several genes encoding key enzymes required for the known autotrophic carbon fixation pathways (Sattley and Blankenship 2010, Tang, Yue et al. 2010). *Heliobacterium modesticaldum*

may have played a key role in the evolution of phototrophic bacteria. The electron transport chain contains a type I photosynthetic reaction center (RC) that employs bacteriochlorophyll (Bchl *g*) as the primary electron donor. The majority of recent studies have focused on characterization of the photosynthetic reaction center and electron transport chain. The energy metabolism of *H. modesticaldum* has been studied to a much lesser extend, and no isolation or biochemical studies have been reported thus far for the *H. modesticaldum* ATP synthase, which is one of the key enzymes involved in bioenergetic energy conversion. Based on the genomic information of *H. modesticaldum*, it is known that this organism contains a gene cluster for an F-type ATP synthase in which all eight subunits are encoded in a single conserved operon (Sattley and Blankenship 2010). However, due to the lack of any biochemical data, the structure, function and regulation of the ATP synthase of *H. modesticaldum* are still poorly understood. The membrane-bound F-type ATP synthase is a multi-subunit membrane protein complex that functions as a universal rotary nano-machine in the energy-transducing membranes of bacteria, mitochondria, and chloroplasts (Turina, Samoray et al. 2003). The chloroplast ATP synthase is a multi-subunit complex comprising 9 different subunits ($\alpha_3\beta_3\gamma\delta\varepsilon I_1 II_1 III_{12\text{-}14} IV_1$) located in two major domains (CF_1 and CF_0). The hydrophilic CF_1 domain comprises 5 different subunits ($\alpha_3\beta_3\gamma\delta\varepsilon$). In most bacteria, the hydrophobic membrane-bound CF_0 domain comprises 3 different subunits (a, b_2, and $c_{10\text{-}15}$), which correspond to the chloroplast subunits (a= IV_1, b_2=I_1 and II_1, and $c_{10\text{-}15}$ = $III_{10\text{-}15}$ IV_1). The CF_1 and CF_0 domains are connected in the CF_1F_0 protein complex by two peripheral stalks: a central interior stalk comprising γ and ε subunits, and the peripheral exterior stalk comprising the I and II subunits as well as the δ subunit (Bottcher, Schwarz et al. 1998). Three ATP molecules are synthesized in the three catalytic sites in CF_1 during one full rotation of the central stalk and the c-ring, driven

by an electrochemical proton gradient. Up to 400 ATP molecules per second are synthesized in the natural environment (Peter Gräber 1984, Pänke 1997, Poetsch, Seelert et al. 1999, Seelert, Poetsch et al. 2000). F-type ATP synthases can act in both synthesis and hydrolysis directions; in the synthesis direction, the enzyme synthesizes ATP, which is driven by an electrochemical proton gradient. In the reverse direction, ATP hydrolysis drives the translocation of protons across the photosynthetic membrane. However, photosynthetic organisms must avoid ATP hydrolysis in the absence of an electrochemical gradient; therefore, the hydrolytic function of CF_1F_O is inactivated at night by redox modulation of a disulfide bridge on its γ subunit via thioredoxin (Junesch and Graber 1991, Ort 1992, Evron, Johnson et al. 2000, Hisabori, Konno et al. 2002, Hisabori, Ueoka-Nakanishi et al. 2003, Richter 2004) (Kohzuma, Dal Bosco et al. 2013). This study is, to the best of our knowledge, the first report of the successful isolation and biochemical characterization of the ATP synthase from *Heliobacterium modesticaldum*. We used an in-gel ATPase activity assay, which is well established and has previously been successfully applied to the detection of the activity of mitochondrial ATP synthases and spinach chloroplast ATP synthases, as well as the ATP synthases from the cyanobacterium *T. elongatus* and the green algae *C. reinhardtii* (Suhai, Heidrich et al. 2009), to study the activity of the ATP synthase in the presence of different detergents. In contrast to mitochondrial ATP synthases, for which high ATP hydrolysis activities have been reported (Suhai, Heidrich et al. 2009), the chloroplast ATP synthase has low ATPase activity due to the inhibition mechanism that prevents wasteful ATP hydrolysis in the dark. This inactivation is mediated by a conformational change of the ε subunit of CF_1 (Richter, Patrie et al. 1984, Gertz, Seelert et al. 2007), which occurs induced by the lack of proton gradient, the binding of Mg^{2+}-ATP (Du and Boyer 1990, Digel, Hightower et al. 1996, Digel, Kishinevsky et al. 1996, Du, Tucker

et al. 2001), and and the oxidation of cysteine residues in the γ subunits to a disulfide bond (Gest H 1983, Nalin and McCarty 1984, Ort 1992). Several studies used harsh pre-treatments of the chloroplast enzyme, including heating, organic solvents, and trypsin, to stimulate the ATPase activity of CF1, which is the hydrophilic part of the enzyme that contains the nucleotide binding sites (Farron 1970, Sakurai, Shinohara et al. 1981, Anthon and Jagendorf 1983, McCarty 2005). The interaction of some harsher detergents with the solubilized CF_1 part of the chloroplast ATP synthases led to enhanced ATPase activity (Pick and Bassilian 1982, Yu and McCarty 1985, Turina, Samoray et al. 2003). The stimulation of CF_1 ATPase activity by harsh detergents that form small micelles may be induced by the dissociation of the ε subunit from the chloroplast CF_1 subcomplex. Various detergents, including alkylglucosides, LDAO, and TDOC, have previously been tested to study the effect of the dissociation of the CF_1- ε subunit (Pick and Bassilian 1982, Yu and McCarty 1985, Turina, Samoray et al. 2003). With an increase of the micelle size by increasing the chain length, the interaction of alkylglucosides with CF_1 becomes less and less effective in removing the ε subunit, resulting in lower ATPase activity (Yu and McCarty 1985). In contrast to the chloroplast enzyme, the hydrolytic function of ATP synthase is a vitally important process in anaerobic bacteria that lack a membrane-bound respiratory chain to establish a gradient of electrochemical potential for protons or sodium ions (Mesbah and Wiegel 2011). The F_1F_O ATP synthase of the alkaliphilic bacterium *Natranaerobius thermophilus* is one example that it does not function in ATP synthesis (Mesbah and Wiegel 2011) but the enzyme catalyzes ATP hydrolysis to expel cytoplasmic Na^+ to avoid Na toxicity. *H. modesticaldum* lacks the internal membranes present in cyanobacteria; the photosynthetic electron transport chain is instead embedded into the cytoplasmic membrane. Therefore, it is commonly assumed that an electrochemical

gradient across the cytoplasmic membrane that is established during the photosynthetic process, drives ATP synthesis. However, whether ATP hydrolysis might also be an essential function of the heliobacterial HF_1F_O remains unknown. It is also unknown whether regulation of the reverse direction of the *H. modesticaldum* ATP synthase is similar to the inactivation mechanism of CF_1F_O at night. In this chapter, we report on the isolation and biochemical characterization of the functional ATP synthase from *H. modesticaldum*. The identities of all subcomplexes and individual subunits of the ATP synthase were determined. We also discovered that the isolated ATP synthase remains active during native gel electrophoresis using an in-gel ATPase activity assay. In contrast to the chloroplast ATP-synthase, no activation is required for the ATPase activity of the ATP synthase from *H. modesticaldum. The H. modesticaldum enzyme is fully active* in the presence of mild detergents, while it is denatured in harsh detergents. Our studies show that the isolated ATP synthase from *H. modesticaldum* is fully functional and is suitable for further functional and structural studies.

6.3 Materials and Methods

6.3.1 Purification of ATP synthase Complex from *Heliobacterium modesticaldum*

The HF_1F_O ATP synthase complex was isolated from *H. modesticaldum* as previously described (Turina, Samoray et al. 2003, Varco-Merth, Fromme et al. 2008, Sarrou, Khan et al. 2012) for the chloroplast ATP synthase. Liquid cultures of *H. modesticaldum* were grown anaerobically using pyruvate-yeast extract medium (pH 6.9) at 52℃ under 4,500-6,000-lux incandescent illumination until the stationary phase is reached (Kimble LK 1995). The cells were harvested by centrifugation at 10,000xg_{max} for 15 min at 4℃ and then re-suspended in 200 ml of harvesting buffer containing 50 mM MOPS (pH 7.0) and 5 mM magnesium chloride. The cells were disrupted by sonication with a

100% duty cycle for 15 cycles at 50% power using an ultrasonic homogenizer, Model 300 V/T (Biologics Inc., Manassas, Virginia). The lysate was subjected to high-speed centrifugation at 200,000xg_{max} for 1 h at 4℃, and the membrane pellets were suspended in the harvesting buffer described above. Prior to detergent solubilization, DL-Dithiothreitol (DTT) was added to reach a final concentration of 50 mM and incubated with agitation for 15 min at 4℃. The membrane proteins were then solubilized in a buffer containing 20 mM Tricine (pH 8.0), 200 mM sucrose, 5 mM magnesium chloride, 400 mM ammonium sulfate, 2 mM Na_2-ATP, 6.25 mM sodium cholate (Sigma, USA), 12 mM n-octyl-β-D-glucoside (OG) (GLYCON, Germany), and 50 mM DTT for 15 min at 4℃ and then subjected to centrifugation at 200,000xg_{max} for 1 h at 4℃ to separate solubilized protein-detergent micelles from non-solubilized membranes. The solubilized protein-detergent micelles were precipitated with ammonium sulfate (45%, v/v) at 4℃. The ammonium sulfate precipitation pellet containing the HF_1F_O ATP synthase was re-suspended in buffer containing 30 mM monobasic sodium phosphate (pH 7.2), 200 mM sucrose, 2 mM magnesium chloride, 0.5 mM Na_2-EDTA, and 4 mM n-dodecyl-β-D-maltopyranoside (β-DDM) (GLYCON, Germany) and was further purified by sucrose density gradient centrifugation at 242,000xg_{max} for 17 h at 44℃ in gradient buffer containing 30 mM monobasic sodium phosphate (pH 7.2) , 2 mM magnesium chloride, 0.5 mM Na_2-EDTA, 8 mM β-DDM, 1 mg/ml asolectin and sucrose at a concentration range from 20%-60% (w/v). The fractions from the sucrose density gradient were collected from the bottom to the top of the gradient. The sucrose was removed by using Sephadex G-25 desalting columns at 4℃ previously equilibrated in buffer containing 10 mM Tricine (pH 8.0), 5 mM magnesium chloride, and 8 mM β-DDM and the ATP synthase was concentrated with a 100-kDa cutoff concentrators membrane filter devices (Millipore, Billerica, MA) prior to further experiments.

The protein concentration was determined according to the modified Lowry method (Lowry, Rosebrough et al. 1951, Hartree 1972).

6.3.2 Protein Analysis by Electrophoresis Techniques

The subunit composition of the HF_1F_O ATP synthase was analyzed using 15% Tricine-SDS–PAGE polyacrylamide gels, according to Schagger (2006) (Schagger 2006) with a few modifications: protein samples were diluted at a 1:2 ratio with sample loading buffer (62.5 mM Tris-HCl pH 6.8 , 2% (w/v) SDS, 25% (w/v) glycerol, 0.01% (w/v) bromophenol blue), and incubated at 80℃ for 30 min to completely disassemble the c-ring of ATP synthase. The gels were run at 4℃ for 3 h. The intact HF_1F_O ATP synthase was analyzed using 4%~16 % native polyacrylamide gels as previously described (Wittig, Carrozzo et al. 2007, Wittig, Karas et al. 2007) with modifications: protein samples, in the presence of β-DDM at 8 mM, were mixed with 2X native sample buffer (100 mM sodium chloride, 100 mM imidazole-HCl, 4 mM 6-aminohexanoic acid, 10% (w/v) glycerol, 2 mM EDTA pH 7.0). Subsequently, protein samples for blue native gel electrophoresis (BN-PAGE) and high-resolution clear native gel electrophoresis (hrCN-PAGE) were additionally supplemented with Coomassie Blue G-250 dye (a detergent/Coomassie ratio of 8) and Ponceau S (0.01%, w/v), respectively. The native electrophoretic buffers were identical except that the BN-PAGE cathode buffer contained the anionic Coomassie Blue G-250 dye (0.02%, w/v), and the hrCN-PAGE cathode buffer contained two detergents (0.05%, w/v) sodium deoxycholate (Sigma, USA) and 0.01% (w/v) non-ionic β-DDM). Native gel electrophoresis was performed at 4℃ to maintain protein-complex integrity. Protein bands were visualized with either the Coomassie Blue staining method or the Silver staining method (Merril, Dunau et al. 1981).

Heme-containing proteins were detected with the heme staining method (Francis and Becker 1984). For immunoblot analysis, performed in principle as previously described (Lawrence, Varco-Merth et al. 2011), the proteins were transferred onto a PVDF membrane in a buffer optimized for the transfer of ATP synthase subunits (25 mM Tris base, 192 mM glycine, 0.1% (w/v) SDS, and 20% (v/v) methanol). The membrane was blocked in 5% (w/v) non-fat milk containing 50 mM Tris-Base, 150 mM sodium chloride, and 0.05% (v/v) Tween-20 for 1 h and then incubated with primary antibodies (AptA and AptH, 1:10,000, Agrisera, Sweden) in 5% (w/v), non-fat dry milk in 1X Tris-buffered saline with Tween-20 (TBST buffer), containing 50 mM Tris–HCl pH 8.0, 150 mM sodium chloride, 0.05% (v/v) Tween-20), washed three times with 1X TBST, incubated with goat anti-rabbit IgG-HRP -conjugated secondary antibodies (1:5,000), washed again, and stained with the Immun-Star HRP substrate reagent.

6.3.3 In-gel Activity of ATP Hydrolysis Assay

The in-gel assay of ATP hydrolysis activity was performed as previously described (Suhai, Heidrich et al. 2009) with modifications, as follows: hrCN-PAGE gel strips were pre-equilibrated in 40 mM Tris-HCl, 4 mM ATP, and 1.5 mM magnesium chloride (pH 8.0) supplemented with 30 mM of various detergents, including beta-dodecylmaltoside (β-DDM) (Glycon), β-octylglycoside (OG) (Glycon), N,N-dimethyl-1-dodecanamine-N-oxide (LDAO) (Affymetrix/Anatrace), or tauro-deoxycholate (TDOC) (Sigma-Aldrich), for 3 hours at room temperature. Following removal of the incubation solution and a 1-min brief rinse with deionized water, the gel strips were incubated in an assay buffer comprising 35 mM Tris-HCl, 270 mM glycine, 14 mM magnesium sulfate, 0.075% (w/v) lead nitrate, and 0.8 mM ATP (pH 7.8) with 20% (v/v) methanol at room temperature for 30 min, 60 min and for 24 h.

Increasing ATP hydrolysis activity leads to increasing lead phosphate precipitate formation. For imaging, the reaction was stopped with 50% (v/v) methanol. The gel strips were incubated for 30 min and then rinsed with deionized water. The transparent gel strips were imaged on top of a blue background to improve the visibility of the lead nitrate bands.

6.4 Results and Discussion

6.4.1 Purification and Subunit Composition of the HF_1F_O ATP Synthase

Since the discovery of heliobacteria, remarkable progress has been made in the understanding of their physiology and energy metabolism, as well as in the characterization of their photosynthetic reaction center, including the pigment composition and electron transfer reactions (Neerken and Amesz 2001, Heinnickel, Agalarov et al. 2006, Heinnickel and Golbeck 2007, Oh-oka 2007, Tang, Yue et al. 2010, Sarrou, Khan et al. 2012, Chauvet, Sarrou et al. 2013). *Heliobacteria* differ from many other photosynthetic organisms as they lack differentiated internal membranes or membrane-bound vesicles. Therefore, the cytoplasmic membrane is the only membrane system found in *Heliobacteria* (Asao and Madigan 2010). All membrane-bound complexes, including all photosynthetic complexes and a large number of various transporters for transporting essential substrates into the cells, are confined to this cytoplasmic membrane (Asao and Madigan 2010, Sattley and Blankenship 2010). According to the complete genome sequence analysis of *H. modesticaldum* (Sattley, Madigan et al. 2008), a gene cluster was identified for the ATP synthase that contains all eight subunits and it is assumed that the enzyme is present in the cytoplasmic membrane (Sattley, Madigan et al. 2008, Sattley and Blankenship 2010). The primary aim of this study was to establish a method to purify the intact ATP synthase complex

from *H. modesticaldum* for further bioenergetic and structural studies. Studies aimed to isolate the photosynthetic reaction center of *H. modesticaldum* used a low percentage of either β-DDM or β-DM to extract the photosynthetic reaction center from the membrane (Sarrou, Khan et al. 2012, Kashey, Cowgill et al. 2014). We modified the protocol developed for the photosynthetic RC by varying the nature of the detergents as well as their concentrations, taking into account procedures established for the chloroplast enzyme from plants and the ATP synthase from cyanobacteria. The maximal yield of ATP synthase extracted from cytoplasmic membranes was obtained using a detergent mixture of 6.25 mM cholate and 15 mM OG, as described in the materials and methods section. Subsequently, the ATP synthase complex was precipitated by ammonium sulfate fractionation at 45% (v/v) saturated ammonium sulfate solution at 4℃ (Figure 6.1, lane 2). The fraction was confirmed by western blotting (the c-subunit, AtpH), as shown in Figure 6.1, lane 3. The fraction also contained a lower amount of heme-containing proteins (cyt c_{533}), as shown in Figure 6.2, lane 7. However, these contaminating heme-proteins were removed by the subsequent sucrose gradient centrifugation step (Figure 6.2, lane 9). To increase enzymatic stability and activity (Varco-Merth, Fromme et al. 2008), the two detergents used in the initial solubilization step (cholate and OG) were replaced by 8 mM β-DDM during the sucrose density gradient centrifugation. As determined by silver-stained SDS-PAGE, the ATP synthase complex is essential in the interfacial fractions between 44% and 52% (w/v) of the sucrose gradient (Figures 6.3 and 6.4). Tricine SDS-PAGE electrophoresis of the isolated ATP synthase complex showed the typical subunit pattern of an F-ATP synthase (Figure 6.5, lane 3), with five F_1 subunits (α, β, γ, δ and ε), and three F_O subunits (a, b and c), according to the molecular mass pattern of the chloroplast enzyme $CF_1F_{O,}$ which was used as a positive control in the SDS-PAGE

analysis (Figure 6.5, lane 2). The identities of the α-subunit (AtpA) and the c-subunit (AtpH) of HF_1F_O were confirmed by western blotting, as shown in Figure 6.5, lanes 4 and 5.

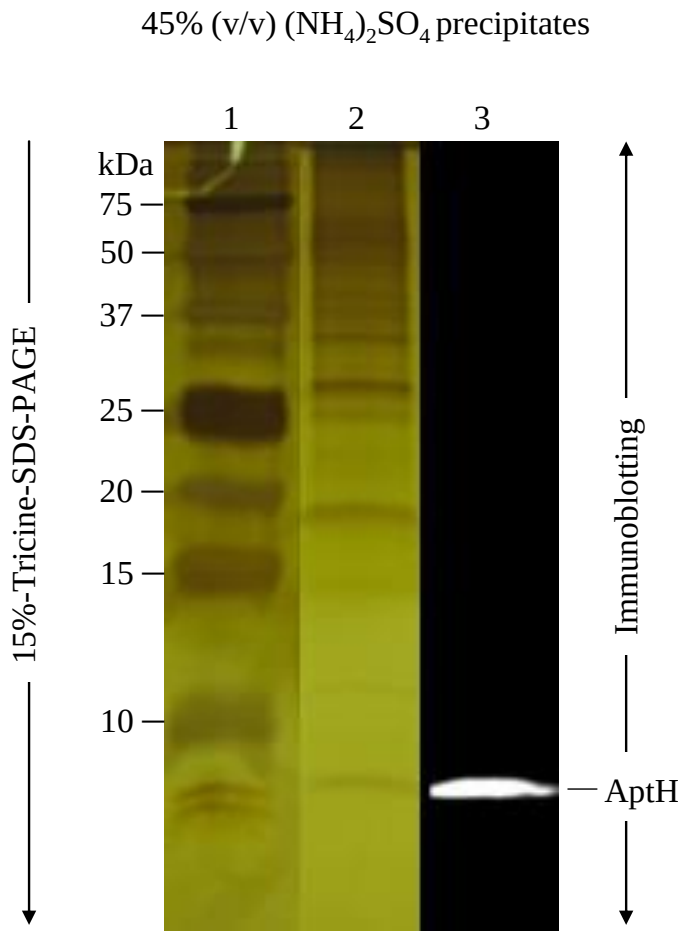

Figure 6.1 Electrophoresis Analysis of the Ammonium Sulfate Precipitate Fractions. Tricine-SDS polyacrylamide gel and immunoblot analysis of the 45% (v/v) ammonium Sulfate precipitate fraction of solubilized membrane proteins of *H. modesticaldum*. The silver-stained 15% Tricine-SDS polyacrylamide gel and immunoblotting detection of the 8-kDa c-subunit (AptH), shows HF_1F_O-ATP synthase complex was enriched in the 45% (v/v) saturated ammonium sulfate ($(NH_4)_2SO_4$) fraction (lanes 2 and 3, respectively). [lane 1, kDa, protein dual color standards (Bio-Rad, USA); lane 2, 45% (v/v) ammonium sulfate precipitate fraction in 15% Tricine-SDS-PAGE; lane 3, 45% (v/v) Western-blot of the ammonium sulfate precipitate fraction using the AptH antibody against the C-subunit of the *H. modesticaldum* ATP synthase].

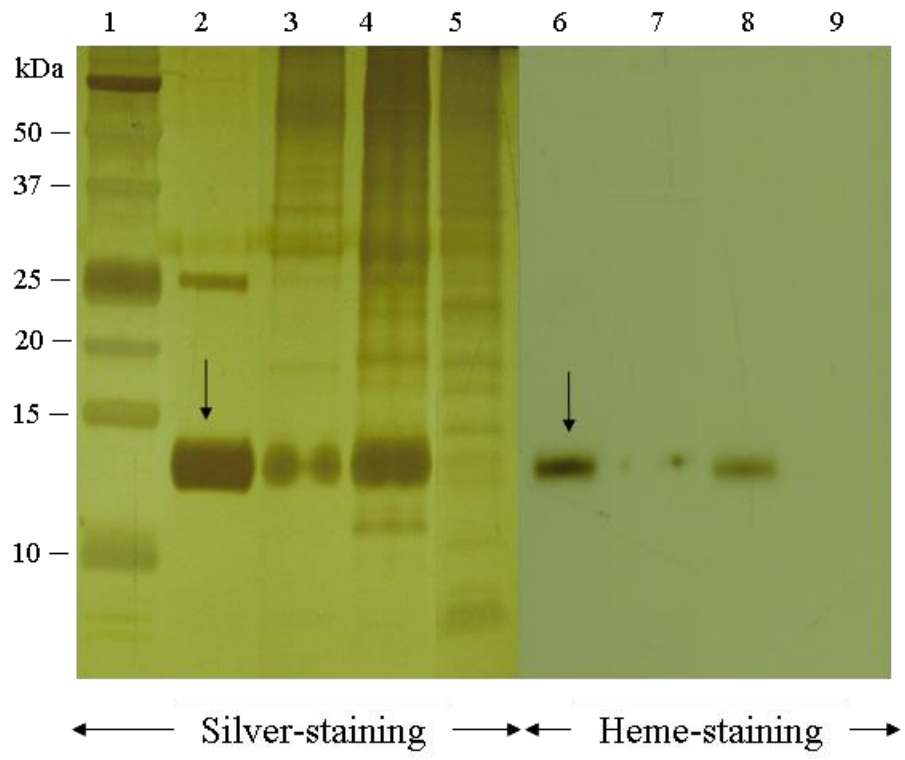

Figure 6.2 Heme-stained SDS-PAGE Gel Analysis of the Ammonium Sulfate Precipitation Fractions. Silver-stained and heme-stained Tricine-SDS polyacrylamide gel analysis in different fractions collected from the ammonium sulfate precipitation and the discontinuous sucrose density gradient centrifugation of H. modesticaldum. Silver-stained and heme-stained Tricine-SDS polyacrylamide gel analysis of different fractions collected from the ammonium sulfate precipitation steps and the discontinuous sucrose density gradient centrifugation of *H. modesticaldum*. The fractions$^{45\%(4P),\ 60\%(6P),\ \text{and}\ 44\%(SG)}$ were analyzed by 15 % Tricine-SDS-PAGE electrophoresis with silver staining (lanes 3, 4 and 5) and heme staining (lanes 7, 8, and 9). The heme staining indicated that fraction$^{45\%(4P)}$ (lanes 3 and 7) and fraction$^{60\%(6P)}$ (lanes 4 and 8) are contaminated by 14-kDa cytochrome *c* according to the molecular mass of the positive control (lanes 1 and 6) cytochrome c (see arrow) (Sarrou, Khan et al. 2012). The majority of cyt. *c* was precipitated by the 60% (v/v) saturated ammonium sulfate solution (fraction$^{60\%(6P)}$, lanes 4 and 8). The fraction$^{45\%\ (4P)}$ enriched the intact HF_1F_O ATP synthase still contained minimal amount of cyt. *c*, which was removed via discontinuous sucrose density gradient centrifugation. Lane 9 shows the 44% sucrose fraction from the density gradient, which contained intact HF_1F_O ATP synthase without cyt. *c* contamination. [lane 1, protein dual color standards (Bio-Rad, USA); lanes 2 and 6, positive control, cytochrome c (provided by Dr. Sarrou); lanes 3 and 7, fraction$^{45\%(4P),}$ proteins fractionated by 45% (v/v) saturated ammonium sulfate solution; lanes 4 and 8, fraction$^{60\%(6P),}$ proteins fractionated by 60% (v/v) saturated ammonium sulfate solution; lanes 5 and 9, fraction$^{44\%(SG),}$ fractions collected between 44% from the sucrose gradient. Abbreviations: P, pellets; SG, sucrose density gradient].

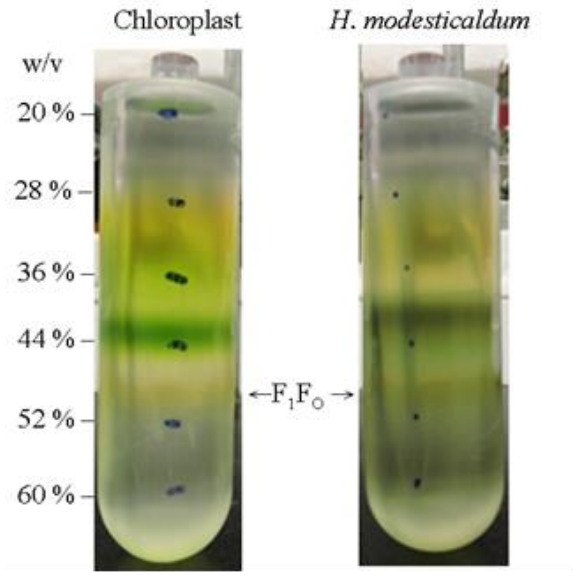

Figure 6.3 Sucrose Gradient Gradient Centrifugation of the HF_1F_O ATP Synthase. The intact ATP synthase was separated from other membrane proteins using discontinuous sucrose density gradient centrifugation. The interface fraction between 44% and 52% (w/v) contains the ATP synthases.The yellowish fraction from the isolated fraction form chloroplast (left) contains chloroplast CF_1F_O ATP synthase, which were isolated according to the method previously described [31], The olive greenish fraction of the isolated fraction (right) of the *H. modesticaldum* contains the HF_1F_O ATP synthase. The indicated numbers on the right represent the concentration of sucrose (w/v) in each fraction of the step gradient.

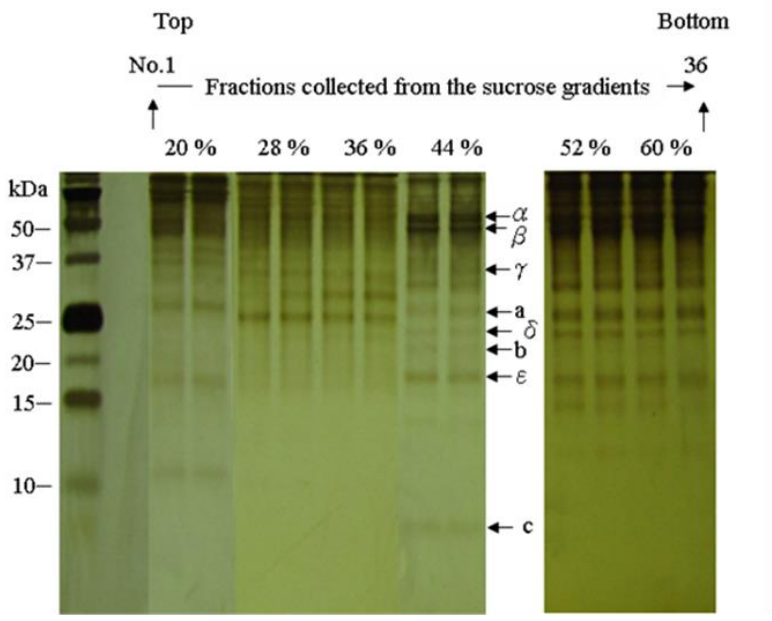

Figure 6.4 Silver-stained SDS-PAGE Gel of the Collected Sucrose Gradient Fractions. Silver-stained 15% Tricine-SDS polyacrylamide gel of the total proteins in the collected sucrose gradient fractions. 1 ml per fraction was collected from top to bottom and successively numbered from 1 to 36. The analysis showed that the interface fractions between 44% and 52% (w/v) were enriched in *H. modesticaldum* HF_1F_O ATP synthase.

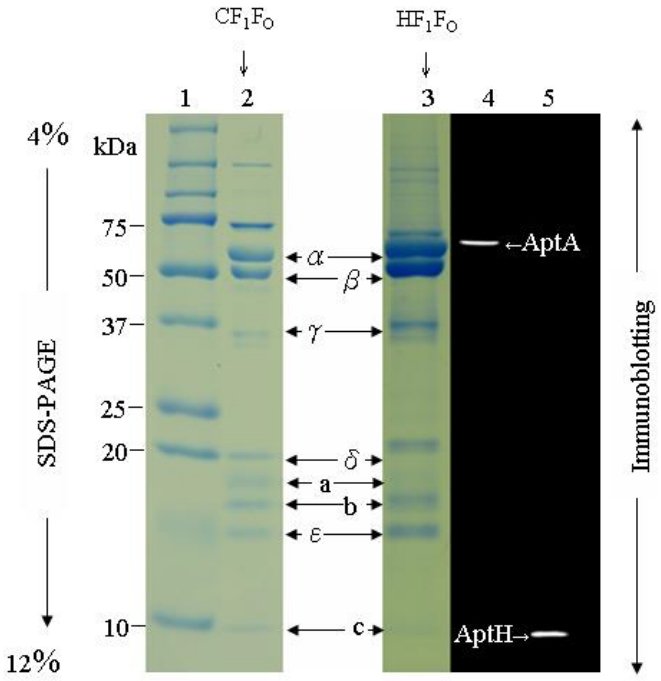

Figure 6.5 Electrophoresis Analysis and of the HF_1F_O ATP Synthase. Tricine-SDS polyacrylamide gel analysis and immunoblotting analysis for subunit c of the *H. modesticaldum* HF_1F_O ATP synthase complexes collected from the interface gradient between 44% and 52% (w/v) of the sucrose gradient. The 5 subunits (α, β, γ, δ, and ε) of the HF_1 subcomplex and the 3 subunits (a, b, and c) of the HF_O subcomplex of the *H. modesticaldum* HF_1F_O ATP synthase complex were identified (lane 3) according to the molecular mass of each subunit and a compared to the positive control chloroplast CF_1F_O ATP synthase (lane 2). The immunoblot detectsthe ~52-kDa α subunit of the HF_1 subcomplex (lane 4) and the ~8-kDa c subunit of the HF_O subcomplex (lane 5). [lane 1, protein dual color standards (Bio-Rad, USA); lane 2, positive control, chloroplast CF_1F_O ATP synthase complex; lanes 3 *H. modesticaldum* HF_1F_O ATP synthase complexes collected from the interface gradient between 44% and 52% (w/v) of the sucrose gradient; Lanes 4 and 5, Western blot analysis with antibodies against the α-subunit (AptA) ans c-subunit (AtpH)].

6.4.2 Native Electrophoresis

The quaternary structure of HF_1F_O was analyzed in more detail by native gel electrophoresis. This technique has been previously used to analyze ATP synthase complexes of mitochondria and chloroplasts. It has also been applied to the analysis of enzymatically active oligomeric states (Poetsch, Neff et al. 2000, Schagger and Pfeiffer 2000, Krause, Reifschneider et al. 2005, Wittig and Schagger 2005, Meyer, Wittig et al. 2007) or in advanced structural studies using 2D-crystallization and electron

microscopic single particle analysis of proteins extracted from BN-PAGE (Poetsch, Neff et al. 2000, Seelert, Dencher et al. 2003, Schafer, Seelert et al. 2006, Schafer, Dencher et al. 2007). The isolated HF_1F_O-ATP synthase complex was analyzed by native electrophoresis techniques to investigate whether it forms oligomers.

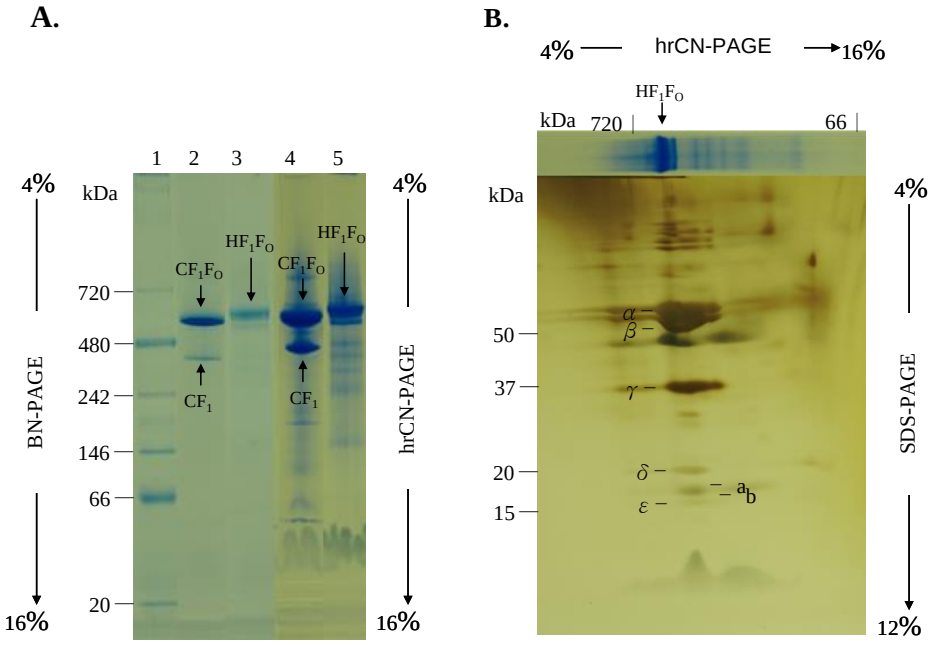

Figure 6.6 Native Electrophoresis and 2D-Electrophoresis Analysis of the HF_1F_O ATP synthase. Native gel electrophoresis analysis and 2D-electrophoresis analysis of the β-DDM-solubilized intact ATP synthase complex of *H. modesticaldum*. (A) The intact F_1F_O complexes and F_1 subcomplexes were identified on the gels of blue native electrophoresis (BN-PAGE) (lanes 2 and 3) and high-resolution clear native electrophoresis (hrCN-PAGE) (lane 4 and 5). Lanes 4 and 5 which represent the clear native gel were stained with Coomassie Blue after completion of the electrophoresis run. (B) A hrCN-PAGE gel strip of the *H. modesticaldum* HF_1F_O ATP synthase complex was analyzed by 2D electrophoresis, which showed all individual subunits of the *H. modesticaldum* HF_1F_O ATP synthase complex. [lane 1, unstained native protein standard (Life Technologies, USA); lane 2, BN-PAGE of the chloroplast CF_1F_O ATP synthase complex; lane 3, BN-PAGE of the *H. modesticaldum* HF_1F_O ATP synthase complex; lane 4, hrCN-PAGE of the chloroplast CF_1F_O ATP synthase complex; lane 5, hrCN-PAGE of the *H. modesticaldum* HF_1F_O ATP synthase complex].

In-gel activity assays were performed to test if the complex still retains its physiologically functional state after the isolation procedure. Under the conditions of native gel electrophoresis, the integral HF_1F_O-ATP synthase complexes migrated as a band with an apparent molecular mass of 600 kDa in both BN-PAGE and hrCN-PAGE

gels and was identified as a monomeric complex according to the native electrophoretic mobility of the CF_1F_O complex in BN-PAGE, as previously described (Fromme, Boekema et al. 1987, Fromme 1988, Neff and Dencher 1999) (Figure 6.6, panel A). The heliobacterial ATP synthase appears to be more stable than the chloroplast enzyme under the stress of the native gel electrophoresis: a significant band for the chloroplast CF_1 subcomplex was identified just below 480 kDa in both BN-PAGE and hrCN-PAGE gels (Figure 6.6, panel A, lanes 2 and 4); however, in the region of the identified CF_1 subcomplex, only a weak band for the HF_1 is identified with Coomassie Blue staining. The gel strips of hrCN-PAGE containing HF_1F_O-ATP synthase complexes were further analyzed using two-dimensional electrophoresis (1-D hrCN-PAGE, 2-D SDS-PAGE), which identified the individual subunits of the HF_1F_O complex on 2-D SDS-PAGE according to the molecular mass shown in Figure 6.6, panel B. The HF_1F_O complex contains all HF_1 and HF_O subunits.

6.4.3 Biochemical Properties of the Isolated HF_1F_O ATP Synthase

The ATP synthesis and hydrolysis functions of ATP synthases isolated from different sources has been studied most frequently via liposome reconstitution and chemiosmotic pH jump experiments. However, the techniques involved are complex and time consuming as they study the function of the enzyme after detergent removal in lipid bilayers. However, these methods cannot analyze the catalytic function of the ATP synthase in form of a protein-detergent complex. Therefore, the combination of native gel electrophoresis techniques and an in-gel functional activity assay has evolved into a powerful tool for protein-protein interaction analysis in mitochondrial respiratory complexes (Wittig and Schagger 2009). One of the established in-gel assays, named here the “in-gel ATP hydrolysis assay,” was remarkably useful in both qualitative and

quantitative analyses of the catalytic activity of the mitochondrial ATP synthase (complex V) (Wittig, Karas et al. 2007). Because ATP hydrolysis activity can be monitored in native gels via an in-gel ATPase assay, it can be used to rapidly screen for enzymatic activity of the isolated ATP synthase complex in detergents directly in the gel without involving reconstitution into liposomes. We used this assay to screen for the best detergent to stabilize the structure and function of the heliobacterial ATP synthase in different protein-detergent complexes. This is not possible using ATP synthesis assays, as they all require removal of the detergent during reconstitution into lipid membranes. The functional properties of the isolated HF_1F_O-ATP synthase complex were examined by monitoring the ATP hydrolysis activity by observing lead phosphate precipitate formation using the in-gel ATPase activity assay at room temperature, as previously described (Suhai, Heidrich et al. 2009). For the in-gel ATPase activity assay, hrCN-PAGE is highly preferred compared with BN-PAGE because the dye Coomassie Blue applied on BN-PAGE can dissociate detergent-labile subunits from the super-complex or disassemble the super-complex into sub-complexes. Furthermore, lead precipitate detection is very difficult in the presence of the Coomassie Blue dye. The hrCN-PAGE gels are colorless; therefore, the in-gel assays can be directly performed without any interference with the Coomassie Blue dye (Wittig and Schagger 2005, Wittig, Karas et al. 2007, Wittig and Schagger 2008, Wittig and Schagger 2009). We compared the CF_1F_O isolated from spinach chloroplast with the HF_1F_O complex isolated from *H. modesticaldum*. Previous studies provided that ATP hydrolysis activity of the chloroplast CF_1F_O-ATP synthase complex is extremely low, but can be improved by activating the CF_1F_O-ATP synthase complex via detergent treatments prior to the in-gel ATPase activity assay (Pick and Bassilian 1982, Yu and McCarty 1985, Suhai, Heidrich et al. 2009). One interesting question was if the

heliobacterial ATP synthase would require activation or if the intact enzyme was fully functional for ATP hydrolysis without any activation such as harsh detergent treatment. The hrCN-PAGE gel strips were treated with selected detergents as described in detail in materials and methods section. We tested the ATP hydrolysis activity of the chloroplast and *H. modesticaldum* ATP synthase in the presence of the following detergents: OG (octyl-glucoside) a non-ionic short length detergent, β-DDM (beta-dodecylmaltoside) a mild non-ionic long chain detergent, LDAO (N,N-dimethyl-1-dodecanamine-N-oxide) an ionic mild long chain detergent, and TDOC (tauro-deoxycholate) a harsh detergent. Using OG treatment, ATP hydrolysis could not be detected for either CF_1F_O or CF_1 within the 0.5 h or 1 h incubation periods (Figure 6.7, panel A, lane 1 and lane 3). After 24 hours of incubation, extremely weak bands indicating hydrolysis activity were visible (Figure 6.7, panel A, lane 5). For ATP HF_1F_O hydrolysis of the intact enzyme was already detectable as a weak band after an incubation period of 0.5 h (Figure 6.7, panel A, lane 2). The intensity of the band increased after 1 hour, and saturated activity was observed after an incubation period of 24 h (Figure 6.7, panel A, lane 6). Interestingly, weak HF_1 hydrolysis activity was only visible after an incubation period of 24 h. Using β-DDM, no ATP hydrolysis of the chloroplast ATP synthase, CF_1F_O, was detected after incubation times of 0.5 h and 1 h (Figure 6.7,panel B, lane l and lane 3), whereas a subcomplex of the chloroplast enzyme showed strong ATP-hydrolysis activity already after 0.5 h and 1 h. In contrast, strong HF_1F_O ATP hydrolysis activity was already observed after an incubation time of 0.5 h (Figure 6.7, panel B, lane 2), and the band was even more pronounced after the 1 h incubation period. (Figure 6.7, panel B, lane 4). In contrast to the chloroplast CF_1F_O subcomplex, the HF_1 subcomplex showed no hydrolysis activity after 0.5 h and 1 h; a weak band became visible only after the 24 h incubation period. This is a very

interesting result because it indicates that the intact HF_1F_O is fully active in the ATP hydrolysis direction in the presence of very mild detergents such as β-DDM without requiring activation.

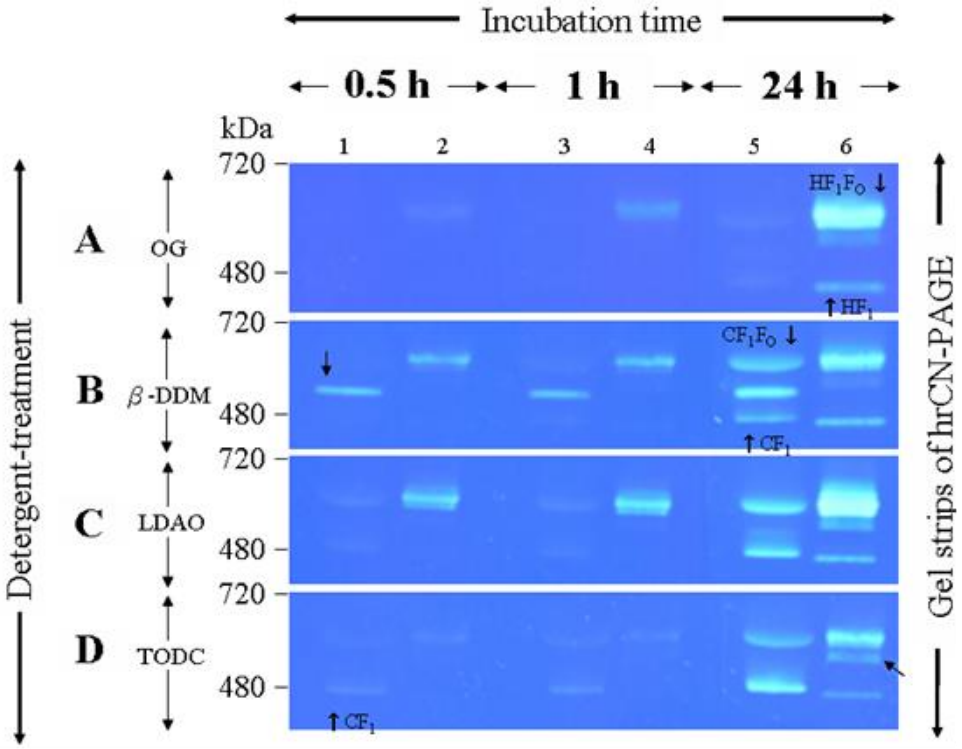

Figure 6.7 In-gel ATPase Hydrolysis Activity of the CF_1F_O and HF_1F_O ATP Synthases. In-gel ATPase hydrolysis activity of ATP synthase complexes isolated from spinach chloroplasts and *H. modesticaldum*. The hrCN-PAGE gel strips, each containing CF_1F_O and HF_1F_O, were incubated in buffers with different detergents to detect whether ATPase activity was dependent on the detergent. The gel strips were preincubated with buffer containing OG (A), β-DDM (B), LDAO (C) (Affymetrix/Anatrace, USA), or TDOC (D) (Sigma, USA). In the in-gel ATPase activity assay, ATP hydrolysis can be visualized as the white band comprising precipitated lead phosphate. Images of the in-gel assays were taken under a blue background after 0.5 h, 1 h and 24 h incubations, respectively. Notably, under some detergent conditions, multiple subcomplex bands appear, as indicated by black arrows. These bands are observed, for example, for CF_1F_O in β-DDM and LDAO and for HF_1F_O in TODC. They might comprise CF_1F_O and HF_1F_O subcomplexes that have lost subunit a and/or b of the F_O domain during hrCN-PAGE electrophoresis. [lanes 1, 3, and 5, spinach chloroplast CF_1F_O ATP synthase complex; lanes 2, 3, and 6, *H. modesticaldum* HF_1F_O synthase complex].

Furthermore, the results indicate that removal of the proton-translocating HF_O domain blocks ATP hydrolysis, as only very weak ATP hydrolysis was detected after 24 h for HF_1 in β-DDM. Using LDAO, only very weak ATP hydrolysis activity of the

chloroplast CF_1F_O and CF_1 was detected after 0.5 and 1 h, whereas HF_1F_O showed very high activity (Figure 6.7, panel C, lanes 1 and lane 2). Interestingly, also using LDAO, no HF_1 hydrolysis activity was detected after 0.5 and 1 h, and only a weak band appeared after an incubation period of 24 h (Figure 6.7, panel C, lane 6). In contrast to the results of the ATP synthase complexes treated with the detergents OG, β-DDM and LDAO, both CF_1F_O and HF_1F_O treated with the harsh detergent TDOC showed extremely low ATP hydrolysis activities after the 0.5 h and 1 h incubation periods (Figure 6.7, panel D, lanes 1, 2, 3, and 4), and significant activity could only be detected after 24 hours of incubation (Figure 6.7, panel D, lanes 5 and lane 6). In summary, these results indicate that HF_1F_O shows high ATPase activity in mild detergents such as LDAO and β-DDM, whereas extremely low ATP hydrolysis activity was detected in harsher detergents such as OG and TDOC. The fastest and highest ATP hydrolysis activity observed was detected when HF_1F_O was treated with LDAO. This result may indicate that long-chain detergents such as β-DDM and especially LDAO, which are known to stabilize membrane protein complexes, stabilize HF_1F_O and maintain its full catalytic activity. In contrast, short-chain detergents such as OG and TDOC may destabilize the heliobacterial ATP synthase and thereby inactivate it. In contrast to the chloroplast enzyme, for which CF_1 shows much higher ATP hydrolysis activity that CF_1F_O, the detachment of the head of the heliobacterial ATP synthase (HF_1) from the intact enzyme does not enhance but rather inhibits ATP hydrolysis activity. Such behavior has thus far not been reported for F-type ATP synthases but has been reported for vacuolar type V ATPases, which are enzymes that function to establish an H^+ gradient across the membrane (Wang and Hiesinger 2013). Our results may provide preliminary evidence that the heliobacterial ATP synthase may act *in vivo* in both ATP synthesis and ATP hydrolysis and that a mechanism may exist in *Heliobacterium*

modesticaldum that leads to switching off of the ATP hydrolysis function when the HF_1 head is decoupled from the transmembrane HF_0 proton inducing channel.

6.5 Conclusion

The combination of a modified isolation method and in-gel ATPase activity assay reported here confirmed that isolation of the functionally intact ATP synthase under anaerobic condition from anaerobic *Heliobacterium modesticaldum* cells can be achieved. We have shown that approximately 20 mg of purified ATP synthase can be routinely obtained from 4 L of anaerobic cell culture. The most critical breakthroughs in achieving these results were modifications in the way the cells were broken down as well as modifications in the isolation of the protein from the membrane. The in-gel ATPase activity assay for the ATP synthase of *H. modesticaldum* allowed us to detect ATP hydrolysis activity directly in the gel and to identify the stability and activity of the ATP synthase in different detergent micelles. The use of the in-gel activity assay method not only offers an expeditious way to screen for activity of sample fractions in a high-throughput manner but also allows for the assessment of the stability and activity of different ATP synthase subcomplexes in different detergents. The intact heliobacterial HF_1F_O enzyme shows fully active ATP hydrolysis activity in mild detergents, whereas the ATP hydrolysis activity is inactivated when the HF_1 head is removed from the HF_O transmembrane part of HF_1F_O. Our reported methods provided a primary isolation process under strictly anaerobic conditions, thereby providing heliobacterial ATP synthase samples for further studies that will include in particular bioenergetics studies, crystallization experiments, and may also be applied to ATP synthases from other anaerobic organisms in the future.

CHAPTER 7

FUTURE PLANS

7.1 Isolation and Purification of the Integral CF_O Subcomplex

There is currently great demand for a new approach to isolate the integral CF_O subcomplex. This demand is motivated by the lack of high-resolution structural information on the integral CF_O subcomplex and the desire to not only verify the currently posposed two-half-channel model for proton entry and release but also understand the interaction between the CF_O-a subunit and CF_O-c ring during proton translocation. Given that the purification method reported in this dissertation proved effective for the purification of CF_1F_O in large quantities from spinach chloroplasts, it is likely that this method can also be successfully applied for the isolation of the CF_O subcomplex, particularly the CF_O-a subunit. Of particular interest are ATP synthases from other organisms, such as the anaerobic photosynthetic bacterium *Heliobacterium modesticaldum*, which have not been isolated or characterized previously. The new ATP synthases from other currently available resources may possess different stoichiometries that enveally are more amenable to crystallization.

7.2 Functional Characterization of the ATP Synthase

Both in vitro qualitative and quantitative analysis techniques for the characterization of the enzymatic activity of ATP synthase were successfully adapted to the purified CF_1F_O. These functional assays will likely lead to new experiments that can be designed to investigate the critical factors that may influence the H^+/ATP ratio and the stability of ATP synthase. Therefore, an alternative characterization approach using an in-gel ATPase assay may possibly facilitate the rapid screening of the optimal detergent to stabilize the native structure and function of the CF_1F_O ATP synthase in different protein-detergent complexes, which may provide a reliable foundation for future

crystallization experiments. This screening cannot be accomplished using ATP synthesis assays because these assays require the removal of the detergent during reconstitution into lipid membranes. Prior to crystallization trails, chemiosmotic assays may facilitate the investigation of the appropriate crystallization conditions such as the optimal molecular weight and concentration of PEGs or the presence of lipids and additives, which may provide better stabilization of the structure and function of ATP synthase. Both the H^+/ATP ratio and the ATP synthesis rate of new ATP synthases from new, previously not studied, organisms can be determined using these functional assays.

7.3 Formation of Two-dimensional Crystals of the CF_1F_O ATP Synthase

The results of reconstitution of intact CF_1F_O into a lipid monolayer to induce the formation of 2D crystals appears to be promising but is not conclusive. The negatively stained electron micrograph images appear to indicate that the CF_1F_O sample has initially formed string-like structures concomitant with the formation of 2D crystals. However, to conclusively determine the effect of the lipid membrane composition on the initial CF_1F_O reconstitution in the lipid monolayer and the subsequent formation of a 2D crystal array, native phospholipids freshly extracted from thylakoid membranes could be investigated. Typically, the phospholipids monogalactosyldiacyl glycerol (MGDG), digalactosyldiacylglycerol (DGDG), sulfoquinovosyldiacylglycerol (SQDG), and phosphatidylglycerol (PG) can be found in thylakoid membranes, where these phospholipids serve as essential cofactors to stabilize the structure and function of photosystem supercomplexes (Loll, Kern et al. 2007). Furthermore, the F-type ATP synthase is inherently instable following solubilization from a native lipid environment, despite sufficient amounts of detergents surrounding its hydrophobic region (Maeda, Shinzawa-Itoh et al. 2013). Therefore, the optimal native lipid composition for the

function of the ATP synthase would be worthwhile to investigate further. Hypothetically, the native lipid association may similarly have a stabilizing effect on either CF_1F_O reconstitution or 2D crystal formation. Preliminary screening using the convenient TEFLON block method of an air-water interface technique successfully resulted in preliminary data for the subsequent 2D crystallization trials. However, to improve the formation of a lipid monolayer, the Langmuir–Blodgett method to compress lipid molecules on the surface of a given subphase for formation of the lipid monolayer would possibly be an alternative approach to systematically produce a lipid monolayer, which will be briefly discussed below. The Langmuir-Blodgett trough (Biolin Scientific, Cat. No. KSV NIMA) is filled with an appropriate volume of the desired buffers to nearly reach the maximual surface tension. The dipper with a freshly cleaned mica plate is lowered at a speed of 1 mm/min until half of the mica plate is immersed in the solution. The system is then incubated for 15 min to allow the surface pressure sensor to become equilibrated in the solution. Following equilibration, the value of the surface pressure should reach a constant, and its variations are recorded until a maximum surface pressure is reached. Subsequently, 25 μL of the lipid working solution is gently deposited as a drop using a cleaned 10-μL Hamilton syringe (Hamilton, Cat. No. 80301) onto the surface area enclosed by both barriers. The drop then immediately spreads over the clean air-water (liquid) interface, and its surface pressure should change only slightly. After an additional 15 min of equilibration to reach a constant surface pressure, the two barriers on the edges of the trough are pressed from both edges to the center of the trough at a speed of 1 mm/min. As the barriers are pressed toward the center, each lipid molecule that is free to move on the enclosed surface also begins to be compressed toward the center, leading to decreases in the free surface of the air-lipid interface. Simultaneously, the surface pressure tension is

measured and recorded by the slowly changing surface pressure sensor. When the surface pressure reaches the initial point of the lipid-expanded phase, the barriers are immediately stopped, and the membrane protein solution is gently delivered into the subphase via a 10-μL Hamilton syringe. This step is followed by incubation for 60 min without lipid compression. During incubation, the membrane proteins are spontaneously inserted into the compressed lipid monolayer, and following incubation, the lipid molecules begin to be compressed until the maximum surface pressure is reached. Once this pressure is reached, there is no free air-liquid interface in the enclosed surface, and the complete interface is occupied by compressed lipid molecules and membrane proteins and can thus be called a lipid monolayer. The membrane protein bound to the lipid monolayer is transferred onto a freshly cleaned mica plate at a constant surface pressure by vertically raising the dipper at a speed of 1 mm/min. Due to coating at a constant surface pressure, the barriers continue to be pressed toward the deep center to maintain constant pressure. After the dipper completely stops, the mica plate is carefully detached and is ready for subsequent imaging.

7.4 Three-dimensional Crystallization Studies

The crystal structure for the CF_O-c_{14} ring has been determined at a resolution of 3.8 Å (Clerico, Maki et al. 2008) and crystals diffrating to 2.8 Å have been reported (Varco-Merth, Fromme et al. 2008) (Figure 7.1). However, 3D crystals and a high-resolution structure of intact ATP synthase, in addition to a crystal structure for the integral CF_O, remain unavailable. The current plan is to utilize systematic approaches including phase diagram determination and high throughput screening for nanocrystals for structure determination with serial femstosecond crystallography, a novel method for the determination of X-ray structures that have been pioneered at Arizona State University

(Chapman, Fromme et al. 2011, Boutet, Lomb et al. 2012, Kupitz, Basu et al. 2014, Kupitz, Grotjohann et al. 2014) . The crystallization plates can be incubated in a crystal incubator controlled at a desired temperature and humidity and will be imaged using white field illumination, polarized light and UV Trp fluorescence. In addition the novel method for SONICC (Wampler, Kissick et al. 2008) can be usewd to detect nanocrystals as small as 100nm. High throughput robotic crystallization screening with the highly pure CF_1F_O samples developed in this dissertation will enable the determination of the optimal crystallization conditions for the formation of 3D crystals of intact CF_1F_O.

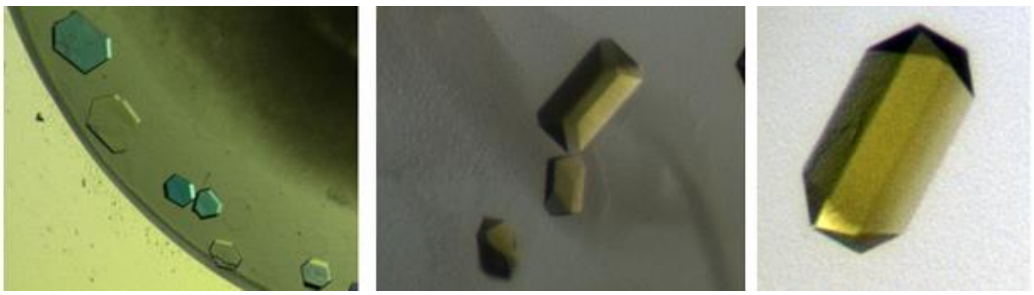

Figure 7.1 Crystal Images of Isolated CF_1F_O c_{14}-ring. The pigment association is observed due to the yellow-green hue of these crystals, Image adapted fromVarco-Merth et al., (2008) (Varco-Merth, Fromme et al. 2008).

In combination with these crystallization conditions, femtosecond nanocrystallography of nanocrystals (Fromme and Spence 2011, Hunter and Fromme 2011, Boutet, Lomb et al. 2012, Koopmann, Cupelli et al. 2012, Kupitz, Basu et al. 2014, Kupitz, Grotjohann et al. 2014, Pedrini, Tsai et al. 2014) has been successfully applied in the structure determination of photosynthetic protein complexes and this technique will likely facilitate the determination of a high-resolution structure of intact ATP synthase. This technique can also potentially be utilized for the structure determination of the CF_O domain and the hydrophobic a-subunit. A native CF_O-c_{14} ring crystal shown in Figure 7.1 (Varco-Merth, Fromme et al. 2008) indicates that the yellow-greenish pigment

association is apparently present in the crystal. Therefore, an additional future plan is to investigate whether these pigments, which serve as cofactors, influence the formation of 3D crystals of intact ATP synthase.

7.5 TEM or AFM Analysis of 2D CF_1F_O Crystals

Although 3D crystals of intact CF_1F_O remain unavailable for X-ray crystallography, electron microcrystallorgaphy (Shi, Nannenga et al. 2013, Doerr 2014, Nannenga and Gonen 2014, Nannenga, Shi et al. 2014, Nannenga, Shi et al. 2014) or atomic force microscopy (AFM) analysis of 2D CF_1F_O crystals would be an alternative approach to achieve the final goal of the structure determination of intact F-type ATP synthase at high resolution. In recent decades, both electron microscopy (TEM) and atomic force microscopy (AFM) have been developed to characterize topographies of large membrane proteins at subnanometer resolution (Henderson and Unwin 1975, Henderson, Baldwin et al. 1990, Kuhlbrandt, Wang et al. 1994) (Milhiet, Gubellini et al. 2006, Raunser and Walz 2009) (Reisinger and Eichacker 2006, Fujiyoshi 2011, Maeda, Shinzawa-Itoh et al. 2013). 2D crystal growth using dialysis-mediated detergent removal techniques have demonstrated success for the mitochondrial and chloroplast ATP synthases (Bottcher, Graber et al. 1995, Neff, Tripathi et al. 1997, Maeda, Shinzawa-Itoh et al. 2013). The combination of TEM and AFM analysis with the lipid monolayer formed using the air-water interface technique has also successfully been applied for characterization of the structure of the mitochondrial ATP synthase (Arechaga and Fotiadis 2007). AFM analysis of 2D crystals has also demonstrated remarkable success in determining the stoichiometry of the *A. platensis* c_{15}-ring (Pogoryelov, Yu et al. 2005), the *I. tartaricus* c_{11}-ring (Stahlberg, Muller et al. 2001), and the *S. oleracea* c_{14}-ring (Figure 7.2) (Seelert, Poetsch et al. 2000), in which the

number of monomeric c-subunits composing the c-ring rotor can be directly visualized and counted. Ongoing work using initial 2D crystals of intact CF_1F_O will be directed toward adapting these techniques to obtain similar high resolution images of intact ATP synthase or its subcomplex. If these techniques can be successfully adapted at Arizona State University to produce comparable high-resolution images, the stoichiometry of the recombinant c-ring (Lawrence, Varco-Merth et al. 2011) can potentially be determined and experiments can be designed to investigate factors influencing the assembly of the c-ring. Furthermore, these techniques would enable the exploration of other stoichiometries of the c-ring (for example of Heliobacterial ATP synthase), which can be readily performed at Arizona State University.

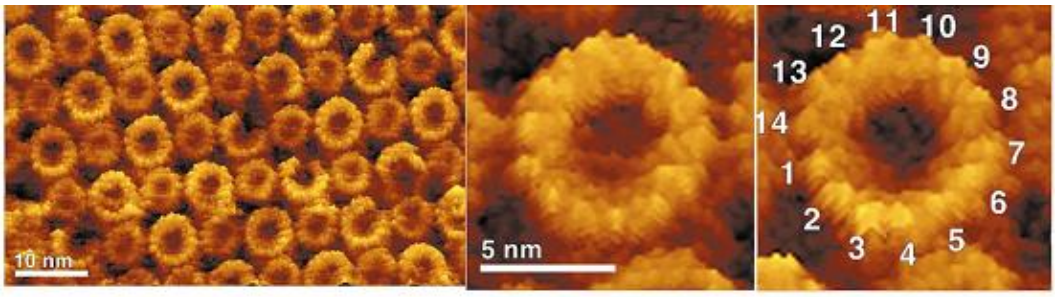

Figure 7.2 Atomic Force Micrograph of Two-dimensional Crystal Arrays of Native Spinach Chloroplast CF_1F_O c_{14}-ring. The number of monomeric c-subunit can be visualized and counted in this high resolution of AFM image. The diameter of c_{14} ring is near 6 nm. Image adapted from Seelert et al., (2000) (Seelert, Poetsch et al. 2000)**.**

CHAPTER 8

CONCLUDING REMARKS

For the past two decades, the ultimate goal of researchers in fields investigating the ATP synthase is to determine the structure of intact ATP synthase at atomic resolution, thereby allowing the elucidation of the ATP synthase coupling mechanism. Although breakthroughs have been accomplished in this field with the structure determination of subcomplexes like F1 and different c-rings, much remains to achieve this ultimate goal. The greatest challenge prior to structure determination is the formation of crystals of intact ATP synthase in three dimensions. Unfortunately, the conditions that allow crystal growth of intact ATP synthase in three dimensions remain to be established. However, investigation of these crystal growth conditions requires significant quantities of protein in high purity. This dissertation provides a large-scale purification procedure for intact ATP synthase for future crystallization experiments. The combination of methods reported herein has resulted in the purification of significant quantities of the integral chloroplast CF_1F_O ATP synthase complex in an active state. Approximately 10 mg of highly pure CF_1F_O can routinely be obtained from 1 kg of baby spinach. Critical to achieving this result was the utilization of isolated intact chloroplast thylakoid membranes for complete removal of water-soluble RuBisCO proteins, the use of discontinuous sucrose gradient ultracentrifugation as an initial purification step, the use of a mixture of phospholipids and n-β-dodecyl-D-maltoside in stabilizing solubilized CF_1F_O, and the use of dye-ligand affinity chromatography in combination with anion exchange chromatography for final purification. Additionally important was the establishment of the described biochemical analytical techniques, particularly various native electrophoresis techniques. The most significant achievement was the successful establishment of an enzymatic functional assay to

determine the CF_1F_O ATP synthesis activity using a combination of liposome reconstitution and $\Delta pH/\Delta\psi$-jump experiments (an acid-base incubation) and the establishment of a fast assay where the ATP hydrolysis activity can be visualized using in-gel ATPase activity. Although the initial crystallization experiments of intact CF_1F_O in two dimensions appear promising based on EM analysis, further experimentation and development of methods for the formation of a lipid monolayer using an air-water interface technique are required. The intention of the work described in this dissertation is to establish a large-scale purification procedure for intact CF_1F_O ATP synthase in an active state for future crystallization experiments that can be designed to investigate the crystallization conditions in two or three dimensions. These crystallization conditions can be interesting targets for future investigations to grow crystals of intact ATP synthase. Although crystals of intact ATP synthase are currently unavailable, these experimental results will likely foster future important and interesting investigations that will drive the crystallization of intact ATP synthase forward toward ultimately determining its structure at atomic resolution, leading to an understanding of the mechanism of proton translocation and its coupling to ATP formation by ATP synthase.

REFERENCES

1. Abrahams, J. P., A. G. Leslie, R. Lutter and J. E. Walker (1994). **"Structure at 2.8 A resolution of F1-ATPase from bovine heart mitochondria"** Nature 370 (6491): 621-628.

2. Adachi, K., K. Oiwa, T. Nishizaka, S. Furuike, H. Noji, H. Itoh, M. Yoshida and K. Kinosita, Jr. (2007). **"Coupling of rotation and catalysis in F_1-ATPase revealed by single-molecule imaging and manipulation"** Cell 130 (2): 309-321.

3. Adachi, K., R. Yasuda, H. Noji, H. Itoh, Y. Harada, M. Yoshida and K. Kinosita, Jr. (2000). **"Stepping rotation of F1-ATPase visualized through angle-resolved single-fluorophore imaging."** Proc Natl Acad Sci U S A 97 (13): 7243-7247.

4. Anthon, G. E. and A. T. Jagendorf (1983). **"Effect of Methanol on Spinach Thylakoid Atpase."** Biochimica Et Biophysica Acta 723 (3): 358-365.

5. Arechaga, I. and D. Fotiadis (2007). **"Reconstitution of mitochondrial ATP synthase into lipid bilayers for structural analysis."** J Struct Biol 160 (3): 287-294.

6. Arnon, D. I. (1949). **"Copper Enzymes in Isolated Chloroplasts. Polyphenoloxidase in Beta Vulgaris."** Plant Physiol 24 (1): 1-15.

7. Asao, M. and M. T. Madigan (2010). **"Taxonomy, phylogeny, and ecology of the heliobacteria."** Photosynth Res 104 (2-3): 103-111.

8. Boekema, E., M. van Heel and P. Graber (1988). **"Structure of the ATP-synthase from chloroplasts studied by electron microscopy and image processing."** Prog Clin Biol Res 273: 75-80.

9. Boekema, E. J., Fromme, P. & Gräber, P. (1988). **"On the Structure of the ATP-Synthase from Chloroplasts."** Ber. Bensen-ges. Phys. Chem. 92: 6.

10. Boekema, E. J., G. Schmidt, P. Graber and J. A. Berden (1988). **"Structure of the ATP-synthase from chloroplasts and mitochondria studied by electron microscopy."** Z Naturforsch C 43 (3-4): 219-225.

11. Bottcher, B. and P. Graber (2000). **"The structure of the H^+-ATP synthase from chloroplasts and its subcomplexes as revealed by electron microscopy."** Biochim Biophys Acta 1458 (2-3): 404-416.

12. Bottcher, B., P. Graber, E. J. Boekema and U. Lucken (1995). **"Electron cryomicroscopy of two-dimensional crystals of the H^+-ATPase from chloroplasts."** FEBS Lett 373 (3): 262-264.

13. Bottcher, B., L. Schwarz and P. Graber (1998). **"Direct indication for the existence of a double stalk in CF_0F_1."** J Mol Biol 281 (5): 757-762.

14. Boutet, S., L. Lomb, G. J. Williams, T. R. Barends, A. Aquila, R. B. Doak, U. Weierstall, D. P. DePonte, J. Steinbrener, R. L. Shoeman, M. Messerschmidt, A. Barty, T. A. White, S. Kassemeyer, R. A. Kirian, M. M. Seibert, P. A. Montanez, C. Kenney, R. Herbst, P. Hart, J. Pines, G. Haller, S. M. Gruner, H. T. Philipp, M. W. Tate, M. Hromalik, L. J. Koerner, N. van Bakel, J. Morse, W. Ghonsalves, D. Arnlund, M. J. Bogan, C. Caleman, R. Fromme, C. Y. Hampton, M. S. Hunter, L. C. Johansson, G. Katona, C. Kupitz, M. Liang, A. V. Martin, K. Nass, L. Redecke, F. Stellato, N. Timneanu, D. Wang, N. A. Zatsepin, D. Schafer, J. Defever, R. Neutze, P. Fromme, J. C. Spence, H. N. Chapman and I. Schlichting (2012). **"High-resolution protein structure determination by serial femtosecond crystallography."** Science 337 (6092): 362-364.

15. Boyer, P. D. (1979). **"The Binding - Change Mechanism of ATP Synthesis."** Membrane Bioenergetics C. P. Lee, Schatz, G., and Ernster, L., . Reading, MA, Addison Wesley: 461-479.

16. Boyer, P. D. (1989). **"A perspective of the binding change mechanism for ATP synthesis."** FASEB J 3 (10): 2164-2178.

17. Boyer, P. D. (1993). **"The binding change mechanism for ATP synthase--some probabilities and possibilities."** Biochim Biophys Acta 1140 (3): 215-250.

18. Boyer, P. D. (1997). **"The ATP synthase--a splendid molecular machine."** Annu Rev Biochem 66: 717-749.

19. Boyer, P. D. (1998). **"ATP synthase--past and future."** Biochim Biophys Acta 1365 (1-2): 3-9.

20. Boyer, P. D. (1998). **"Energy, life, and ATP."** Biosci Rep 18 (3): 97-117.

21. Boyer, P. D. (2000). **"Catalytic site forms and controls in ATP synthase catalysis."** Biochim Biophys Acta 1458 (2-3): 252-262.

22. Boyer, P. D., and Kohlbrenner, W. E. (1981). **" The present status of the binding-change mechanism and its relation to ATP formation by chloroplast."** Energy Coupling in Photosynthesis. B. R. Selman, Selma-Reimer S. North-Holland, Amsterdam, Elsevier: 231-240.

23. Boyer, P. D., R. L. Cross and W. Momsen (1973). **"A new concept for energy coupling in oxidative phosphorylation based on a molecular explanation of the oxygen exchange reactions."** Proc Natl Acad Sci U S A 70(10): 2837-2839.

24. Chapman, H. N., P. Fromme, A. Barty, T. A. White, R. A. Kirian, A. Aquila, M. S. Hunter, J. Schulz, D. P. DePonte, U. Weierstall, R. B. Doak, F. R. Maia, A. V. Martin, I. Schlichting, L. Lomb, N. Coppola, R. L. Shoeman, S. W. Epp, R. Hartmann, D. Rolles, A. Rudenko, L. Foucar, N. Kimmel, G. Weidenspointner, P. Holl, M. Liang, M. Barthelmess, C. Caleman, S. Boutet, M. J. Bogan, J. Krzywinski, C. Bostedt, S. Bajt, L. Gumprecht, B. Rudek, B. Erk, C. Schmidt, A. Homke, C. Reich, D. Pietschner, L. Struder, G. Hauser, H. Gorke, J. Ullrich, S. Herrmann, G. Schaller, F. Schopper, H. Soltau, K. U. Kuhnel, M. Messerschmidt, J. D. Bozek, S. P. Hau-Riege, M. Frank, C. Y. Hampton, R. G. Sierra, D. Starodub, G. J. Williams, J. Hajdu, N. Timneanu, M. M. Seibert, J. Andreasson, A. Rocker, O. Jonsson, M. Svenda, S. Stern, K. Nass, R. Andritschke, C. D. Schroter, F. Krasniqi, M. Bott, K. E. Schmidt, X. Wang, I. Grotjohann, J. M. Holton, T. R. Barends, R. Neutze, S. Marchesini, R. Fromme, S. Schorb, D. Rupp, M. Adolph, T. Gorkhover, I. Andersson, H. Hirsemann, G. Potdevin, H. Graafsma, B. Nilsson and J. C. Spence (2011). **"Femtosecond X-ray protein nanocrystallography."** Nature 470 (7332): 73-77.

25. Chauvet, A., J. Sarrou, S. Lin, S. P. Romberger, J. H. Golbeck, S. Savikhin and K. E. Redding (2013). **"Temporal and spectral characterization of the photosynthetic reaction center from Heliobacterium modesticaldum."** Photosynth Res 116 (1): 1-9.

26. Cingolani, G. and T. M. Duncan (2011). **"Structure of the ATP synthase catalytic complex (F_1) from Escherichia coli in an autoinhibited conformation."** Nat Struct Mol Biol 18 (6): 701-707.

27. Clerico, E. M., J. L. Maki and L. M. Gierasch (2008). **"Use of synthetic signal sequences to explore the protein export machinery."** Biopolymers 90 (3): 307-319.

28. Cohen, R. O., G. Shen, J. H. Golbeck, W. Xu, P. R. Chitnis, A. I. Valieva, A. van der Est, Y. Pushkar and D. Stehlik (2004). **"Evidence for asymmetric electron transfer in cyanobacterial photosystem I: analysis of a methionine-to-leucine mutation of the ligand to the primary electron acceptor A_0."** Biochemistry 43 (16): 4741-4754.

29. Cox, G. B., J. A. Downie, D. R. Fayle, F. Gibson and J. Radik (1978). **"Inhibition, by a protease inhibitor, of the solubilization of the F_1-portion of the Mg^{2+}-stimulated adenosine triphosphatase of Escherichia coli."** J Bacteriol 133 (1): 287-292.

30. Cross, R. L. and C. M. Nalin (1982). **"Adenine nucleotide binding sites on beef heart F_1-ATPase. Evidence for three exchangeable sites that are distinct from three noncatalytic sites."** J Biol Chem 257 (6): 2874-2881.

31. Dashdorj, N., W. Xu, R. O. Cohen, J. H. Golbeck and S. Savikhin (2005). **"Asymmetric electron transfer in cyanobacterial Photosystem I: charge separation and secondary electron transfer dynamics of mutations near the primary electron acceptor A_0."** Biophys J 88 (2): 1238-1249.

32. Delucas, L. (2009). **"Membrane Protein crystallization."** Current Topics in membranes 63: 3.

33. Diez, M., B. Zimmermann, M. Borsch, M. Konig, E. Schweinberger, S. Steigmiller, R. Reuter, S. Felekyan, V. Kudryavtsev, C. A. Seidel and P. Graber (2004). **"Proton-powered subunit rotation in single membrane-bound F_0F_1-ATP synthase."** Nat Struct Mol Biol 11 (2): 135-141.

34. Digel, J. G., K. E. Hightower and R. E. McCarty (1996). **"Subunit movement during catalysis by F_1-F_0-ATP synthases."** J Bioenerg Biomembr 28 (5): 439-442.

35. Digel, J. G., A. Kishinevsky, A. M. Ong and R. E. McCarty (1996). **"Differences between two tight ADP binding sites of the chloroplast coupling factor 1 and their effects on ATPase activity."** J Biol Chem 271 (33): 19976-19982.

36. Dimroth, P. and G. M. Cook (2004). **"Bacterial Na^+ - or H^+ -coupled ATP synthases operating at low electrochemical potential."** Adv Microb Physiol 49: 175-218.

37. Dimroth, P., G. Kaim and U. Matthey (1998). **"The motor of the ATP synthase."** Biochim Biophys Acta 1365 (1-2): 87-92.

38. Dmitriev, O., P. C. Jones, W. Jiang and R. H. Fillingame (1999). **"Structure of the membrane domain of subunit b of the Escherichia coli F_0F_1 ATP synthase."** J Biol Chem 274 (22): 15598-15604.

39. Dmitriev, O. Y., P. C. Jones and R. H. Fillingame (1999). **"Structure of the subunit c oligomer in the F_1F_o ATP synthase: model derived from solution structure of the monomer and cross-linking in the native enzyme."** Proc Natl Acad Sci U S A 96 (14): 7785-7790.

40. Doerr, A. (2014). **"Electron crystallography goes 3D with MicroED."** Nat Methods 11 (1): 6-7.

41. Du, Z., W. C. Tucker, M. L. Richter and Z. Gromet-Elhanan (2001). **"Assembled F1-(alpha beta) and Hybrid F_1-alpha 3beta 3gamma -ATPases from Rhodospirillum rubrum alpha, wild type or mutant beta, and chloroplast gamma subunits. Demonstration of Mg^{2+}versus Ca^{2+}-induced differences in catalytic site structure and function."** J Biol Chem 276 (15): 11517-11523.

42. Du, Z. Y. and P. D. Boyer (1990). **"On the mechanism of sulfite activation of chloroplast thylakoid ATPase and the relation of ADP tightly bound at a catalytic site to the binding change mechanism."** Biochemistry 29 (2): 402-407.

43. Elston, T., H. Wang and G. Oster (1998). **"Energy transduction in ATP synthase."** Nature 391 (6666): 510-513.

44. Engelbrecht, S. and W. Junge (1997). **"ATP synthase: a tentative structural model."** FEBS Lett 414 (3): 485-491.

45. Evron, Y., E. A. Johnson and R. E. McCarty (2000). **"Regulation of proton flow and ATP synthesis in chloroplasts."** J Bioenerg Biomembr 32 (5): 501-506.

46. Farron, F. (1970). **"Isolation and properties of a chloroplast coupling factor and heat-activated adenosine triphosphatase."** Biochemistry 9 (19): 3823-3828.

47. Feniouk, B. A., Yoshida, M. (2008). **"Regulatory mechanisms of proton-translocating F_OF_1-ATP synthase."** Results Probl Cell Differ. 45: 30.

48. Fillingame, R. H., C. M. Angevine and O. Y. Dmitriev (2002). **"Coupling proton movements to c-ring rotation in F_1F_o ATP synthase: aqueous access channels and helix rotations at the a-c interface."** Biochim Biophys Acta 1555 (1-3): 29-36.

49. Fillingame, R. H., C. M. Angevine and O. Y. Dmitriev (2003). **"Mechanics of coupling proton movements to c-ring rotation in ATP synthase."** FEBS Lett 555 (1): 29-34.

50. Fillingame, R. H. and P. R. Steed (2014). **"Half channels mediating H^+ transport and the mechanism of gating in the Fo sector of Escherichia coli F1Fo ATP synthase."** Biochim Biophys Acta 1837 (7): 1063-1068.

51. Fischer, S., C. Etzold, P. Turina, G. Deckers-Hebestreit, K. Altendorf and P. Graber (1994). **"ATP synthesis catalyzed by the ATP synthase of Escherichia coli reconstituted into liposomes."** Eur J Biochem 225 (1): 167-172.

52. Fischer, S. and P. Graber (1999). **"Comparison of DeltapH- and Delta***φ***-driven ATP synthesis catalyzed by the H^+-ATPases from *Escherichia coli* or chloroplasts reconstituted into liposomes."** FEBS Lett 457 (3): 327-332.

53. Francis, R. T. and R. R. Becker (1984). **"Specific Indication of Hemoproteins in Polyacrylamide Gels Using a Double-Staining Process."** Analytical Biochemistry 136 (2): 509-514.

54. Fromme, P. (1988).**"Die ATP-synthase aus Chloroplast: Biochemische Untersuchungen zur Struktur and Kinetische Messungen zum Mechanismus des Enzyme."** Technical University Berlin.

55. Fromme, P., E. J. Boekema and P. Graber (1987). **"Isolation and Characterization of a Supramolecular Complex of Subunit-Iii of the Atp-Synthase from Chloroplasts."** Zeitschrift Fur Naturforschung C-a Journal of Biosciences 42 (11-12): 1239-1245.

56. Fromme, P., Boekema, E. J. & Gräber, P. (1987). **"Isolation and Characterisation of a Supramolecular Complex of Subunit III of the ATP-Synthase from Chloroplasts."** Z. Naturforsch. 42c: 10.

57. Fromme, P. and J. C. Spence (2011). **"Femtosecond nanocrystallography using X-ray lasers for membrane protein structure determination."** Curr Opin Struct Biol 21 (4): 509-516.

58. Fujiyoshi, Y. (2011). **"Electron crystallography for structural and functional studies of membrane proteins."** J Electron Microsc (Tokyo) 60 Suppl 1: S149-159.

59. Gertz, M., H. Seelert, N. A. Dencher and A. Poetsch (2007). **"Interactions of rotor subunits in the chloroplast ATP synthase modulated by nucleotides and by $Mg2^+$."** Biochim Biophys Acta 1774(5): 566-574.

60. Gest H, F. J. (1983). **"Heliobacterium chlorum, an anoxygenic brownish-green photosynthetic bacterium containing a “new” form of bacteriochlrophyll."** Arch Microbiol 136: 6.

61. Girvin, M. E., V. K. Rastogi, F. Abildgaard, J. L. Markley and R. H. Fillingame (1998). **"Solution structure of the transmembrane H^+-transporting subunit c of the F_1F_0 ATP synthase."** Biochemistry 37(25): 8817-8824.

62. Gogol, E. P., E. Johnston, R. Aggeler and R. A. Capaldi (1990). **"Ligand-dependent structural variations in *Escherichia coli* F_1 ATPase revealed by cryoelectron microscopy."** Proc Natl Acad Sci U S A 87 (24): 9585-9589.

63. Groth, G. (2002). **"Structure of spinach chloroplast F_1-ATPase complexed with the phytopathogenic inhibitor tentoxin."** Proc Natl Acad Sci U S A 99 (6): 3464-3468.

64. Groth, G., D. A. Mills, E. Christiansen, M. L. Richter and B. Huchzermeyer (2000). **"Characterization of a phosphate binding domain on the alpha-subunit of chloroplast ATP synthase using the photoaffinity phosphate analogue 4-azido-2-nitrophenyl phosphate."** Biochemistry 39 (45): 13781-13787.

65. Groth, G. and E. Pohl (2001). **"The structure of the chloroplast F_1-ATPase at 3.2 A resolution."** J Biol Chem 276 (2): 1345-1352.

66. Groth. G. and Strotmann, H. (1999). **"New results about structure, function and regulation of the chloroplast ATP synthase (CF_0CF_1)."** Physiologia Plantarum 106 (1): 7.

67. Hakulinen, J. K., A. L. Klyszejko, J. Hoffmann, L. Eckhardt-Strelau, B. Brutschy, J. Vonck and T. Meier (2012). **"Structural study on the architecture of the bacterial ATP synthase Fo motor."** Proc Natl Acad Sci U S A 109 (30): E2050-2056.

68. Hall, M., Y. Mishra and W. P. Schroder (2011). **"Preparation of stroma, thylakoid membrane, and lumen fractions from Arabidopsis thaliana chloroplasts for proteomic analysis."** Methods Mol Biol 775: 207-222.

69. Hartree, E. F. (1972). **"Determination of protein: a modification of the Lowry method that gives a linear photometric response."** Anal Biochem 48 (2): 422-427.

70. Heinnickel, M., R. Agalarov, N. Svensen, C. Krebs and J. H. Golbeck (2006). **"The identification of f(x) in the heliobacterial reaction center as a [4Fe-4S] cluster with a ground spin state of S = 3/2."** Biochimica Et Biophysica Acta-Bioenergetics: 76-76.

71. Heinnickel, M. and J. H. Golbeck (2007). **"Heliobacterial photosynthesis."** Photosynthesis Research 92 (1): 35-53.

72. Henderson, R., J. M. Baldwin, T. A. Ceska, F. Zemlin, E. Beckmann and K. H. Downing (1990). **"Model for the structure of bacteriorhodopsin based on high-resolution electron cryo-microscopy."** J Mol Biol 213 (4): 899-929.

73. Henderson, R. and P. N. Unwin (1975). **"Three-dimensional model of purple membrane obtained by electron microscopy."** Nature 257 (5521): 28-32.

74. Hirono-Hara, Y., H. Noji, M. Nishiura, E. Muneyuki, K. Y. Hara, R. Yasuda, K. Kinosita, Jr. and M. Yoshida (2001). **"Pause and rotation of F_1-ATPase during catalysis."** Proc Natl Acad Sci U S A 98 (24): 13649-13654.

75. Hisabori, T., H. Konno, H. Ichimura, H. Strotmann and D. Bald (2002). **"Molecular devices of chloroplast F_1-ATP synthase for the regulation."** Biochim Biophys Acta 1555 (1-3): 140-146.

76. Hisabori, T., H. Ueoka-Nakanishi, H. Konno and F. Koyama (2003). **"Molecular evolution of the modulator of chloroplast ATP synthase: origin of the conformational change dependent regulation."** FEBS Lett 545 (1): 71-75.

77. Holloway, P. W. (1973). **"A simple procedure for removal of Triton X-100 from protein samples."** Anal Biochem 53 (1): 304-308.

78. Hunter, M. S. and P. Fromme (2011). **"Toward structure determination using membrane-protein nanocrystals and microcrystals."** Methods 55 (4): 387-404.

79. Jancarik, J. K., S.-H. (1991). **"Sparse matrix sampling: a screening method for crystallization of proteins."** Journal of Applied Crystallography 24: 33.

80. Jiang, W. and R. H. Fillingame (1998). **"Interacting helical faces of subunits a and c in the F_1F_O ATP synthase of Escherichia coli defined by disulfide cross-linking."** Proc Natl Acad Sci U S A 95(12): 6607-6612.

81. Jones, P. C., W. Jiang and R. H. Fillingame (1998). **"Arrangement of the multicopy H^+-translocating subunit c in the membrane sector of the Escherichia coli F_1F_0 ATP synthase."** J Biol Chem 273 (27): 17178-17185.

82. Junesch, U. and P. Graber (1991). **"The rate of ATP-synthesis as a function of delta pH and delta psi catalyzed by the active, reduced H^+-ATPase from chloroplasts."** FEBS Lett 294 (3): 275-278.

83. Junge, W. (1999). **"ATP synthase and other motor proteins."** Proc Natl Acad Sci U S A 96 (9): 4735-4737.

84. Junge, W., H. Lill and S. Engelbrecht (1997). **"ATP synthase: an electrochemical transducer with rotatory mechanics."** Trends Biochem Sci 22 (11): 420-423.

85. Junge, W. and S. McLaughlin (1987). **"The role of fixed and mobile buffers in the kinetics of proton movement."** Biochim Biophys Acta 890 (1): 1-5.

86. Kabaleeswaran, V., N. Puri, J. E. Walker, A. G. Leslie and D. M. Mueller (2006). **"Novel features of the rotary catalytic mechanism revealed in the structure of yeast F_1 ATPase."** EMBO J 25 (22): 5433-5442.

87. Kashey, T. S., J. B. Cowgill, M. D. McConnell, M. Flores and K. E. Redding (2014). **"Expression and characterization of cytochrome c553 from *Heliobacterium modesticaldum*."** Photosynth Res 120 (3): 291-299.

88. Kato-Yamada, Y., D. Bald, M. Koike, K. Motohashi, T. Hisabori and M. Yoshida (1999). **"Epsilon subunit, an endogenous inhibitor of bacterial F_1-ATPase, also inhibits F_0F_1-ATPase."** J Biol Chem 274 (48): 33991-33994.

89. Kayalar, C., J. Rosing and P. D. Boyer (1977). **"An alternating site sequence for oxidative phosphorylation suggested by measurement of substrate binding patterns and exchange reaction inhibitions."** J Biol Chem 252 (8): 2486-2491.

90. Kimble LK, M. L., Woese CR, Madigan MT (1995). **"*Heliobacterium modesticaldum*, sp. nov., a thermophilic heliobacterium of hot springs and volcanic soils."** Arch Microbiol 163 (4): 259-267.

91. Kinosita, K., Jr., K. Adachi and H. Itoh (2004). **"Rotation of F_1-ATPase: how an ATP-driven molecular machine may work."** Annu Rev Biophys Biomol Struct 33: 245-268.

92. Kinosita, K., Jr., R. Yasuda and H. Noji (2000). **"F_1-ATPase: a highly efficient rotary ATP machine."** Essays Biochem 35: 3-18.

93. Kinosita, K., Jr., R. Yasuda, H. Noji and K. Adachi (2000). **"A rotary molecular motor that can work at near 100% efficiency."** Philos Trans R Soc Lond B Biol Sci 355 (1396): 473-489.

94. Kohzuma, K., C. Dal Bosco, J. Meurer and D. M. Kramer (2013). **"Light- and metabolism-related regulation of the chloroplast ATP synthase has distinct mechanisms and functions."** J Biol Chem 288 (18): 13156-13163.

95. Konno, H., T. Suzuki, D. Bald, M. Yoshida and T. Hisabori (2004). **"Significance of the epsilon subunit in the thiol modulation of chloroplast ATP synthase."** Biochem Biophys Res Commun 318 (1): 17-24.

96. Koopmann, R., K. Cupelli, L. Redecke, K. Nass, D. P. Deponte, T. A. White, F. Stellato, D. Rehders, M. Liang, J. Andreasson, A. Aquila, S. Bajt, M. Barthelmess, A. Barty, M. J. Bogan, C. Bostedt, S. Boutet, J. D. Bozek, C. Caleman, N. Coppola, J. Davidsson, R. B. Doak, T. Ekeberg, S. W. Epp, B. Erk, H. Fleckenstein, L. Foucar, H. Graafsma, L. Gumprecht, J. Hajdu, C. Y. Hampton, A. Hartmann, R. Hartmann, G. Hauser, H. Hirsemann, P. Holl, M. S. Hunter, S. Kassemeyer, R. A. Kirian, L. Lomb, F. R. Maia, N. Kimmel, A. V. Martin, M. Messerschmidt, C. Reich, D. Rolles, B. Rudek, A. Rudenko, I. Schlichting, J. Schulz, M. M. Seibert, R. L. Shoeman, R. G. Sierra, H. Soltau, S. Stern, L. Struder, N. Timneanu, J. Ullrich, X. Wang, G. Weidenspointner, U. Weierstall, G. J. Williams, C. B. Wunderer, P. Fromme, J. C. Spence, T. Stehle, H. N. Chapman, C. Betzel and M. Duszenko (2012). **"In vivo protein crystallization opens new routes in structural biology."** Nat Methods 9 (3): 259-262.

97. Krah, A., D. Pogoryelov, T. Meier and J. D. Faraldo-Gomez (2010). **"On the structure of the proton-binding site in the F_O rotor of chloroplast ATP synthases."** J Mol Biol 395 (1): 20-27.

98. Krause, F., N. H. Reifschneider, S. Goto and N. A. Dencher (2005). **"Active oligomeric ATP synthases in mammalian mitochondria."** Biochem Biophys Res Commun 329 (2): 583-590.

99. Krause, F. and H. Seelert (2008). **"Detection and analysis of protein-protein interactions of organellar and prokaryotic proteomes by blue native and colorless native gel electrophoresis."** Curr Protoc Protein Sci Chapter 19: Unit 19 18.

100. Kuhlbrandt, W., D. N. Wang and Y. Fujiyoshi (1994). **"Atomic model of plant light-harvesting complex by electron crystallography."** Nature 367 (6464): 614-621.

101. Kupitz, C., S. Basu, I. Grotjohann, R. Fromme, N. A. Zatsepin, K. N. Rendek, M. S. Hunter, R. L. Shoeman, T. A. White, D. Wang, D. James, J. H. Yang, D. E. Cobb, B. Reeder, R. G. Sierra, H. Liu, A. Barty, A. L. Aquila, D. Deponte, R. A. Kirian, S. Bari, J. J. Bergkamp, K. R. Beyerlein, M. J. Bogan, C. Caleman, T. C. Chao, C. E. Conrad, K. M. Davis, H. Fleckenstein, L. Galli, S. P. Hau-Riege, S. Kassemeyer, H. Laksmono, M. Liang, L. Lomb, S. Marchesini, A. V. Martin, M. Messerschmidt, D. Milathianaki, K. Nass, A. Ros, S. Roy-Chowdhury, K. Schmidt, M. Seibert, J. Steinbrener, F. Stellato, L. Yan, C. Yoon, T. A. Moore, A. L. Moore, Y. Pushkar, G. J. Williams, S. Boutet, R. B. Doak, U. Weierstall, M. Frank, H. N. Chapman, J. C. Spence and P. Fromme (2014). **"Serial time-resolved crystallography of photosystem II using a femtosecond X-ray laser."** Nature 513 (7517): 261-265.

102. Kupitz, C., I. Grotjohann, C. E. Conrad, S. Roy-Chowdhury, R. Fromme and P. Fromme (2014). **"Microcrystallization techniques for serial femtosecond crystallography using photosystem II from *Thermosynechococcus elongatus* as a model system."** Philos Trans R Soc Lond B Biol Sci 369(1647): 20130316.]

103. Laget, P. P. and J. B. Smith (1979). **"Inhibitory properties of endogenous subunit epsilon in the Escherichia coli F_1 ATPase."** Arch Biochem Biophys 197 (1): 83-89.

104. Lawrence, R. M. (2011). **"Recombinant Expression, Purification, and Reconstitution of the Chloroplast ATP Synthase c-subunit Ring."** Doctor of Philiosophy, Arizona State University

105. Lawrence, R. M., B. Varco-Merth, C. J. Bley, J. J. Chen and P. Fromme (2011). **"Recombinant production and purification of the subunit c of chloroplast ATP synthase."** Protein Expr Purif 76 (1): 15-24.

106. Lebeau, L. and C. Venien-Bryan (2013). **"Monolayer two-dimensional crystallization of membrane proteins."** Methods Mol Biol 955: 59-71.

107. Levy, D., G. Mosser, O. Lambert, G. S. Moeck, D. Bald and J. L. Rigaud (1999). **"Two-dimensional crystallization on lipid layer: A successful approach for membrane proteins."** J Struct Biol 127 (1): 44-52.

108. Loll, B., J. Kern, W. Saenger, A. Zouni and J. Biesiadka (2007). **"Lipids in photosystem II: interactions with protein and cofactors."** Biochim Biophys Acta 1767 (6): 509-519.

109. Lowry, O. H., N. J. Rosebrough, A. L. Farr and R. J. Randall (1951). **"Protein measurement with the Folin phenol reagent."** J Biol Chem 193 (1): 265-275.

110. Maeda, S., K. Shinzawa-Itoh, K. Mieda, M. Yamamoto, Y. Nakashima, Y. Ogasawara, C. Jiko, K. Tani, A. Miyazawa, C. Gerle and S. Yoshikawa (2013). **"Two-dimensional crystallization of intact F-ATP synthase isolated from bovine heart mitochondria."** Acta Crystallogr Sect F Struct Biol Cryst Commun 69 (Pt 12): 1368-1370.

111. Matthies, D., W. Zhou, A. L. Klyszejko, C. Anselmi, O. Yildiz, K. Brandt, V. Muller, J. D. Faraldo-Gomez and T. Meier (2014). **"High-resolution structure and mechanism of an F/V-hybrid rotor ring in a Na^+-coupled ATP synthase."** Nat Commun 5: 5286.

112. McCarty, R. E. (2005). **"ATP synthase of chloroplast thylakoid membranes: a more in depth characterization of its ATPase activity."** J Bioenerg Biomembr 37 (5): 289-297.

113. McPherson, A. (2009). **"Introduction to the crystallization of biological macromolecules."** Current Topics in membranes 63: 19.

114. Meier, T., P. Polzer, K. Diederichs, W. Welte and P. Dimroth (2005). **"Structure of the rotor ring of F-Type Na^+-ATPase from Ilyobacter tartaricus."** Science 308 (5722): 659-662.

115. Merril, C. R., M. L. Dunau and D. Goldman (1981). **"A rapid sensitive silver stain for polypeptides in polyacrylamide gels."** Anal Biochem 110 (1): 201-207.

116. Mesbah, N. M. and J. Wiegel (2011). **"The Na^+-translocating F_1F_0-ATPase from the halophilic, alkalithermophile *Natranaerobius thermophilus*."** Biochim Biophys Acta 1807(9): 1133-1142.

117. Meyer, B., I. Wittig, E. Trifilieff, M. Karas and H. Schagger (2007). **"Identification of two proteins associated with mammalian ATP synthase."** Mol Cell Proteomics 6 (10): 1690-1699.

118. Milhiet, P. E., F. Gubellini, A. Berquand, P. Dosset, J. L. Rigaud, C. Le Grimellec and D. Levy (2006). **"High-resolution AFM of membrane proteins directly incorporated at high density in planar lipid bilayer."** Biophys J 91 (9): 3268-3275.

119. Mills, J. D. and P. Mitchell (1982). **"Modulation of Coupling Factor Atpase Activity in Intact Chloroplasts - Reversal of Thiol Modulation in the Dark."** Biochimica Et Biophysica Acta 679 (1): 75-83.

120. Mula, S., A. Savitsky, K. Mobius, W. Lubitz, J. H. Golbeck, M. D. Mamedov, A. Y. Semenov and A. van der Est (2012). **"Incorporation of a high potential quinone reveals that electron transfer in Photosystem I becomes highly asymmetric at low temperature."** Photochem Photobiol Sci 11 (6): 946-956.

121. Nadanaciva, S., J. Weber and A. E. Senior (2000). **"New probes of the F_1-ATPase catalytic transition state reveal that two of the three catalytic sites can assume a transition state conformation simultaneously."** Biochemistry 39 (31): 9583-9590.

122. Nakamoto, R. K., J. A. Baylis Scanlon and M. K. Al-Shawi (2008). **"The rotary mechanism of the ATP synthase."** Arch Biochem Biophys 476 (1): 43-50.

123. Nalin, C. M. and R. E. McCarty (1984). **"Role of a disulfide bond in the gamma subunit in activation of the ATPase of chloroplast coupling factor 1."** J Biol Chem 259(11): 7275-7280.

124. Nannenga, B. L. and T. Gonen (2014). **"Protein structure determination by MicroED."** Curr Opin Struct Biol 27: 24-31.

125. Nannenga, B. L., D. Shi, J. Hattne, F. E. Reyes and T. Gonen (2014). **"Structure of catalase determined by MicroED."** Elife 3: e03600.

126. Nannenga, B. L., D. Shi, A. G. Leslie and T. Gonen (2014). **"High-resolution structure determination by continuous-rotation data collection in MicroED."** Nat Methods 11 (9): 927-930.

127. Neerken, S. and J. Amesz (2001). **"The antenna reaction center complex of heliobacteria: composition, energy conversion and electron transfer."** Biochim Biophys Acta 1507 (1-3): 278-290.

128. Neff, D. and N. A. Dencher (1999). **"Purification of multisubunit membrane protein complexes: isolation of chloroplast F_OF_1-ATP synthase, CF_O and CF_1 by blue native electrophoresis."** Biochem Biophys Res Commun 259 (3): 569-575.

129. Neff, D., S. Tripathi, K. Middendorf, H. Stahlberg, H. J. Butt, E. Bamberg and N. A. Dencher (1997). **"Chloroplast F0F1 ATP Synthase Imaged by Atomic Force Microscopy."** J Struct Biol 119 (2): 139-148.

130. Nishizaka, T., K. Oiwa, H. Noji, S. Kimura, E. Muneyuki, M. Yoshida and K. Kinosita, Jr. (2004). **"Chemomechanical coupling in F_1-ATPase revealed by simultaneous observation of nucleotide kinetics and rotation."** Nat Struct Mol Biol 11 (2): 142-148.

131. Noji, H., R. Yasuda, M. Yoshida and K. Kinosita, Jr. (1997). **"Direct observation of the rotation of F_1-ATPase."** Nature 386 (6622): 299-302.

132. Oh-oka, H. (2007). **"Type 1 reaction center of photosynthetic heliobacteria."** Photochem Photobiol 83(1): 177-186.

133. Ort, D. R. and K. Oxborough (1992). **"Insitu Regulation of Chloroplast Coupling Factor Activity."** Annual Review of Plant Physiology and Plant Molecular Biology 43: 269-291.

134. Ort, D. R., Oxborough, K. (1992). **"In Situ Regulation of Chloroplast Coupling Factor Activity."** Annual Review of Plant Physiology and Plant Molecular Biology 43: 23.

135. Pänke, O., and Rumberg, B. (1997). **"Energy and entropy balance of ATP synthesis."** Biochimica et Biophysica Acta 1322 (2-3).

136. Pedrini, B., C. J. Tsai, G. Capitani, C. Padeste, M. S. Hunter, N. A. Zatsepin, A. Barty, W. H. Benner, S. Boutet, G. K. Feld, S. P. Hau-Riege, R. A. Kirian, C. Kupitz, M. Messerschmitt, J. I. Ogren, T. Pardini, B. Segelke, G. J. Williams, J. C. Spence, R. Abela, M. Coleman, J. E. Evans, G. F. Schertler, M. Frank and X. D. Li (2014). **"7 A resolution in protein two-dimensional-crystal X-ray diffraction at Linac Coherent Light Source."** Philos Trans R Soc Lond B Biol Sci 369 (1647): 20130500.

137. Perry, S. E., H. M. Li and K. Keegstra (1991). **"In vitro reconstitution of protein transport into chloroplasts."** Methods Cell Biol 34: 327-344.

138. Peter Gräber, U. J. a. G. H. S. (1984). **"Kinetics of Proton-Transport-Coupled ATP Synthesis in Chloroplasts. Activation of the ATPase by an Artificially Generated ΔpH and $\Delta\phi$."** Berichte der Bunsengesellschaft für physikalische Chemie 88 (7): 10.

139. Petersen, J., K. Forster, P. Turina and P. Graber (2012). **"Comparison of the H^+/ATP ratios of the H^+-ATP synthases from yeast and from chloroplast."** Proc Natl Acad Sci U S A 109 (28): 11150-11155.

140. Pfeiffer, K., V. Gohil, R. A. Stuart, C. Hunte, U. Brandt, M. L. Greenberg and H. Schagger (2003). **"Cardiolipin stabilizes respiratory chain supercomplexes."** J Biol Chem 278 (52): 52873-52880.

141. Pick, U. (1982). **"Isolation of the ATPase cmplex (CF_O-CF_1)"**. Methods in Chloroplast Molecular Biology. R. B. H. a. N.-H. C. M. Edelman, Elsevier Biomedical Press: 8.

142. Pick, U. and S. Bassilian (1982). **"Activation of magnesium ion specific adenosinetriphosphatase in chloroplast coupling factor 1 by octyl glucoside."** Biochemistry 21 (24): 6144-6152.

143. Poetsch, A., D. Neff, H. Seelert, H. Schagger and N. A. Dencher (2000). **"Dye removal, catalytic activity and 2D crystallization of chloroplast H+-ATP synthase purified by blue native electrophoresis."** Biochim Biophys Acta 1466 (1-2): 339-349.

144. Poetsch, A., D. Neff, H. Seelert, H. Schagger and N. A. Dencher (2000). **"Dye removal, catalytic activity and 2D crystallization of chloroplast H^+-ATP synthase purified by blue native electrophoresis."** Biochimica Et Biophysica Acta-Biomembranes 1466 (1-2): 339-349.

145. Poetsch, A., H. Seelert, J. Meyer zu Tittingdorf and N. A. Dencher (1999). **"Detergent effect on anion exchange perfusion chromatography and gel filtration of intact chloroplast H^+-ATP synthase."** Biochem Biophys Res Commun 265 (2): 520-524.

146. Pogoryelov, D., J. Yu, T. Meier, J. Vonck, P. Dimroth and D. J. Muller (2005). **"The c_{15} ring of the Spirulina platensis F-ATP synthase: F_1/F_0 symmetry mismatch is not obligatory."** EMBO Rep 6 (11): 1040-1044.

147. Rastogi, V. K. and M. E. Girvin (1999). **"Structural changes linked to proton translocation by subunit c of the ATP synthase."** Nature 402 (6759): 263-268.

148. Raunser, S. and T. Walz (2009). **"Electron crystallography as a technique to study the structure on membrane proteins in a lipidic environment."** Annu Rev Biophys 38: 89-105.

149. Rees, D. M., A. G. Leslie and J. E. Walker (2009). **"The structure of the membrane extrinsic region of bovine ATP synthase."** Proc Natl Acad Sci U S A 106 (51): 21597-21601.

150. Reisinger, V. and L. A. Eichacker (2006). **"Analysis of membrane protein complexes by blue native PAGE."** Proteomics 6 Suppl 2: 6-15.

151. Rexroth, S., J. M. Meyer Zu Tittingdorf, H. J. Schwassmann, F. Krause, H. Seelert and N. A. Dencher (2004). **"Dimeric H^+-ATP synthase in the chloroplast of Chlamydomonas reinhardtii."** Biochim Biophys Acta 1658 (3): 202-211.

152. Richard, P., J. L. Rigaud and P. Graber (1990). **"Reconstitution of CF_0F_1 into liposomes using a new reconstitution procedure."** Eur J Biochem 193 (3): 921-925.

153. Richter, M. L. (2004). **"Gamma-epsilon Interactions Regulate the Chloroplast ATP Synthase."** Photosynth Res 79 (3): 319-329.

154. Richter, M. L., R. Hein and B. Huchzermeyer (2000). **"Important subunit interactions in the chloroplast ATP synthase."** Biochim Biophys Acta 1458 (2-3): 326-342.

155. Richter, M. L., W. J. Patrie and R. E. McCarty (1984). **"Preparation of the epsilon subunit and epsilon subunit-deficient chloroplast coupling factor 1 in reconstitutively active forms."** J Biol Chem 259 (12): 7371-7373.

156. Sakurai, H., K. Shinohara, T. Hisabori and K. Shinohara (1981). **"Enhancement of Adenosine-Triphosphatase Activity of Purified Chloroplast Coupling Factor-I in an Aqueous Organic-Solvent."** Journal of Biochemistry 90 (1): 95-102.

157. Sarrou, I., Z. Khan, J. Cowgill, S. Lin, D. Brune, S. Romberger, J. H. Golbeck and K. E. Redding (2012). **"Purification of the photosynthetic reaction center from *Heliobacterium modesticaldum*."** Photosynth Res 111 (3): 291-302.

158. Sattley, W. M. and R. E. Blankenship (2010). **"Insights into heliobacterial photosynthesis and physiology from the genome of *Heliobacterium modesticaldum*."** Photosynthesis Research 104 (2-3): 113-122.

159. Sattley, W. M., M. T. Madigan, W. D. Swingley, P. C. Cheung, K. M. Clocksin, A. L. Conrad, L. C. Dejesa, B. M. Honchak, D. O. Jung, L. E. Karbach, A. Kurdoglu, S. Lahiri, S. D. Mastrian, L. E. Page, H. L. Taylor, Z. T. Wang, J. Raymond, M. Chen, R. E. Blankenship and J. W. Touchman (2008). **"The genome of Heliobacterium modesticaldum, a phototrophic representative of the Firmicutes containing the simplest photosynthetic apparatus."** J Bacteriol 190 (13): 4687-4696.

160. Schafer, E., N. A. Dencher, J. Vonck and D. N. Parcej (2007). **"Three-dimensional structure of the respiratory chain supercomplex $I_1III_2IV_1$ from bovine heart mitochondria."** Biochemistry 46 (44): 12579-12585.

161. Schafer, E., H. Seelert, N. H. Reifschneider, F. Krause, N. A. Dencher and J. Vonck (2006). **"Architecture of active mammalian respiratory chain supercomplexes."** J Biol Chem 281 (22): 15370-15375.

162. Schagger, H. (2006). **"Tricine-SDS-PAGE."** Nat Protoc 1 (1): 16-22.

163. Schagger, H. and K. Pfeiffer (2000). **"Supercomplexes in the respiratory chains of yeast and mammalian mitochondria."** EMBO J 19 (8): 1777-1783.

164. Schmidt-Krey, I. (2007). **"Electron crystallography of membrane proteins: two-dimensional crystallization and screening by electron microscopy."** Methods 41(4): 417-426.

165. Schmidt, G. G., P. (1985). **"The rate of ATP synthesis by reconstituted CF_0F_1 liposomes."** Biochim. Biophys. Acta 808, 46–51.

166. Schwem, B. E. and R. H. Fillingame (2006). **"Cross-linking between helices within subunit a of *Escherichia coli* ATP synthase defines the transmembrane packing of a four-helix bundle."** J Biol Chem 281 (49): 37861-37867.

167. Seelert, H., N. A. Dencher and D. J. Muller (2003). **"Fourteen protomers compose the oligomer III of the proton-rotor in spinach chloroplast ATP synthase."** J Mol Biol 333 (2): 337-344.

168. Seelert, H. and F. Krause (2008). **"Preparative isolation of protein complexes and other bioparticles by elution from polyacrylamide gels."** Electrophoresis 29 (12): 2617-2636.

169. Seelert, H., A. Poetsch, N. A. Dencher, A. Engel, H. Stahlberg and D. J. Muller (2000)**. "Structural biology. Proton-powered turbine of a plant motor."** Nature 405 (6785): 418-419.

170. Seelert, H., A. Poetsch, M. Rohlfs and N. A. Dencher (2000). **"Dye-ligand chromatographic purification of intact multisubunit membrane protein complexes: application to the chloroplast H^+-F_OF_1-ATP synthase."** Biochem J 346 Pt 1: 41-44.

171. Senior, A. E., J. Weber and S. Nadanaciva (2000). **"The catalytic transition state in ATP synthase."** J Bioenerg Biomembr 32 (5): 523-529.

172. Shi, D., B. L. Nannenga, M. G. Iadanza and T. Gonen (2013). **"Three-dimensional electron crystallography of protein microcrystals."** Elife 2: e01345.

173. Shimabukuro, K., R. Yasuda, E. Muneyuki, K. Y. Hara, K. Kinosita, Jr. and M. Yoshida (2003). **"Catalysis and rotation of F_1 motor: cleavage of ATP at the catalytic site occurs in 1 ms before 40 degree substep rotation."** Proc Natl Acad Sci U S A 100 (25): 14731-14736.

174. Shirakihara, Y., A. G. Leslie, J. P. Abrahams, J. E. Walker, T. Ueda, Y. Sekimoto, M. Kambara, K. Saika, Y. Kagawa and M. Yoshida (1997). **"The crystal structure of the nucleotide-free alpha 3 beta 3 subcomplex of F_1-ATPase from the thermophilic *Bacillus PS3* is a symmetric trimer."** Structure 5 (6): 825-836.

175. Sone, N., M. Yoshida, H. Hirata and Y. Kagawa (1977). **"Reconstitution of vesicles capable of energy transformation from phospholipids and adenosine triphosphatase of a thermophilic bacterium."** J Biochem 81 (2): 519-528.

176. Stahlberg, H., D. J. Muller, K. Suda, D. Fotiadis, A. Engel, T. Meier, U. Matthey and P. Dimroth (2001). **"Bacterial Na^+-ATP synthase has an undecameric rotor."** EMBO Rep 2 (3): 229-233.

177. Steigmiller, S., P. Turina and P. Graber (2008). **"The thermodynamic H^+/ATP ratios of the H^+-ATPsynthases from chloroplasts and *Escherichia coli*."** Proc Natl Acad Sci U S A 105 (10): 3745-3750.

178. Stock, D., A. G. Leslie and J. E. Walker (1999). **"Molecular architecture of the rotary motor in ATP synthase."** Science 286 (5445): 1700-1705.

179. Suhai, T., N. G. Heidrich, N. A. Dencher and H. Seelert (2009). **"Highly sensitive detection of ATPase activity in native gels."** Electrophoresis 30 (20): 3622-3625.

180. Tang, K. H., H. Yue and R. E. Blankenship (2010). **"Energy metabolism of *Heliobacterium modesticaldum* during phototrophic and chemotrophic growth."** BMC Microbiol 10: 150.

181. Tikhonov, A. N. (2013). **"pH-dependent regulation of electron transport and ATP synthesis in chloroplasts."** Photosynth Res 116 (2-3): 511-534.

182. Turina, P., D. Samoray and P. Graber (2003). **"H^+/ATP ratio of proton transport-coupled ATP synthesis and hydrolysis catalysed by CF_0F_1-liposomes."** Embo Journal 22 (3): 418-426.

183. Turina, P., D. Samoray and P. Graber (2003). **"H^+/ATP ratio of proton transport-coupled ATP synthesis and hydrolysis catalysed by CF_0F_1-liposomes."** EMBO J 22 (3): 418-426.

184. Valiyaveetil, F. I. and R. H. Fillingame (1998). **"Transmembrane topography of subunit a in the Escherichia coli F_1F_0 ATP synthase."** J Biol Chem 273 (26): 16241-16247.

185. van Wijk, K. J., J. B. Peltier and L. Giacomelli (2007). **"Isolation of chloroplast proteins from Arabidopsis thaliana for proteome analysis."** Methods Mol Biol 355: 43-48.

186. Varco-Merth, B., R. Fromme, M. Wang and P. Fromme (2008). **"Crystallization of the c14-rotor of the chloroplast ATP synthase reveals that it contains pigments."** Biochim Biophys Acta 1777 (7-8): 605-612.

187. Vik, S. B. and B. J. Antonio (1994). **"A mechanism of proton translocation by F_1F_0 ATP synthases suggested by double mutants of the a subunit."** J Biol Chem 269 (48): 30364-30369.

188. Vik, S. B. and R. R. Ishmukhametov (2005). **"Structure and function of subunit a of the ATP synthase of *Escherichia coli*."** J Bioenerg Biomembr 37 (6): 445-449.

189. Vollmar, M., D. Schlieper, M. Winn, C. Buchner and G. Groth (2009). **"Structure of the c_{14} rotor ring of the proton translocating chloroplast ATP synthase."** J Biol Chem 284 (27): 18228-18235.

190. von Ballmoos, C., A. Wiedenmann and P. Dimroth (2009). **"Essentials for ATP synthesis by F_1F_0 ATP synthases."** Annu Rev Biochem 78: 649-672.

191. Wada, T., J. C. Long, D. Zhang and S. B. Vik (1999). **"A novel labeling approach supports the five-transmembrane model of subunit a of the *Escherichia coli* ATP synthase."** J Biol Chem 274 (24): 17353-17357.

192. Walker, J. E. (2013). **"The ATP synthase: the understood, the uncertain and the unknown."** Biochem Soc Trans 41 (1): 1-16.

193. Wampler, R. D., D. J. Kissick, C. J. Dehen, E. J. Gualtieri, J. L. Grey, H. F. Wang, D. H. Thompson, J. X. Cheng and G. J. Simpson (2008). **"Selective detection of protein crystals by second harmonic microscopy."** J Am Chem Soc 130 (43): 14076-14077.

194. Wang, D. and P. R. Hiesinger (2013). **"The vesicular ATPase: a missing link between acidification and exocytosis."** J Cell Biol 203 (2): 171-173.

195. Watt, I. N., M. G. Montgomery, M. J. Runswick, A. G. Leslie and J. E. Walker (2010). **"Bioenergetic cost of making an adenosine triphosphate molecule in animal mitochondria."** Proc Natl Acad Sci U S A 107 (39): 16823-16827.

196. Weber, J. and A. E. Senior (1997). **"Binding of TNP-ATP and TNP-ADP to the non-catalytic sites of *Escherichia coli* F_1-ATPase."** FEBS Lett 412 (1): 169-172.

197. Weber, J. and A. E. Senior (1997). **"Catalytic mechanism of F_1-ATPase."** Biochim Biophys Acta 1319 (1): 19-58.

198. Weber, J. and A. E. Senior (2000). **"ATP synthase: what we know about ATP hydrolysis and what we do not know about ATP synthesis."** Biochim Biophys Acta 1458 (2-3): 300-309.

199. Weber, J. and A. E. Senior (2000). **"Features of F_1-ATPase catalytic and noncatalytic sites revealed by fluorescence lifetimes and acrylamide quenching of specifically inserted tryptophan residues."** Biochemistry 39(18): 5287-5294.

200. Wellburn, A. R. a. H. L. (1984). **"Formulae and program to determine total carotenoids and chlorophyll a and b of leaf extracts in different solvents."** The Hague, The Netherlands.

201. Wittig, I., H. P. Braun and H. Schagger (2006). **"Blue native PAGE."** Nat Protoc 1 (1): 418-428.

202. Wittig, I., R. Carrozzo, F. M. Santorelli and H. Schagger (2007). **"Functional assays in high-resolution clear native gels to quantify mitochondrial complexes in human biopsies and cell lines."** Electrophoresis 28 (21): 3811-3820.

203. Wittig, I., M. Karas and H. Schagger (2007). **"High resolution clear native electrophoresis for in-gel functional assays and fluorescence studies of membrane protein complexes."** Mol Cell Proteomics 6 (7): 1215-1225.

204. Wittig, I. and H. Schagger (2005). **"Advantages and limitations of clear-native PAGE."** Proteomics 5 (17): 4338-4346.

205. Wittig, I. and H. Schagger (2008). **"Features and applications of blue-native and clear-native electrophoresis."** Proteomics 8 (19): 3974-3990.

206. Wittig, I. and H. Schagger (2009). **"Native electrophoretic techniques to identify protein-protein interactions."** Proteomics 9 (23): 5214-5223.

207. Yasuda, R., H. Noji, K. Kinosita, Jr. and M. Yoshida (1998). **"F_1-ATPase is a highly efficient molecular motor that rotates with discrete 120 degree steps."** Cell 93 (7): 1117-1124.

208. Yoshida, M. and W. S. Allison (1986). **"Characterization of the catalytic and noncatalytic ADP binding sites of the F_1-ATPase from the thermophilic bacterium, PS3."** J Biol Chem 261 (13): 5714-5721.

209. Yoshida, M., E. Muneyuki and T. Hisabori (2001). **"ATP synthase--a marvellous rotary engine of the cell."** Nat Rev Mol Cell Biol 2 (9): 669-677.

210. Yu, F. and R. E. McCarty (1985). **"Detergent activation of the ATPase activity of chloroplast coupling factor 1."** Arch Biochem Biophys 238 (1): 61-68.

211. Zerbetto, E., L. Vergani and F. Dabbeni-Sala (1997). **"Quantification of muscle mitochondrial oxidative phosphorylation enzymes via histochemical staining of blue native polyacrylamide gels."** Electrophoresis 18 (11): 2059-2064.

APPENDIX A

FORMULA OF SOLUBILIZAION PROCESS

Formula of solubilization solutions suitable for 100 mL of the mixture of reduced thylakoid membrane-suspension

1. 25 ml of Solubilization Buffer	Initial		Volume		Final	
Tricine-NaOH, pH 8.0	80	mM	25	mL	10	mM
Sucrose	800	mM			100	mM
$MgCl_2$	20	mM			2.5	mM
KCl	20	mM			2.5	mM

2. 4 ml of Na_2-ATP Solution	100	mM	4	mL	2	mM

3. 20 ml of Saturated $(NH_4)_2SO_4$ Solution	100	% (w/v)	20	mL	10	% (w/v)
pH 8.0, adjusted by titration with NH_3OH						

4. 14 ml of Deionized H_2O	0	mM	14	mL	0	mM

5. 20 ml of DL-dithiotreitol Solution	500	mM	20	mL	50	mM

6. 5 ml of Sodium cholate Solution	500	mM	5	mL	12.5	mM
pH 8.0, adjusted by titration with NaOH, and filtered						

7. 12 ml of β-D-octylglucoside Solution	500	mM	12	mL	30	mM

APPENDIX B

EQUATIONS OF CONCENTRATION DETERMINATION

The ammonium sulfate precipitation step

Equation 4.4.3:

$$v = [\, V_{supernatant} \cdot (b_{\text{end concentration in \%}} - a_{\text{start concentration in \%}})] \,/\, (100\% - b_{\text{end concentration in \%}})$$

v	=	volume of saturated ammonium sulfate solution
a	=	initial concentration of ammonium sulfate in %(v/v)
b	=	final concentration of ammonium sulfate in %(v/v)

Protein concentration determination at 280nm and 278nm

Equation 4.5.1.1 (280 nm):

$$c = (A_{280} / d) \cdot (D)$$

c	=	concentration of total proteins, mg/ mL
$A_{280\ nm}$	=	absorbance value at 280 nm
d	=	path length of a quartz cuvette, 1 cm
D	=	dilution factor, total volume/volume of the sample

Equation 4.5.2.2 (278 nm):

$$c = [A_{278} / (\varepsilon \cdot d)] \cdot D$$

c	=	concentration of CF_1F_O in the protein sample solution, M
$A_{278\ nm}$	=	absorbance value at 278 nm
d	=	path length of a quartz cuvette, 1 cm
$\varepsilon_{278\ nm}$	=	extinction coefficient at 278 nm, 22,800 M^{-1} cm^{-1}
D	=	dilution factor, total volume /volume of the sample

Chlorophyll Concentration determination at 652 nm for Intact Chloroplasts Isolation

Equation 4.5.3 (652 nm):

$$c_{mg/mL} = 0.02899 \cdot A_{652\,nm} \cdot (D)$$

c	=	concentration of chlorophyll, mg/mL
$A_{652\,nm}$	=	absorbance value at 652 nm
D	=	dilution factor, total volume/volume of the sample

Chlorophyll Concentration determination of CF_1F_O for ATP Synthase Isolation

Equation 4.5.4 (664 nm and 700 nm):

$$c = [(A_{664\,nm} - A_{700\,nm}) / (\varepsilon_{664nm})] \cdot (D)$$

c	=	concentration of total chlorophyll, mg /mL
$A_{664\,nm}$	=	absorbance value at 664 nm
$A_{700\,nm}$	=	absorbance value at 700 nm
$\varepsilon_{664\,nm}$	=	extinction coefficient at 664 nm in 80% (v/v) acetone solution, 76,780 M^{-1} cm^{-1}
D	=	dilution factor, total volume/volume of the sample

APPENDIX C

GRADIENT GEL SETUP AND ELECTROELUTION DEVICE

1. Setup for preparing native gradient gels (Krause and Seelert 2008).

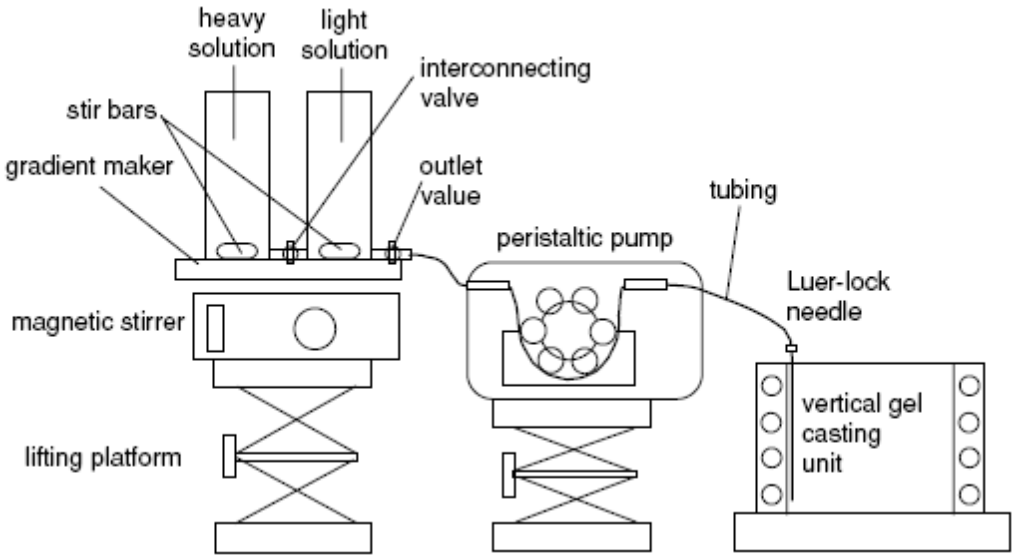

2. Setup of the electroelution device (Krause and Seelert 2008).

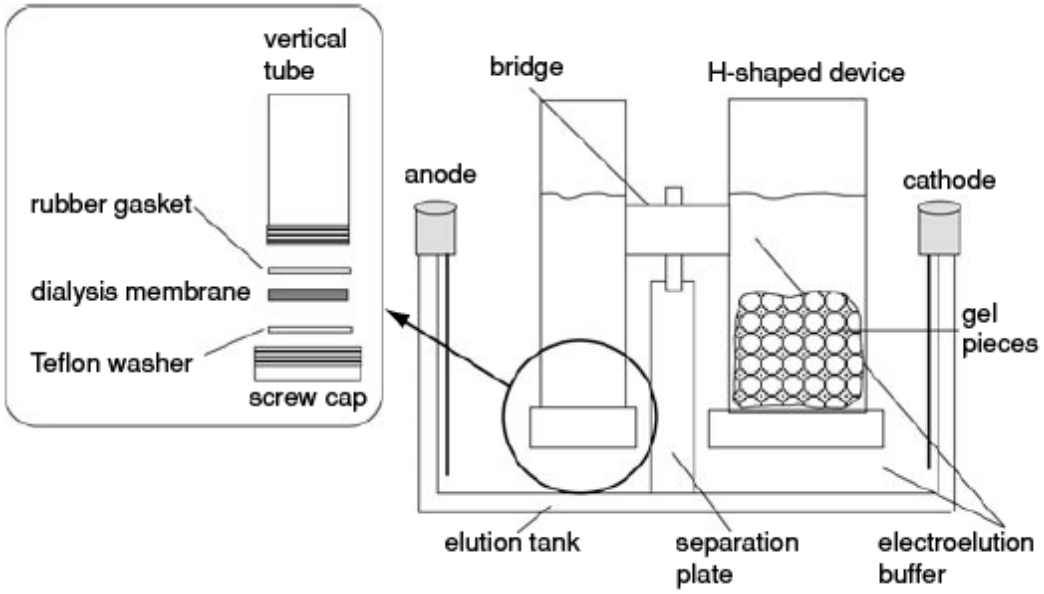

APPENDIX D

CF_1F_O PROTEIN RECONSTITUTION

Pipetting scheme of the CF_1F_O reconstitution experiment

Substance	Initial con.		Volume		Final con.	
Freshly prepared liposome	16	g/L	100	µL	8	g/L
$MgCl_2$	1	M	0.5	µL	2.5	mM
1X Reconstitution-Buffer	-------		81.5	µL	-------	
	-				-	
Protein	10	µM	2	µL	100	nM
Triton X-100	100	g/L	16	µL	8	g/L

APPENDIX E

CHROMATOGRAPHIC PARAMETERS

Parameters for anion affinity chromatography

Column volume	1.7	mL
Column material	POROS, 20 HQ, strong anion exchange packing	
Equilibration buffer	1X Equilibration buffer	
Elution buffer	2M NaCl in 1X equilibration buffer	
Equilibration buffer volume (10CV)	17	mL
Elution buffer volume (30CV)	51	mL
Regeneration buffer	1X Equilibration buffer	
Pump A	1X Equilibration buffer	
Pump B	1X Elution Buffer	
Flow rate	5	mL/min
Fraction volume	0.5	mL per fraction
Detection	UV-VIS 280 nm	
Gradient	0~25% 1X Elution buffer in 30 CV	
Column storage buffer	20% (v/v) Ethanol	

Parameter of R-120 negative affinity chromatography

Column volume	4	mL
Column material	Reactive Red 120-agarose (R0503, Sigma)	
Equilibration buffer	1X R120 Equilibration buffer	
Elution buffer	1X R120 Elution buffer (1.5 M NaCl)	
Equilibration buffer volume (6 CV)	24	mL
Elution buffer volume (12CV)	48	mL
Pump A	1X R120 equilibration buffer	
Pump B	1X R120 Elution buffer	
Flow rate	2	mL/min
Fraction volume	1	mL per fraction
Detection	UV-VIS 280 nm	
Column washing buffer (6CV)	1X R120 Washing buffer	
Column storage buffer	1X R120 Storage buffer	

APPENDIX F

EQUATION OF ATP SYNTHESIS ACTIVITY ASSAY

Calibration and Baseline Recording

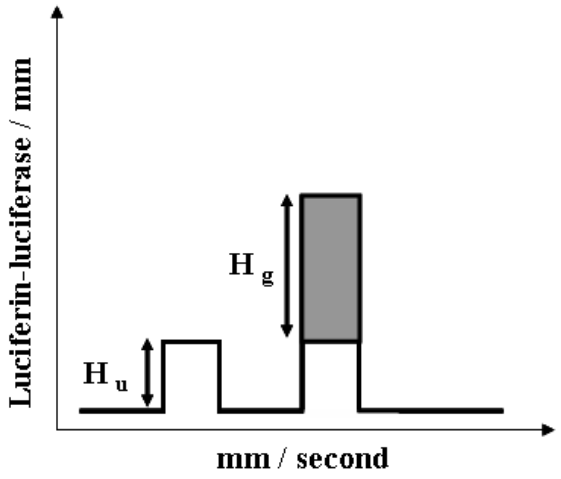

Schematic of calibration and baseline recording data

Eqution 4.11.3.1

$$C_{Basic\text{-}Buffer} = (H_u \cdot V_{Basic\text{-}Buffer + luciferin/luciferase\ kit} \cdot C_{st}) / (H_g \cdot V_{Basic\text{-}Buffer})$$

$C_{Basic\text{-}Buffer}$	=	ATP concentration in 1X basic incubation buffer (nM)
H_u	=	Height of the underground signal (cm)
H_g	=	Height of the generated signal (cm)
C_{st}	=	ATP standard concentration (nM)
V_1	=	volume of 1X basic incubation buffer (μL)
V_2	=	volume of 1X basic incubation buffer + luciferin/luciferase kit (μL)

The rate of ATP synthesis activity

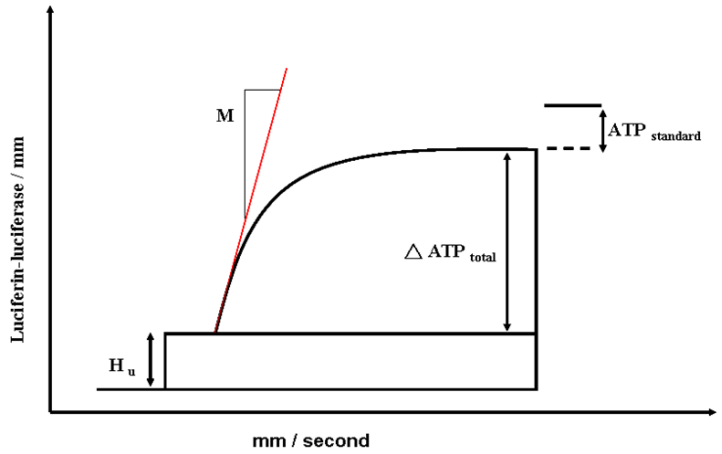

Schematic of ATP synthesis recording data

Eqution 4.11.3.2

$$T_S = (M \cdot C_{Basic\text{-}Buffer} \cdot V_1) / (H_u \cdot C_{CF1F0} \cdot V_2)$$

Ts	=	turnover per ATP synthase (S^{-1})
$C_{Basic\text{-}Buffer}$	=	ATP concentration in the basic incubation buffer (nM)
H_u	=	height of the underground signal (cm)
V_1	=	volume of the basic incubation buffer (μL)
V_2	=	volume of the basic buffer + luciferin/luciferase kit (μL)
M	=	slope (initial rate per ATP synthase) (mm S^{-1})
C_{CF1F0}	=	CF_1F_0 concentration (nM)